AD-A064 159 KAMAN AEROSPACE CORP BLOOMFIELD CONN F/G 1/3
PRELIMINARY DESIGN STUDY OF A COMPOSITE MAIN ROTOR BLADE FOR TH--ETC(U)
SEP 78 C HARDERSEN, W BLACKBURN DAAJ02-77-C-0075
UNCLASSIFIED R-1532-VOL-1 USARTL-TR-78-29A NL


3
59

USARTL-TR-78-29A

LEVEL II

C016402

PRELIMINARY DESIGN STUDY OF A COMPOSITE MAIN ROTOR BLADE FOR THE OH-58 HELICOPTER

VOLUME I - Trade Analysis and Preliminary Design Study of Composite OH-58 Main Rotor Blade

Charles Hardersen, William Blackburn

KAMAN AEROSPACE CORPORATION
Old Windsor Road
Bloomfield, Conn. 06002

September 1978

Final Report for Period October 1977 - February 1978

Approved for public release; distribution unlimited.

Prepared for

APPLIED TECHNOLOGY LABORATORY
U. S. ARMY RESEARCH AND TECHNOLOGY LABORATORIES (AVRADCOM)
Fort Eustis, Va. 23604

APPLIED TECHNOLOGY LABORATORY POSITION STATEMENT

The preliminary design and analysis in this report provides insight into the feasibility and technical gains associated with the application of a composite main rotor blade to the OH-58 helicopter. Results from this program will be of benefit when establishing requirements and objectives for any follow-on blade Product Improvement Program for the OH-58 helicopter.

Mr. Harold K. Reddick, Jr., Structures Technical Area, Aeronautical Technology Division, served as project engineer for this effort.

DISCLAIMER NOTICE

THIS DOCUMENT IS BEST QUALITY PRACTICABLE. THE COPY FURNISHED TO DDC CONTAINED A SIGNIFICANT NUMBER OF PAGES WHICH DO NOT REPRODUCE LEGIBLY.

Unclassified

SECURITY CLASSIFICATION OF THIS PAGE (When Data Entered)

REPORT DOCUMENTATION PAGE

READ INSTRUCTIONS BEFORE COMPLETING FORM

1. REPORT NUMBER: USARTL-TR-78-29A
2. GOVT ACCESSION NO.:
3. RECIPIENT'S CATALOG NUMBER:
4. TITLE (and Subtitle): PRELIMINARY DESIGN STUDY OF A COMPOSITE MAIN ROTOR BLADE FOR THE OH-58 HELICOPTER. Volume I. Trade Analysis and Preliminary Design Study of Composite OH-58 Main Rotor Blade.
5. TYPE OF REPORT & PERIOD COVERED: Final rept. Oct 77 - Feb 78
6. PERFORMING ORG. REPORT NUMBER: R-1532-VOL-1
7. AUTHOR(s): Charles Hardersen, William Blackburn
8. CONTRACT OR GRANT NUMBER(s): DAAJ02-77-C-0075
9. PERFORMING ORGANIZATION NAME AND ADDRESS: Kaman Aerospace Corporation, Old Windsor Road, Bloomfield, Conn. 06002
10. PROGRAM ELEMENT, PROJECT, TASK AREA & WORK UNIT NUMBERS: 62209AIL262209AH76 00 227 EK
11. CONTROLLING OFFICE NAME AND ADDRESS: Applied Technology Laboratory, U.S. Army Research & Technology Laboratories (AVRADCOM), Fort Eustis, Va. 23604
12. REPORT DATE: Sept[illegible] 1978
13. NUMBER OF PAGES: 206
14. MONITORING AGENCY NAME & ADDRESS (if different from Controlling Office): 212p.
15. SECURITY CLASS. (of this report): Unclassified
15a. DECLASSIFICATION/DOWNGRADING SCHEDULE:

16. DISTRIBUTION STATEMENT (of this Report)

Approved for public release; distribution unlimited.

AD A064021 V2

17. DISTRIBUTION STATEMENT (of the abstract entered in Block 20, if different from Report)

18. SUPPLEMENTARY NOTES

Volume I of a two-volume report.

19. KEY WORDS (Continue on reverse side if necessary and identify by block number)

Helicopter
Composites
Erosion
Ice Protection
Rotor Blade
Damage Tolerance

20. ABSTRACT (Continue on reverse side if necessary and identify by block number)

The objective of this program was to design a composite rotor blade for the OH-58C/A helicopter which has reduced life-cycle costs, 6% improved hover performance, improved reliability and maintainability, reduced radar signature and increased ballistic survivability. A trade-study approach was used to select the final configuration for the preliminary design phase. A monolithic composite structure evolved which utilizes winding in the production of the main spar, skins and the trailing edge spline. The blade satisfies

Over

DD FORM 1 JAN 73 1473 EDITION OF 1 NOV 65 IS OBSOLETE

Unclassified

SECURITY CLASSIFICATION OF THIS PAGE (When Data Entered)

404 362 LB

20. Abstract (Continued)

basic objectives using a double-tapered planform and a VR-7 airfoil. Composite materials selected include S-glass, E-glass and carbon graphite. This report is presented in two volumes. Volume I is contained herein. Volume II, with security classification of CONFIDENTIAL, is titled "Ballistic Survivability Analysis and Radar Reflectivity Analysis" and is presented under separate cover.

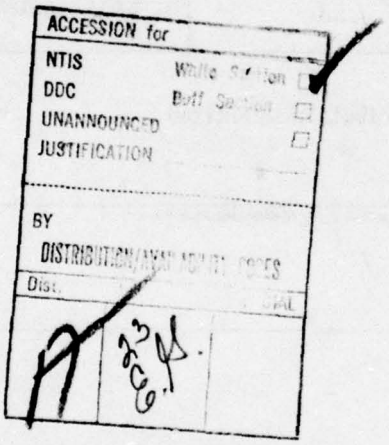

SUMMARY

This report covers activities performed at Kaman Aerospace Corporation in two task areas. Task I consisted of trade studies to determine the best state-of-the-art design of a composite blade for the OH-58C/A helicopter. Task II covered the preliminary design and analysis of the selected configuration.

The Task I trade study examines the characteristics of five distinct root-end designs, two cross section variations and two tip configurations. Several airfoils and planforms were examined in a performance study phase, and at least 20 materials/fabrication combinations were investigated. Fatigue life, damage tolerance, reliability and maintainability were determining factors in the study. Cost was of prime consideration, as well as radar reflectivity. Using a ranking system, a best configuration was selected for the preliminary design phase of Task II.

In Task II, the selected configuration, designated the K757 rotor blade, is submitted to detailed analysis. Laminate stress analyses were completed and a final adjustment of mass and stiffness distribution was made. Blade first, second and third flapwise and chordwise natural frequencies replicated those of the standard OH-58 blade within 8%. Load calculations were in good agreement with observed OH-58 flight, but in some instances were unconservative and replaced by extrapolated flight measured loadings for the design analysis. The fatigue life was conservatively calculated to be 4703 hours. Performance analyses, reliability and maintainability analyses, life cycle costs, radar reflectivity and ballistic survivability analyses were completed in detail.

With the exception of radar signature, the selected K757 blade design was shown to meet or exceed all desired objectives, including an increase in polar moment of inertia for improved autorotation characteristics. Figure 1 presents data comparing the attributes of the K757 OH-58 composite blade with the present OH-58 metal blade.

The configuration selected is a double tapered blade having a twelve degree twist from tip to rotor mast station zero (0). Solidity is .0364 and a VR-7 airfoil is used between station 36.5 and the tip. Materials selected consist of fiber E- and S-glass, Thornel 300 carbon graphite and epoxy molding compound. Other materials are cast steel and lead for ballast weight and steel bushings, bolts and washers. Fabrication of the main spar is by filament winding using the tip inertia ballast weight as a built-in mandrel component. A carved Nomex-core afterbody and a linear filament-wound trailing edge piece and leading edge piece make up the blade cross section. The blade tip cap is an integral part of the cast steel tip ballast member. Figure 2 presents the root-end details.

The blade is retained within the yoke clevis by the present OH-58 main pin. It is also restrained in the edgewise direction using the existing OH-58 latch mechanism. Rotor loads are transferred to the inboard all composite

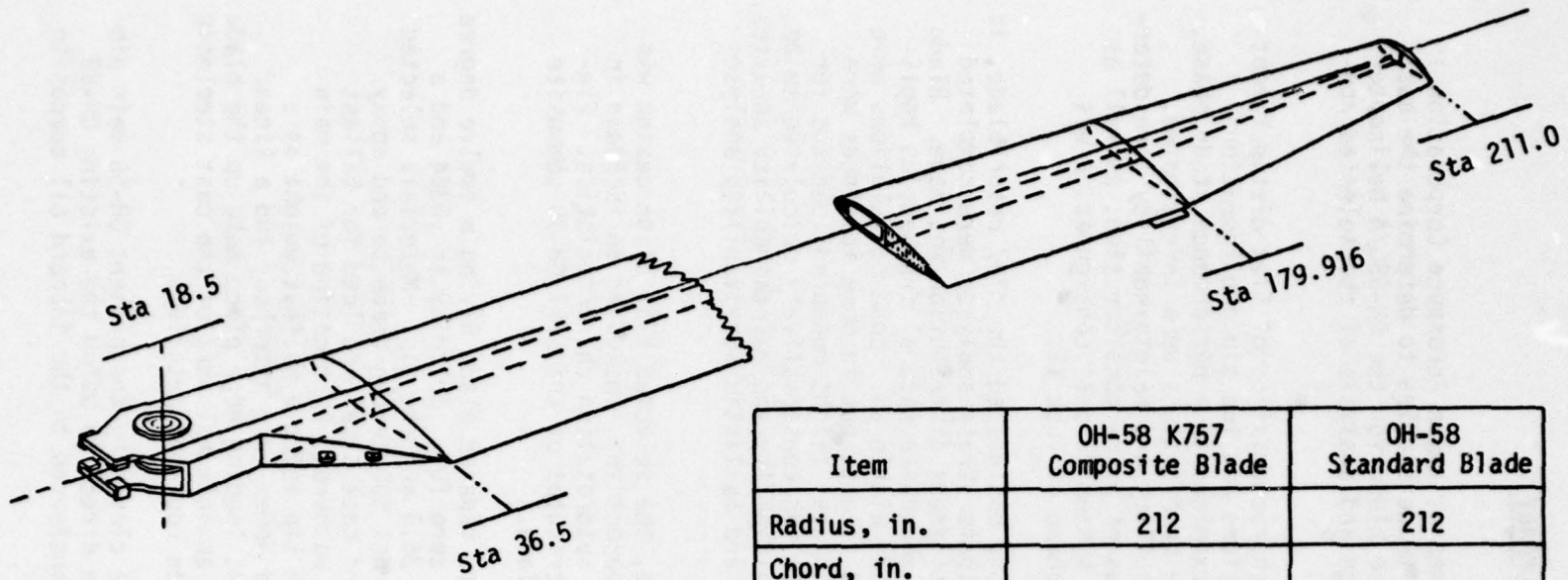

Item	OH-58 K757 Composite Blade	OH-58 Standard Blade
Radius, in.	212	212
Chord, in.		
Sta 36.5	15	13
Sta 179.916	12.5	13
Sta 211	6.25	13
Weight, lb	89.36	95
Mass moment in.-lb	10535.6	10117.5
Polar moment slug-ft^2	341	327
C.F., lb	37516.6	37673

Figure 1. Comparative information - OH-58 blade.

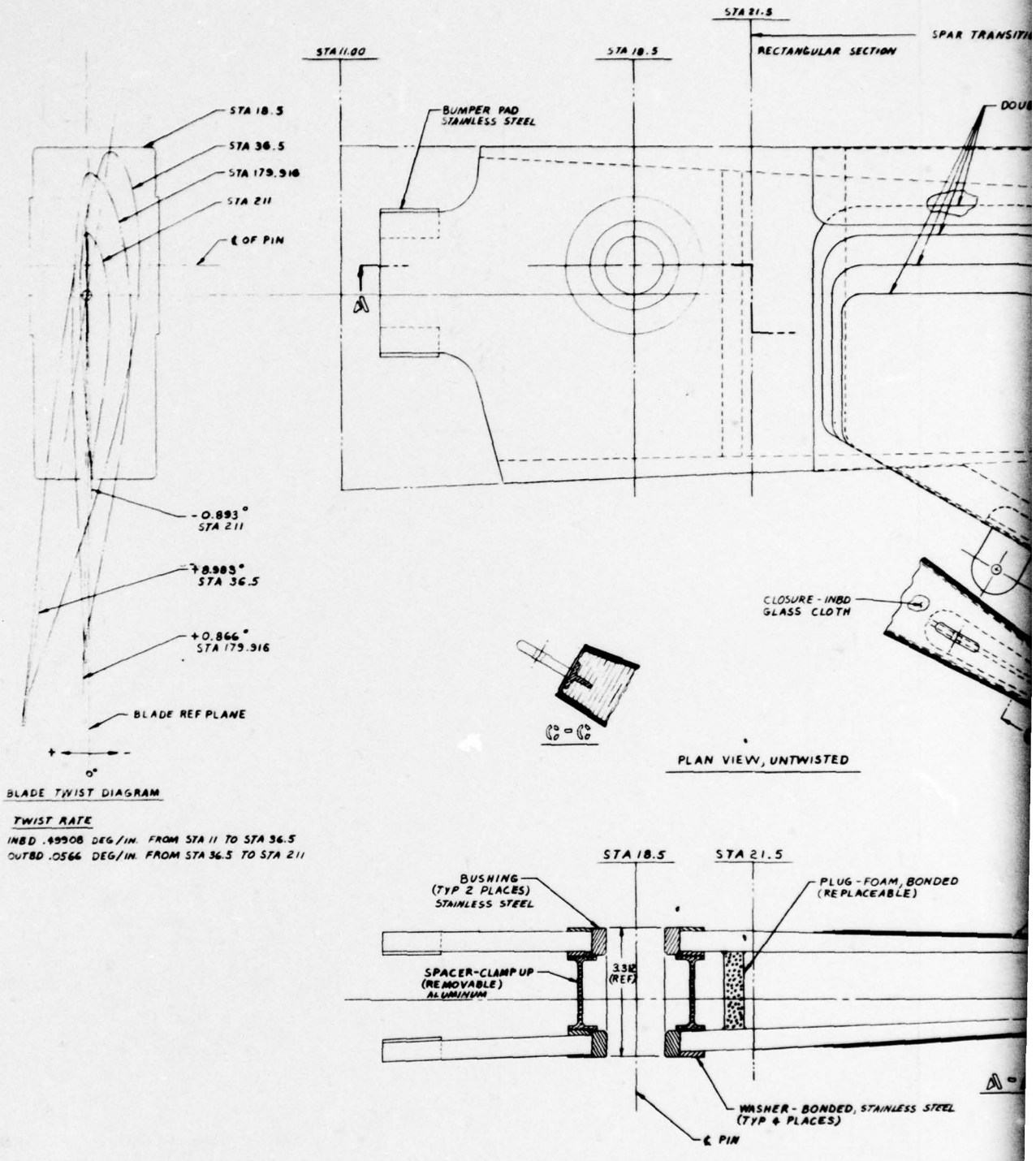

Figure 2. K757 root end details - OH-58 blade.

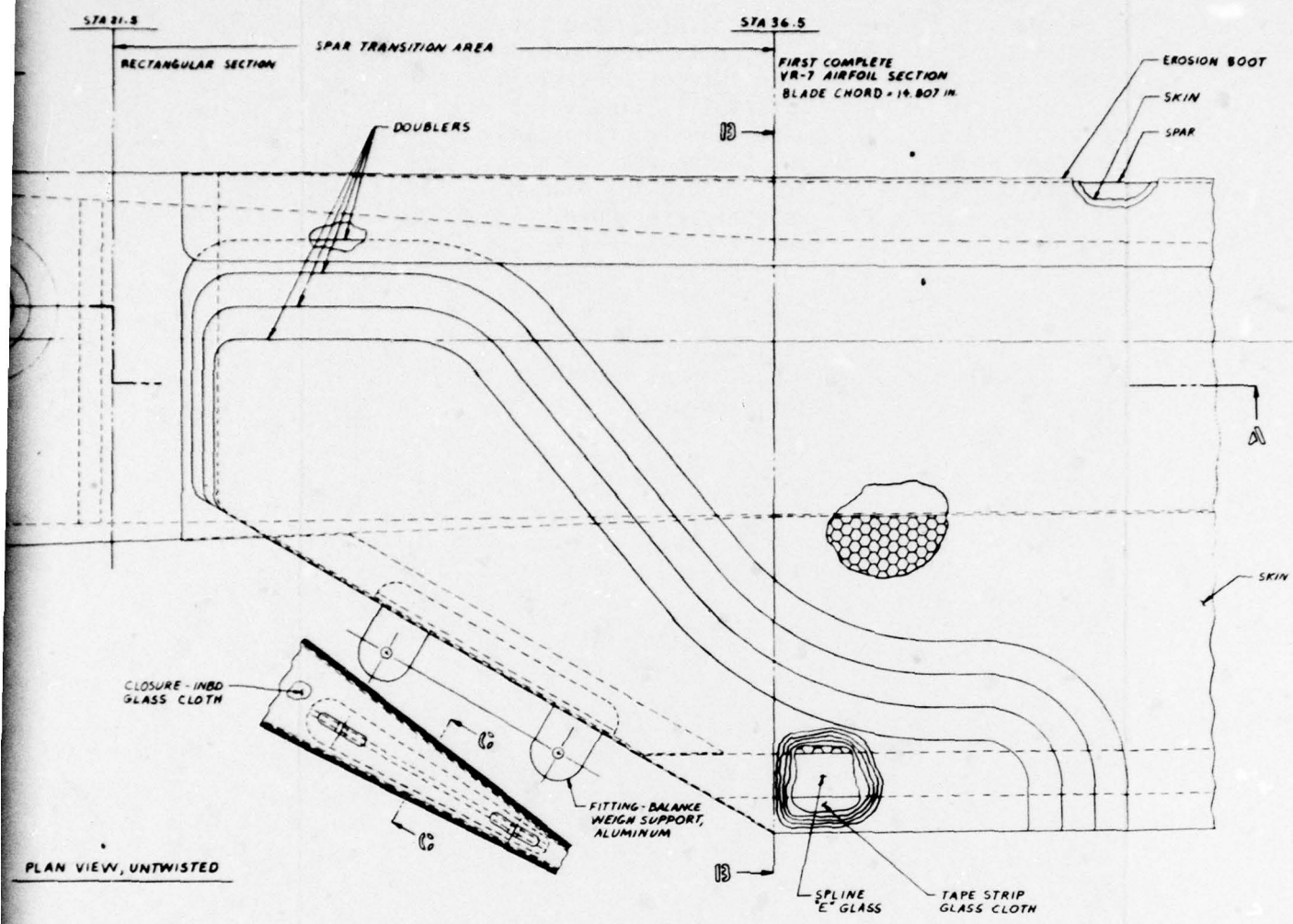

PLAN VIEW, UNTWISTED

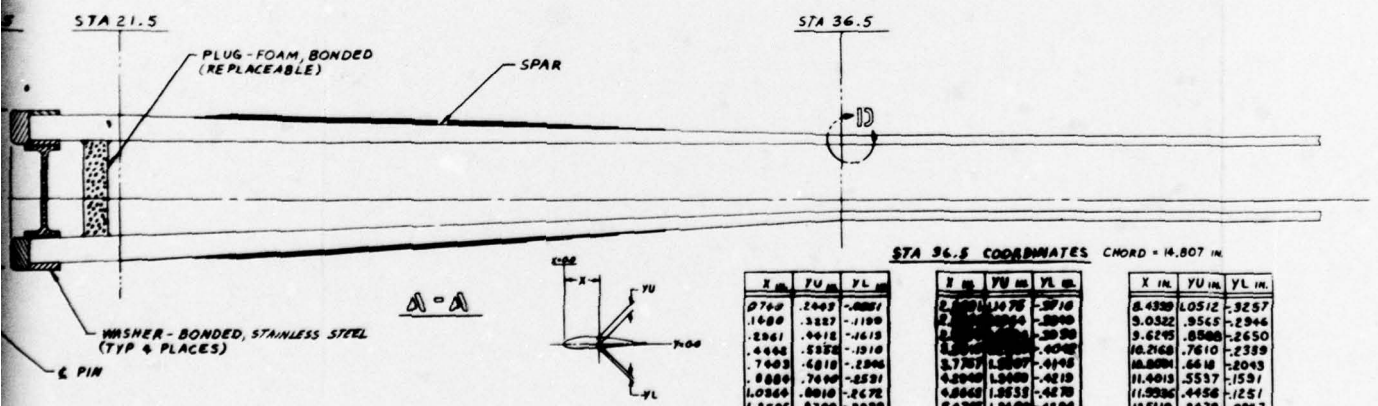

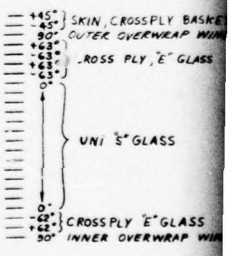

13 LAYUP SCHEDULE AT STA 36.

STA 36.5 COORDINATES CHORD = 14.807 IN.

X IN.	YU IN.	YL IN.
.0760	.2403	-.0881
.1688	.3227	-.1190
.2961	.4418	-.1615
.4466	.5378	-.1910
.7603	.6818	-.2346
.9884	.7699	-.2591
1.0364	.8010	-.2672
1.2685	.8780	-.2933
1.5103	.9550	-.3176
1.7768	1.0831	-.3383
2.0729	1.0912	-.3568

X IN.	YU IN.	YL IN.
[illegible]	[illegible]	-.3716
[illegible]	[illegible]	-.3848
[illegible]	[illegible]	-.3958
[illegible]	[illegible]	-.4042
3.7387	1.5807	-.4105
4.2048	1.5903	-.4119
4.6868	1.5833	-.4078
5.4788	1.5688	-.4284
6.0788	1.5188	-.4819
6.6838	1.2674	-.5071
7.8677	1.1556	-.5553

X IN.	YU IN.	YL IN.
8.4339	1.0512	-.5257
9.0322	.9565	-.4946
9.6295	.8588	-.4650
10.2168	.7610	-.4389
10.8091	.6618	-.4043
11.4013	.5537	-.1591
11.9986	.4456	-.1251
12.5819	.3479	-.0947
13.0301	.2472	-.0629
13.4743	.1564	-.0347
13.8946	.0818	-.0088
14.2197	.0790	-.0000
14.3658	.1141	+.0401

58 blade.

COMPLETE
AIRFOIL SECTION
E CHORD = 14.807 IN.

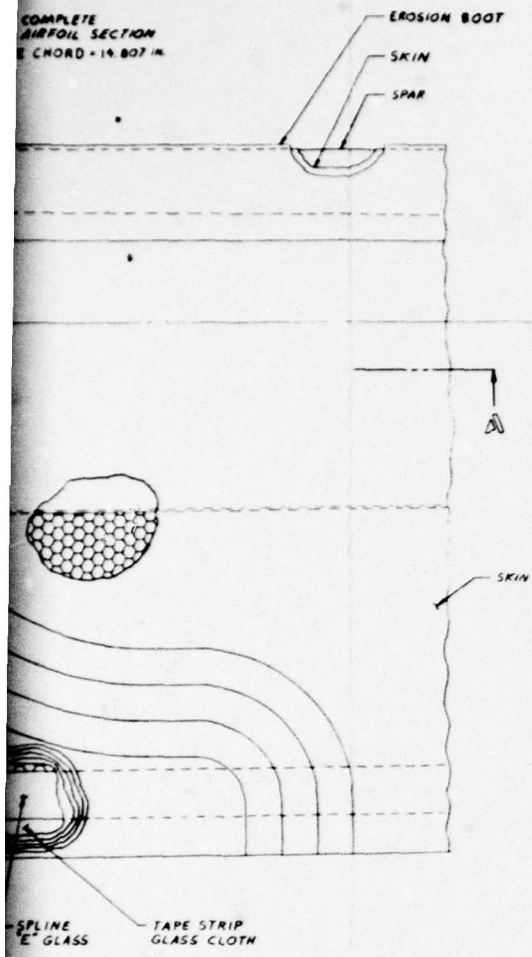

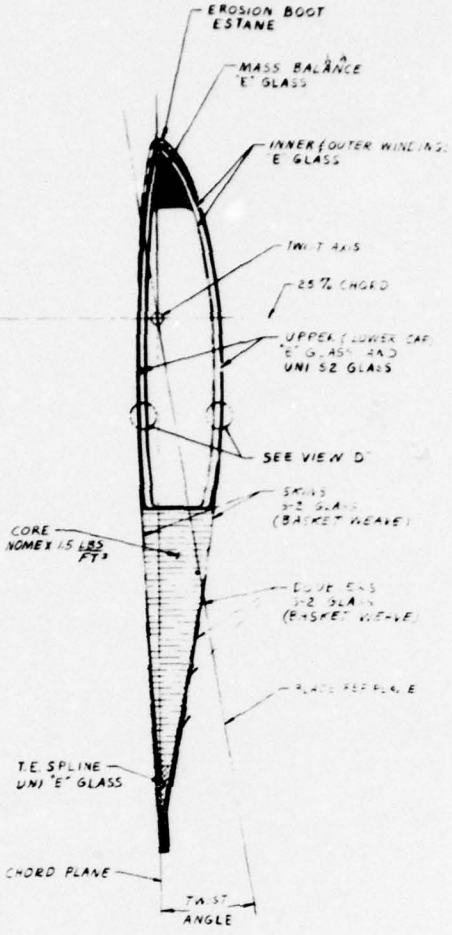

D - D

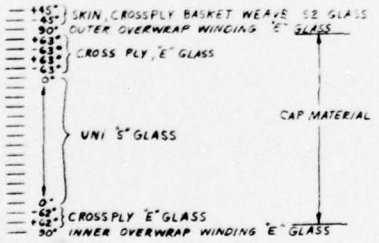

D LAYUP SCHEDULE AT STA 36.5

STA 36.8 COORDINATES CHORD = 14.807 IN.

X IN.	YU IN.	YL IN.
8.4339	L0512	-.3257
9.0322	.9565	-.2944
9.6245	.8588	-.2650
10.2168	.7610	-.2339
10.8091	.6618	-.2043
11.4013	.5537	-.1591
11.9936	.4456	-.1251
12.5819	.3479	-.0947
13.0301	.2472	-.0623
13.4743	.1564	-.0347
13.8948	.0818	-.0088
14.2147	.0740	-.0000
14.3958	.1141	+.0401

reinforcement plates to be reacted at the oversize bushings and latch-bearing pads. The filament-wound spar consists of optimized combinations of fiber angles to reproduce desired stiffness and stress conditions. At the reinforcement plates, cross-ply graphite material is finely interspersed to impart the required shear, bearing and tensile properties. The trailing edge spline transfers shear and bending to the spar bearing plate by means of a series of interconnecting doublers. Chordwise balance weights, compatible with the present balance weights, are shown. The spar twist is reversed inboard of station 36.5 (17.2% blade radius) to develop a maximum beamwise cross section for structural purposes. The reverse twist is facilitated by high spar taper and a separate inboard mandrel span-segment.

Figure 3 shows the details of the outer region and tip of the K757 blade. A cast-to-shape tip inertia weight serves as the mandrel for the tip winding. This inertia weight transfers centrifugal loads to the fiberglass spar through a molded rubber blanket. Blade tuning is facilitated by the lead tuning mass. The tip cap cavity is integral with the tip ballast weight and allows the incorporation of a variable lead weight package. The afterbody tip cap is a shaped compression molded closure. The complete blade assembly is designed to be co-cured to insure high quality, lowest cost and maximum structural efficiency.

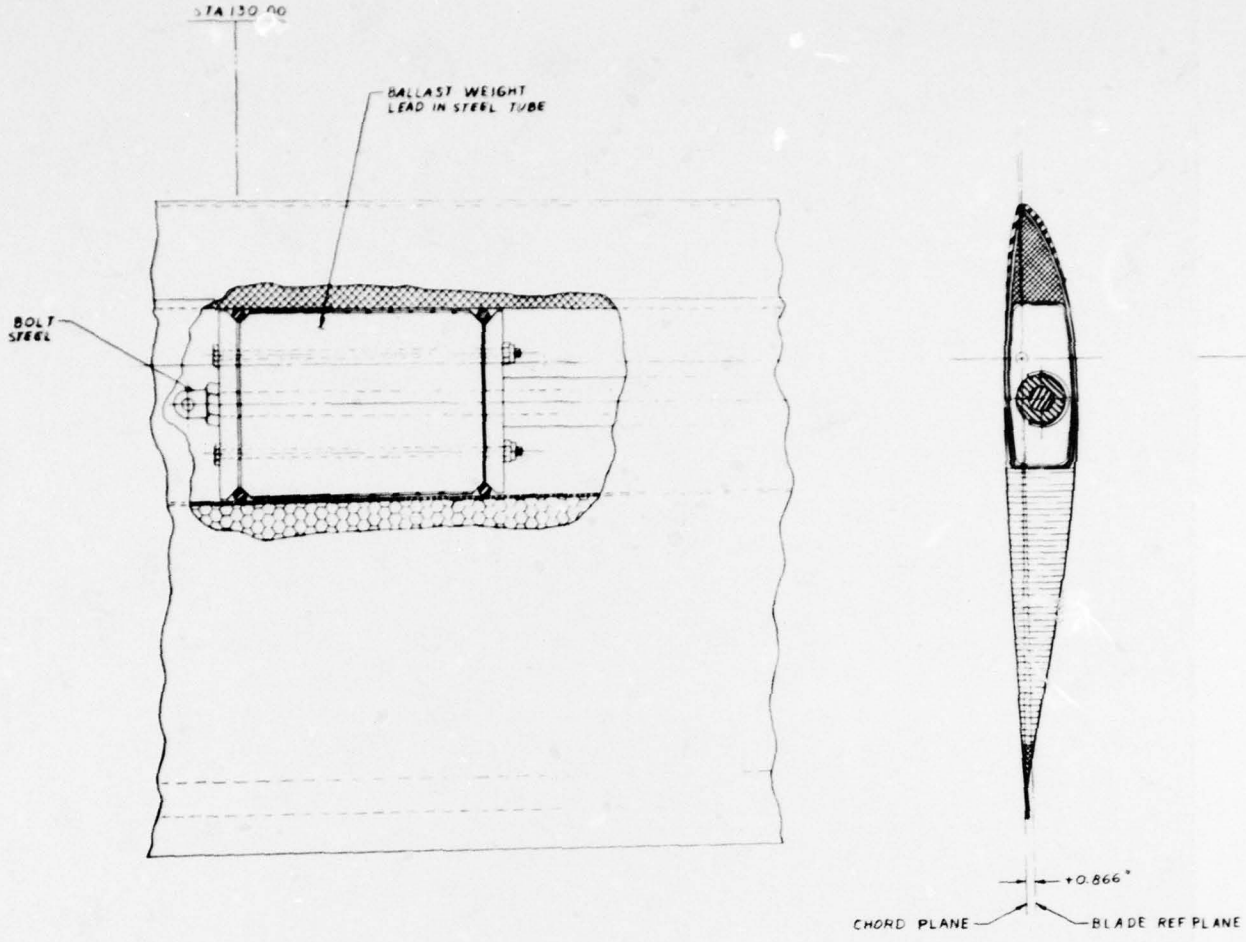

X IN.	YU IN.	YL IN.
.0625	.2062	-.0718
.1250	.2725	-.1012
.2500	.3725	-.1362
.3750	.4518	-.1612
.5000	.5187	-.1806
.6250	.5756	-.1981
.7500	.6281	-.2137
.8750	.6762	-.2256
1.0625	.7412	-.2481
1.2750	.8062	-.2681
1.5000	.8637	-.2856
1.7500	.9212	-.3012
2.0000	.9687	-.3137
2.2500	1.0100	-.3250
2.5000	1.0725	-.3325
2.8125	1.0837	-.3412
3.1875	1.1150	-.3500
3.6250	1.1362	-.3562

X IN.	YU IN.	YL IN.
4.1250	1.1425	-.3612
4.6250	1.1312	-.3625
5.1250	1.1087	-.3562
5.6250	1.0700	-.3437
6.6250	.9587	-.3000
7.1250	.8875	-.2750
7.6250	.8075	-.2487
8.1250	.7250	-.2237
8.6250	.6425	-.1975
9.1250	.5587	-.1725
9.6250	.4675	-.1343
10.1250	.3762	-.1056
10.5625	.2937	-.0800
11.0000	.2087	-.053
11.3750	.1312	-.02
11.6875	.0775	.0075
12.0000	.0425	.0000
12.6250	.0763	+.0338

STA 179.916 COORDINATES
CHORD = 12.500 IN.

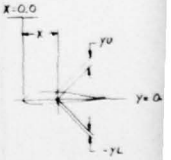

Figure 3. K757 tip details - OH-58 blade.

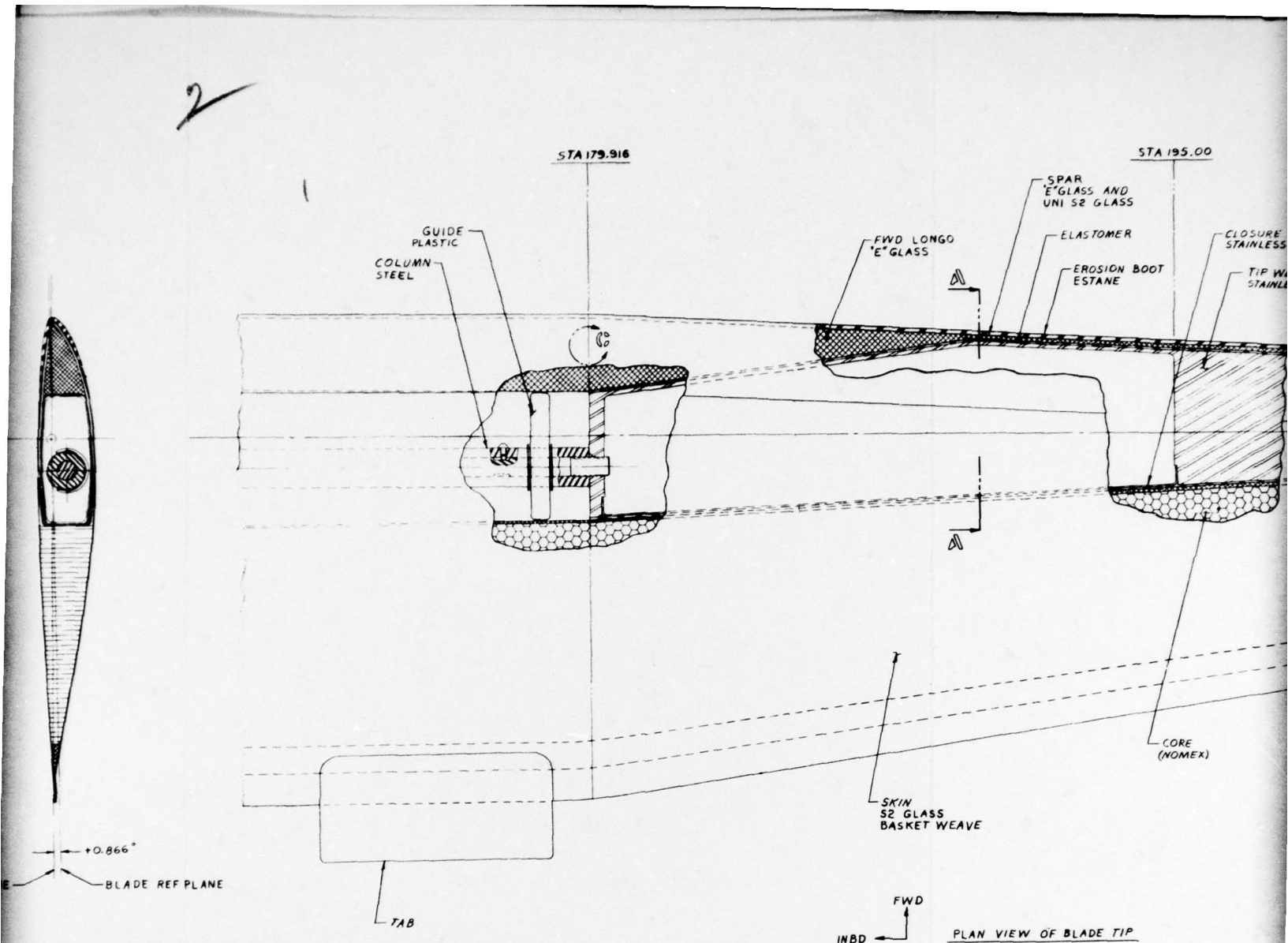

PLAN VIEW OF BLADE TIP

COVER STAINLESS STEEL

	YL IN.
2	-.0719
5	-.1012
5	-.1362
8	-.1612
7	-.1806
6	-.1981
1	-.2137
2	-.2256
1	-.2481
2	-.2681
7	-.2856
2	-.3012
7	-.3137
0	-.3250
5	-.3325
7	-.3412
0	-.3500
2	-.3562

X IN.	YU IN.	YL IN.
4.1250	1.1425	-.3612
4.6250	1.1312	-.3625
5.1250	1.1087	-.3562
5.6250	1.0700	-.3437
6.6250	.9587	-.3000
7.1250	.8875	-.2750
7.6250	.8075	-.2487
8.1250	.7250	-.2237
8.6250	.6425	-.1975
9.1250	.5587	-.1725
9.6250	.4675	-.1343
10.1250	.3762	-.1056
10.5625	.2937	-.0800
11.0000	.2087	-.0531
11.3750	.1312	-.0293
11.6875	.0775	-.0075
12.0000	.0625	-.0000
12.6250	.0743	+.0338

STA 179.916 COORDINATES
CHORD = 12.500 IN.

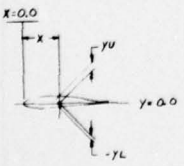

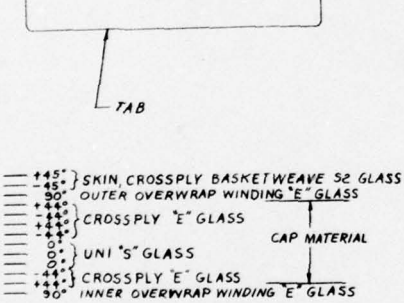

℄ LAYUP SCHEDULE AT STA 179.916

A-A

078

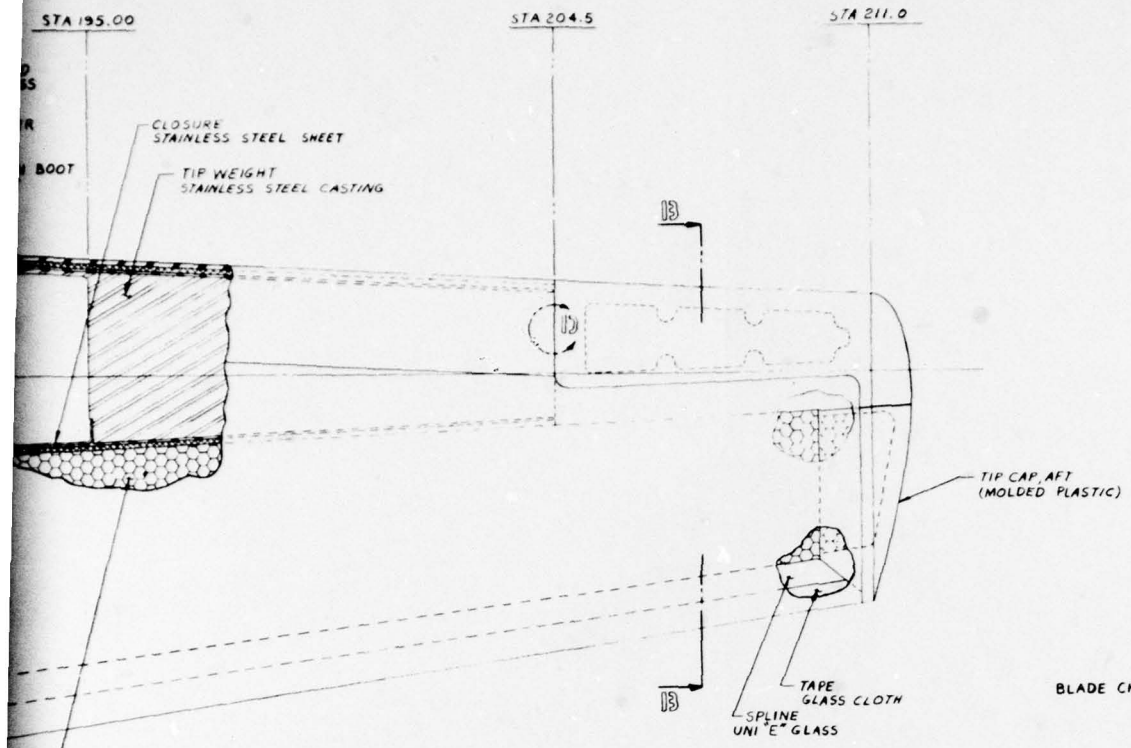

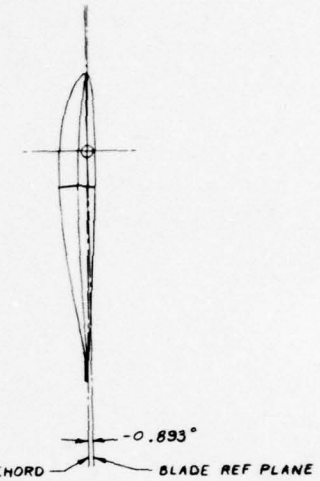

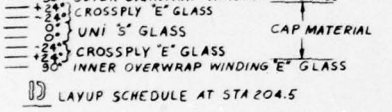

13 LAYUP SCHEDULE AT STA 204.5

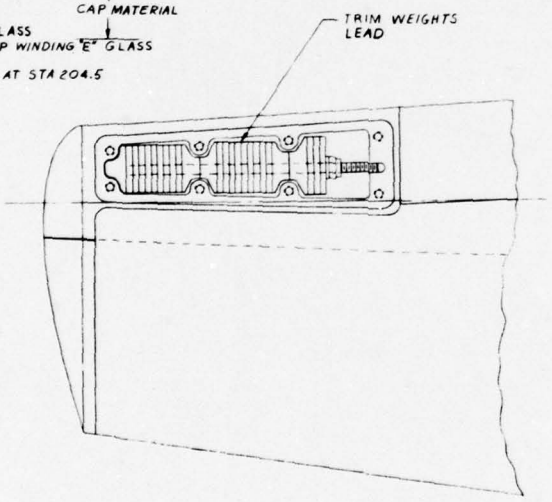

VIEW OF LOWER SIDE OF BLADE TIP

X IN.	YU IN.	YL IN.
.0312	.1031	-.0359
.0825	.1362	-.0506
.1250	.1862	-.0681
.1875	.2259	-.0806
.2500	.2593	-.0903
.3125	.2878	-.0990
.3750	.3140	-.1068
.4375	.3381	-.1128
.5312	.3706	-.1240
.6375	.4031	-.1340
.7500	.4318	-.1428
.8750	.4606	-.1506
1.0000	.4843	-.1568
1.1250	.5050	-.1625
1.2500	.5362	-.1662
1.4062	.5418	-.1706
1.5937	.5575	-.1750
1.8125	.5681	-.1781

X IN.	YU IN.	YL IN.
2.0625	.5712	-.1806
2.3125	.5656	-.1812
2.5625	.5543	-.1781
2.8125	.5350	-.1718
3.3125	.4793	-.1500
3.5625	.4437	-.1375
3.8125	.4037	-.1243
4.0625	.3625	-.1118
4.3125	.3212	-.0987
4.5625	.2793	-.0862
4.8125	.2337	-.0671
5.0625	.1881	-.0528
5.2812	.1468	-.0400
5.5000	.1043	-.0265
5.6875	.0656	-.0146
5.8437	.0387	-.0037
6.0000	.0312	-0.0000
6.3125	.0481	+0.0169

STA 211.00 COORDINATES
CHORD = 6.250 IN.

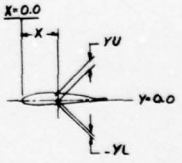

TIP

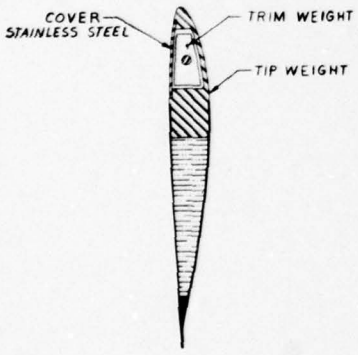

13 - 13

PREFACE

Composite materials and the associated fabrication techniques are resulting in a new generation of superior helicopter rotor blades. Kaman Aerospace Corporation, at the forefront of this technology, has produced the K747 composite blade for the AH-1 helicopter. This blade has demonstrated increased performance, superior flying qualities, substantially improved damage tolerance, long life, and increased reliability and maintainability. With this very substantial background experience, Kaman herein defines a similar state-of-the-art blade for the OH-58C/A helicopter. In this endeavor, significant contributions were made by the following Kaman personnel: Messrs. R. E. Collins, R. Jones, J. E. Miller, G. Haire, H. C. Freeman, M. White, H. E. Showalter, E. Janssen, M. Bowes, J. Fitzpatrick and P. F. Maloney.

We would also like to acknowledge the assistance of Mr. H. K. Reddick of the Applied Technology Laboratory in the performance of this program.

TABLE OF CONTENTS

TABLE OF CONTENTS (continued)

TABLE OF CONTENTS (continued)

LIST OF ILLUSTRATIONS

LIST OF ILLUSTRATIONS (continued)

LIST OF ILLUSTRATIONS (continued)

LIST OF ILLUSTRATIONS (continued)

LIST OF TABLES

LIST OF TABLES (continued)

TECHNICAL APPROACH

Composite materials are inherently well-suited to the requirements of helicopter blades for several reasons. Preferred orientation can be provided by a number of manufacturing processes which can, in most cases, use a wide range of fibers and resin systems. Blade geometry can be variable, approaching optimum aerodynamic shapes, with only minor constraints imposed by most manufacturing processes. Several different material choices are available to provide efficient structural/dynamic tailoring. The best of these materials have high fatigue strength, low crack propagation rates, and favorable strength/weight and stiffness/weight ratios. Ballistic damage is of less concern with helicopter blades made of composites. Experience has shown that post-impact lives can be substantially more than those of metallic configurations. These materials are extremely durable and have high repairability which leads to low life-cycle costs.

The Kaman K747 composite blade for the AH-1 helicopter represents a breakthrough in low cost fabrication technology. This is the first production composite blade in the Army system. Knowledge gained in this program has been put to direct use in the OH-58 composite blade program. The OH-58 blade is designed as a state-of-the-art blade. In this context, it is the result of practical confrontations with present limitations in each of the required disciplines. Kaman has used validated computer design tools and techniques to examine an array of concepts and evolve one objective configuration. This has been fortified with practical experience gained in our many composite programs.

The OH-58 composite blade program was performed in two distinct phases. Task I was an objective trade study in which the primary disciplines were called on to evaluate numerous configurations in order to conclude with one best blade design. The major analysis activity in this stage is in aerodynamics/performance and in structures/dynamics. In Task II, considerable detailed structural and dynamics analysis was performed for final configuration detail. The life-cycle cost analysis was of particular interest, since this is the area of major concern. The following pages report all the activities of this program. The inclusion of voluminous computer printout data has been resisted; however, this information is on file at Kaman if a further review is desired.

Trade Study Methodology

Trade analyses were performed evaluating merit based on the following prime attributes, listed in order of assigned importance:

- Life-cycle cost
- Performance
- Reliability and maintainability

- Radar reflectivity
- Ballistic survivability

Each of these items is individually assessed and a grade is assigned or calculated. To reflect this order of importance, a graduated maximum score for each was assigned as shown below. Since operational costs were considered under the Reliability and Maintainability section, only acquisition costs were considered under the life-cycle cost evaluation at this time.

Item	Maximum Score
Cost	10
Performance	9
Reliability and maintainability	8
Radar reflectivity	7
Ballistic survivability	6
	40

To determine a grade for cost, the DTUPC objective of $3400 per blade was used as a basis:

$$\frac{3400}{\text{Configuration Cost}} \times 10 = \text{Grade} \quad (10 \text{ maximum})$$

To determine a grade for performance, the minimum objective hover performance increase of 6% was used as a basis:

$$\frac{6}{\% \text{ Performance Increase}} \times 9 = \text{Grade} \quad (9 \text{ maximum})$$

A reliability and maintainability grade was obtained based on a combined ranking of sub-tier items multiplied by 8.

For radar reflectivity, it was considered that any of the configurations envisioned would have radar signatures similar to those observed on the K747 AH-1 composite blade, and that treatments could nearly equalize these. Therefore, there is no anticipated distinction among any of the composite configurations. An arbitrary grade of 7 was assigned to all, although any lower number could have been selected without affecting the overall results.

The ballistic survivability grade was determined using generally accepted techniques to calculate a relative P_K for each of the final candidates.

This technique analyzes the blade as a series of span and chordwise sections, each of which has an exclusive P_K determined for it. From this, an overall P_K can be calculated.

The results were proportioned to the best design and multiplied by six:

$$\frac{(100 - P_K)\ (\text{Best})}{100 - P_K} \times 6 = \text{Grade}$$

All grades were thereafter summed and compared to each other to determine the best of the configurations.

The trade study commenced with configuration analyses to determine the aerodynamic geometry requirements and the structural/fabrication constraints. Analysis was performed initially to define desired planform, airfoil geometry and twist geometry. A structural/fabrication survey was then used to determine the fabrication scheme(s) and resultant structural properties of the configurations meeting the aerodynamic requirements. This led to the segregation of the blade structure into three span-elements; namely, root end, clean section and tip. This is illustrated in the configuration equation, Figure 4. The numbers assigned to each element are used to define the configuration; thus, an AH-1 type root end, ① , with a filament-wound spar/Nomex afterbody and spline, ① , and a cast steel plus molded tip, ② , is designated configuration 112.

The root end elements appear in Figure 5, blade clean section variations in Figures 6 and 7, and the two tip variations in Figure 8. Two detailed versions of pultruded afterbodies appear in Figures 9 and 10.

Although 20 combinations are possible here, it is clear that clean section and tip configuration ideas are not mutually independent. For example, the molded tip configuration was a spin-off requirement of the pultruded afterbody and, because of the increased complexity, weight and cost, is not considered a logical part of clean section #1 having a Nomex afterbody. Also, the Nomex afterbody tip #1 does not allow through-bagging of the pultruded afterbody #2 during the cure cycle to support and pressurize the surface, and, therefore, is not a logical mate. Additionally, the preliminary stress analyses indicated that bond line shear stresses were much too high in the root end race-track #4, and fiber tension stresses too high for the race-track-plus-drag-brace #5. These were eliminated as structurally unsound. The screening progress is illustrated in Figure 11. Six configurations remain for consideration: 111, 211, 311, 122, 222 and 322.

Performance Trade-Off Analysis

Background. One of the most important considerations affecting the design of either a new helicopter or the modification of an existing one is performance. For this investigation, the criteria defining the impact of the new rotor blade design on helicopter performance capabilities specify that a 6% reduction in total power required for hover under a given set of conditions is desired, but that it must be achieved without compromise of forward flight performance.

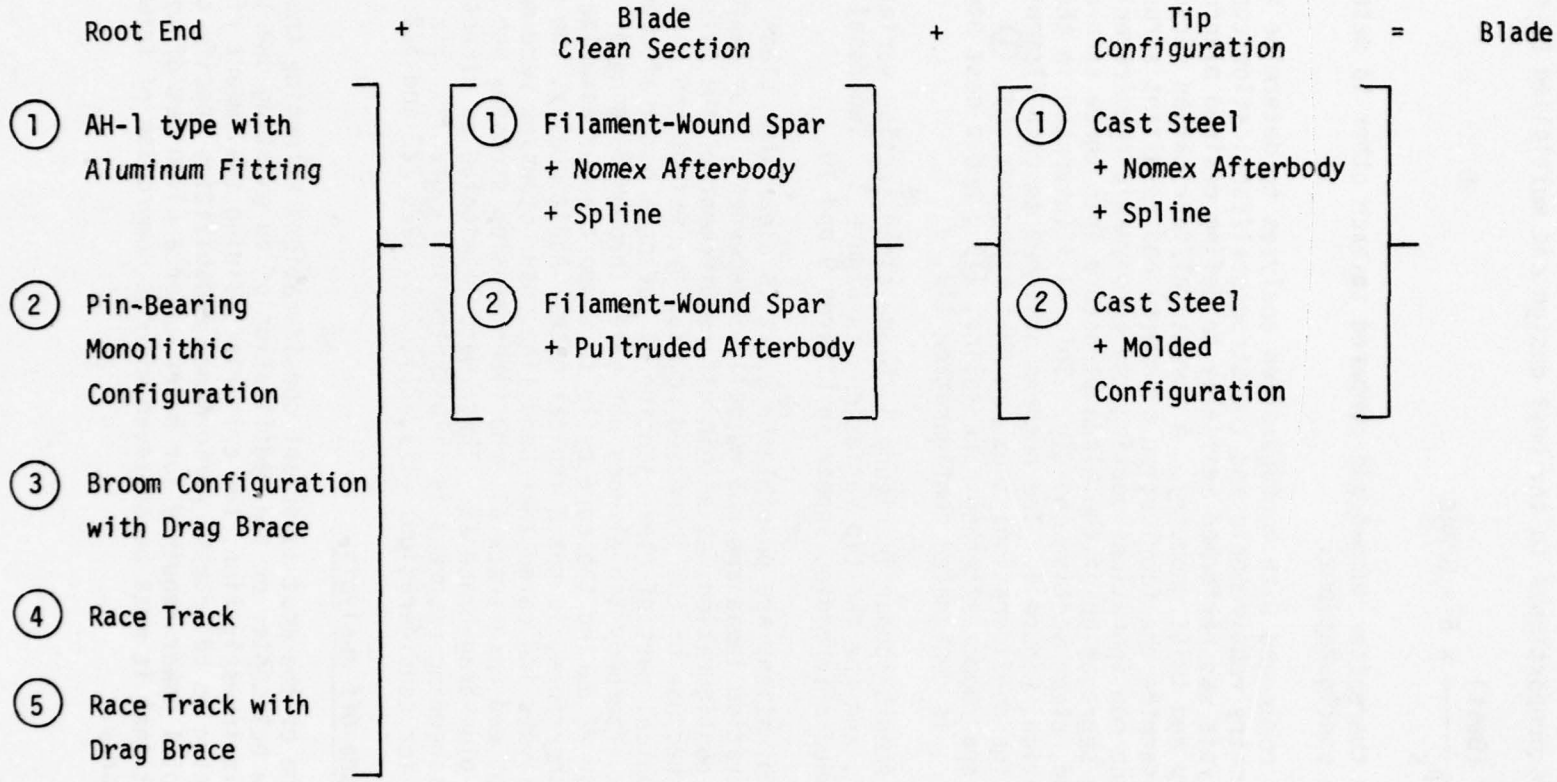

Figure 4. Configuration equation.

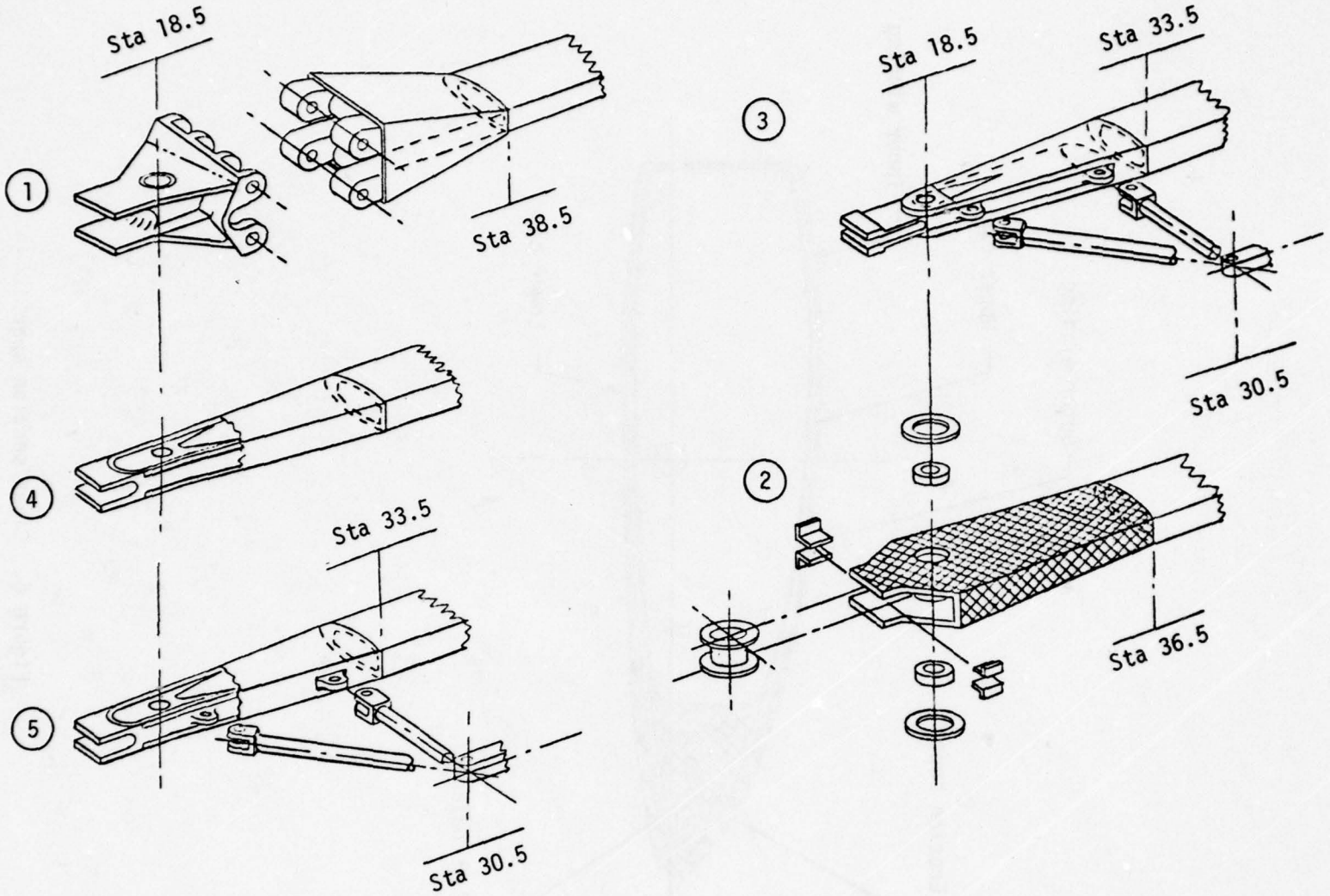

Figure 5. Root end configuration.

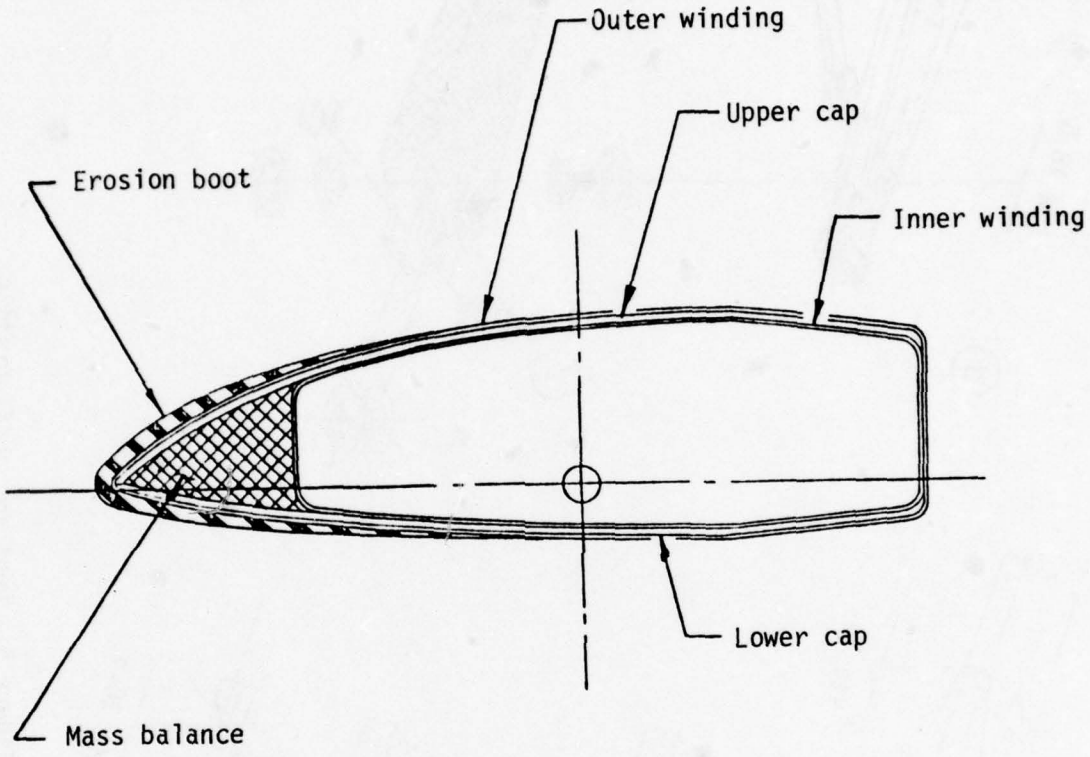

Figure 6. Clean section spar.

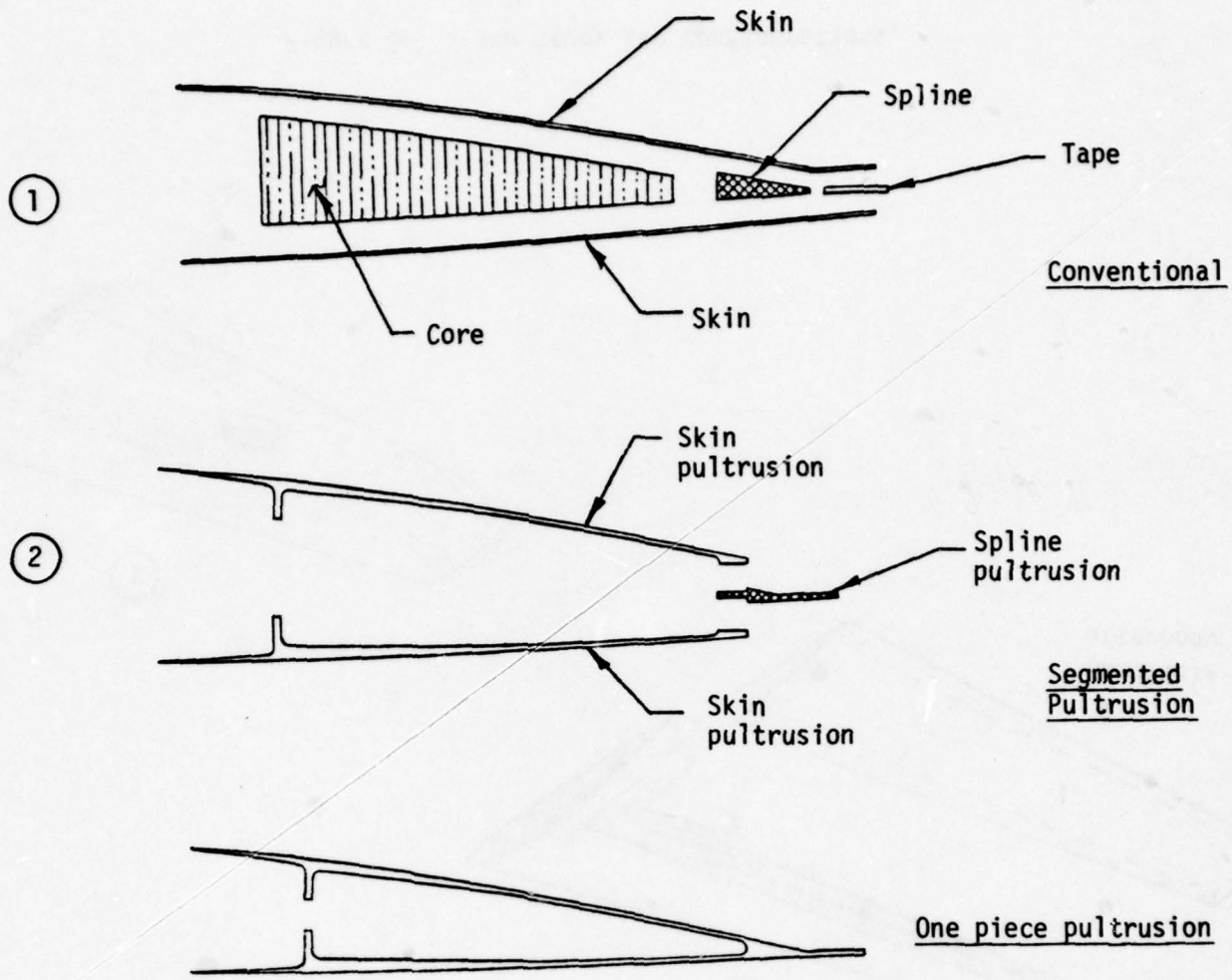

Figure 7. Clean section afterbody concepts.

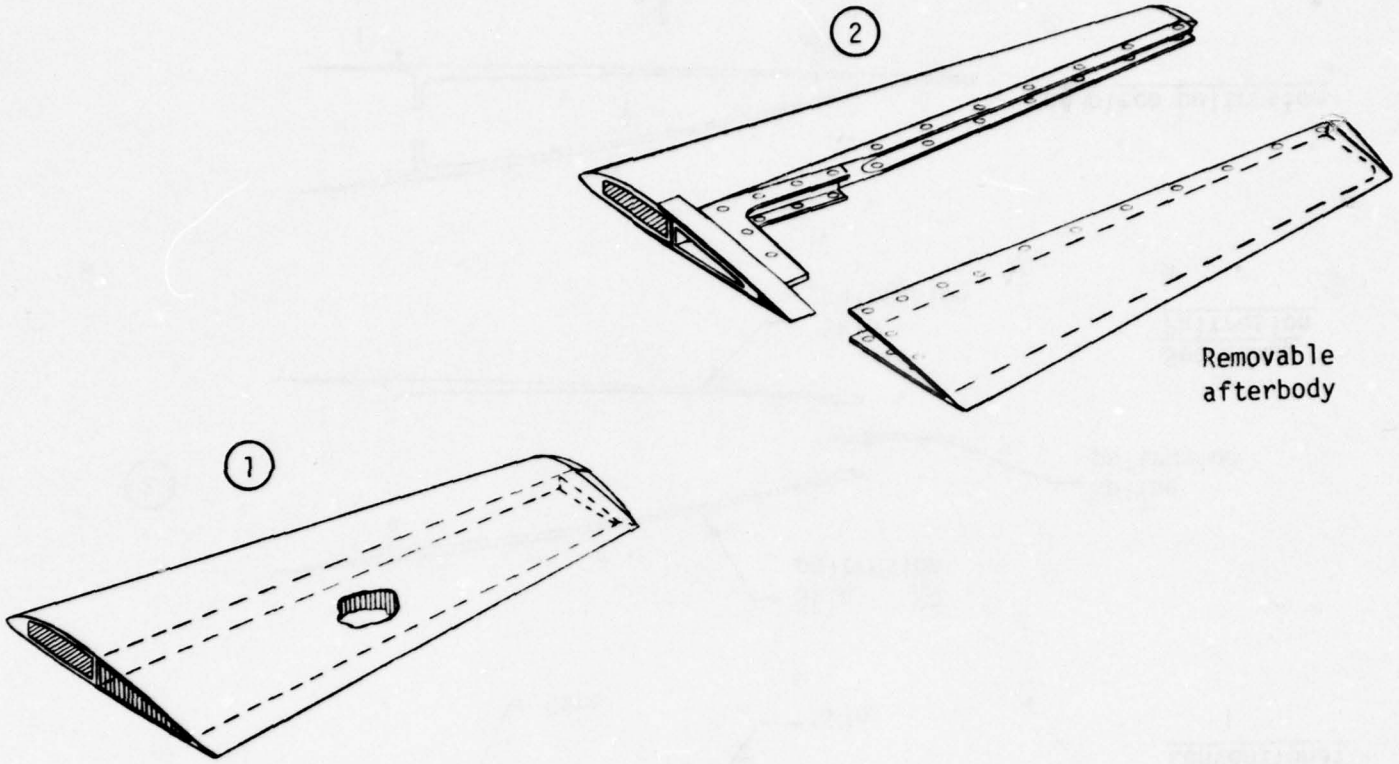

Figure 8. Trade study tip configurations.

X IN.	CONTOUR UPPER Y IN.	CONTOUR LOWER Y IN.
0.00	+1.040	-.382
.386	+1.025	-.377
1.053	+.984	-.362
1.721	+.918	-.335
2.388	+.845	-.305
3.056	+.757	-.271
3.723	+.663	-.237
4.390	+.568	-.203
5.058	+.470	-.165
5.725	+.368	-.127
6.393	+.264	-.088
6.926	+.177	-.057
7.327	+.112	-.032
7.661	+.074	-.014
7.861	+.053	-.007
8.528	+.077	+.017

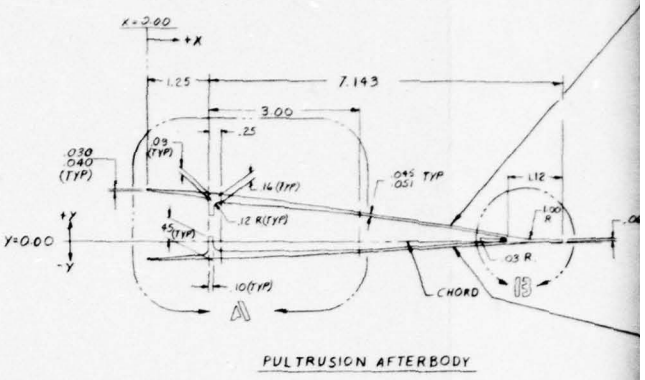

PULTRUSION AFTERBODY

MATER

RES

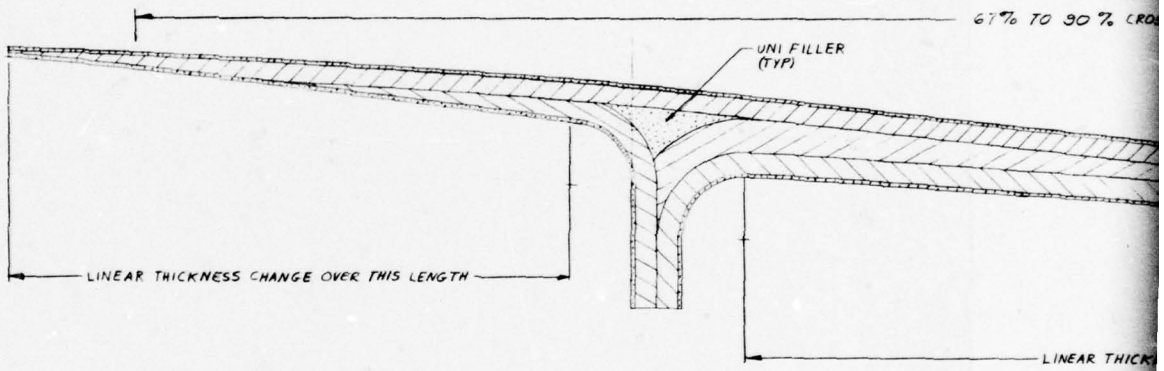

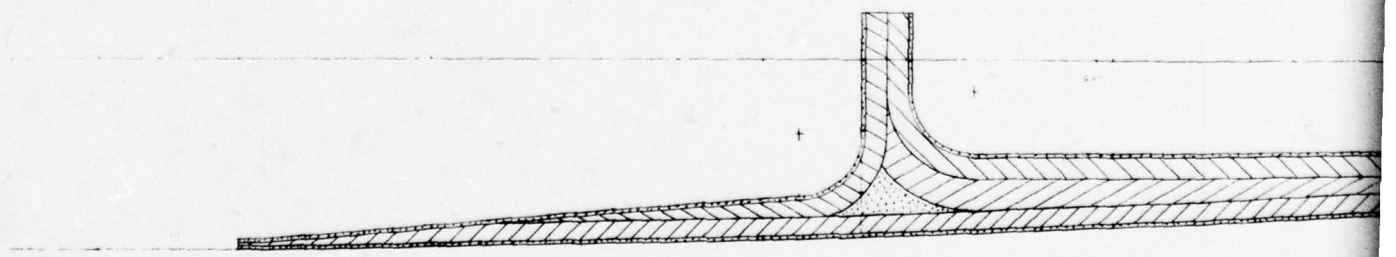

SCALE 10:1

Figure 9. One-piece pultruded afterbody.

2

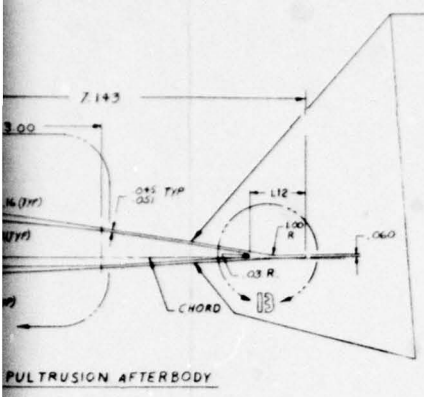

THE UPPER AND LOWER LEGS OF THE PULTRUSION MAY BE FORMED FLAT AND SEMI CURED (GREEN), PROVIDED THEIR LENGTHS ARE SUFFICIENT TO BE FORMED INTO THE CONTOURS SHOWN.

PULTRUSION AFTERBODY

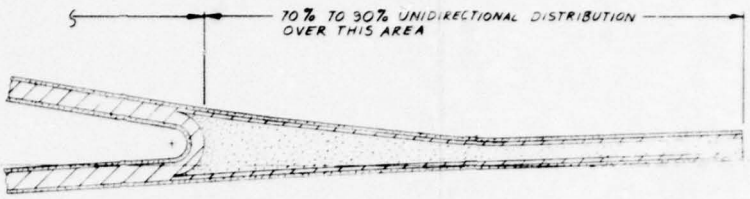

13

SCALE 10:1

MATERIALS

SYMBOL DENOTES UNIDIRECTIONAL KEVLAR 29

SYMBOL DENOTES CROSS PLY KEVLAR 29

RESIN SYSTEM : EPOXY

67 % TO 90 % CROSSPLY DISTRIBUTION OVER THIS AREA

(SEE -E- F)

FILLER

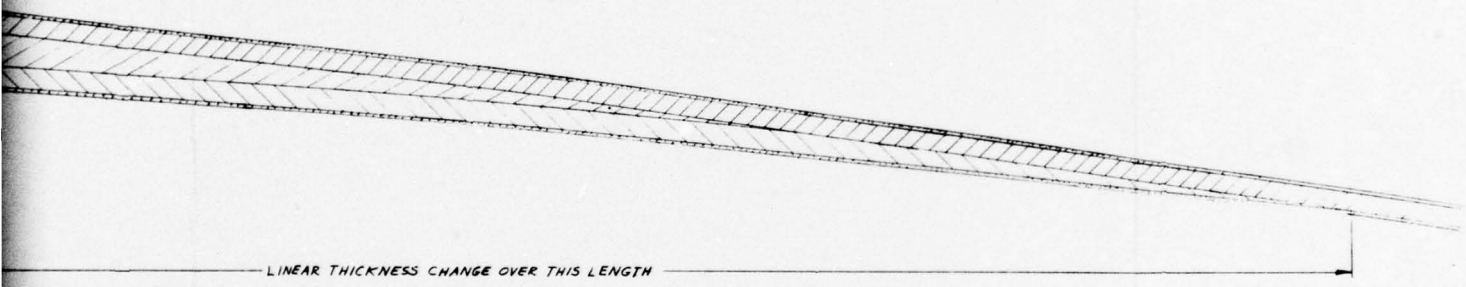

LINEAR THICKNESS CHANGE OVER THIS LENGTH

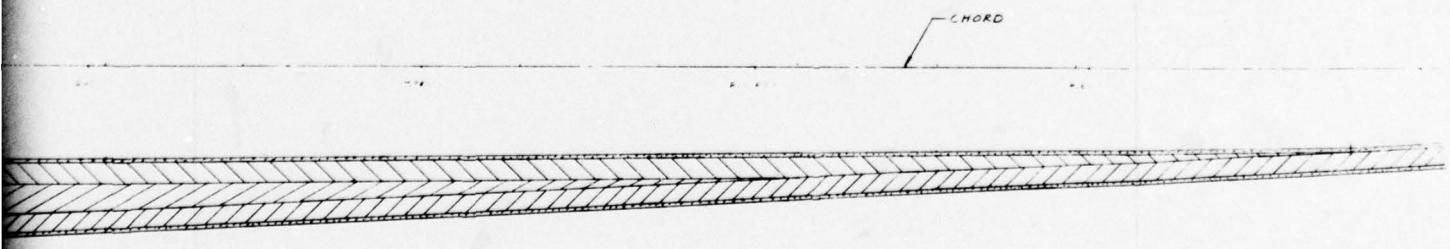

A

SCALE 10:1

X (IN)	CONTOUR UPPER Y (IN)	CONTOUR LOWER Y (IN)
.000	+1.090	-.392
.396	+1.035	-.377
1.028	+.984	-.366
1.721	+.918	-.355
2.398	+.845	-.308
3.052	+.757	-.271
3.705	+.665	-.237
4.359	+.568	-.203
5.013	+.470	-.165
5.666	+.368	-.131
6.333	+.264	-.098
6.926	+.177	-.067
7.5[illegible]	+.[illegible]	-.036
7.6[illegible]	+.[illegible]	-.014
[illegible]	+.[illegible]	-.007
[illegible]	+.[illegible]	+.017

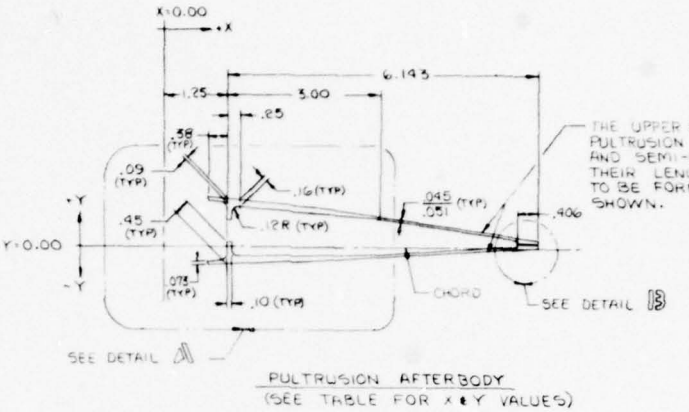

PULTRUSION AFTERBODY
(SEE TABLE FOR X & Y VALUES)

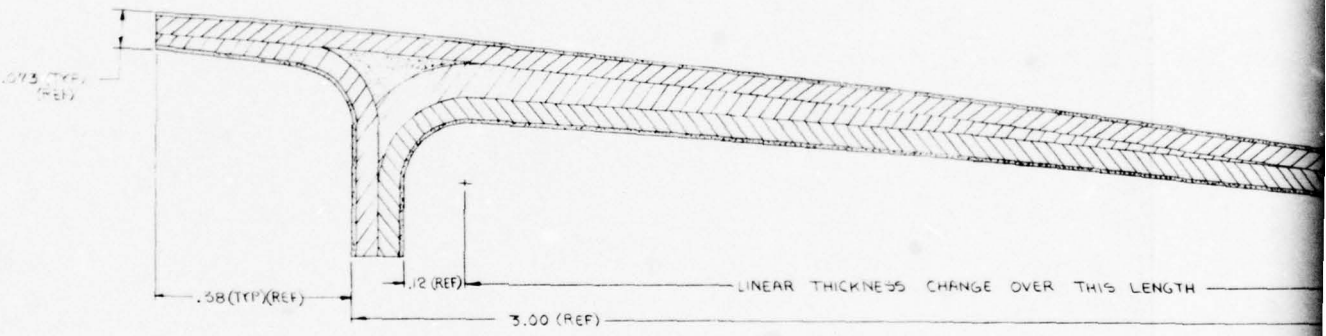

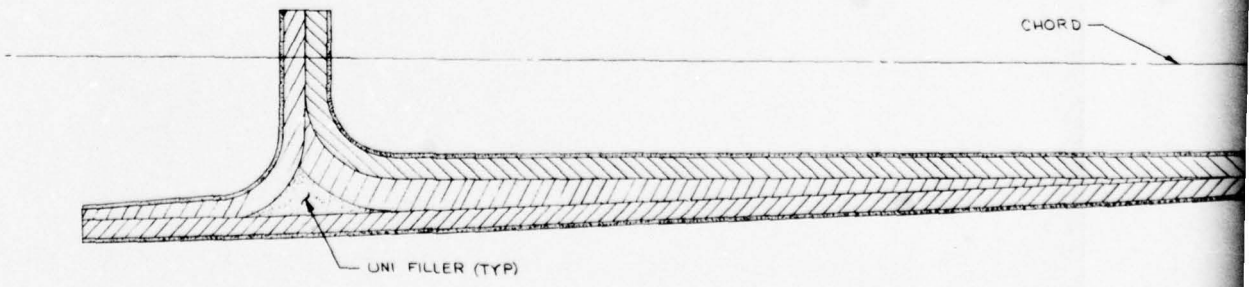

DETAIL A
SCALE 10:1

Figure 10. Two-piece pultruded afterbody.

2

1

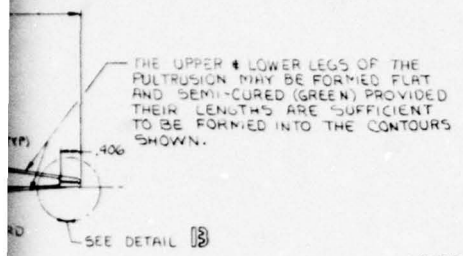

ODY
Y VALUES)

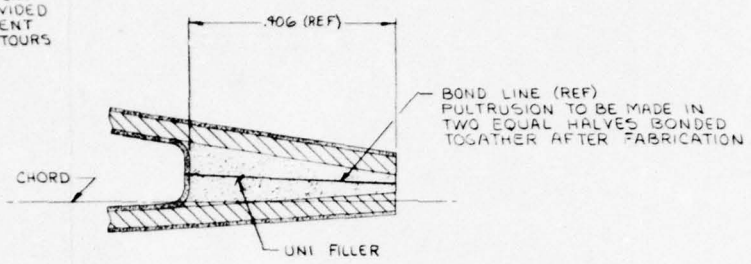

DETAIL B
SCALE 10:1

SYMBOL DENOTES UNIDIRECTIONAL KEVLAR 29

SYMBOL DENOTES CROSS PLY KEVLAR 29

PULTRUSION TO BE FABRICATED USING AN EPOXY RESIN SYSTEM

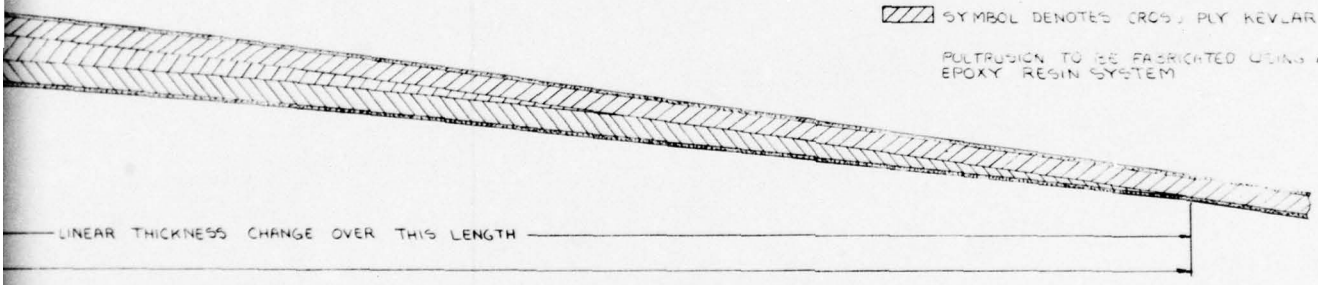

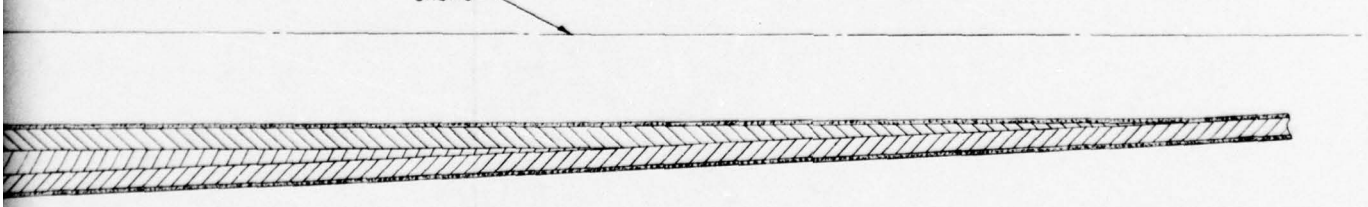

terbody.

DETAIL A
SCALE 10:1

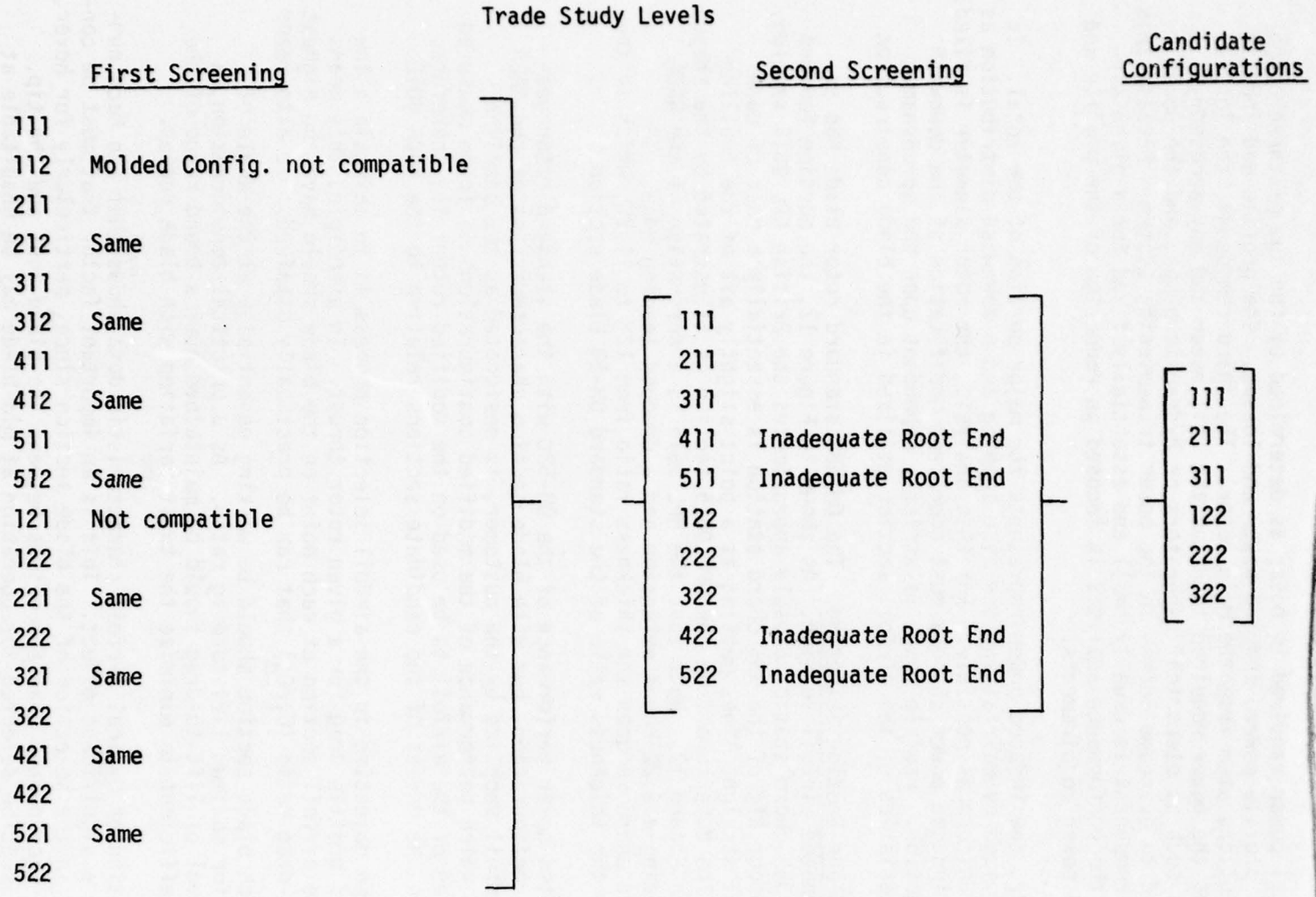

Figure 11. Trade screening levels.

The total power required to hover is determined by the sum of three components: profile power, induced power and losses. The profile and induced contributions stem from the main rotor. The third component, the losses, includes the power required to drive the tail rotor and any accessory devices such as electrical generators or hydraulic pumps, and the power required to overcome losses in the power transmission system. Because this latter component is usually small and essentially fixed for a given aircraft, the performance analysis is focused on reduction of the profile and induced power requirements.

In hover, the induced power represents the major portion of the total. It is minimized by maintaining low disc loading and a downwash distribution as nearly uniform as possible. For this analysis, the rotor diameter is fixed, so any induced power changes must come from modification of the downwash distribution. Profile power is strictly dependent upon the aerodynamic characteristics of the airfoil section utilized in the blade construction.

Rotor Blade Section Selection. The OH-58C standard rotor blade has an undesignated airfoil section. As shown in Figure 12, the portion forward of the 35% chord station closely approximates the British NPL 9615 section. The contour aft of the 35% chord station is essentially a pair of non-parallel straight lines meeting at a point slightly aft of the trailing edge. The departure from the NPL 9615 section is illustrated by the shaded areas in Figure 12. Note that the NPL 9615 is a derivative of the NACA 0012 having a 6.2% chord extension and a drooped leading edge. The extended chord reduces the thickness ratio from 12% to 11.3%, which is the same as the thickness ratio of the standard OH-58 blade section.

Calculated hover performance of the OH-58C with the standard rotor geometric configuration, but with blade section characteristics of the NACA 0012 airfoil supplied by the customer, is designated as the baseline against which performance of the modified configurations is to be measured. Selection of the airfoil to be used on the modified rotors is, therefore, based on the merits of the candidate sections relative to the NACA 0012.

The prime objective in the airfoil selection process is to maintain a low level of profile drag for a given rotor thrust. In principle, this means that the airfoil section at each point on the blade should have the highest lift-to-drag ratio (C_l/C_d) that can be practically attained. It also means that each blade section should be working essentially at the angle of attack for maximum lift-to-drag ratio. As a practical consideration, a high level of lift-to-drag should be maintained over a broad range of the lift coefficient to minimize the twist variation with blade radius.

Examination of typical airfoil characteristic data shows that the Mach number has a significant effect. This is an important factor that must be considered in the selection of the blade section since, particularly for hover, a large Mach number gradient exists between the blade root and the tip. Thus, a section selected for operation at mid-blade may be unsuitable at the tip.

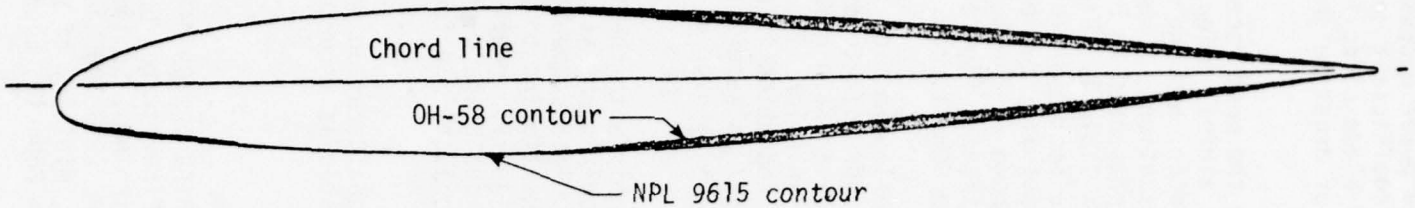

Shaded areas denote deviation of OH-58C blade section from the NPL 9615 contour

Figure 12. OH-58 C/A main rotor blade contour compared to British NPL 9615 section.

The maximum section lift coefficient attained on an airfoil section does not bear directly on the rotor profile power because the blade area can be adjusted to maintain an average lift coefficient well below stall. It should be considered, however, in the blade airfoil selection because it affects the flight envelope in terms of gross weight, normal load factor, and speed.

Review of the literature published on the most recently developed airfoil sections, along with the work done on airfoil selection for the improved main rotor blade for the AH-1Q helicopter, has indicated several airfoils that may be suited to the OH-58C application. A summary of the aerodynamic characteristics of the candidates is presented in Figures 13 and 14 with appropriate References 1 and 2, and in Table 1. Figure 13 shows the maximum lift-to-drag ratio for each of the sections plotted versus blade radius. The variation in the curves actually reflects the variation of the lift-to-drag ratio with Mach number shown in the lower scale for a temperature of 95°F and a tip speed of 655 ft/sec. Figure 14 shows the variation of the maximum lift coefficient in the same format.

Based on these data, the optimum airfoil selection appears to be the VR-7. Although the FX-69-H-098 shows a superior lift-to-drag ratio at low Mach number, it loses this advantage rapidly as Mach number increases. Compared to the VR-7, the FX-69-H-098 shows an inferior lift-to-drag ratio over the outboard 15% of blade span where drag reduction is particularly important. It should be observed also that the VR-7 is superior to the FX-69-H-098 with regard to the maximum lift coefficient over at least the outboard 50% of the blade radius.

The 23010-1.58 section compares favorably with the VR-7 in terms of both lift-to-drag ratio and maximum lift coefficient at low Mach number, but it loses its advantage over the outboard blade segment. Using the 23010-1.58 on the inboard blade segments and transitioning to a VR-7 on outboard blade segments would improve performance slightly. However, the additional complications attendant to changing from one blade section to another at some point on the blade do not appear to be justified for the small performance benefits that might accrue.

The VR-8 section is eliminated from consideration for OH-58C application primarily because the low thickness ratio is structurally unsuitable at

1. Dadone, L. U., U. S. ARMY HELICOPTER DESIGN DATCOM, VOLUME I - AIRFOILS, USAAMRDL-TR-76-2, Eustis Directorate, U. S. Army Air Mobility R & D Laboratory, Fort Eustis, Virginia, September 1976.
2. Gregory, N., and Wilby, P. G., NPL 9615 AND NACA 0012 - A COMPARISON OF AERODYNAMIC DATA, CP No. 1261, Ministry of Defence (Procurement Executive), Aeronautical Research Council, London, England, November 1968.

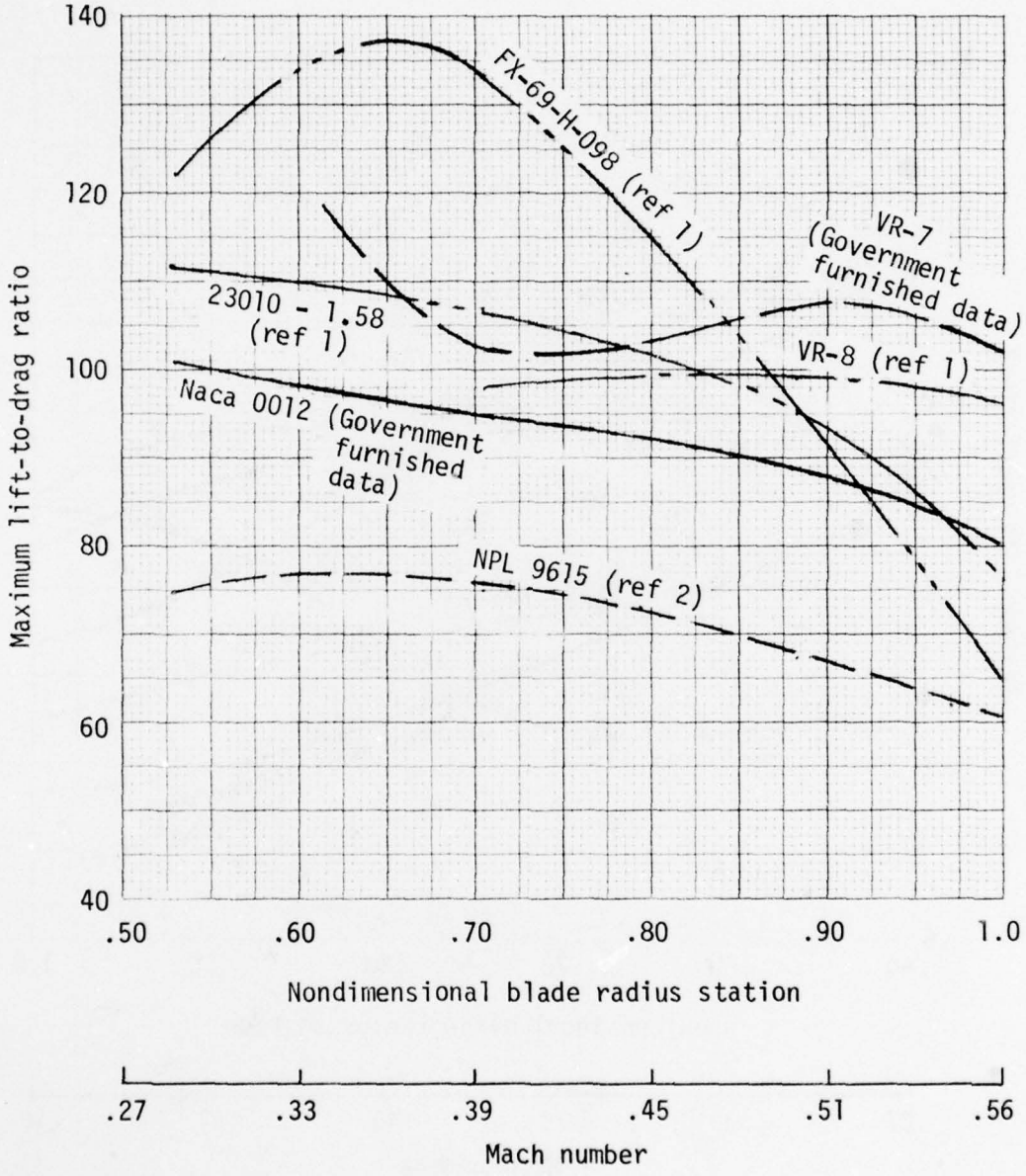

Figure 13. Maximum lift-to-drag ratio obtainable with candidate airfoil sections.

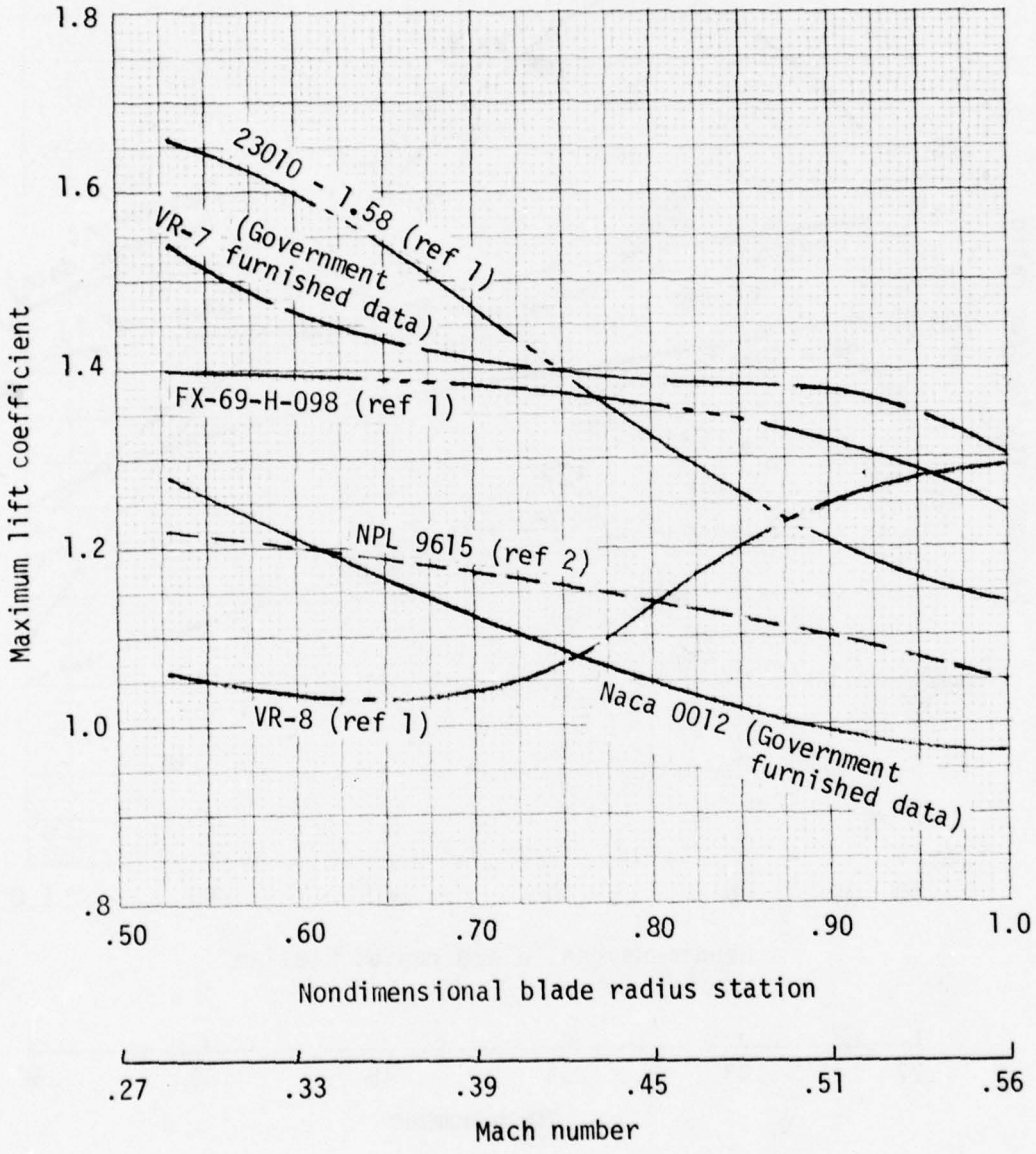

Figure 14. Maximum lift coefficient for candidate airfoil sections.

TABLE 1. SUMMARY OF AERODYNAMIC CHARACTERISTICS OF CANDIDATE AIRFOIL SECTIONS

Item	Airfoil Section					
	FX-69-H-098	VR-7	VR-8	23010-1.58	NPL 9615	NACA 0012
$C_{l_{max}}$ @ .75R	1.37	1.40	1.07	1.40	1.16	1.08
$(L/D)_{max}$ @ .75R	125	102	99	105	74	94
C_d @ C_l = 0.6 @ .75R	.0061	.0085	.0068	.0083	.0113	.0075
M_{DD}	.790	.742	.811	.794	.785	.765
Test Facility	UTC	NASAL	BVWT	BSWT	NPL	NASAL

UTC - United Technologies two-dimensional channel
BVWT - Boeing-Vertol wind tunnel
BSWT - Boeing-Seattle two-dimensional insert
NPL - National Physical Laboratory transonic wind tunnel
NASAL - Langley 6 x 28 inch transonic tunnel

the inboard stations and because its advantages with regard to maximum lift-to-drag at higher Mach number ratio are never realized at the outboard stations due to the relatively low tip Mach number, 0.57 for the OH-58C/A in hover under hot day conditions.

With the exception of the NPL 9615, all candidate airfoil sections considered display an advantage relative to the NACA 0012 with respect to the maximum lift-to-drag ratio. All but the VR-8 also have higher maximum lift coefficients over the range of Mach numbers of interest for the OH-58C/A application.

Blade Geometry

The design of the optimum rotor requires that the blade angle of attack be constant at all points on the blade radius to minimize the profile power required and that the downwash velocity remain constant at all points on the rotor disc to minimize the induced power required. To achieve these goals, the most fundamental analysis reveals that both the blade pitch and chord distribution with radius should be hyperbolic with the solidity selected so that the angle of attack is equal to that for maximum lift-to-drag ratio. The optimum rotor may achieve a 6 - 8 % performance improvement over the untwisted, untapered configuration. The hyperbolic variation of blade chord and twist distributions results in impractical blade geometry, and a more accurate analysis is required to optimize a realistic rotor design. For this purpose, a Goldstein-Lock analysis is used which accounts for a finite number of blades and assumes the blades are lifting lines and the rotor wake is uncontracted. The method has been adapted by Kaman to computer solution and has been found to yield results substantially in agreement with test results. It has the advantage that blade geometry can be readily changed and, since actual airfoil characteristics are an integral part of the program, the effects of Mach number and stall can be accounted for. Thus, a wide variety of blade geometric and aerodynamic configurations can be analyzed in a minimum of computer time. In addition, the computer printout includes angle of attack distribution with blade radius, which tends to minimize the number of computer runs, as well as to give better insight into the impact of various geometric changes.

The Goldstein-Lock analytical procedure was used to evaluate a wide range of geometric blade configurations utilizing the VR-7 airfoil characteristics. The configurations included three planforms with linear chord taper from root to tip and a two-step chord taper. The basic planforms are shown in Figure 15. The simple taper with a 6:1 taper ratio was selected as an approximation to the optimum hyperbolic chord distribution. The two smaller taper ratios were analyzed to determine the sensitivity of hover performance to this parameter. The dual taper configuration is based on the AH-1 blade geometry which represents a compromise configuration considering hover performance, structural and dynamic requirements, and forward flight performance. The dual taper and the linear 2:1 taper ratio configuration were further analyzed to determine the effect of blade twist distribution and solidity.

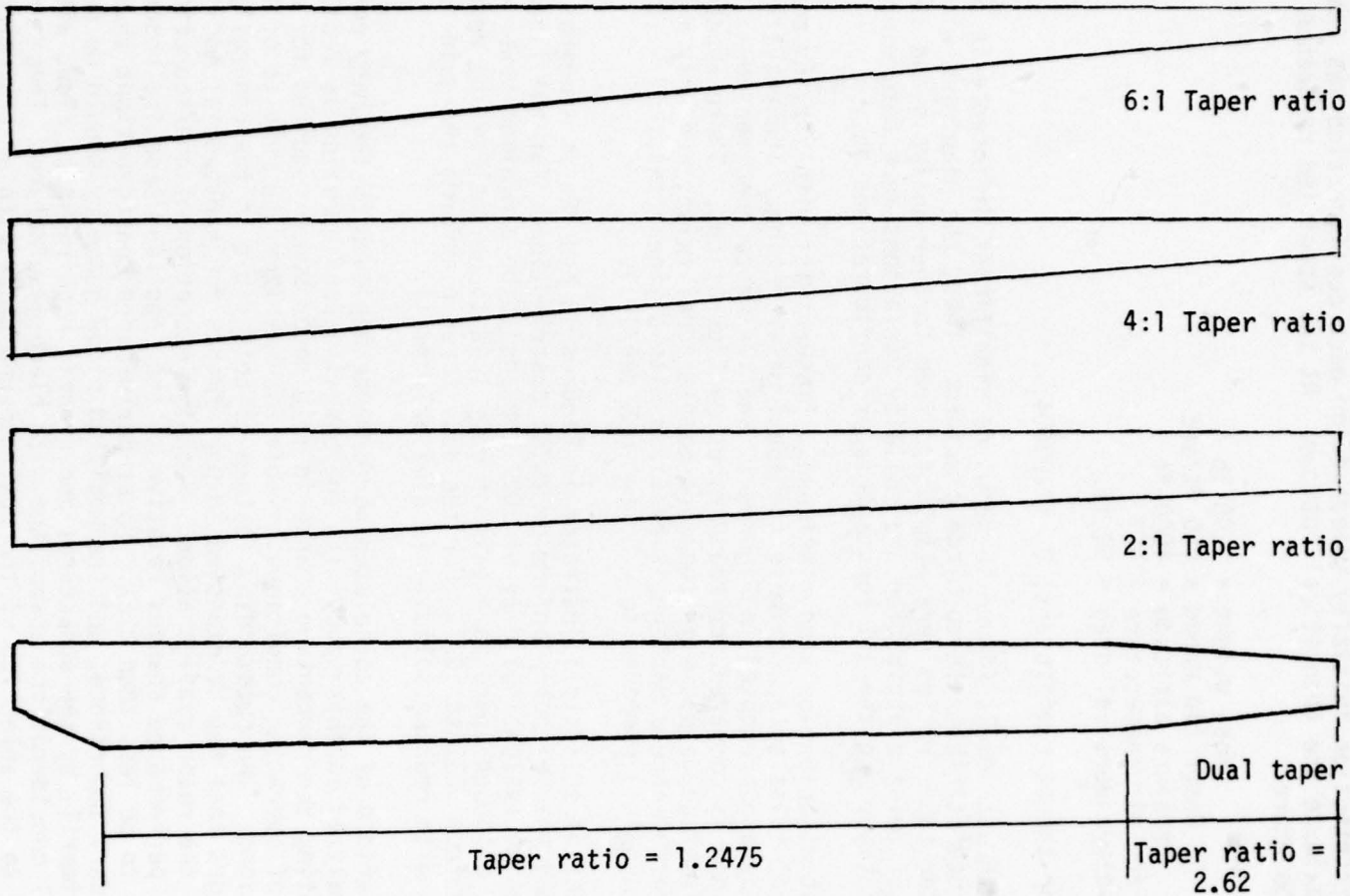

Figure 15. Planform geometry used in analysis of main rotor hover performance.

Hover performance calculated for the main rotor with the above blade planforms is presented in Figure 16 at a thrust-weighted solidity of .03. The twist distribution initially selected for each configuration was intended to approximate the theoretical optimum. At the specified reference hover condition where:

Gross weight = 3200 lb
Rotor tip speed = 655 ft/sec
Pressure altitude = 4000 ft
Free air temperature = 95°
Fuselage vertical drag = 64 lb

the rotor thrust coefficient, C_T = .00404.

At this thrust level, Figure 16 shows no significant difference in hover performance attributable to blade planform. Thus, the planforms with the two higher taper ratios were eliminated from further analysis and the effects of twist distribution and solidity variations were determined for the dual taper and the 2:1 constant taper configurations only.

The twist distribution study included a linear twist with varying magnitude and a dual twist to approximate the ideal distribution. The results of this study are presented in Figures 17 and 17a where nondimensional hover performance is compared for the various configurations. There appears to be no advantage gained with the more complex dual twist, and only a very slight performance advantage is realized with a linear twist of - 12° (- .057 deg/in.) compared to - 8° (- .038 deg/in.).

The effect of solidity illustrated in Figures 18 and 18a is somewhat more pronounced than either planform or twist distribution. For the linear taper, an equivalent solidity of .027 appears to be a minimum power configuration, although there is a gain of only 1.4% to be realized by reducing solidity from .037 to .027. For the dual taper planform, the gain in performance with reduced solidity is similarly small.

The comparison of the calculated performance achieved by the many configurations analyzed in this study with the baseline configuration is facilitated by computing the percentage change in main rotor power required for a specific set of operating conditions. Table 2 summarizes the results of these computations. The outstanding feature of this table is the generally minimal changes that may be expected in performance for substantial modifications in the rotor configuration. With the exception of configuration 4 in Table 2, performance changes relative to the specified baseline rotor are computed to be less than 2.5%. Hover performance considerations thus become of secondary importance, and the modified blade geometry should be determined primarily by the structural and dynamic requirements, along with the practical considerations associated with blade manufacture. These criteria have led to the selection of the dual tapered blade with an equivalent solidity of .036 and a total twist of 12° distributed linearly from the center of rotation to the blade tip. This configuration is listed in Table 2 as Number 18. Pertinent geometric details are illustrated in Figure 1, and tabular data is provided in Table 3.

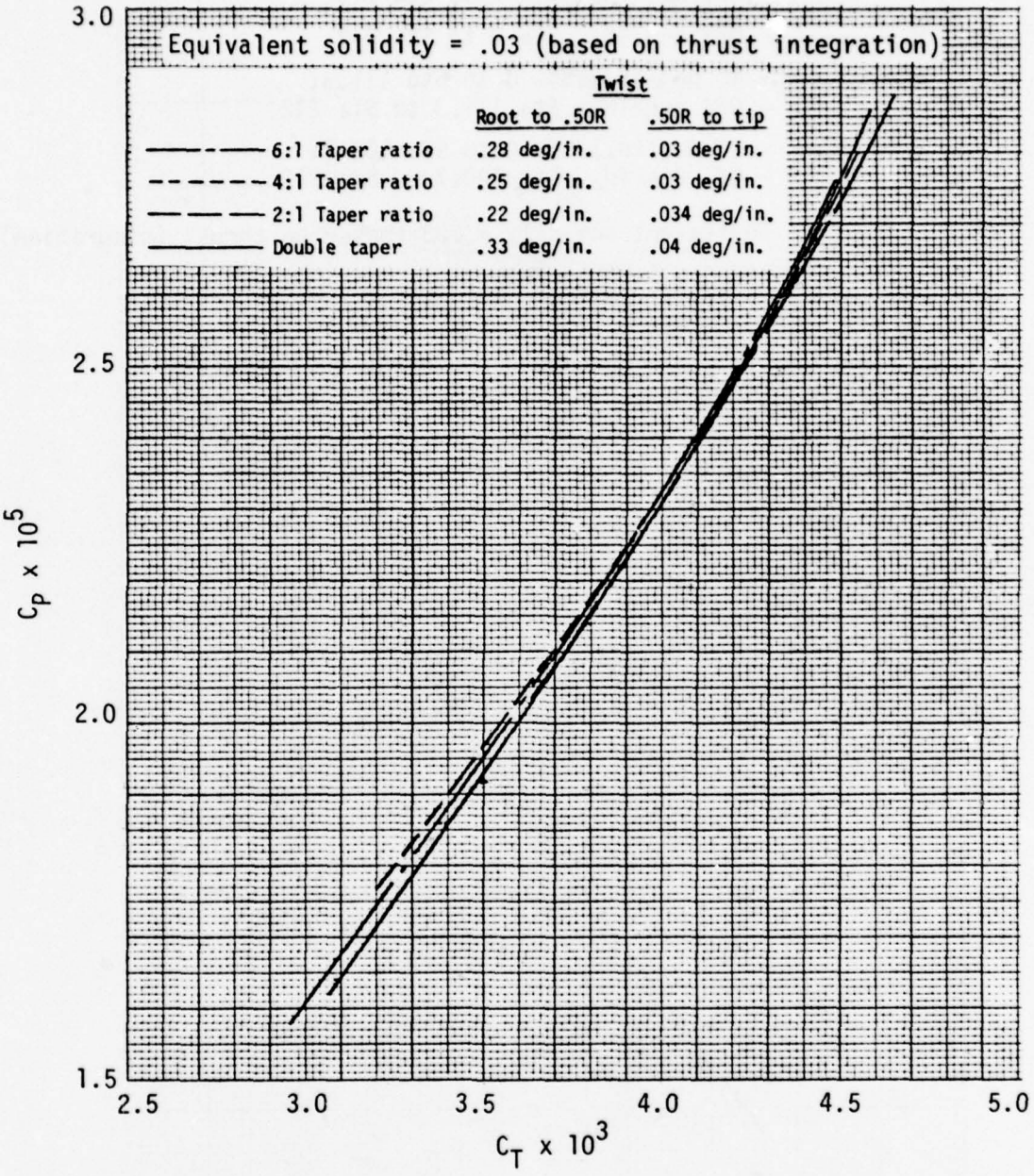

Figure 16. Effect of blade planform on main rotor hover performance.

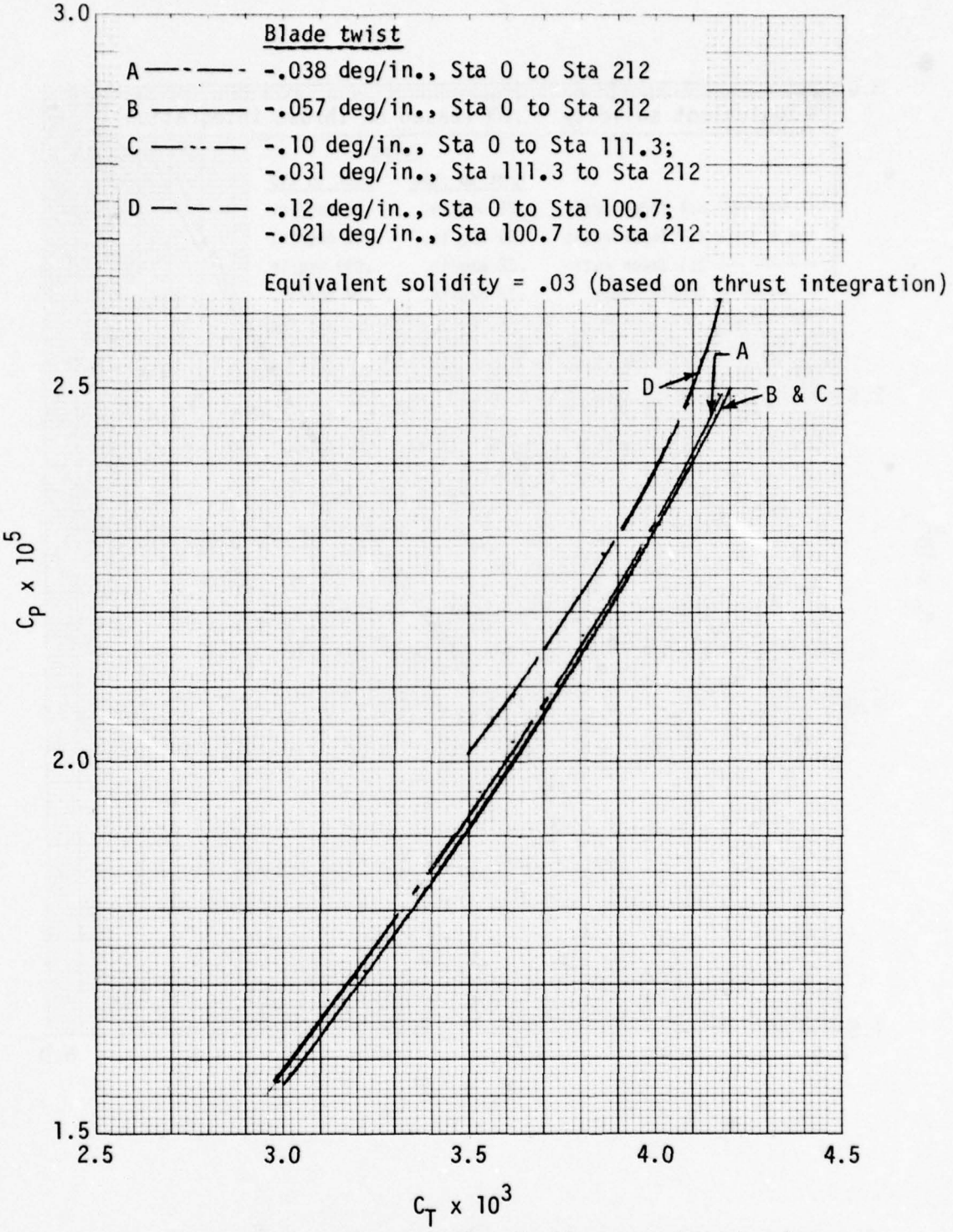

Figure 17. Effect of twist distribution on main rotor hover performance - dual taper planform.

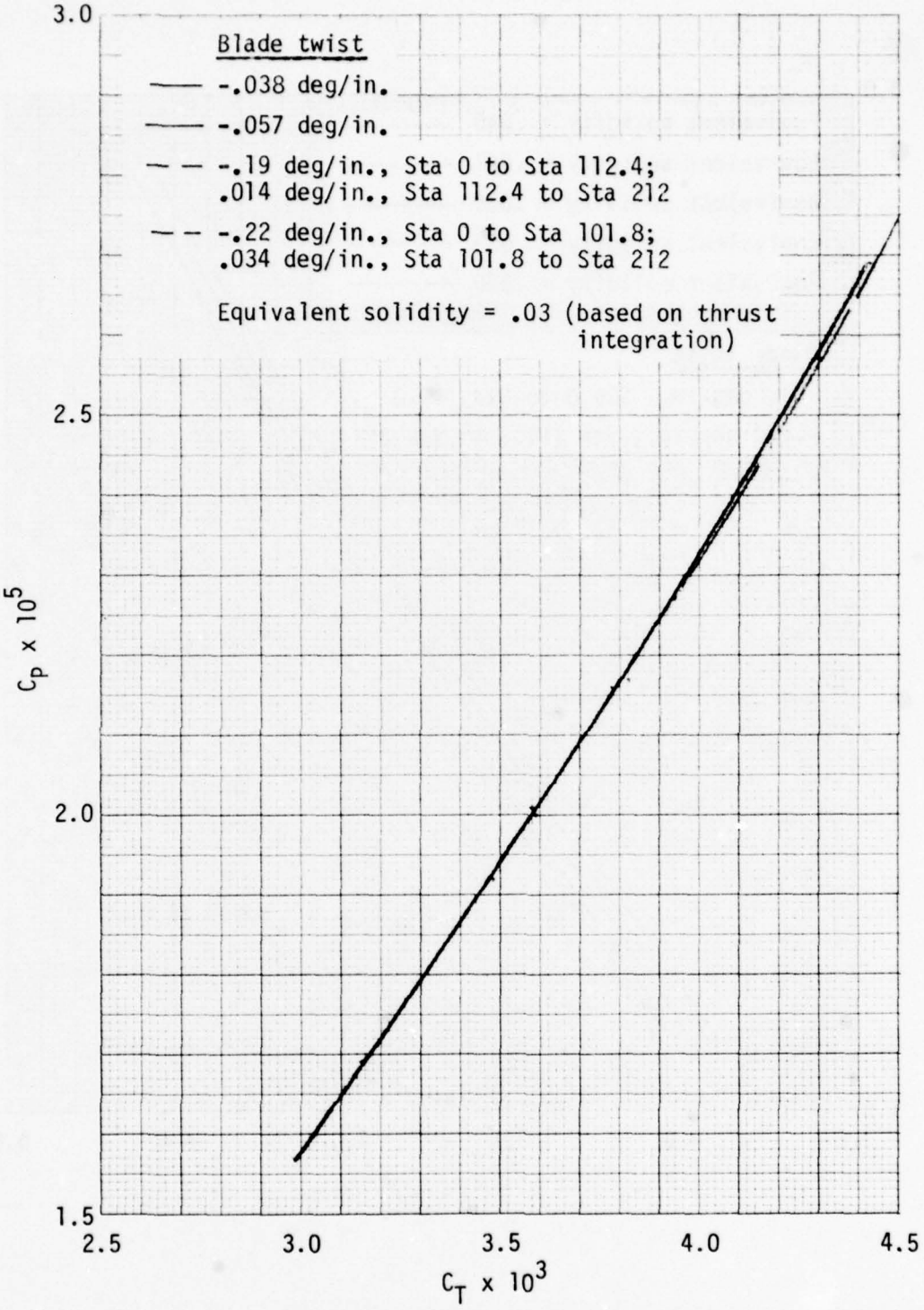

Figure 17a. Effect of twist distribution on main rotor hover performance - taper ratio 2:1.

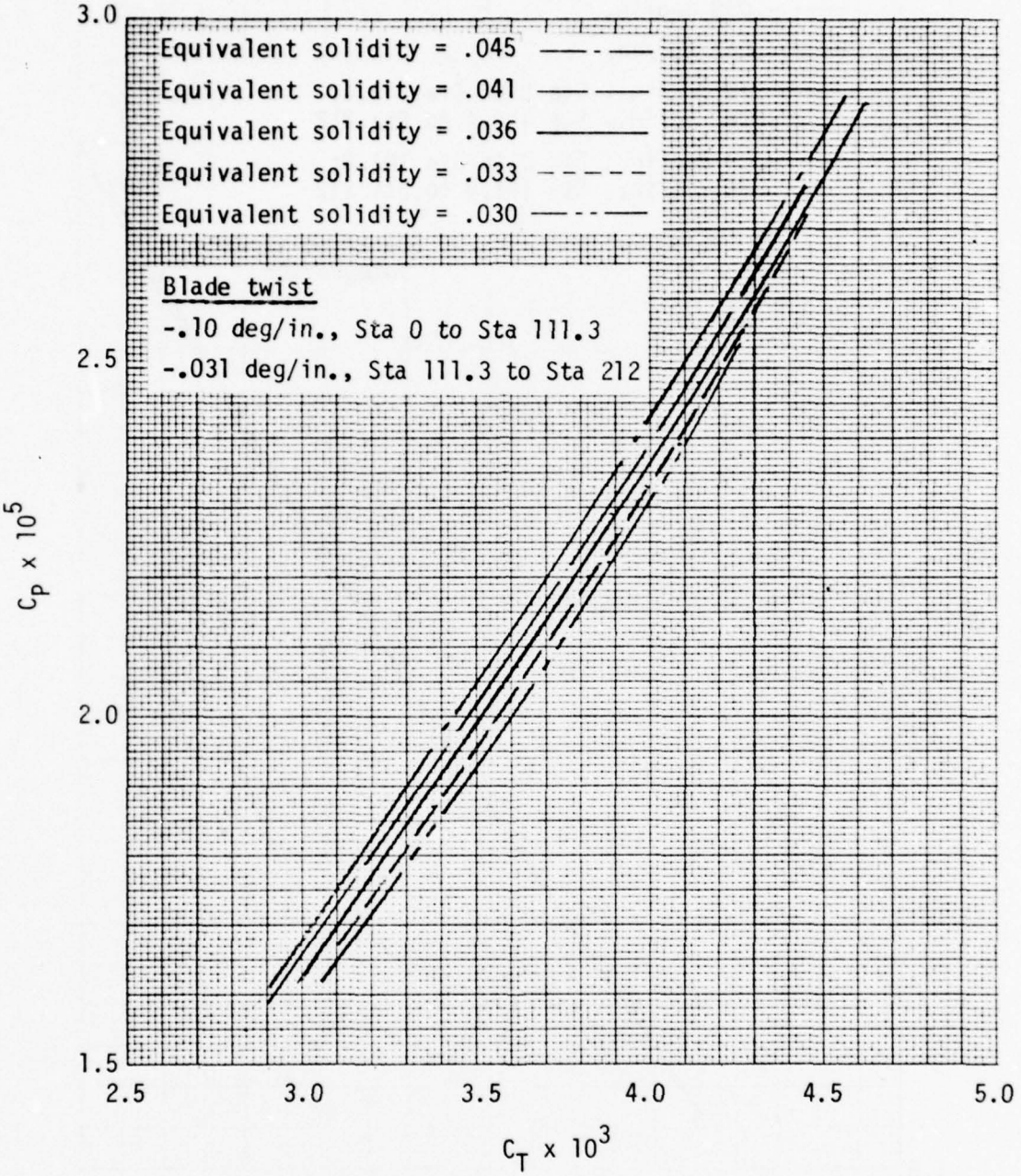

Figure 18. Effect of equivalent solidity on main rotor hover performance - dual taper planform.

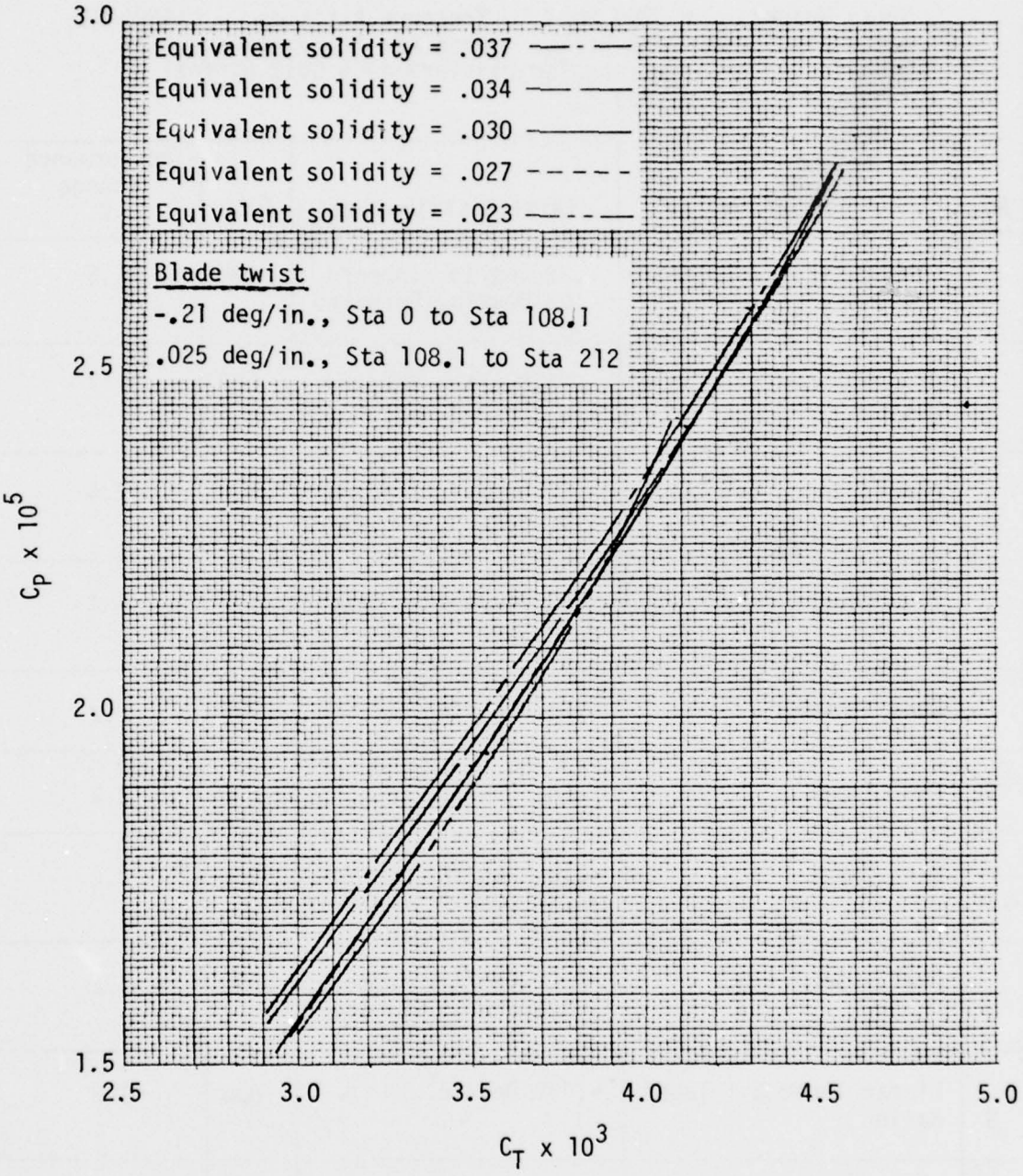

Figure 18a. Effect of equivalent solidity on main rotor hover performance - taper ratio 2:1.

TABLE 2. SUMMARY OF HOVER PERFORMANCE CAPABILITY OF CANDIDATE ROTOR CONFIGURATIONS RELATIVE TO BASELINE

Gross Weight = 3200 Lb Pressure Altitude = 4000 Ft
Rotor Tip Speed = 655 Ft/Sec Free Air Temperature = 95°F
Baseline Rotor = Rectangular Planform NACA 0012 Airfoil
Section σ_{CT} = .039

No.	Planform	Twist Distribution	σ_{CT}	Performance Change %
1	Linear Taper 6:1 Taper Ratio	-.23 Deg/In. Inboard -.03 Deg/In. Outboard	.030	1.8
2	Linear Taper 4:1 Taper Ratio	-.25 Deg/In. Inboard -.03 Deg/In. Outboard	.030	1.7
3	Linear Taper 2:1 Taper Ratio	-.22 Deg/In. Inboard -.03 Deg/In. Outboard	.030	2.4
4	Dual Taper	-.33 Deg/In. Inboard -.04 Deg/In. Outboard	.030	-4.2
5	Dual Taper	-.038 Deg/In.	.030	1.2
6	Dual Taper	-.057 Deg/In.	.030	2.2
7	Dual Taper	-.10 Deg/In. Inboard -.031 Deg/In. Outboard	.030	2.0
8	Dual Taper	-.12 Deg/In. Inboard -.021 Deg/In. Outboard	.030	-1.2
9	Linear Taper 2:1 Taper Ratio	-.038 Deg/In.	.030	1.3
10	Linear Taper 2:1 Taper Ratio	-.057 Deg/In.	.030	1.9

TABLE 2. SUMMARY OF HOVER PERFORMANCE CAPABILITY OF CANDIDATE ROTOR CONFIGURATIONS RELATIVE TO BASELINE (continued)

No.	Planform	Twist Distribution	σ_{CT}	Performance Change %
11	Linear Taper 2:1 Taper Ratio	-.19 Deg/In. Inboard -.014 Deg/In. Outboard	.030	1.9
12	Linear Taper 2:1 Taper Ratio	-.22 Deg/In. Inboard -.034 Deg/In. Outboard	.030	2.4
13	Dual Taper	-.10 Deg/In. Inboard -.031 Deg/In. Outboard	.045	-2.3
14	Dual Taper	Same as Config No. 13	.041	-1.2
15	Dual Taper	Same as Config No. 13	.036	0
16	Dual Taper	Same as Config No. 13	.033	1.3
17	Dual Taper	Same as Config No. 13	.030	2.0
18	Dual Taper	-.057 Deg/In.	.036	1.3
19	Linear Taper 2:1 Taper Ratio	-.21 Deg/In. Inboard -.025 Deg/In. Outboard	.037	0.6
20	Linear Taper 2:1 Taper Ratio	Same as Config No. 18	.034	1.4
21	Linear Taper 2:1 Taper Ratio	Same as Config No. 18	.030	1.8
22	Linear Taper 2:1 Taper Ratio	Same as Config No. 18	.027	2.0
23	Linear Taper 2:1 Taper Ratio	Same as Config No. 18	.023	0.5

TABLE 3. SELECTED BLADE DESCRIPTION - K757

RADIAL STATION								
inches	0.0	18.5	25.0	36.5	172.916	178.916	179.916	212.0
feet	0.0	1.5417	2.0837	3.0422	14.41	14.91	14.9258	17.6667
nondimensional	0.0	.087264	.117925	.172170	.8156	.8439	.848660	1.00000
CHORD[1]								
inches - with tab	---	---	8.2	14.955	14.113	14.016	12.6257	6.3125
- without tab	---	---	8.2	14.807	12.613	12.516	12.5	6.25
feet - with tab	---	---	.683333	1.24625	1.176	1.168	1.052	.526
- without tab	---	---	N/A	1.2339	1.051	1.043	1.042	.5208
TWIST - deg	0.0	0.0	- 7.863	- 2.124	- 9.845	- 10.184	- 10.241	- 12.
AIRFOIL	← HUB →		← SPAR →	← TRANSITION →	← VR-7 →			

SHORT TRAILING EDGE TAB

Chord - inches	1.5
- feet	.125
Deflection - degrees	0°

1. Note Chord includes trailing edge tab on VR-7 airfoil with tab setting 4.7° trailing edge up. See airfoil data table in Appendix A which includes tab characteristics.

Comparative Performance

Nondimensionalized hover performance obtained for the selected configuration is presented in Figure 19. All data shown in this and previous graphs includes only main rotor power requirements. For the complete aircraft, the tail rotor power, accessory power and gearing losses, as well as the fuselage vertical drag, must be considered.

Fuselage vertical drag is a function of the rotor thrust. It is accounted for by increasing the thrust coefficient at a given gross weight by a specified factor of 1.02.

The total is written:

$$SHP = \frac{MRHP + TRHP + ACHP}{\eta}$$

Flight experience indicates that the tail rotor horsepower, TRHP, is close to 10% of the main rotor power, MRHP, for normal hover conditions. Since the tail rotor power, treated as a percentage of main rotor power, has no influence in the power comparison between various main rotor configurations, this value is used throughout the analysis. The accessory power is specified at 12.74 horsepower and a power transmission loss of 1%/mesh is assumed. For three meshing gears, the transmission efficiency, η, is .97. Then,

$$SHP = \frac{1.1\ MRHP + 12.74}{.97}$$

The main rotor horsepower is calculated from the nondimensionalized main rotor power coefficient presented, typically, in Figure 19 as a function of the thrust coefficient.

The overall helicopter hover performance, calculated according to the foregoing discussion, is presented in Figure 20 for the OH-58C/A with the composite rotor and with the standard rotor. Data included in Figure 20 illustrates the hover performance as it is presented in the OH-58C Detail Specification (Reference 3). This performance shows excellent agreement with the performance determined from flight test and reported in Reference 4.

3. Hill, David A., DETAIL SPECIFICATION FOR THE OH-58C HELICOPTER INTERIM SCOUT, BHC 206-947-203, Bell Helicopter Company, Fort Worth, Texas, September 1975.
4. Yamakawa, George M., and Watts, Joseph C., AIRWORTHINESS AND FLIGHT CHARACTERISTICS TEST, PRODUCTION OH-58A HELICOPTER, UNARMED AND ARMED WITH XM27E1 WEAPON SYSTEM, USSAASTA 68-30, U. S. Army Aviation Systems Test Activity, Edwards Air Force Base, California, September 1970, AD875793L.

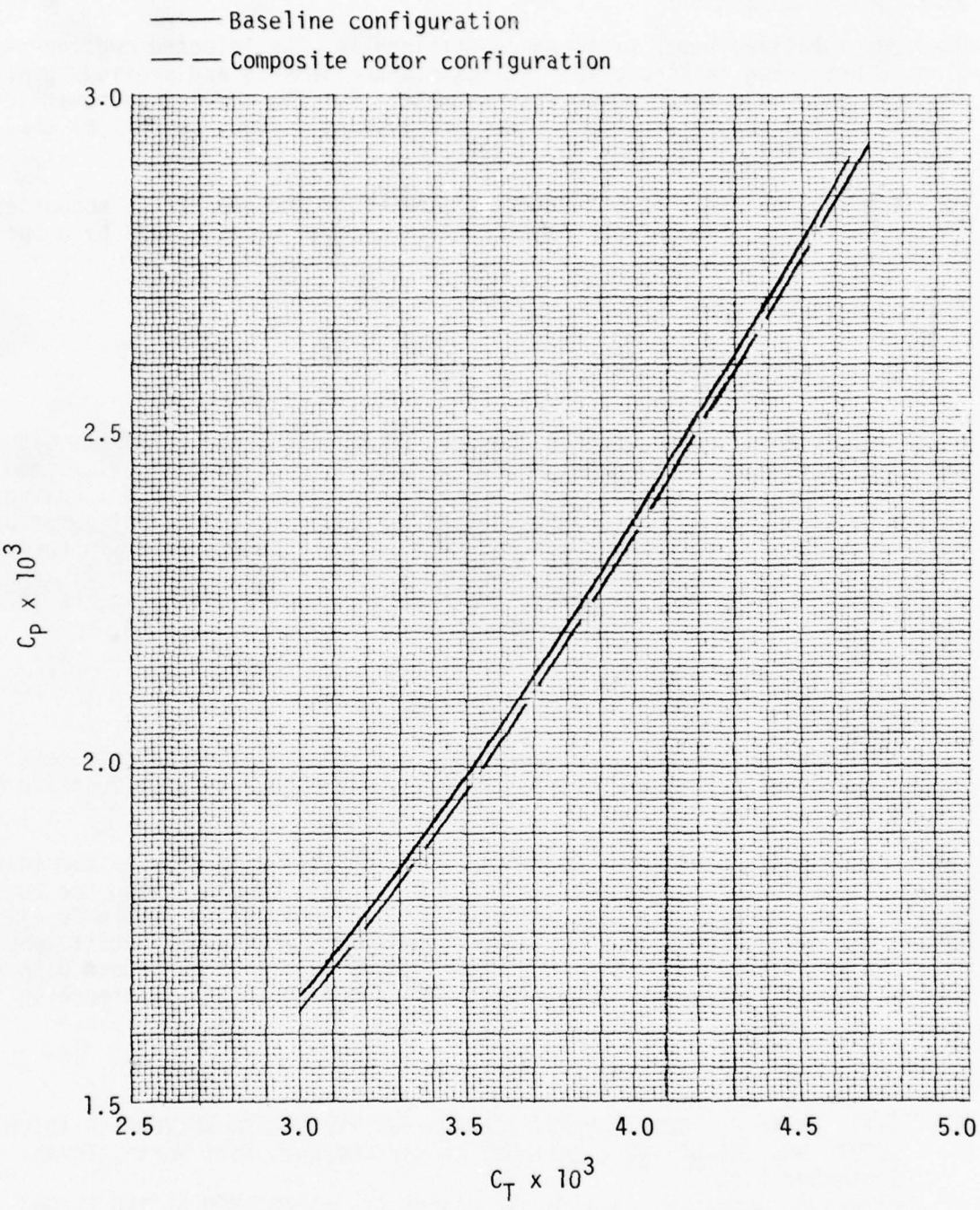

Figure 19. Nondimensional hover performance.

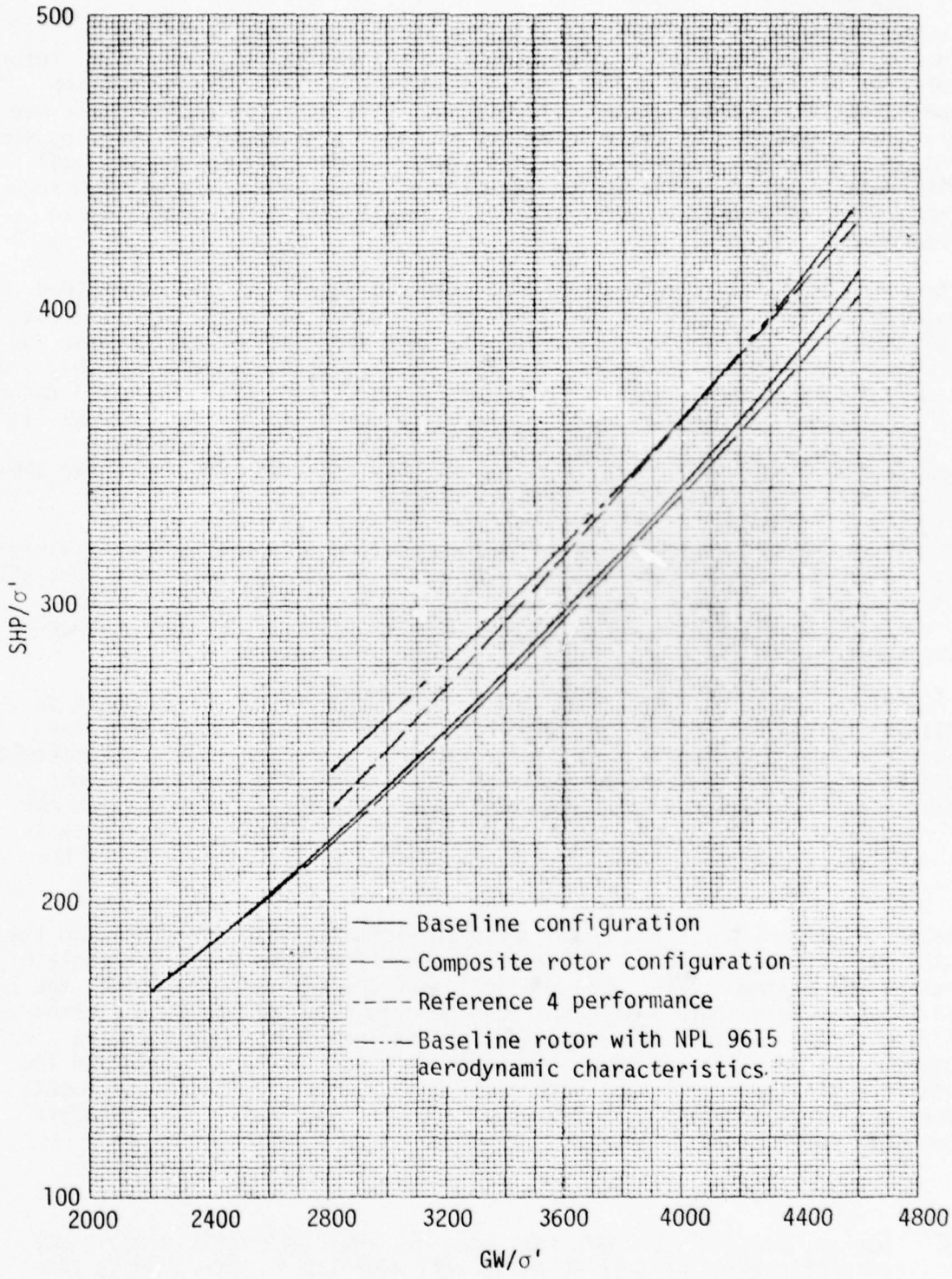

Figure 20. Hover performance comparison.

The performance of the OH-58C/A with the composite rotor installed is calculated for the dual taper blade with - 12° linear twist. Equivalent rotor solidity is 0.036 based on integrated thrust. The VR-7 airfoil section characteristics were Government-furnished. Lift and drag coefficients are given as a function of angle of attack at various Mach numbers covering the range of operation considered in this study. These data agree very well with data measured in the Boeing-Vertol wind tunnel where the maximum section lift coefficient is corrected for sidewall effects as indicated in Reference 5.

The calculated hover performance with standard main rotor was determined using the NACA 0012 and the NPL 9615 section aerodynamic characteristics. The NACA 0012 lift and drag coefficients were supplied by the customer for a wide range of section angles of attack at various Mach numbers. They are based on measurements made in the Langley 6- x 19-inch transonic wind tunnel and reported in Reference 5 with appropriate correction to the maximum lift coefficient for tunnel sidewall effects. The baseline configuration is designated as that which utilizes the OH-58C/A standard rotor with the specified NACA 0012 aerodynamic characteristics.

As discussed previously, the actual blade section of the OH-58C/A is similar to the British NPL 9615, particularly in the portion forward of the 35% chord point. In view of this similarity, the hover performance of the OH-58C/A with the standard rotor was estimated using blade section characteristics for the NPL 9615 airfoil listed in Reference 2.

Comparison of the calculated and measured performance of the OH-58C/A is illustrated in Figure 20. The calculated performance with the baseline specification performance over a wide range of gross weight and atmospheric conditions. A 7% improvement in performance at the specified reference condition is achieved by the composite rotor relative to the measured performance of the standard rotor. This is due primarily to the increase in the lift-to-drag ratio exhibited by the VR-7 airfoil relative to the NPL 9615.

Detailed comparison of the aerodynamic characteristics of the VR-7 and the NACA 0012 airfoil shows no significant drag differences until the angle of attack for maximum lift-to-drag ratio is approached. At this point, the VR-7 begins to exhibit a slight advantage primarily because of the camber. At low thrust loading, therefore, any performance difference existing between the baseline and composite rotor configurations is attributed to planform variation. As shown previously, this is a very small increment even for large deviations from the rectangular planforms of the standard OH-58C/A rotor blade.

5. Noonan, Kevin W., and Bingham, Gene J., TWO-DIMENSIONAL AERODYNAMIC CHARACTERISTICS OF SEVERAL ROTORCRAFT AIRFOILS AT MACH NUMBERS FROM 0.35 TO 0.90, NASA TM X-73990, January 1977.

Comparative level forward flight performance for the baseline and the composite rotor configurations is presented in Figure 21. At low thrust coefficients and airspeeds there is essentially no difference in performance. This is consistent with the hover results where only a small improvement in performance is predicted due to the composite rotor. At speeds beyond transition, the composite rotor begins to show improvement relative to the baseline configuration, and the improvement increases with increasing rotor loading. This result is expected in view of the improved lift-to-drag ratio and the higher maximum lift coefficient exhibited by the VR-7 airfoil relative to the NACA 0012.

As in the hover comparison, forward flight performance for the standard main rotor was also calculated using the NPL 9615 section aerodynamic characteristics. In this case, the agreement of the calculated performance with that reported in Figure 11 of Reference 3 is not as good as in the hover case, but it is significantly improved over that shown using the NACA 0012 aerodynamic data.

Aerodynamic Characteristics Distribution

Table 4 summarizes the distribution of the aerodynamic characteristics with respect to spanwise location on the blade for the baseline and composite rotor configurations. Note that the last three columns in the table are proportional to the thrust and the induced and profile torque loading distributions, since

$$\frac{dT}{Dr} = \frac{dC_T}{dx} \frac{\rho\pi R^2(\Omega R)^2}{Rb} \quad \text{Lb/Ft}$$

$$\frac{dQ_i}{dr} = \frac{dC_{Qi}}{dx} \frac{\rho\pi R^2(\Omega R)^2}{b} \quad \text{Ft-lb/Ft}$$

$$\frac{dQ_o}{dr} = \frac{dC_{Qo}}{dx} \frac{\rho\pi R^2(\Omega R)^2}{b} \quad \text{Ft-lb/Ft}$$

and

$$CT = \frac{dC_T}{dx}$$

$$CPIND = \frac{dC_{Qi}}{dx}$$

$$CPPRO = \frac{dC_{Qo}}{dx}$$

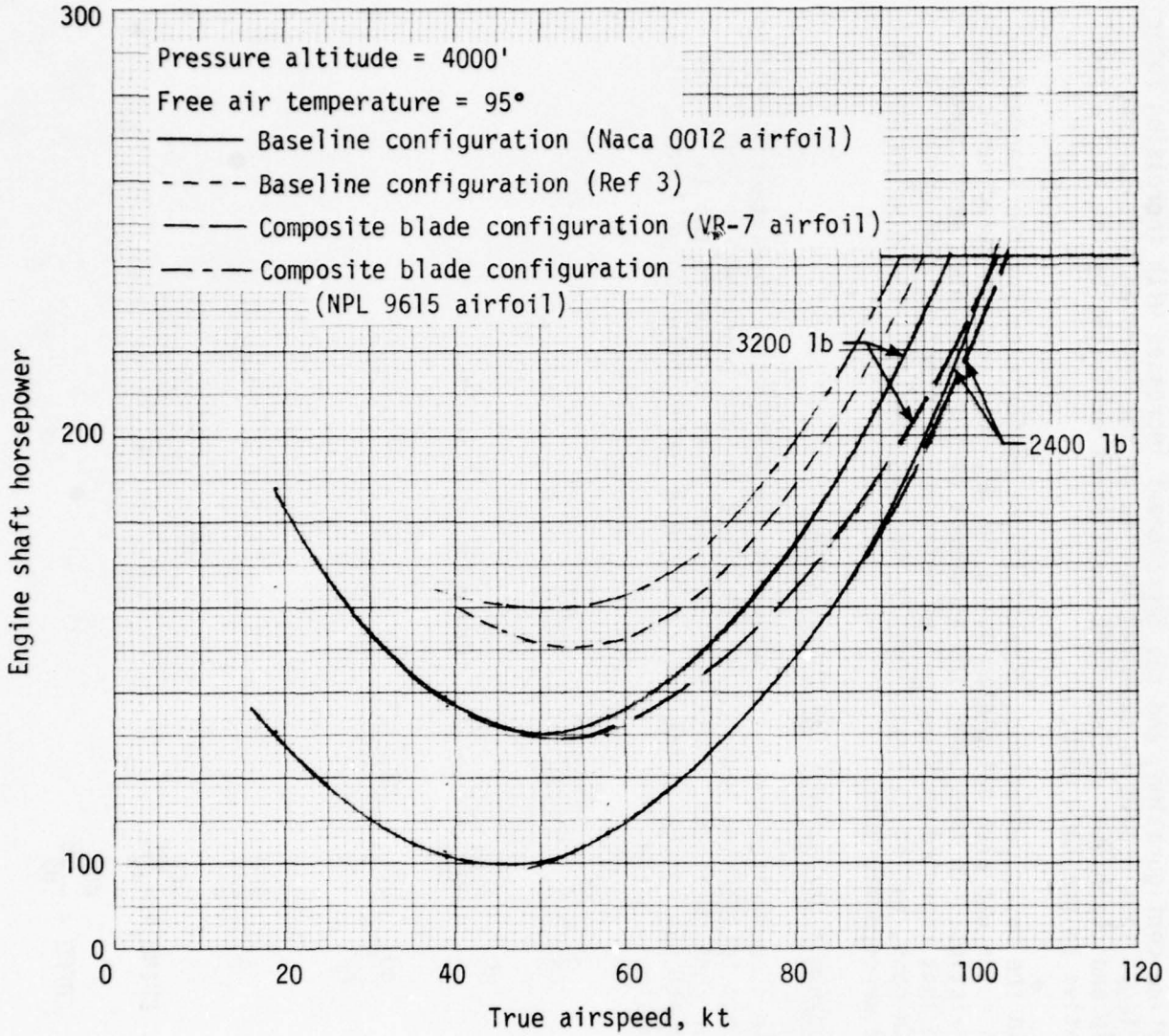

Figure 21. Forward flight performance comparison.

TABLE 4. SPANWISE DISTRIBUTION OF AERODYNAMICS HOVER CHARACTERISTICS

(a) Baseline

STATION	MACH NO.	ALPHA	CL	CD	L/D	PHI	CT	CP IND.	CP PRO.
0.172	0.200	7.50	0.8199	0.0092	88.64	8.531	0.0004564	0.0000119	0.0000009
0.300	0.200	7.80	0.8622	0.0095	90.55	6.969	0.0014610	0.0000544	0.0000049
0.450	0.255	7.51	0.8341	0.0093	90.04	5.666	0.0022486	0.0001451	0.0000163
0.600	0.340	6.82	0.7922	0.0087	91.11	4.765	0.0055082	0.0002757	0.0000363
0.700	0.397	6.28	0.7520	0.0084	89.88	4.252	0.0071299	0.0003714	0.0000556
0.750	0.425	5.93	0.7207	0.0082	87.68	4.074	0.0078508	0.0004197	0.0000672
0.800	0.454	5.58	0.6876	0.0080	85.72	3.891	0.0085280	0.0004643	0.0000796
0.850	0.482	5.22	0.6523	0.0078	83.91	3.719	0.0091374	0.0005051	0.0000926
0.875	0.496	4.96	0.6239	0.0076	82.37	3.719	0.0102220	0.0005817	0.0001087
0.900	0.510	4.83	0.6156	0.0078	79.20	3.583	0.0096710	0.0005453	0.0001100
0.924	0.524	4.56	0.5921	0.0078	75.70	3.583	0.0097966	0.0005670	0.0001196
0.952	0.540	4.30	0.5706	0.0077	73.77	3.583	0.0100357	0.0005991	0.0001297
0.977	0.554	4.03	0.5479	0.0074	73.76	3.583	0.0101345	0.0006206	0.0001343

(b) Composite rotor

STATION	MACH NO.	ALPHA	CL	CD	L/D	PHI	CT	CP IND.	CP PRO.
0.172	0.350	6.30	0.8981	0.0082	109.14	9.631	0.0005647	0.0000165	0.0000009
0.300	0.350	6.72	0.9500	0.0085	111.24	7.680	0.0017964	0.0000727	0.0000049
0.450	0.350	6.48	0.9197	0.0084	110.04	6.122	0.0038107	0.0001840	0.0000156
0.600	0.350	5.82	0.8385	0.0080	105.04	4.979	0.0059796	0.0003128	0.0000342
0.700	0.397	5.23	0.7919	0.0092	85.80	4.372	0.0075089	0.0004022	0.0000613
0.750	0.425	4.83	0.7578	0.0091	83.67	4.167	0.0081507	0.0004457	0.0000731
0.800	0.454	4.44	0.7235	0.0089	81.47	3.956	0.0087403	0.0004839	0.0000859
0.850	0.482	4.04	0.6866	0.0088	78.11	3.757	0.0092497	0.0005167	0.0001007
0.875	0.496	3.94	0.6799	0.0088	77.50	3.559	0.0088190	0.0004802	0.0000997
0.900	0.510	3.84	0.6712	0.0088	76.63	3.361	0.0083716	0.0004428	0.0000984
0.924	0.524	3.70	0.6562	0.0087	75.07	3.215	0.0077797	0.0004039	0.0000958
0.952	0.540	3.50	0.6350	0.0087	72.75	3.073	0.0069509	0.0003557	0.0000911
0.977	0.554	3.34	0.6167	0.0087	70.64	2.940	0.0061886	0.0003107	0.0000857

DESIGN CONSIDERATIONS, CONFIGURATIONS 111, 211, 311, 122, 222, 322

Structural Description

Three basic structural areas are considered in the design of a composite rotor blade: the root end attachment, the basic blade section, and the tip structure. The root end demands the most innovative design approach, since the classical composite joint problem is so prominent. The clean section design is largely one of selecting a manufacturing technique and structural layout that is simple, efficient and economical. In essence, the clean section determines the overall fabrication philosophy for the blade. The tip has termination joints and is likely to have other features such as balance weights and inertia weights. The tip planform, which is an aerodynamic requirement, and the manufacturing procedures exert significant influence on the overall tip configuration.

Since the first two screening levels reduced the number of configurations to six, each of the remaining will be discussed in detail. Sketches of the configuration elements appear in Figures 5 through 8.

Configuration 111. Configuration 111 consists of a K747 (Kaman AH-1) type root attachment, a filament-wound spar with Nomex core afterbody and spline, and a cast steel tip Nomex afterbody and spline. This root end allows the composite blade to terminate inboard in multiple structural bows which are adapted by an aluminum root fitting to the OH-58 main retention yoke. The adapter results in two joints: one between the composite and the adapter, and the other between the adapter and the yoke. Since the weight and cost impact of the adapter-fitting is substantial, it must be as short and compact as possible. This results in short, tortuous load paths with attendant substantial stress configuration concentration effects which must be dealt with.

Because the root fitting must react chordwise bending, as well as flapwise bending and centrifugal force, it is a more severe application than it was for the AH-1 blade. Also, it has the potentially detrimental effect of moving the first clean aerodynamic section somewhat further outboard. The chief advantage lies in that it allows design freedom of the composite end of the blade. The filament-wound spar is a simple single cell with an integrally wound structural leading edge balance weight (Figure 6). The carved Nomex afterbody is foam-adhesive attached to the back of this spar with upper and lower skins forming the top and bottom plates. A trailing edge spline is sandwiched between the skins and bonded to the aft surface of the Nomex core. The tip configuration employs a cast steel "permanent" mandrel to provide inertia properties. Spar and afterbody are similar to the clean section in description.

Configuration 122. The root fitting adapter is coupled to a filament-wound spar/pultruded afterbody clean section. Configuration 2 clean section has a somewhat lighter section spar due to the increased properties

provided by the pultruded afterbody. However, because of the heavy afterbody, a considerably larger nose balance weight is required. Thus, this becomes a relatively heavy section. Since pressure must be applied internally to bond the pultruded afterbody to the spar, it is necessary for the afterbody to be open at each end. Therefore, tip configuration number 2 provides a fully cured, removable, molded afterbody as a closure.

Configuration 211. The root attachment is all composite, excepting bushings, washers, etc. This root end greatly resembles the present blade, having a substantial wall thickness buildup of carbon-graphite and S-glass to sustain the high structural requirements. The clean section includes a filament-wound single cell spar with Nomex afterbody and trailing edge spline. The tip configuration incorporates the steel tip weight with Nomex core afterbody and trailing edge spline. This configuration is one of the simplest, with low fabrication development risk.

Configuration 222. This has an all-composite root end, excepting bushings, washers, etc. The clean section consists of a filament-wound spar with a pultruded afterbody. The tip has the filament-wound cast steel inertia weight and molded afterbody pieces.

Configuration 311. Root end configuration 3 consists of a broom-type composite root end with an auxiliary aluminum drag-brace structure to react chordwise shear and moments. The metallic parts are in three pieces: a drag strut cross-member, a drag-brace diagonal member, and an internal reacting member which is attached at the main retention pin and extends inboard to react edgewise shears at the blade latch. The broom is a uniaxial filament winding which is consolidated into the basic blade section. The clean section is a filament-wound spar with Nomex core and trailing edge spline, and the tip consists of the filament-wound spar containing the cast steel weight with a continuation of the Nomex core and trailing edge spline.

Configuration 322. This configuration has a broom-type composite root end with auxiliary drag-brace structure. The clean section is a basic filament-wound spar with a pultruded afterbody, and the tip has a filament-wound spar containing the inertia weight with a molded afterbody.

Materials Consideration

Materials and manufacturing process trade studies were performed in conjunction with the mutually dependent design and performance evaluations. Characteristics of the dry fibers, matrices and fabrication methods considered are as follows:

Fiber Characteristics

- E-glass is lowest in cost. It has low strength and modulus and high density with very good inherent damage tolerance and fatigue characteristics.

- S-glass is still a low cost material, although it is presently approximately 2-1/2 times E-glass costs. Modulus and strength are significantly higher. Density is slightly lower. Damage tolerance and crack propagation properties are very good. Fatigue strengths are higher than E-glass.

- Kevlar 29 is a moderate cost material at seven to eight times the cost of E-glass. The modulus is similar to S-glass, but density is substantially lower than the glass fibers. Although tensile strengths are moderately high, compressive strengths are very low. Fatigue properties are undocumented, but damage tolerance and crack propagation are believed to be similar to glass.

- Kevlar 49 is a moderate cost material at eight to nine times the cost of E-glass. The modulus is high and the density quite low, yielding a very favorable stiffness/weight ratio. Tensile strength is high, but compressive strength is low. Damage tolerance and crack propagation characteristics are slightly poorer than glass, but substantially better than graphite. Fatigue strength is greater than glass. Processing is slightly more difficult.

- Moderate modulus graphite is moderately high in cost at about 20 times E-glass. The modulus is about three times S-glass and 50% greater than Kevlar 49. This material has substantially poorer damage tolerance and crack propagation characteristics than glass. Tensile strength is moderately high, but fatigue strength is substantially greater than glass or Kevlar. Graphite is a conductive material.

- High modulus graphite is high in cost, but has a very high modulus. Tensile strength is lower than glass, but fatigue strength is very high. Damage tolerance is poor. High modulus graphite material is conductive.

- Boron is very costly. It has a high modulus and possesses higher compression strength than other fibers. Boron is also a conductive material.

In consideration of the desire to have low costs, excellent damage tolerance and low crack propagation rates, it is apparent that fiberglass is the optimum material if dynamic, structural and weight objectives can be met. Weight, balance and dynamic requirements can be effectively adjusted by judicious use of Kevlar 49. Graphite and boron will adversely affect the cost and weight needed to achieve adequate lightning protection and reduced radar cross section. Because of this, their use will be limited to areas where local stiffening or strengthening is required.

Matrix Characteristics

- Epoxy matrices have a long history of use in aircraft structural components. The processing characteristics, environmental response, and fatigue performance of epoxy matrix composites are well understood. Evolutionary application of epoxies to main rotor blades began in the early 1950s with such components as skins and local reinforcements. All-composite blades using epoxy matrices are now in production by Kaman and others.

- Polyester resin matrix fiberglass composites have been used extensively in commercial applications and in some nonstructural aircraft components, such as fairings. Their chief drawback is lower fiber/resin bonding strength than epoxies, with attendant poorer fatigue characteristics. Adequate design fatigue data, particularly under severe environmental conditions, is not available, and a substantial fatigue characterization effort would be required in advance of a blade design in order to minimize technical risk. Raw material costs are somewhat lower than epoxies and fabrication characteristics better suited to some fabrication methods of interest, particularly pultrusion.

- Recently developed polysulfone thermoplastic matrices offer promise of low-cost composite fabrication for some structural configurations. Material fabrication characteristics are similar to epoxy prepregs, except for shortened thermal cycles, and do not appear advantageous for major blade components, such as spars. The process is advantageous in making formed parts from reinforced sheets. It does not harmonize with an overall spar fabrication scheme. Again, fatigue performance is inadequately characterized for blade design, and a major material test program would be required.

Fabrication Methods

- Filament winding is a proven, automated method of blade fabrication which uses low-cost raw materials (basic fiber and resin).

- Braiding is promising as a high-laydown rate, low-cost method of fabrication. Available equipment limits the spar circumference/fiber orientation obtainable, but in the future, it appears suitable for a blade of OH-58 size. Unknowns pose high risk for production blade development programs, but braiding appears worthy of further study and development.

- Pultrusion appeared attractive as a low-cost method for producing blade afterbodies and was the subject of major evaluation. The present state-of-the-art was found to impose severe restrictions on the section thickness, shapes and fiber orientations attainable, and, therefore, on design efficiency. Further, most pultrusion experience is with polyester resins. Both the use of polyester resins in blade designs and the use of epoxy resins in complex pultrusions are considered to involve significant development and technical risk.

- Prepreg layup is the conventional low risk method of composite manufacture. Continuing evaluation of automatic layup technology and prepreg costs leads to the conclusion that prepreg fabrication of major blade components, such as spars, is incompatible with the Army's cost goals.

Materials and Fabrication Trade Selections

Preliminary stress analysis and section property calculations indicated that combinations of E-glass and S-glass were optimum material for the basic spar cross section. An epoxy matrix was selected because of high strength, relatively low cost and good damage tolerance. In configuring the pultruded afterbody, it became apparent that weight was a serious problem since minimum section thickness must be at least .045 inch. In order to keep this configuration competitive, it was necessary to specify Kevlar 29 for the pultrusion. Kevlar 29 was selected over Kevlar 49 because of lower cost. For the conventional afterbody, a 1.5 lb/ft^3 Nomex core was selected with S-glass filament-wound cross-ply skins for plates. The trailing edge spline is made from E-glass. For structural reasons, interspersed layers of cross-ply graphite are included at the root end configuration 2. A stainless steel casting was selected as a tip ballast member for all. This provides corrosion protection and promotes better bonding. Aluminum alloy 7049 was selected for configuration 1 root end.

Wet filament winding was selected for all six candidates because of its low cost and advanced state of development. Braiding appears to be a quite attractive alternative, although there is not presently a machine capable of producing a spar perimeter as large as that of the OH-58 with $\pm$ 45° fibers. Pultruding appeared to be very cost competitive. The necessity of having straight uniform sections limited its possibilities, however. Configurations 122, 222 and 322 mated a uniform section pultruded afterbody to a slightly tapered spar inboard of station 180. The large amount of development required and the possibility of having to compromise the cross section to facilitate pultruding puts this process in the category of "moderate risk." The other fabrication methods were discarded due to unfavorable cost factors.

Material Properties

Design allowables for metallic parts were derived from MIL-HDBK-5 where necessary. Composite properties orginate with test data obtained from very similar materials and actual fatigue levels attained in the composite AH-1 blade. These data were obtained under severe temperature and humidity conditions. Static properties appear in Table 5 for S-2 fiberglass.

Fatigue properties are shown in Figures 22 and 23 for S- and E-glass. The S-glass values were conservatively used for Kevlar materials also. Critical strain points in the composite AH-1 blade were used to determine an endurance limit point for each material. The Goodman diagram was constructed using the curve shapes from Reference 6 as a guide. The selected points are based on a conservatively determined endurance limit, having experienced no failures, for the AH-1 composite spar. All configurations were sized using these properties.

Structural Requirements

Preliminary stress analysis was performed to define the required structure for the six remaining configurations. The structural requirements are summarized as follows:

- Structural compatibility must be maintained with existing OH-58C/A main rotor hardware. The Bell/Kaman interface is identified at the retention yoke (206-010-102), blade retention bolt (206-010-152) and the blade latch (206-010-121).

- The limit load condition is defined for a 3200-lb helicopter with vertical accelerations of 2.5 G to - .5 G applied as appropriate. Maneuver cases derive from MIL-S-8698.

- A minimum fatigue life of 3600 hours is required. In determining fatigue lives, all material properties are to be documented and validated with considerations made for damage tolerance, thermal effects and environmental effects.

6. McKenzie, F. G., HLH/ATC ROTOR SYSTEM STRUCTURAL SUBSTANTIATION REPORT, Boeing-Vertol Report D301-10227-1, Boeing Company, Vertol Division, Morton, Pennsylvania, July 1973.

TABLE 5. S-2 FIBERGLASS PROPERTIES

	Test Panel	Laminate Layup	Test Direction	-65F Dry Avg	-65F Dry Max	-65F Dry Min	-65F Wet Avg	-65F Wet Max	-65F Wet Min	75F Dry Avg	75F Dry Max	75F Dry Min	75F Wet Avg	75F Wet Max	75F Wet Min	160F Dry Avg	160F Dry Max	160F Dry Min	160F Wet Avg	160F Wet Max	160F Wet Min
TENSION																					
Ultimate Stress, ksi	1	Uni	0°	260	269	248	251	260	243	226	235	222	206	213	197	213	220	206	193	206	187
	10	±45°	0°	42.7	45.3	40.5	38.0	39.3	37.6	27.7	28.0	27.0	20.9	21.4	20.4	21.5	22.0	21.2	12.7	13.1	12.3
	4	Uni	90°	6.12	7.42	5.23	7.37	7.55	7.15	5.75	6.21	5.44	4.60	4.81	4.47	3.77	3.97	3.51	2.08	2.32	1.86
Ultimate Strain, %	1	Uni	0°	3.2	3.3	3.2	3.1	3.2	3.0	3.0	3.3	2.9	2.8	3.2	2.6	3.1	3.2	3.0	2.5	2.6	2.3
	10	±45°	0°	--	--	--	--	--	--	>10	>10	>10	11.0	15.0	10.0	--	--	--	--	--	--
	4	Uni	90°	0.24	0.27	0.21	0.28	0.29	0.28	0.24	0.26	0.22	0.22	0.24	0.21	0.26	0.29	0.23	0.31	0.34	0.28
Initial Modulus, 10^6 psi	1	Uni	0°	8.02	8.14	7.91	8.01	8.35	7.79	7.80	7.99	7.60	7.82	7.97	7.74	7.71	7.77	7.64	7.72	7.94	7.50
	10	±45°	0°	3.80	4.23	3.59	3.63	3.97	3.29	3.33	3.83	2.80	3.18	3.28	3.10	3.30	3.65	2.68	2.38	2.50	2.10
	4	Uni	90°	2.72	3.06	2.30	2.82	2.90	2.64	3.00	3.16	2.87	2.65	2.83	2.48	2.05	2.19	1.86	1.04	1.13	0.98
Poisson's Ratio at 1/3 Ultimate Stress	1	Uni	0°	--	--	--	--	--	--	.251	.260	.243	.268	.270	.266	--	--	--	--	--	--
	10	±45°	0°	--	--	--	--	--	--	.661	.707	.614	.605	.632	.578	--	--	--	--	--	--
	4	Uni	90°	--	--	--	--	--	--	.092	.092	.092	.092	.096	.088	--	--	--	--	--	--
COMPRESSION																					
Ultimate Stress, ksi	3	Uni	0°	104	115	99.2	122	127	116	85.5	90.8	76.9	75.6	84.9	60.9	59.1	64.0	52.1	48.4	53.6	37.9
	10	±45°	0°	25.9	26.9	24.7	25.5	27.2	23.5	19.2	19.6	18.9	14.0	14.8	13.7	11.3	11.9	10.9	8.31	8.64	7.88
	3	Uni	90°	25.4	27.8	23.4	23.8	25.0	23.1	17.8	18.6	17.1	14.2	14.5	13.6	12.2	12.7	11.3	8.99	9.77	8.16
Initial Modulus, 10^6 psi	3	Uni	0°	--	--	--	--	--	--	8.08	8.45	7.60	7.37	7.59	7.04	--	--	--	--	--	--
	10	±45°	0°	--	--	--	--	--	--	3.00	3.17	2.75	--	--	--	--	--	--	--	--	--
	3	Uni	90°	--	--	--	--	--	--	2.42	2.52	2.31	--	--	--	--	--	--	--	--	--
INPLANE(RAIL) SHEAR																					
Ultimate Stress, ksi	3	Uni	0-90°	--	--	--	--	--	--	4.79	5.45	4.35	--	--	--	--	--	--	--	--	--
	9	±45°	0°	--	--	--	--	--	--	37.9	38.1	37.5	--	--	--	--	--	--	--	--	--
	3	Uni	90-0°	9.60	--	--	--	--	--	6.78	7.08	6.25	--	--	--	5.56	5.81	5.19	--	--	--
Modulus at 1/3 Ultimate Stress, 10^6 psi	3	Uni	0-90°	--	--	--	--	--	--	--	--	--	--	--	--	--	--	--	--	--	--
	9	±45°	0°	--	--	--	--	--	--	--	--	--	--	--	--	--	--	--	--	--	--
	3	Uni	90-0°	.800	--	--	--	--	--	.850	.865	.840	--	--	--	.654	.688	.625	--	--	--
FLEXURE																					
Ultimate Stress, ksi	3	Uni	0°	268	283	247	--	--	--	215	233	204	--	--	--	156	162	148	--	--	--
	10	±45°	0°	88.4	91.5	82.4	--	--	--	66.3	71.4	62.2	--	--	--	51.0	51.3	50.2	--	--	--
Initial Modulus, 10^6 psi	3	Uni	0°	6.43	6.76	6.18	--	--	--	6.35	6.60	6.14	--	--	--	6.21	6.42	6.08	--	--	--
	10	±45°	0°	2.64	2.83	2.52	--	--	--	2.33	2.42	2.19	--	--	--	2.17	2.29	2.03	--	--	--
SHORT BEAM SHEAR																					
Ultimate Stress, ksi	3	Uni	0°	10.6	11.1	10.3	11.3	11.8	10.9	7.68	7.87	7.35	7.13	7.21	7.00	6.26	6.45	6.13	4.42	4.56	4.29
	10	±45°	0°	6.85	7.12	6.60	6.34	6.60	6.07	4.43	4.59	4.26	4.20	4.33	4.04	3.48	3.67	3.23	3.04	3.12	2.98

PHYSICAL PROPERTIES				THICKNESS Avg	THICKNESS Max	THICKNESS Min	SPECIFIC GRAVITY Avg	SPECIFIC GRAVITY Max	SPECIFIC GRAVITY Min	RESIN WEIGHT (%) Avg	RESIN WEIGHT (%) Max	RESIN WEIGHT (%) Min	FIBER VOLUME (%) Avg	FIBER VOLUME (%) Max	FIBER VOLUME (%) Min	VOID CONTENT (%) Avg	VOID CONTENT (%) Max	VOID CONTENT (%) Min
	1	Uni	--	.0302	.0308	.0295	1.955	2.009	1.871	20.84	24.43	17.94	64.72	69.08	60.13	4.12	5.41	3.62
	3	Uni	--	.0809	.0846	.0746	1.981	1.996	1.968	19.68	20.34	19.16	66.50	67.20	65.51	3.59	4.12	3.24
	4	Uni	--	.0811	.0846	.0788	1.994	2.017	1.978	19.32	20.27	17.89	67.01	69.08	65.65	3.41	3.88	3.07
	9	±45°	--	.0639	.0647	.0622	1.993	2.009	1.966	20.99	22.32	20.22	64.70	65.77	62.88	2.09	2.29	1.91
	10	±45°	--	.0807	.0867	.0770	1.980	1.996	1.959	21.19	22.83	20.01	64.43	66.06	62.20	2.49	2.74	2.20

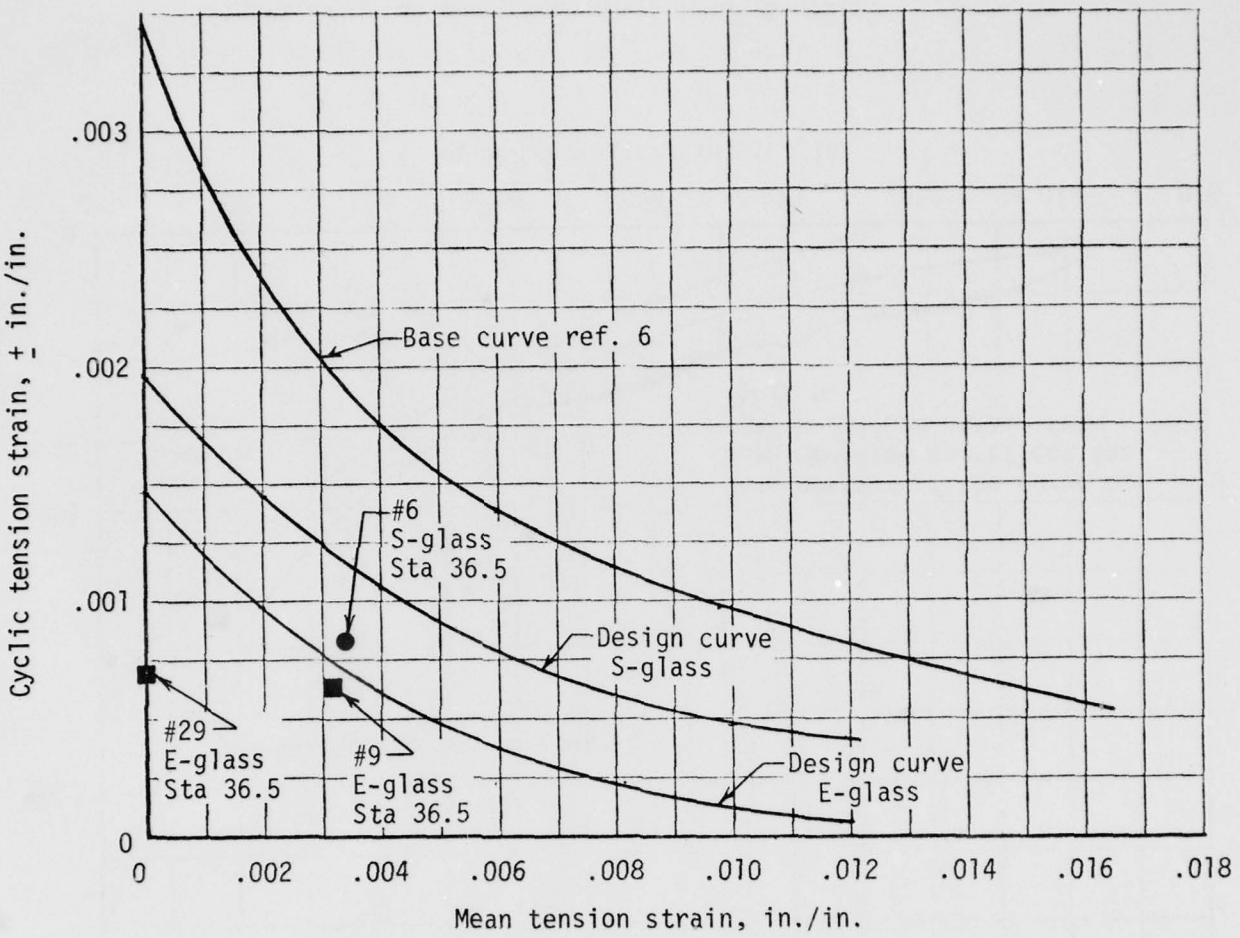

Figure 22. Fatigue properties, uniaxial S- and E-glass.

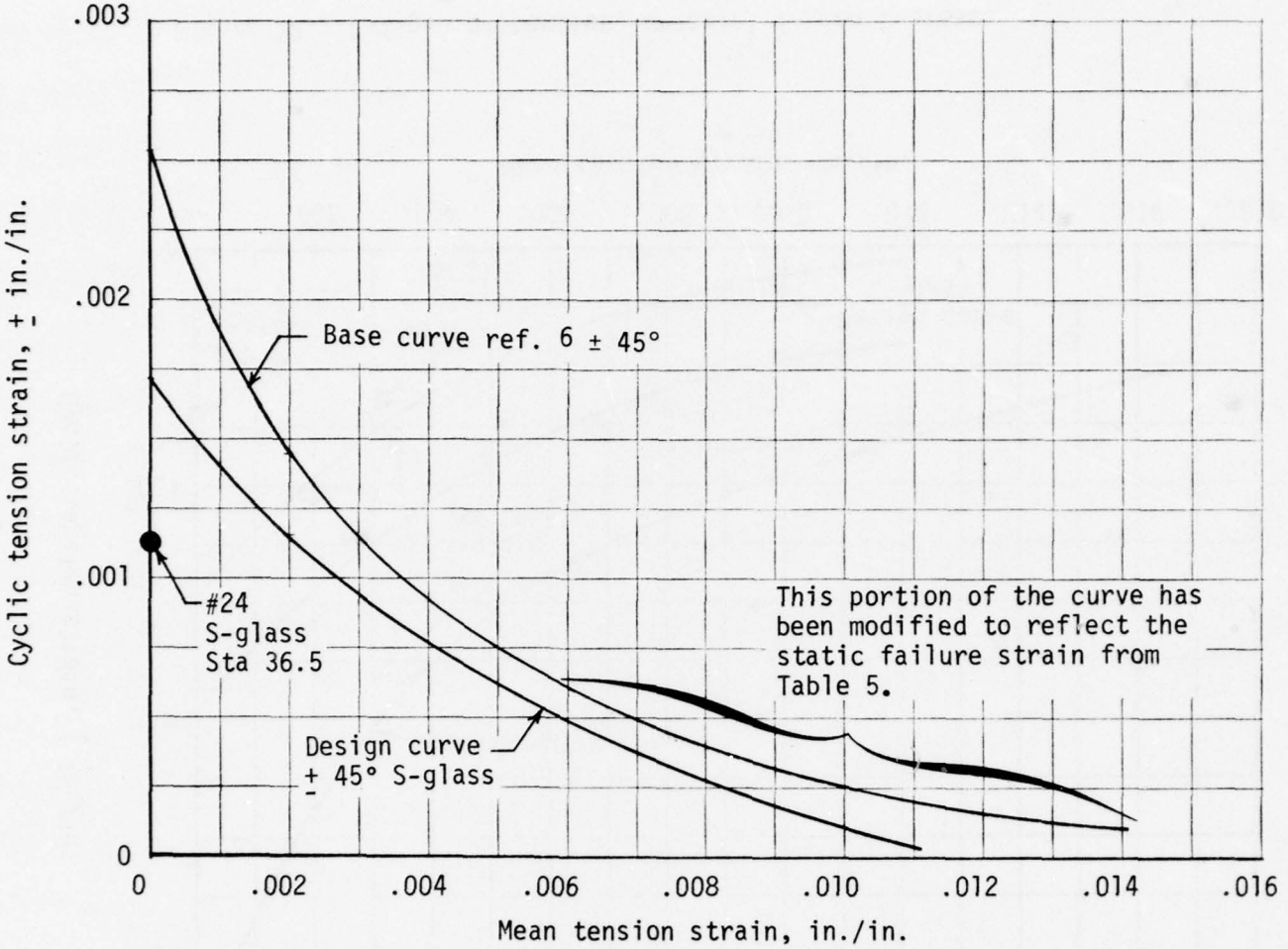

Figure 23. Fatigue properties, ± 45° S-glass.

Static Load Considerations

A review of calculated maneuver load cases in Reference 7 indicated that conditions III and IX were critical for the Kaman blade. Preliminary loads for these cases were determined as follows. For limit beam moment, the values shown on page 2.08 of Reference 8 were adjusted to a 3200-lb GW/ 2.5 G basis by multiplying all values by 2.5/2.34. This results in Figure 24. Since chord moments are affected by tension beam effects due to CG/ neutral axis offsets, they are considered unique to each blade. Therefore, only a drag load, distributed over the outer 3/4 span, was considered for preliminary purposes. The resulting calculated limit chord moment distribution appears in Figure 25. Limit blade torque (pitching moment) was estimated using the limit pitch link load reported in Reference 8 and an estimated moment distribution based on the similar K747 AH-1 blade. The resulting torque distribution is shown in Figure 26. Centrifugal force was calculated for configuration 111 which was first to be completely drawn and weighted. The resulting CF distribution appears in Figure 27. These loads were used in all preliminary static analyses.

Fatigue Load Considerations

It was desired to derive fatigue load criteria which could be used for blade design. Loads thus used must insure that the desired 3600-hour life can be achieved. Therefore, the preliminary fatigue analyses were performed to insure adequate life. The specified flight profiles appear in Tables 6 and 7. To employ a schedule of this type, it must be recognized that calculated life is inversely proportional to the time accrued in accelerated flight maneuvers, resulting in loads above the endurance limit; almost all of the remaining time falls at or below this limit. A breakdown of the flight profile damage appears in Tables 8 and 9.

Preliminary load calculations indicated that blade bending moments are predicted to be somewhat lower. Therefore, a conservative approach is to select fatigue loads from data available in flight strain survey reports (Reference 9). Although the Statement of Work did not specify a forward flight performance objective, it is considered unconservative not to anticipate the possible effects of such an increase. One approach would be to

7. Jordan, G. L., STRUCTURAL DESIGN CRITERIA FOR 206A-1/OH-58A, BHC Report 206-099-200, Bell Helicopter Corporation, Fort Worth, Texas, August 1968.
8. Clinard, R. L., LOAD DETERMINATION AND STRUCTURAL ANALYSIS OF THE 206-011-001-3 MAIN ROTOR HUB AND BLADE ASSEMBLY FOR THE 206A-1 HELICOPTER, BHC Report 206-099-107, Bell Helicopter Corporation, Fort Worth, Texas, January 1969.
9. Martin, Bill, MODEL 206A-1 CERTIFICATION FLIGHT LOAD SURVEY, VOLUME II OF VI, BHC Report 206-194-062, Bell Helicopter Corporation, Fort Worth, Texas, April 1969.

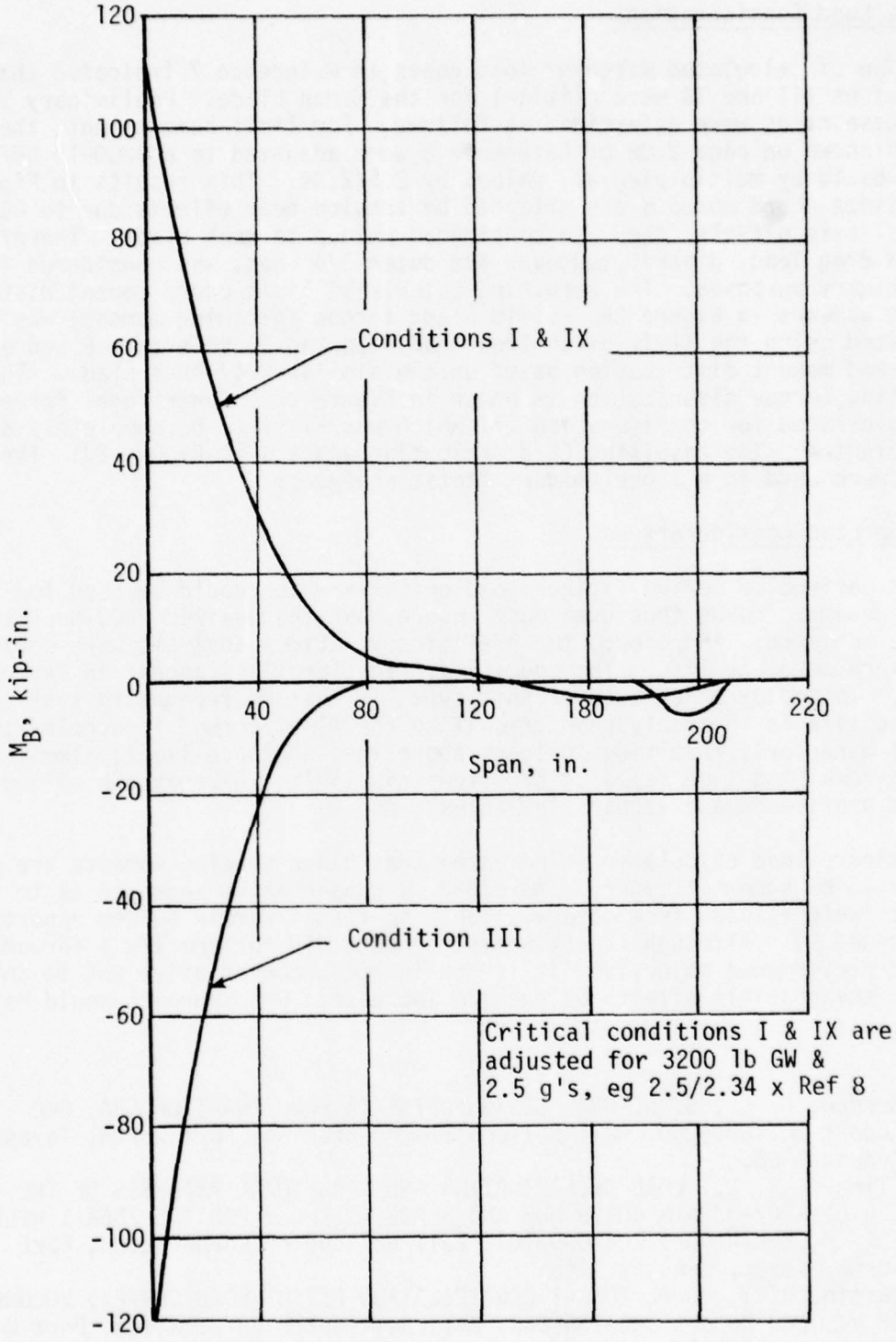

Figure 24. Limit beam moment distribution.

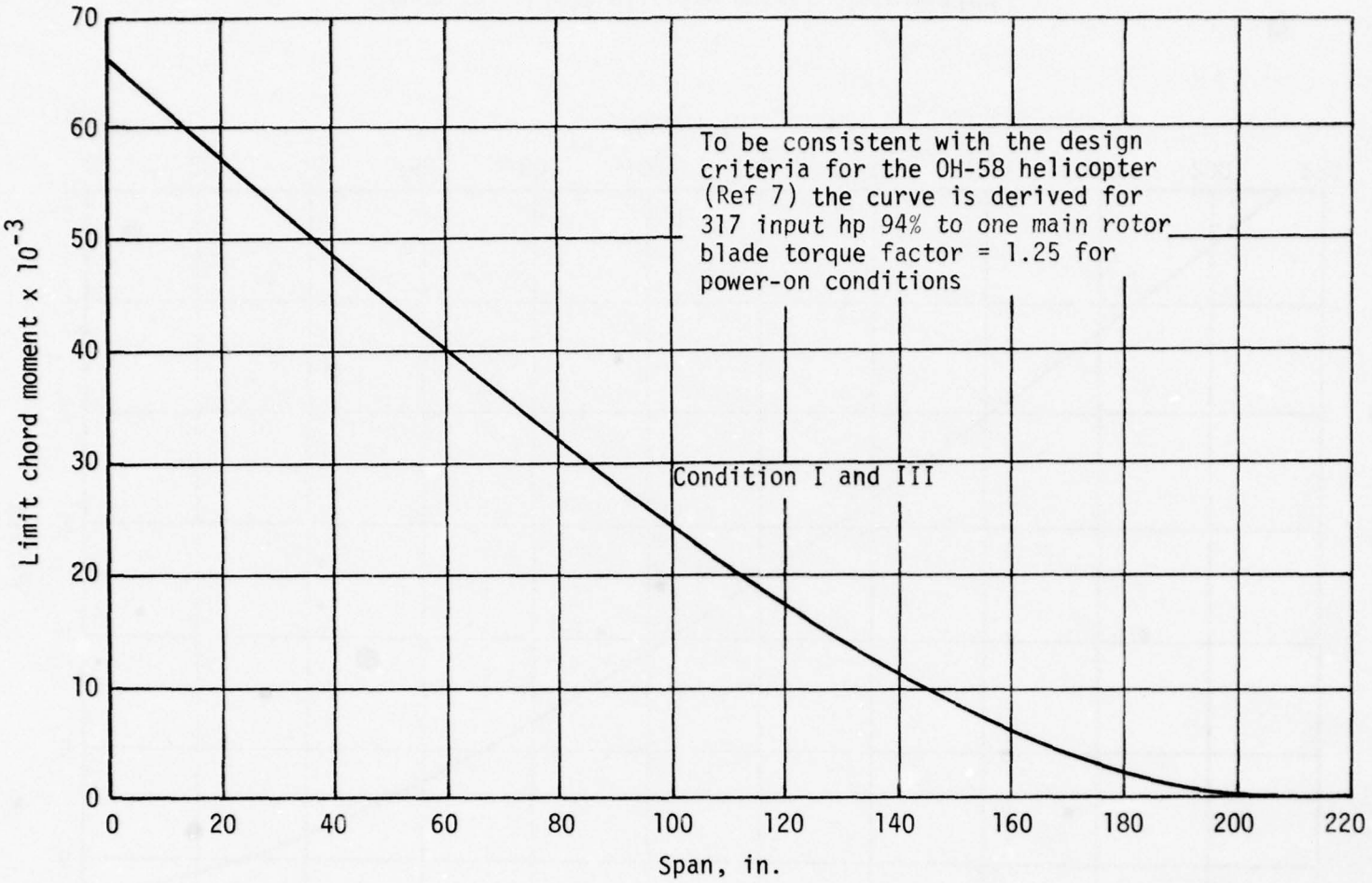

Figure 25. OH-58 limit chord moment.

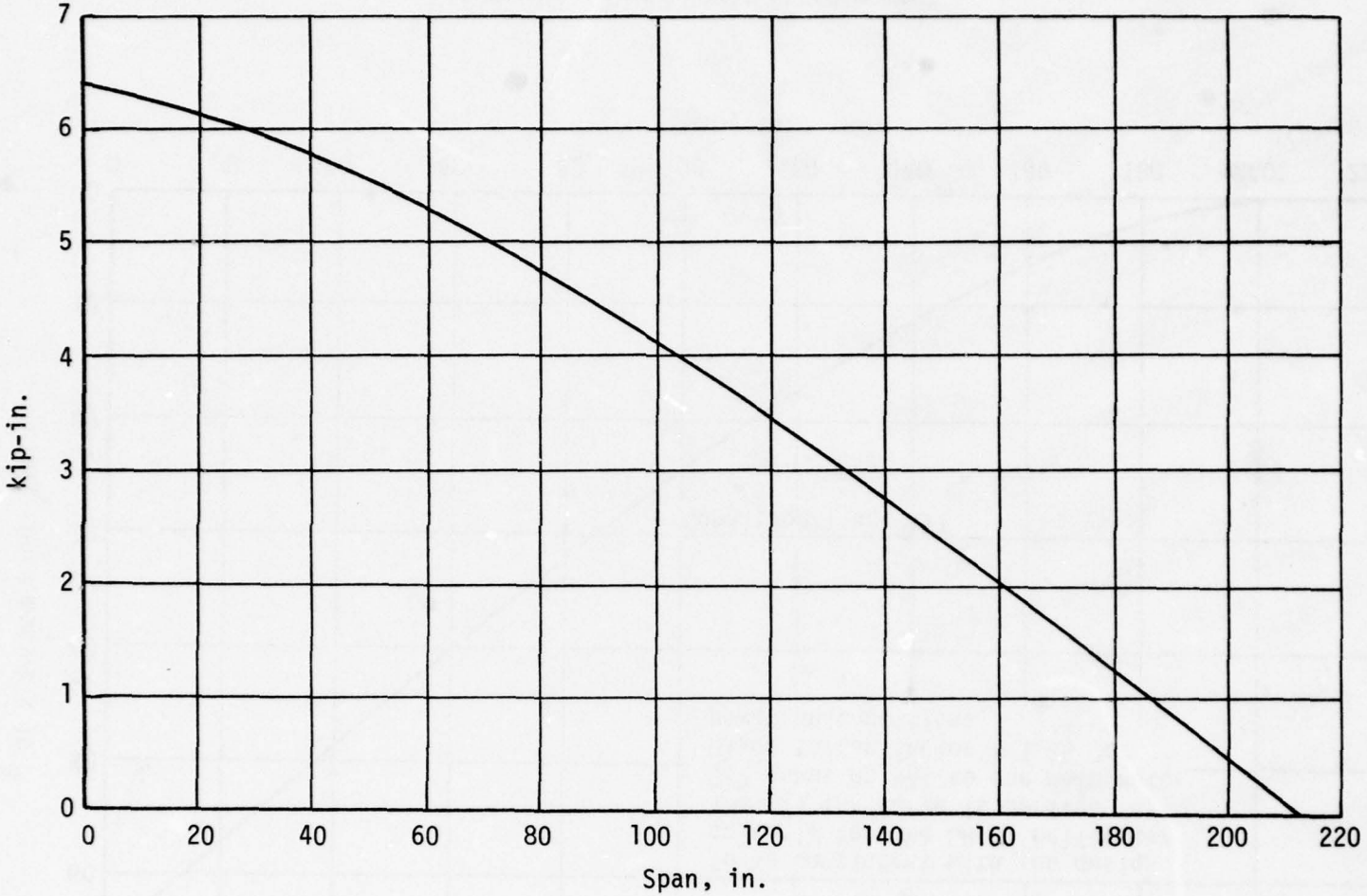

Figure 26. Limit pitching moment distribution.

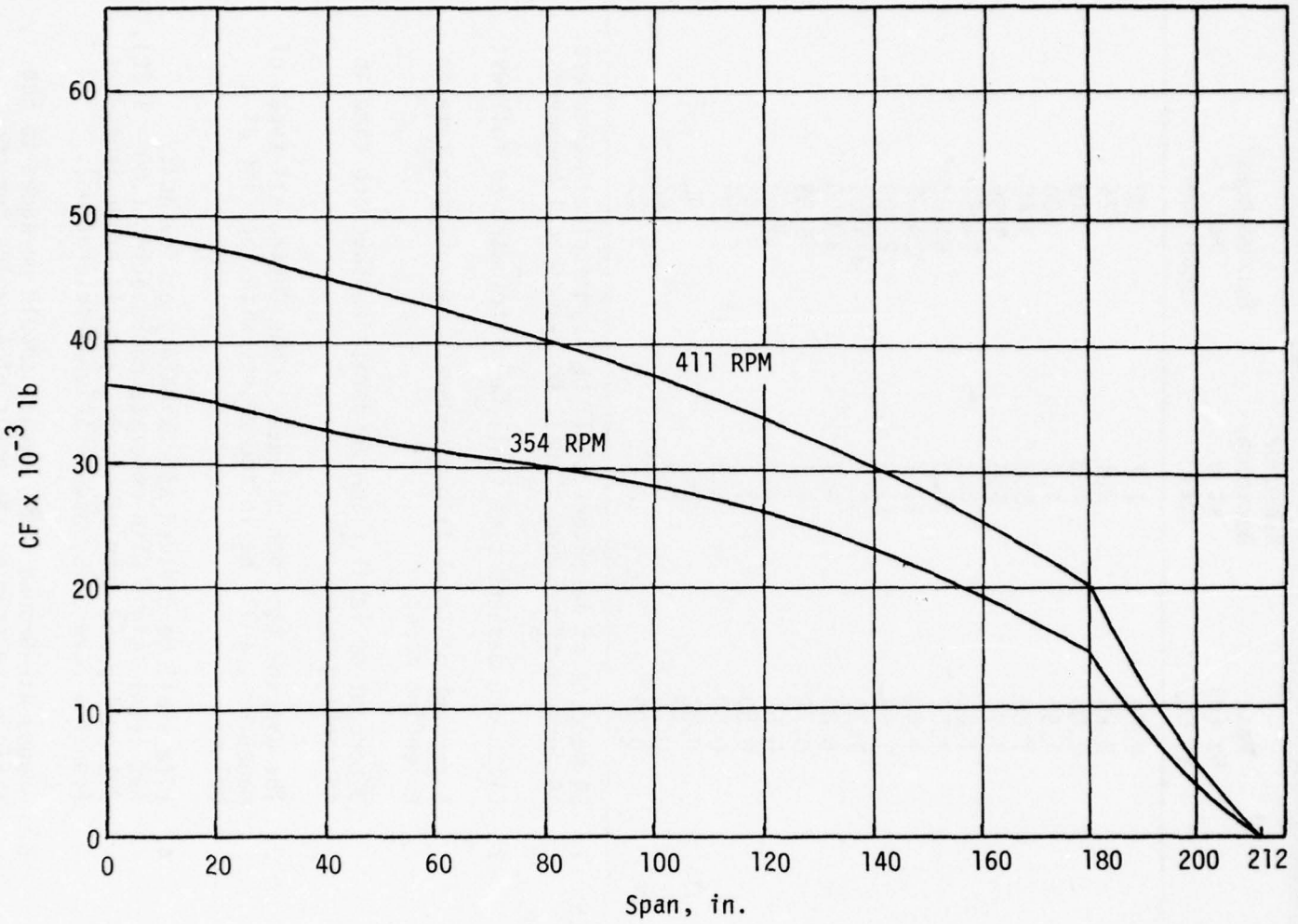

Figure 27. Preliminary calculated CF distribution.

TABLE 6. FLIGHT PROFILE

Peak Nz (g) at CG	Maneuver Duration at g (Sec)	Exceedances per 3600 Hours
2.50	1.7	90
2.25	2.8	225
2.00	4.0	819
1.90	4.7	1800
1.80	5.6	3748
1.70	6.6	9999
1.60	8.2	24997
1.50	10.0	64287
1.40	11.1	128565
1.30	11.7	225000
1.20	12.2	374985
0.80	4.7	45000
0.70	4.1	6133
0.60	3.5	1363
0.50	3.1	643
0.40	2.8	207
0.30	2.6	90
0.20	2.3	42
0.00	2.0	20

NOTES:

1. 64 percent of maneuvers shall be asymmetrical maneuvers. 36 percent of maneuvers shall be symmetrical maneuvers.

2. Climb and descent time shall be distributed as follows:

   5 percent of level flight/moderate maneuvering time in ascending mode.

   8 percent of level flight/moderate maneuvering time in descending mode.

3. The average time per maneuver, considering all types of maneuvers, shall be in accordance with the time at g column.

4. Life shall be divided approximately as follows: 69% level flight with moderate maneuvering (.80 - 1.20), 20% pullup and turn maneuvers, and 11% other maneuvers (control reversals, acceleration/deceleration).

5. Ground-Air-Ground (GAG) cycles should be added to the fatigue spectrum on the basis of 4 cycles per hour.

TABLE 7. EXCEEDANCE PER 3600 HOURS

%VH	N_Z = 2.50	N_Z = 2.00	N_Z = 1.75	N_Z = 1.50	N_Z = 1.40	N_Z = 1.30	N_Z = 1.20
110			4	40	72	139	243
100		4	22	144	261	508	972
90		27	90	441	981	2043	8523
80	18	85	301	1228	3316	7146	15003
70	18	189	715	4725	8304	11749	18846
50	60	292	985	7249	12978	20952	34326
30	18	198	2569	25875	43006	58707	86022
20		18	1210	20340	37039	69543	95760
10		4	99	4243	22707	54211	115200
TOTAL	114	819	5998	64287	128565	225000	374985

TABLE 8. TIME DISTRIBUTION

Time	Condition	N_Z (Range)	Load Cond
69% 48.710	Level Flight	.8 - 1.2	1 (E.L.)
69% 20.29	Climb and Descent Mod Maneuver	1.3	1.08
11% 6	Control Reversals	1.3	1.08
11% 5	Accelerations/ Decelerations	1.4	1.17
.501	Pull-Ups and Push-Overs	1.3	1.08
9.523		1.4	1.17
6.5424	Asymmetrical Maneuvers (64%) Left & Right	1.5	1.25
2.086		1.6	1.33
.6716		1.7	1.42
20% .2136	Symmetrical Maneuvers (36%)	1.8	1.5
.0861		1.8	1.5
.03339		1.9	1.58
.00641		2.0	1.67
.0015		2.5	2.08
.33447		.6	--
100%			

TABLE 9. FLIGHT PROFILE SUMMARY

N_Z	Duration	Exceedances/ 3600 HR	Time (sec)	5.9 Cy/sec Cys 1/Rev	% Time
2.5	1.7	90	150.0	902.7	.0015
2.25	2.8	225	630.0	3,717.0	.00641
2.0	4.0	819	3,276.0	19,328.4	.03339
1.9	4.7	1,800	8,460.0	49,914.0	.0861
1.8	5.6	3,748	20,988.8	123,833.9	.2136
1.7	6.6	9,999	65,993.4	389,361.1	.6717
1.6	8.2	24,997	204,975.4	1,209,354.9	2.086
1.5	10.0	64,287	642,870.0	3,792,933.0	6.5425
1.4	11.1	128,565	1,427,071.5	8,419,721.9	14.523
1.3	11.7	225,000	2,632,500.0	15,531,750.0	26.791
1.2	12.2	374,985	4,574,817.0	26,991,420.3	46.558
.8	4.7	45,000	211,500.0	1,247,850.0	2.152
.7	4.1	6,133	25,145.3	148,357.0	.256
.6	3.5	1,363	4,770.5	28,149.9	.0485
.5	3.1	643	1,993.3	11,760.5	.0203
.4	2.8	207	579.6	3,419.6	.0059
.3	2.6	90	234.0	1,380.6	.00238
.2	2.3	42	96.6	569.9	.0098
0	2.0	20	40	236.0	.00041

proportion all documented beamwise loads by the 3200/3000 thrust increase ratio. This would have been consistent with Figure 24. Another approach would be to consider that a higher forward speed coupled with intermediate gross weights usually results in higher beam and chord bending moments. Accordingly, data was selected from Reference 9 for 124 knots (V_H) and 3000 lb GW, CG location at 112.1 inches and 6000 ft density altitude. These curves were extrapolated to 130 knots using the prevailing curve end-slope. This approach yielded higher load magnitudes than the use of 3200/3000 thrust ratio on the same data. Fatigue loads thus generated appear in Figures 28 and 29. Steady and vibratory blade torques (pitching moments) were derived from the corresponding extrapolated pitch link load, Figure 30.

Using this condition as an endurance limit level with a life of 100×10^6 cycles, a conservative estimate of blade life for all configurations may be determined using the S-N curve in Figure 31 which originates in Reference 10. The damage summation and resulting calculated life is shown in Table 10 as a minimum value of 4703 hours.

Performance

Since all six configurations could attain the desired performance, no trade-off distinction was made among them and a perfect score (9) was assigned to each.

Reliability and Maintainability

As a preliminary step for decision-making purposes, a ranking procedure was used considering the overall reliability and maintainability objectives. These objectives are summarized in Table 11. The results of this qualitative ranking appear in Table 12. The only significant variation appears for Maintenance Man-Hour/Flight Hour which is dependent on the number of mechanical joints to inspect and maintain. Thus, configuration 322, which has a drag-brace and molded tip pieces, has a low score. No score (0) was given if it was judged that an objective could not presently be met.

Radar Reflectivity

From Kaman's experience with the AH-1 composite blade, it was concluded that any of the six candidate configurations could be modified to a minimum radar signature which would be approximately the same. Therefore, an arbitrary score of 7 was assigned to each.

10. Hardersen, C. P., FINAL STRESS ANALYSIS OF K747 MAIN ROTOR BLADE FOR AH-1Q/S HELICOPTER, Kaman Report S230-1, Kaman Aerospace Corporation, Bloomfield, Connecticut, June 1977.

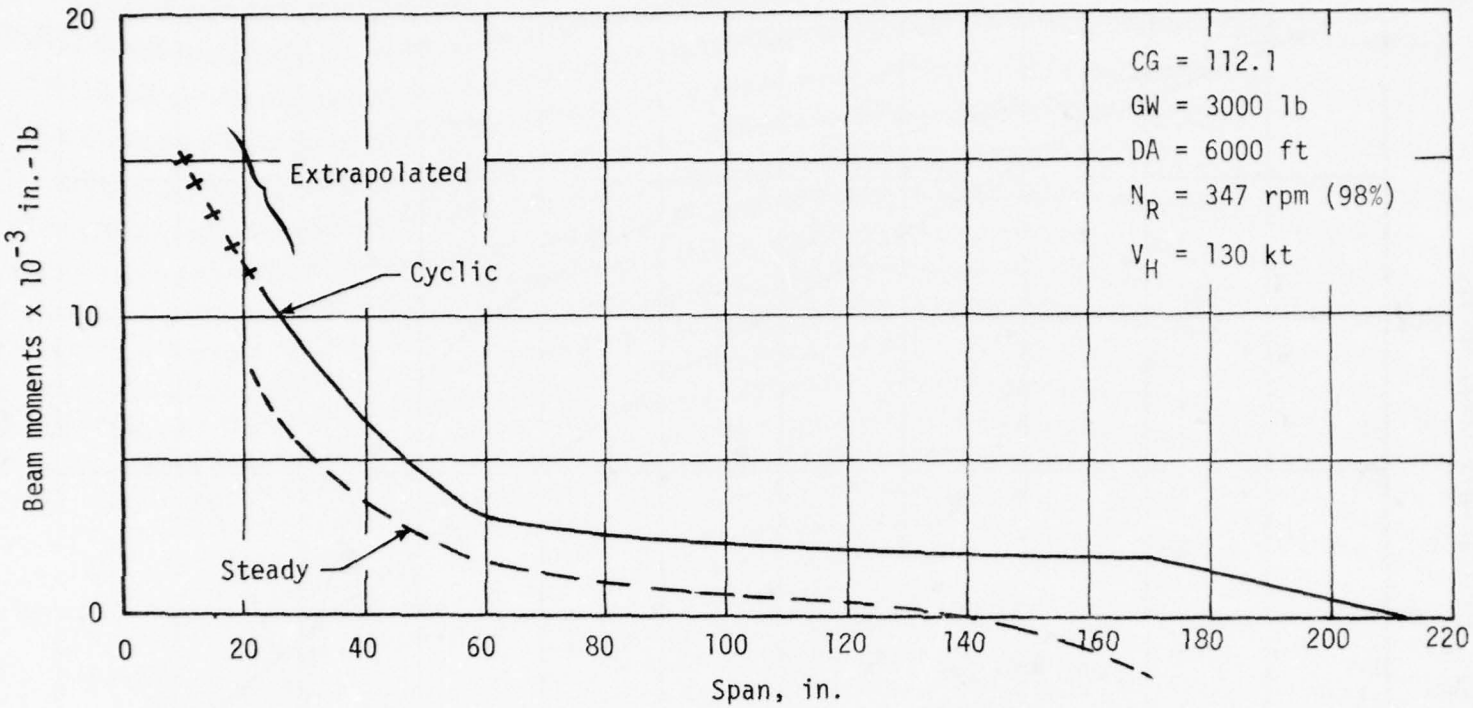

Figure 28. OH-58 beam moment distribution, forward flight.

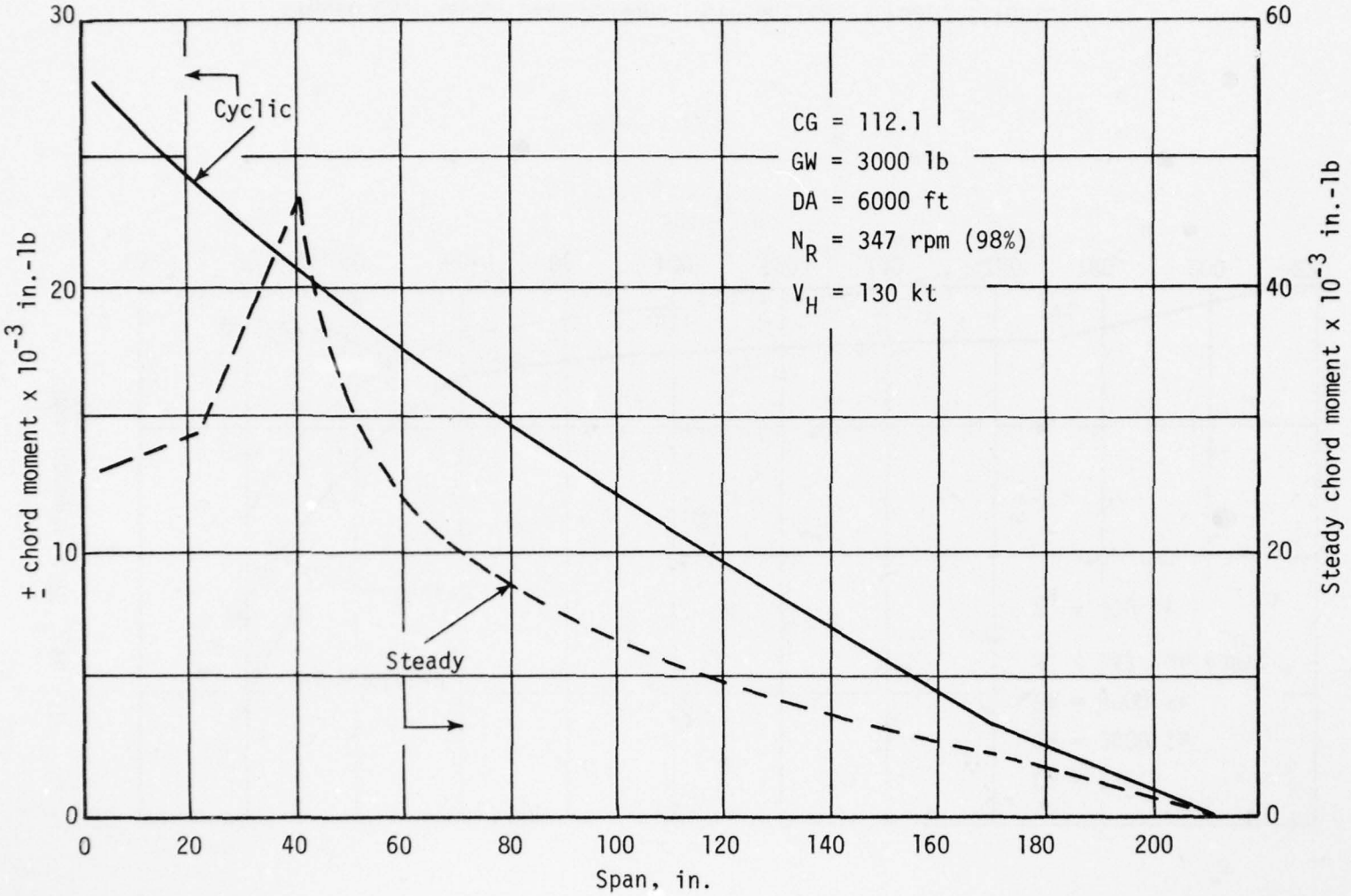

Figure 29. OH-58 chord moment distribution vs span.

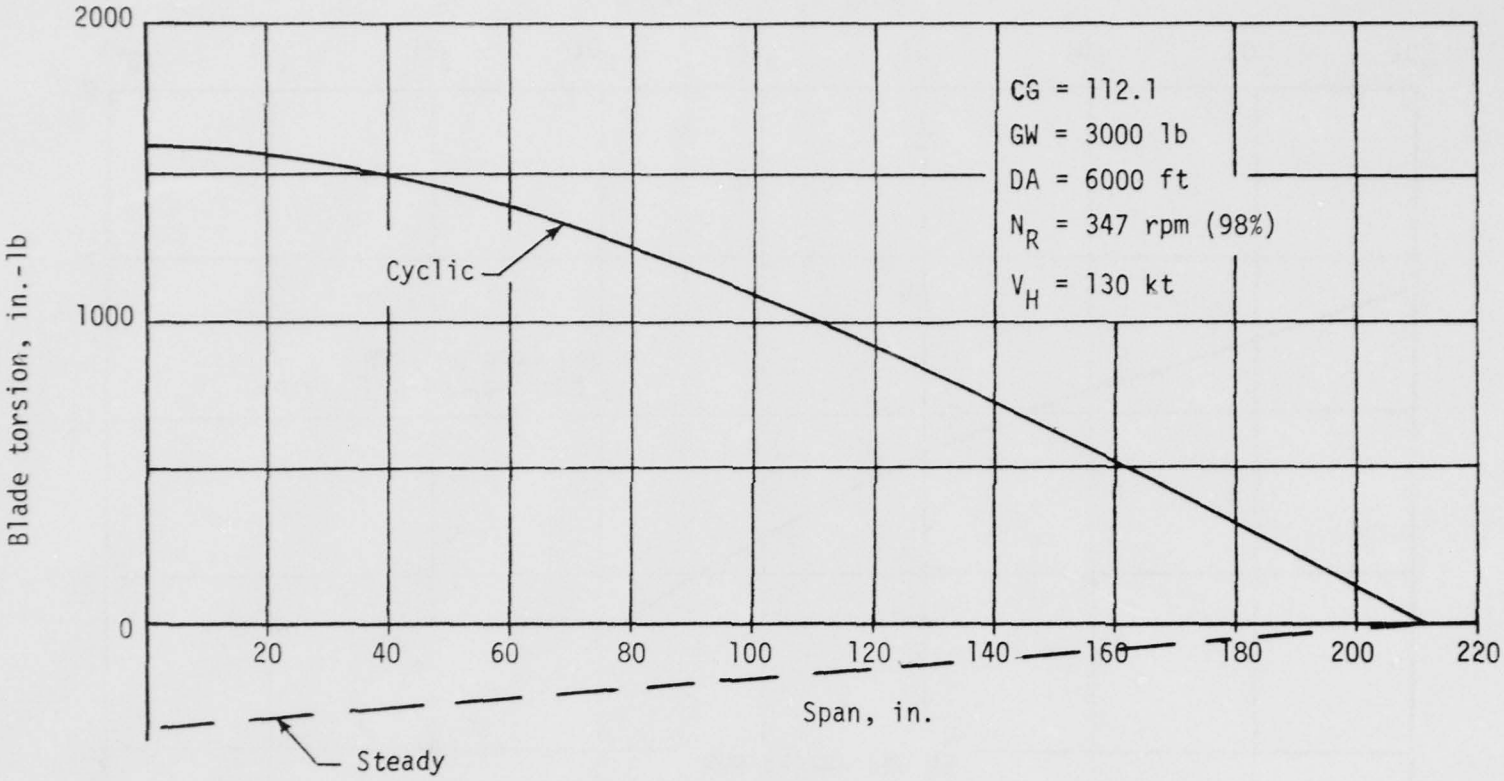

Figure 30. OH-58 pitching moment distribution.

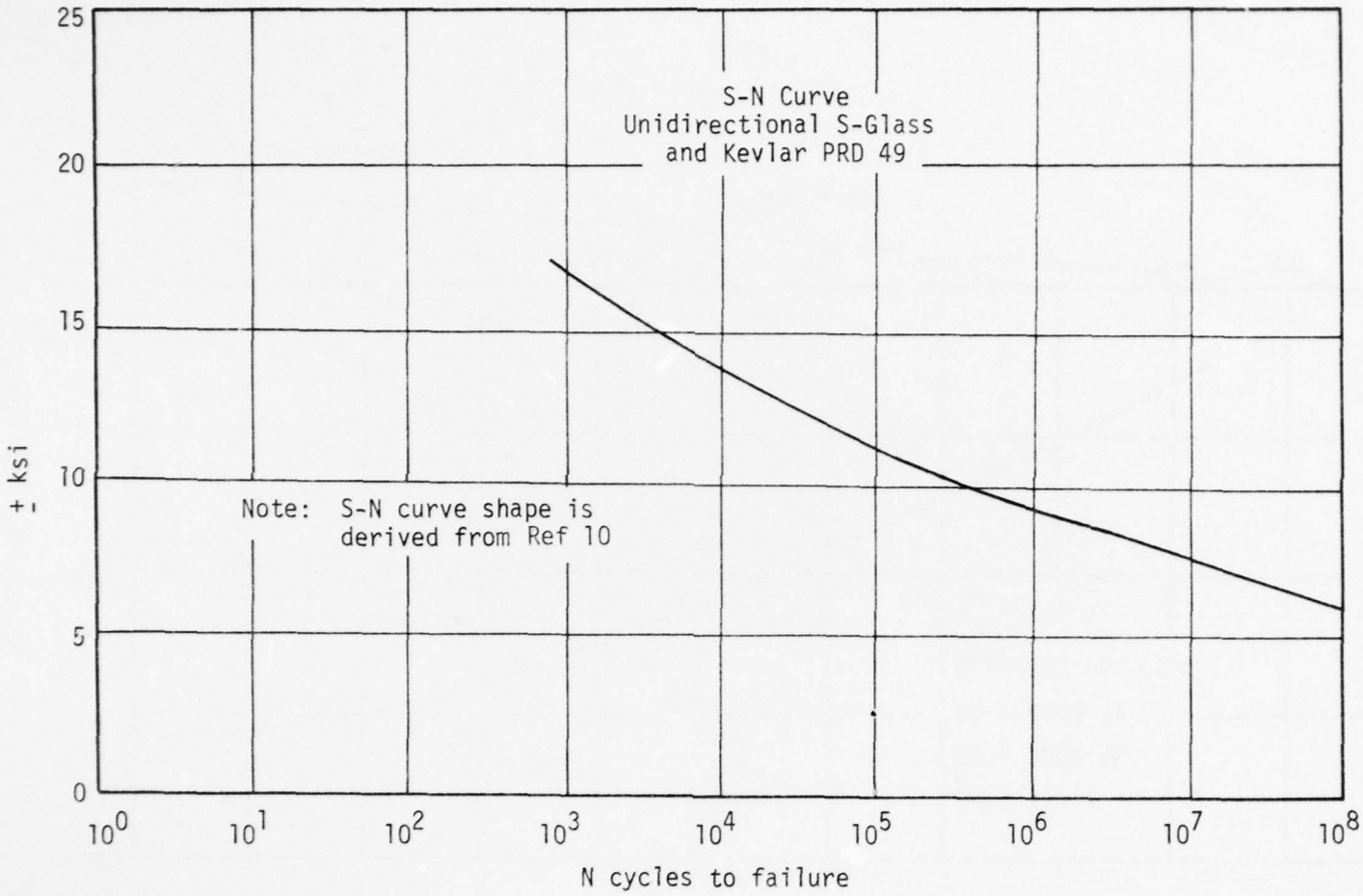

Figure 31. S-N curve composite blade.

TABLE 10. LIFE CALCULATION

% Time	Endurance Limit Multiplier*	Damage Cycles/Hr n	Life at Load N	n/N
48.71	1	10346.0	100×10^6	
26.791	1	5690.4	100×10^6	
14.523	1	3084.7	100×10^6	
6.5425	1	1389.6	100×10^6	
2.086	1	443.06	100×10^6	.0002116
.672	1	142.6	100×10^6	
.2136	1	45.4	100×10^6	
.0861	1	18.3	100×10^6	
.03339	1.053	7.2	55×10^6	.00000013
.00641	1.1842	1.36	13×10^6	.00000011
.00151	1.316	.32	5×10^6	.00000006
.33447	1	71.0	100×10^6	.00000071
100.				.00021261

L = 4703 hr

*A study of Reference 9 indicates that critical cyclic beam moments do not exceed the V_H condition up to g levels of 1.9 g and down to -.5 g. Therefore, the multiplier is calculated as Nz/1.9.

TABLE 11. RELIABILITY AND MAINTAINABILITY OBJECTIVES

Reliability

1. FSR $\geq$ .999998
2. 90% Ps Surviving inherent failure modes for 3600 hours
3. MTBUM Due to inherent failures $\geq$ 1500 hours

Maintainability

1. MMH/FH $\leq$ .01 man-hour/flight hour
2. 95% Pc Field level repairs in 3 hours
3. Pr Probability of repair required above field level $\leq$ 20%
4. Minimum tools
5. Skill levels per Army 67N20 MOS personnel
6. "On Aircraft" repairs desired
7. Single repair kit desirable/repair task
8. Repairability compatible with field level tools for 7.62mm API damage
9. Spar repairability desired (it is likely that items 3 and 8 above would not be met)

TABLE 12. RANKING OF RELIABILITY AND MAINTAINABILITY OBJECTIVES

Item	Configuration					
	111	211	311	122	222	322
R1	10	10	10	10	10	10
R2	10	10	10	10	10	10
R3	10	10	10	10	10	10
M1	7	10	6	6	9	5
M2	10	10	10	--	--	--
M3	10	10	10	10	10	10
M4	10	10	10	--	--	--
M5	10	10	10	10	10	10
M6	9	10	9	9	10	9
M7	10	10	10	10	10	10
M8	10	10	10	--	--	--
M9	10	10	10	10	10	10
ΣI =	116	120	115	85	89	84
$\Sigma I/12 \times 8$ =	7.73	8.00	7.67	5.67	5.93	5.60

Ballistic Survivability

Preliminary estimates of a 23mm API threat damage to the six configurations were the basis for comparison. A kill probability (P_K) was calculated for each candidate based on the threat-zone partitioning shown in Figure 32. A score was assigned inversely proportional to the lowest P_K of the group for decision-making purposes. Table 13 presents comments relative to the ballistic properties of each configuration. Table 14 provides the preliminary dimensional parameters needed for calculation purposes. Table 15 lists element kill probabilities, and Table 16 summarizes the overall kill probability and effective score.

Cost

Preliminary cost estimates were performed on the six configurations. The relative cost results appear in Table 17 for one blade of 3000 in constant 1976 dollars.

Trade Study Results

Table 18 presents the trade study results. The two top scoring configurations, 111 and 211, were completed in layout detail and are illustrated in Figures 33 and 34 and Figures 2 and 3. Configuration 111 was of particular interest because it is somewhat similar to the present AH-1 composite blade. However, sever requirements are imposed on the aluminum adapter root-fitting in the case of the OH-58. This is due to two factors: the requirement to react edgewise bending moments and the requirement to accommodate blade twist locally at the root end. These increased the weight complexity and cost. Pultruded afterbodies appear to offer lower costs; however, the increased weight and higher development risk militated against their selection at this time. Configuration 211 is clearly the winner by virtue of its simplicity, low cost, low weight and ballistic survivability. As indicated, the configuration number has been replaced with the Kaman 757 designation.

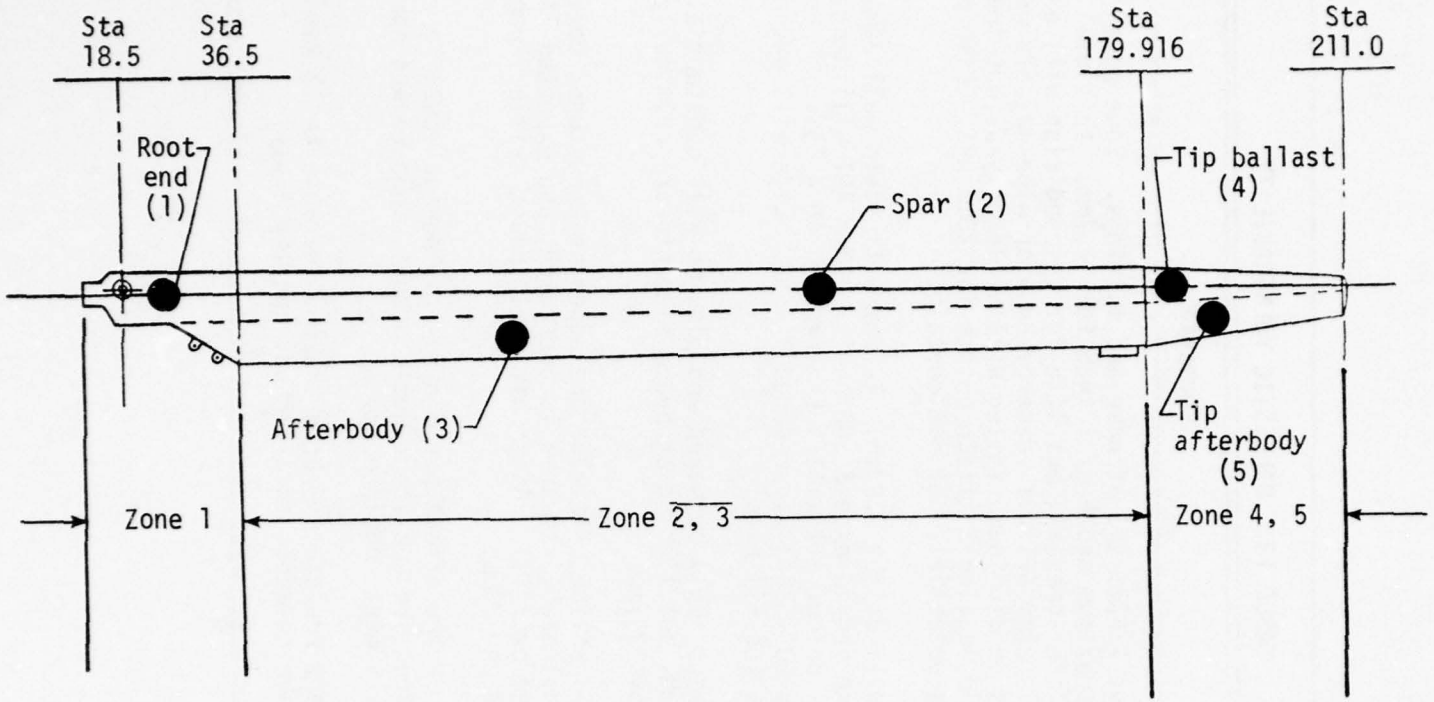

Figure 32. Threat zones.

TABLE 13. BALLISTIC VULNERABILITY

Config	Comments
111	Will defeat 7.62mm API at nose and fittings. Some nose damage to maximum depth of 1 inch for 12.7mm. This will decrease life somewhat, but life for V_H condition will exceed 500 hours. 23mm API will destroy nose or wipe out aft wall. Outer ears on aluminum fitting will be destroyed, but inner should hold leaving 3 attach points for 23mm API. Life of 30 minutes is potential, but not certain.
211	The nose will defeat 7.62mm. 12.7mm will yield wall damage but V_H life should exceed 500 hours. 23mm API will destroy nose and wipe out aft wall. EI_F reduced 10 - 15%; GJ reduced 20 - 30%; EI_C reduced 3 - 5%. Life will exceed 30 minutes for all hits.
311	Same comments apply outboard and pinwrap will substantially defeat 22mm, but light drag brace elements are critically defeated by 12.7mm.
122	Since A.B. provides flatwise and edgewise structure, more critical vulnerability area is presented, and expected lives are reduced over 111. A tip hit could cause critical unbalance for 12.7mm and 23mm.
222	Afterbody damage effect per above - tip damage could be critical since destructive unbalance would occur. Inboard and spar would easily meet requirement.
322	Pinwrap very resistant - Drag brace vulnerable to 12.7mm and 23mm. Above comments on afterbody and tip apply.

TABLE 14. BLADE SEGMENT DIVISIONS

Dimension	Span Segment d_1	Span Segment $d_{2,3}$	Span Segment d_4
a_{AVG}	8	6.509	3.826
b_{AVG}	---	7.145	5.549
C	8	13.654	9.375
a/C	1	.477	.408
b/C	---	.523	.592
S	200	200	200
d_1	25.5		
$d_{2,3}$		143.5	
d_4			31
d_1/S	.1275		
$d_{2,3}/S$		.7175	
d_4			.155

TABLE 15. ESTIMATED KILL PROBABILITY (P_K) DISTRIBUTION FOR 23mm API

Impact Angle	Chd Section	111			211			311			122			222			322		
		d_1	$d_{2,3}$	d_4	d_1	$d_{2,3}$	d_4	d_1	$d_{2,3}$	d_4	d_1	$d_{2,3}$	d_4	d_1	$d_{2,3}$	d_4	d_1	$d_{2,3}$	d_4
0°	a	.20	.05	.02	.10	.05	.02	.15	.05	.02	.20	.05	.02	.10	.05	.02	.15	.05	.02
0°	b	---	.01	.02	---	.01	.02	---	.01	.02	---	.02	.02	---	.02	.02	---	.02	.02
45°	a	.15	.02	.01	.08	.02	.01	.12	.02	.01	.15	.02	.01	.08	.02	.01	.12	.02	.01
45°	b	---	.01	.01	---	.01	.01	---	.01	.01	---	.02	.02	---	.02	.02	---	.02	.02
90°	a	.01	.01	.01	.01	.01	.01	.01	.01	.01	.01	.01	.01	.01	.01	.01	.01	.01	.01
90°	b	---	.01	.01	---	.01	.01	---	.01	.01	---	.02	.05	---	.02	.05	---	.02	.05
135°	a	.15	.02	.02	.08	.02	.02	.30	.02	.02	.15	.05	.05	.08	.05	.05	.30	.05	.05
135°	b	---	.01	.02	---	.01	.02	---	.01	.02	---	.02	.05	---	.02	.05	---	.02	.05
180°	a	.20	.05	.02	.10	.05	.02	.5	.05	.02	.20	.08	.06	.10	.08	.06	.50	.08	.06
180°	b	---	.01	.02	---	.01	.02	---	.01	.02	---	.02	.06	---	.02	.06	---	.02	.06

TABLE 16. P_K SUMMARY FOR ALL CONFIGURATIONS

Configuration	Span Segment	0°	45°	90°	135°	180°	P_C	% P_K	Ranking Score
111	d_1	.2	.15	.01	.15	.2	.12525		
	$d_{2,3}$	.02908	.01477	.01	.01477	.02908	.017155		
	d_4	.02	.01	.01	.02	.02	.015	3.0603	$\frac{2.324}{3.0603} \times 6 = 4.56$
211	d_1	.10	.08	.01	.08	.10	.0675		
	$d_{2,3}$	.02908	.01477	.01	.01477	.02908	.017155		
	d_4	.02	.01	.01	.02	.02	.015	2.324	$\frac{2.324}{2.324} \times 6 = 6.0$
311	d_1	.15	.12	.01	.20	.25	.18875		
	$d_{2,3}$	.02908	.01477	.01	.01477	.02908	.017155		
	d_4	.02	.01	.01	.02	.02	.015	3.87	$\frac{2.324}{3.87} \times 6 = 3.6$
122	d_1	.2	.15	.01	.15	.20	.1275		
	$d_{2,3}$	.03431	.02	.01523	.03431	.04862	.02775		
	d_4	.02	.01523	.03092	.05	.06	.034038	4.144	$\frac{2.324}{4.144} \times 6 = 3.37$
222	d_1	.1	.08	.01	.08	.1	.0675		
	$d_{2,3}$	.03431	.02	.01523	.03431	.04862	.02775		
	d_4	.02	.01523	.03092	.05	.06	.03404	3.379	$\frac{2.324}{3.38} \times 6 = 4.125$
322	d_1	.15	.12	.01	.3	.5	.18875		
	$d_{2,3}$	.03431	.02	.01523	.03431	.04862	.02775		
	d_4	.02	.01523	.03092	.05	.06	.03404	4.925	$\frac{2.324}{4.9252} \times 6 = 2.83$

TABLE 17. BLADE RELATIVE COSTS - NO DEICING OR TUNING PROVISIONS					
111	122	211	222	311	322
4340.88	4273.65	3295.84	3274.83	4340.88	4273.65

TABLE 18. FINAL RANKING SUMMARY							
	111	211	311	122	222	322	Perfect Score
L. C. C.	7.8	10	7.8	7.9	10	7.9	10
Performance	9	9	9	9	9	9	9
Reliability/ Maintainability	7.7	8	7.7	5.7	5.9	5.6	8
Radar Reflectivity	7	7	7	7	7	7	7
Ballistic Survivability	4.6	6	3.6	3.4	4.1	2.8	6
	36.1	40	35.1	33	36	32.3	40

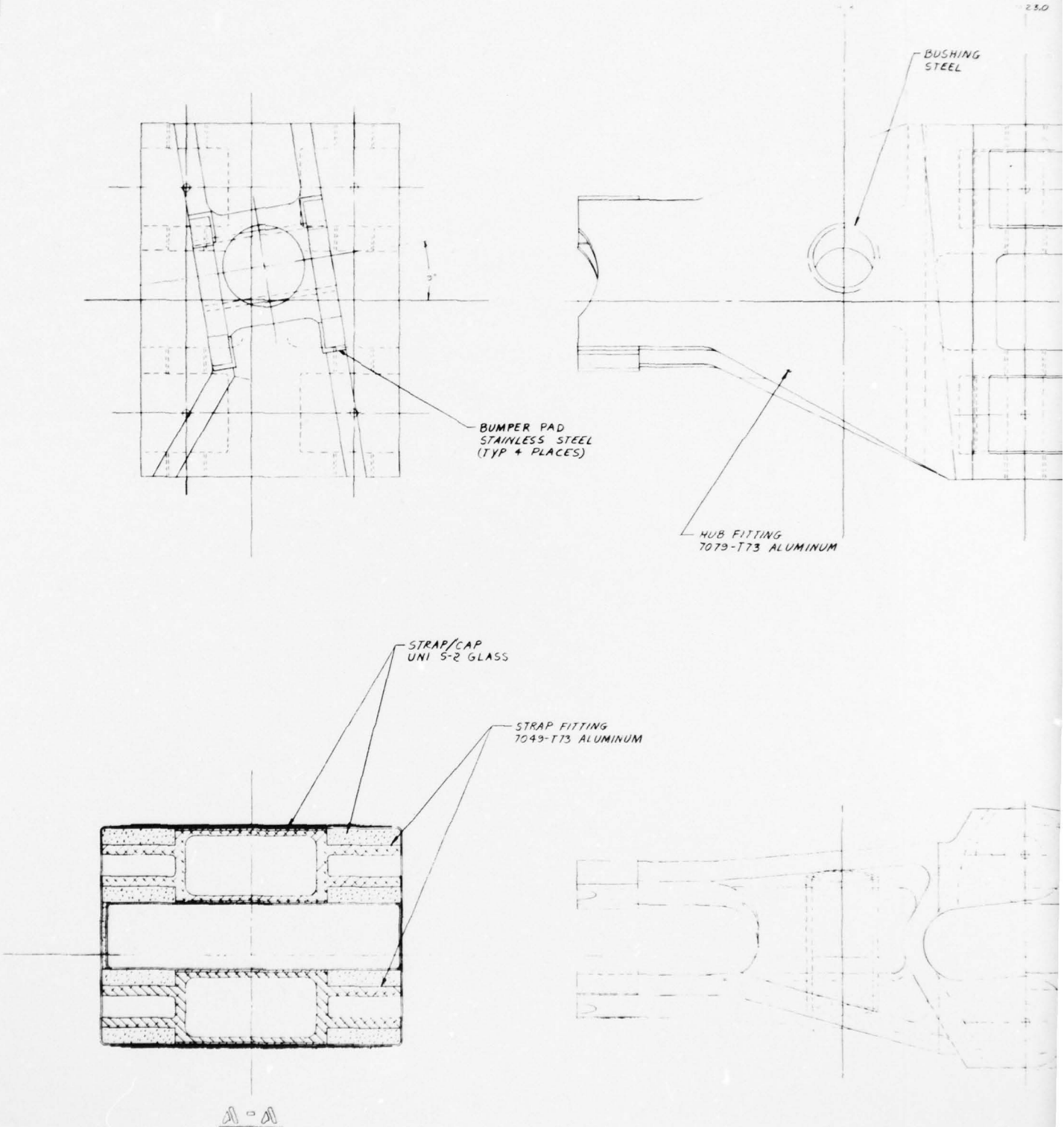

Figure 33. Root end details - configuration III.

2-1

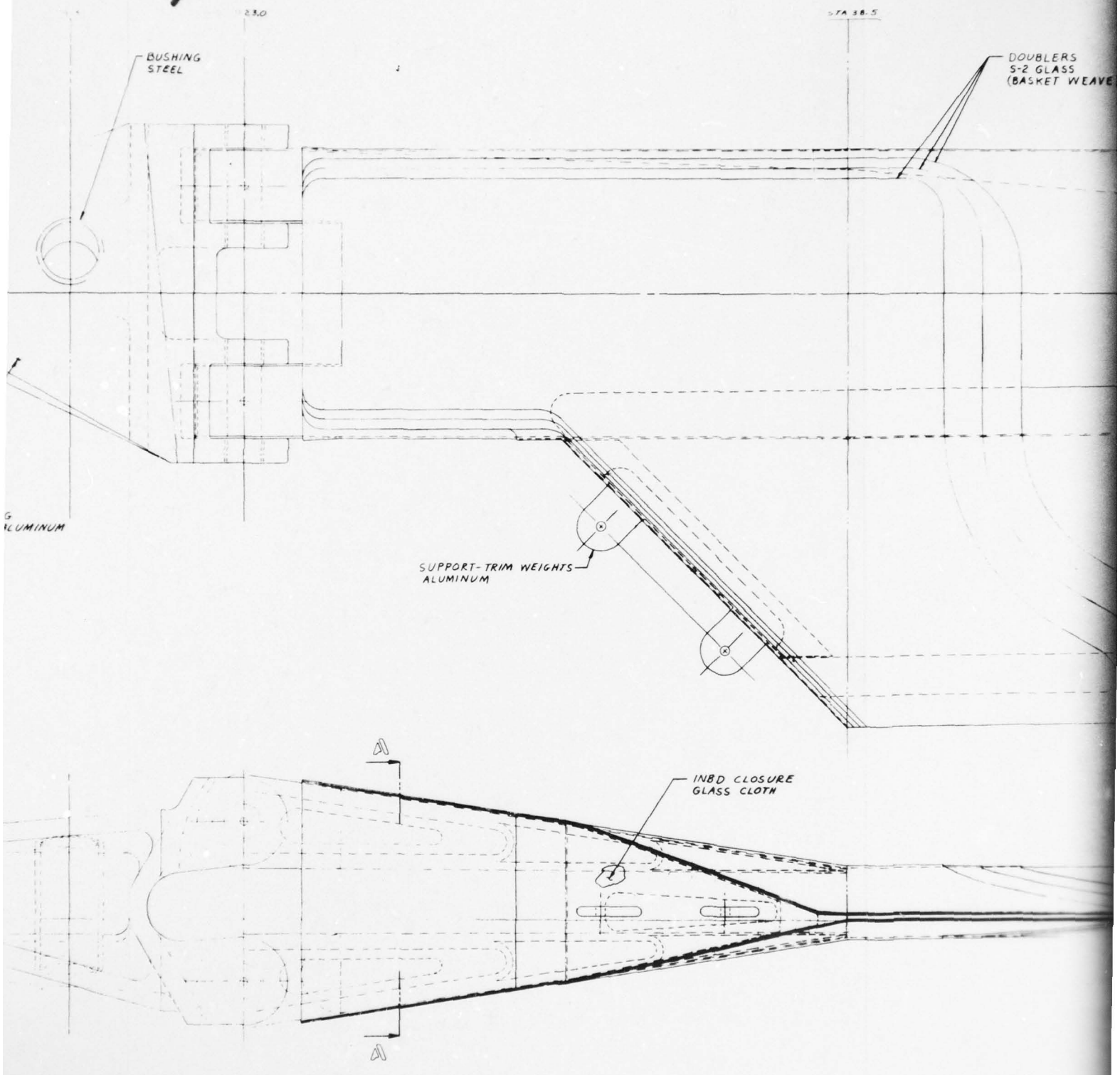
BUSHING
STEEL
DOUBLERS
S-2 GLASS
(BASKET WEAVE)
SUPPORT-TRIM WEIGHTS
ALUMINUM
INBD CLOSURE
GLASS CLOTH

AD-A064 159 KAMAN AEROSPACE CORP BLOOMFIELD CONN F/G 1/3
PRELIMINARY DESIGN STUDY OF A COMPOSITE MAIN ROTOR BLADE FOR TH--ETC(U)
SEP 78 C HARDERSEN, W BLACKBURN DAAJ02-77-C-0075
UNCLASSIFIED R-1532-VOL-1 USARTL-TR-78-29A NL

2 OF 3
AD
A064 159

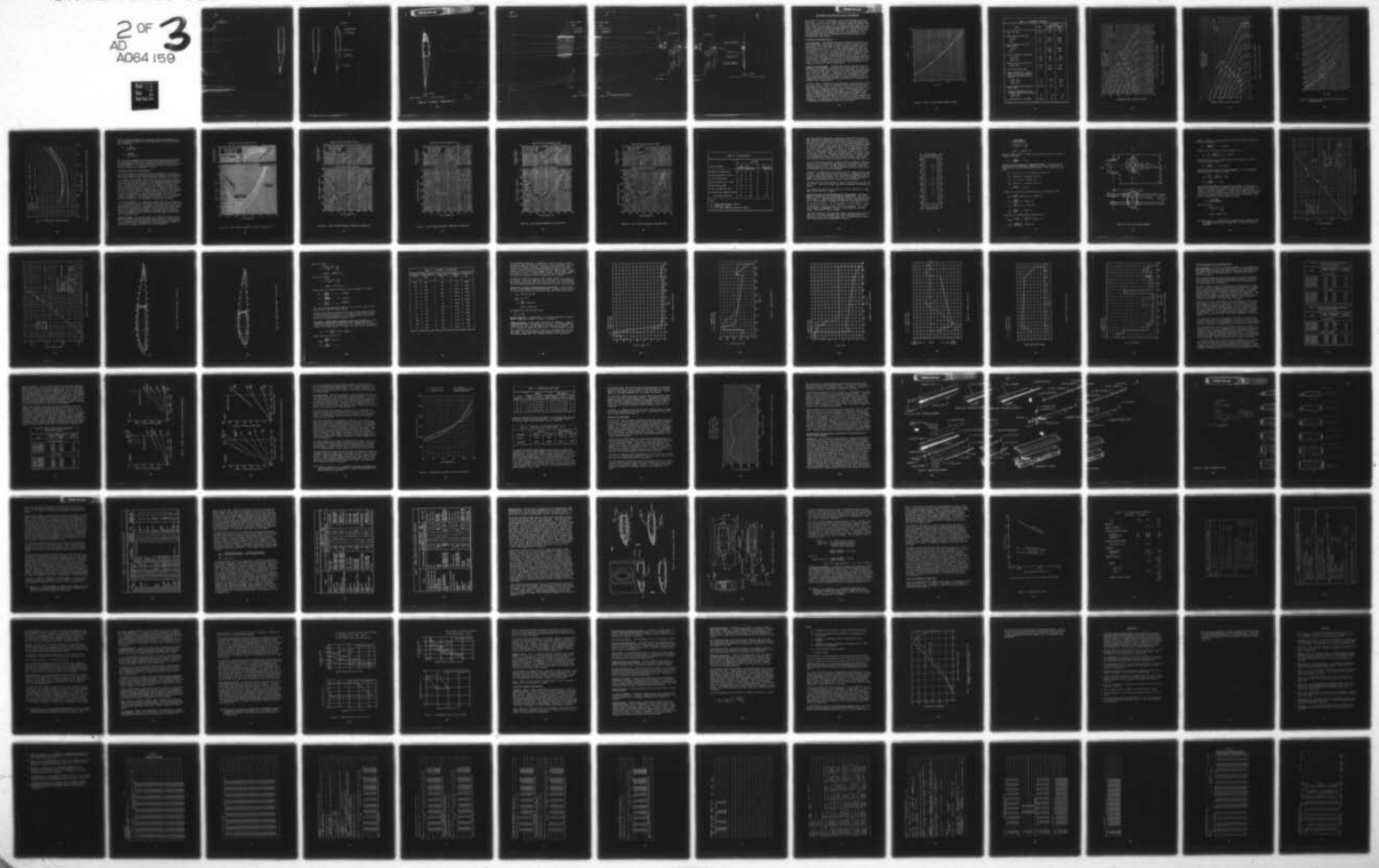

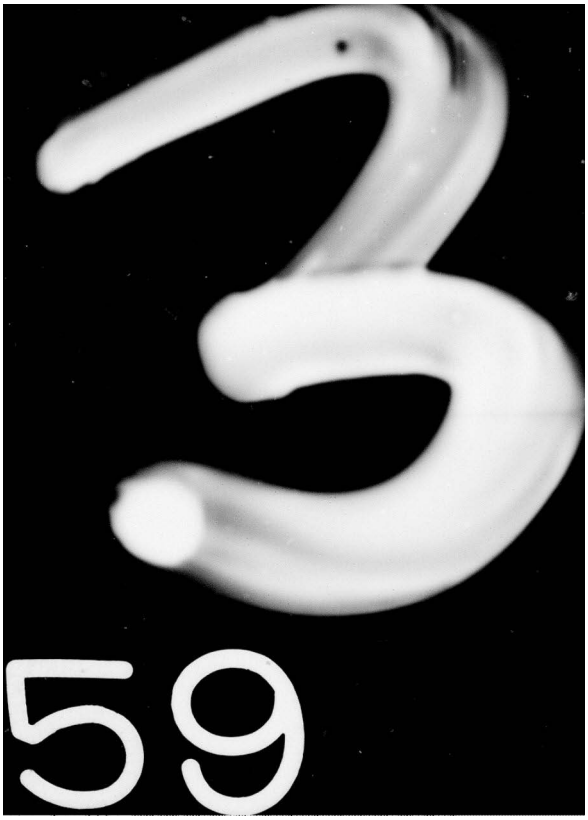
59

3

STA 38.5

STA 19.5

DOUBLERS
S-2 GLASS
(BASKET WEAVE)

STA 38.5

STA 38.5

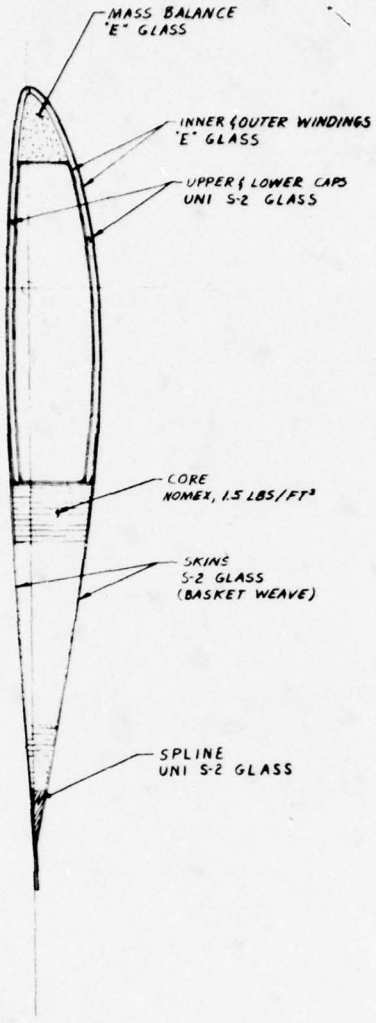

STA 48.5

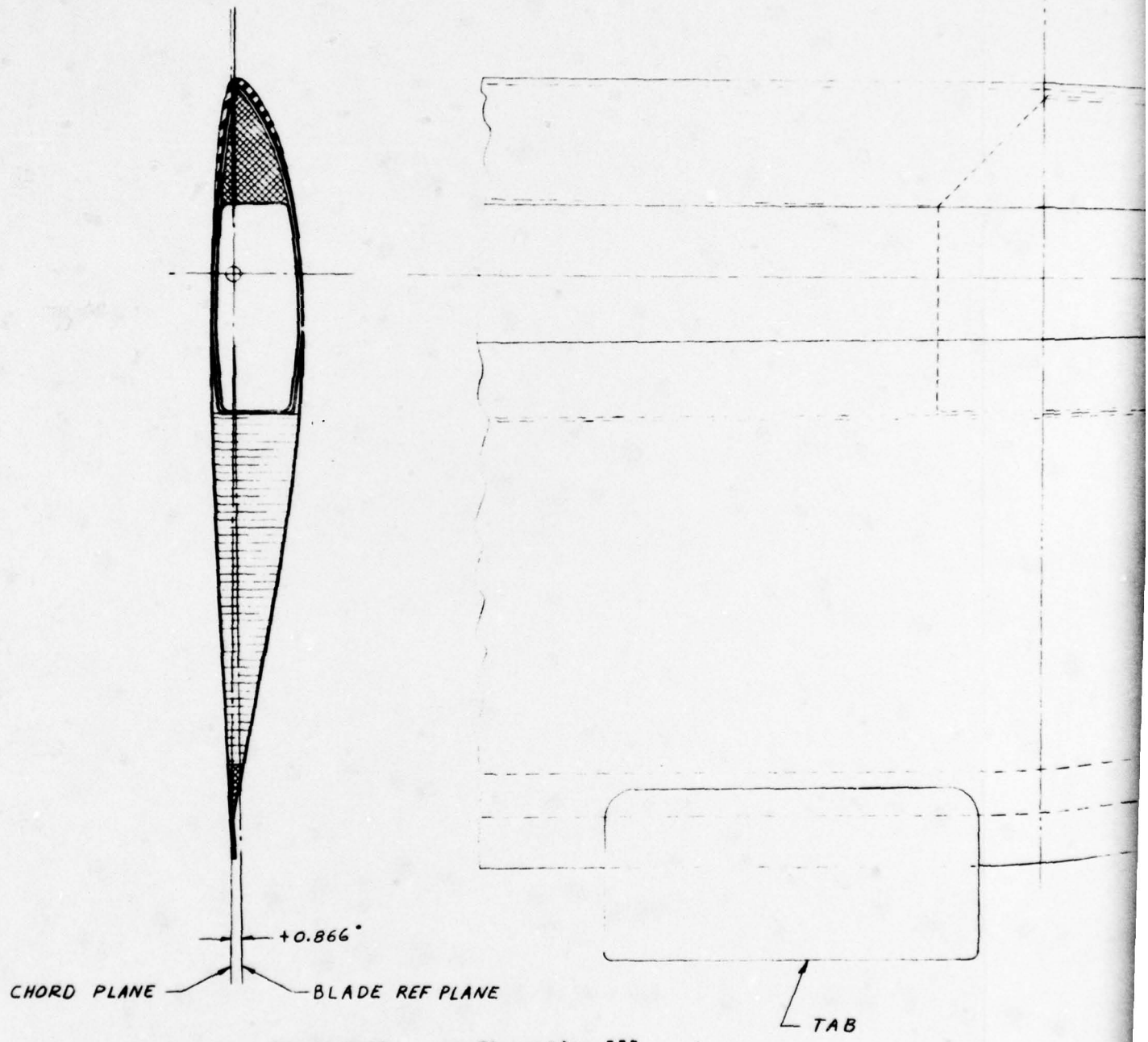

Figure 34. Tip details - configuration 111.

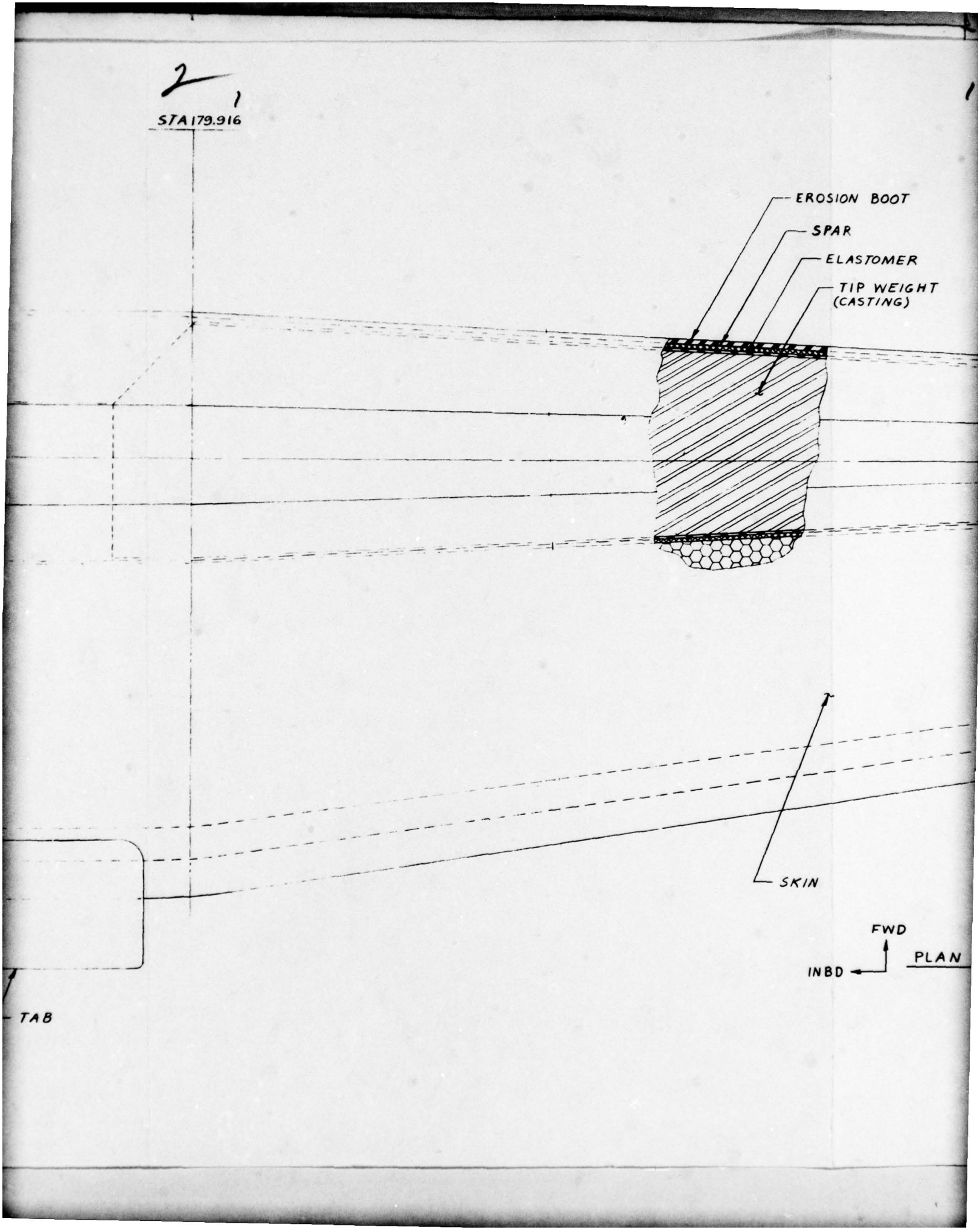
STA 179.916
EROSION BOOT
SPAR
ELASTOMER
TIP WEIGHT
(CASTING)
SKIN
FWD
INBD
PLAN
TAB

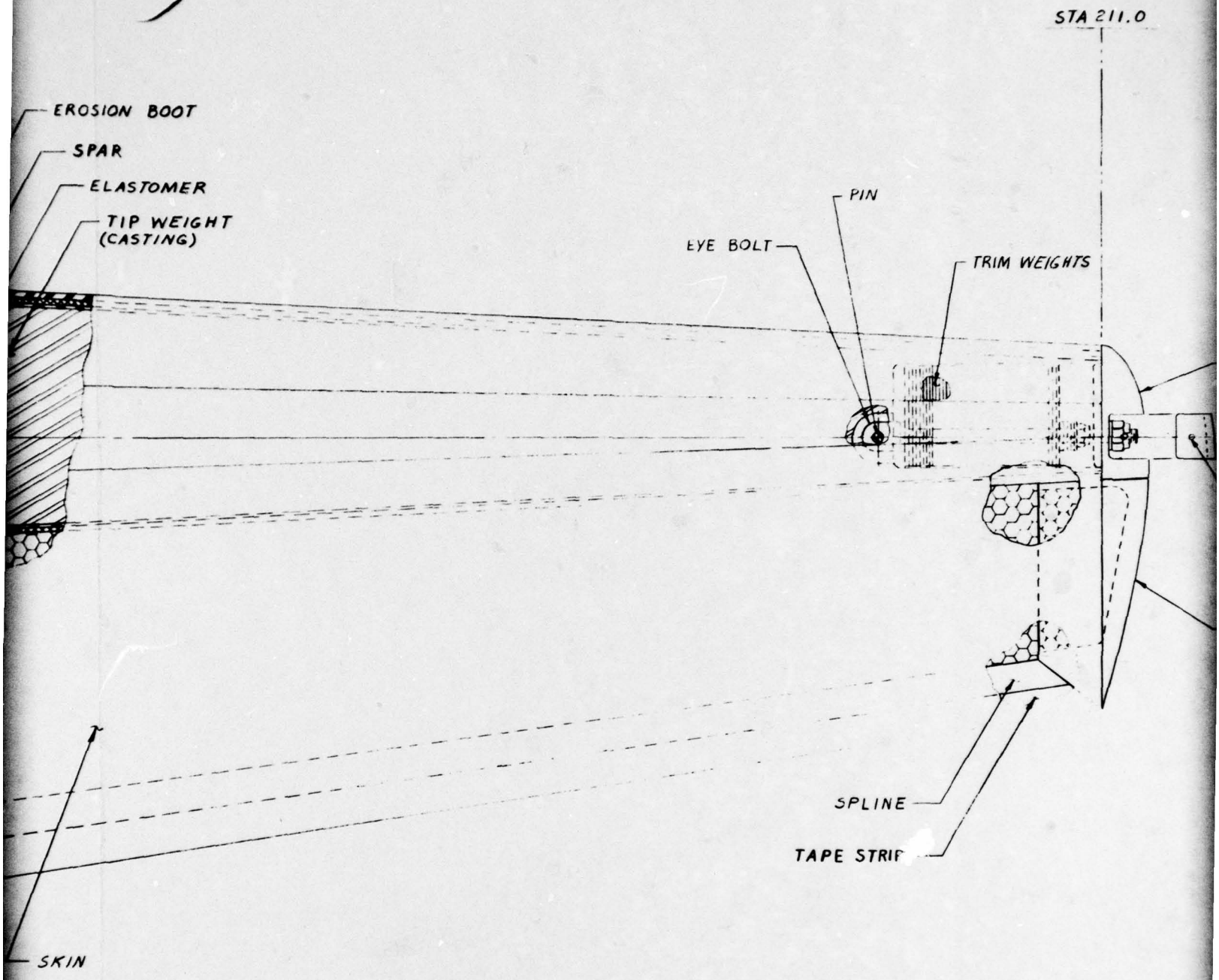

PLAN VIEW - BLADE TIP

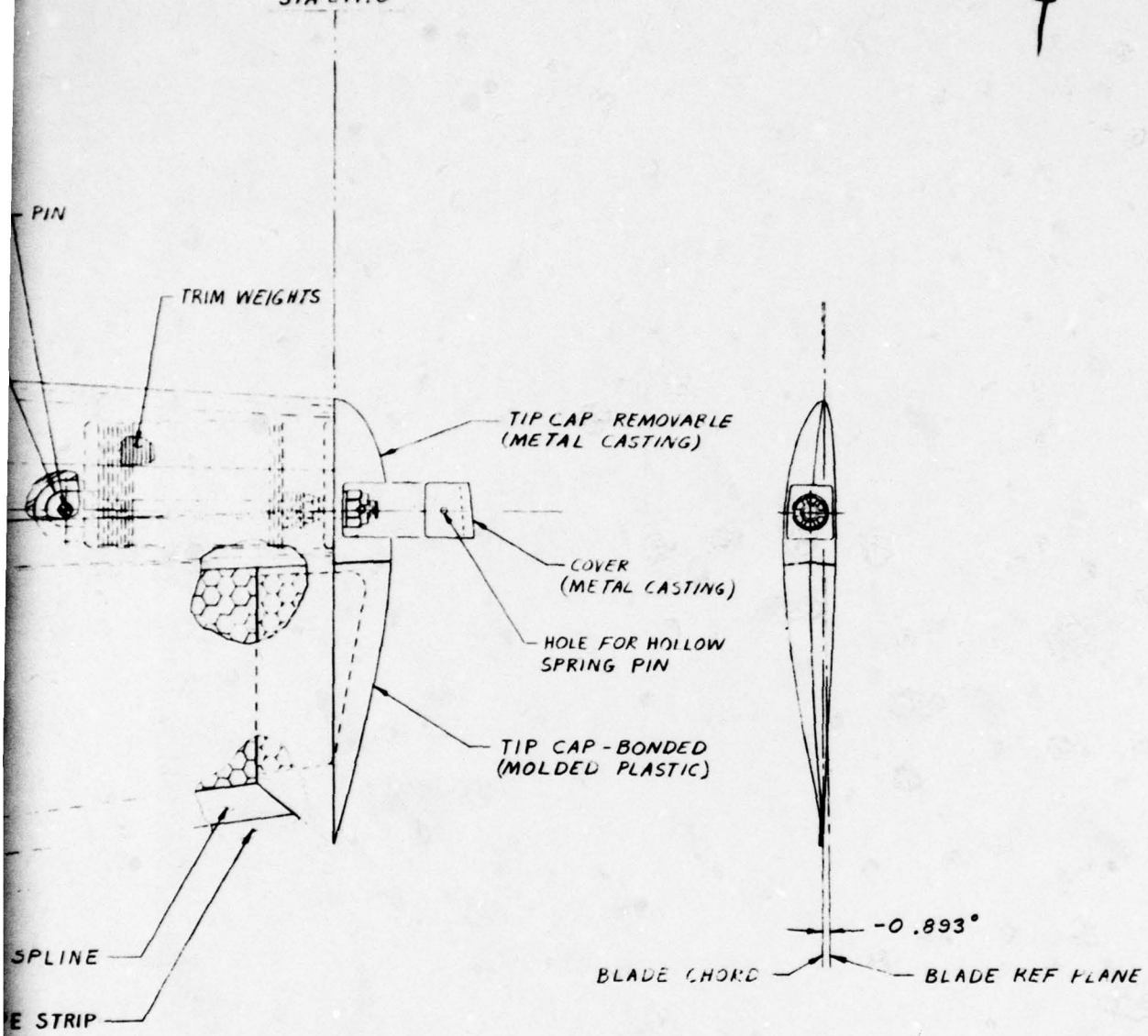
STA 211.0
PIN
TRIM WEIGHTS
TIP CAP REMOVABLE
(METAL CASTING)
COVER
(METAL CASTING)
HOLE FOR HOLLOW
SPRING PIN
TIP CAP - BONDED
(MOLDED PLASTIC)
SPLINE
E STRIP
-0.893°
BLADE CHORD
BLADE REF PLANE

PRELIMINARY DESIGN PHASE OF SELECTED CONFIGURATION

Having selected a final configuration, there remains the task of preliminary design. In Task I, it was found necessary to undertake advanced portions of the overall effort in order to solidify some of the necessary decisions. Because of this, some of the information presented under Task II is revised Task I material because of design changes or more detailed considerations. References to work accomplished under Task I merely indicate the level of completion of activities at that time. The results of the trade study phase indicated that configuration 211 is the best design. This design has been given the Kaman designation K757 which will be used for the remainder of this report.

Preliminary Performance Analysis

Hover Performance. The nondimensional hover performance of the K757 composite rotor blade configuration selected as a result of the analyses conducted under Task I requirements has been expanded to include a range of ambient temperatures from - 65°F to 120°F, corresponding to tip Mach numbers varying from 0.67 to 0.57. The relationship between the shaft power coefficient and rotor thrust coefficient at the limiting temperature conditions appears in Figure 35. The effect of Mach number is seen to be small in this instance, and zero airspeed performance can be modified for the composite rotor based on a linear interpolation between the two temperature extremes shown. The comparison of the zero airspeed performance achieved by the baseline configuration and the composite rotor configuration is presented in Table 19, and in the modified curves, Figures 36 and 37, which compare with Figures 14 and 15 of Reference 3.

Forward Flight Performance. Nondimensional forward flight performance is presented in Figure 38 for the composite rotor configuration in terms of the shaft power coefficient versus the thrust coefficient at various values of the rotor tip speed ratio. These data are derived from the performance shown in Figures 7 through 11 of Reference 3 for the baseline configuration. They are converted to the composite rotor configuration by subtracting the power difference obtained from Figure 39 which compares the nondimensional forward flight performance calculated for the baseline and composite rotor configurations.

From this figure, it appears that the performance of both configurations is essentially equal at low thrust coefficients from transition speed to maximum speed for level flight. At high thrust coefficients, the composite rotor exhibits a slight advantage up to speeds approaching 80 kts ($\mu = 0.2$) and an increasing advantage at higher speeds. It is therefore conservatively assumed that the specific performance maneuvers conducted at low speed are unaffected by the change to the composite main rotor. These maneuvers include the maximum rate of climb, service ceiling, endurance and all but the hover portions of the mission profile described in Figure 13 of Reference 3. At speeds above 80 knots, the effect on pertinent performance is determined by the magnitude of the thrust coefficient.

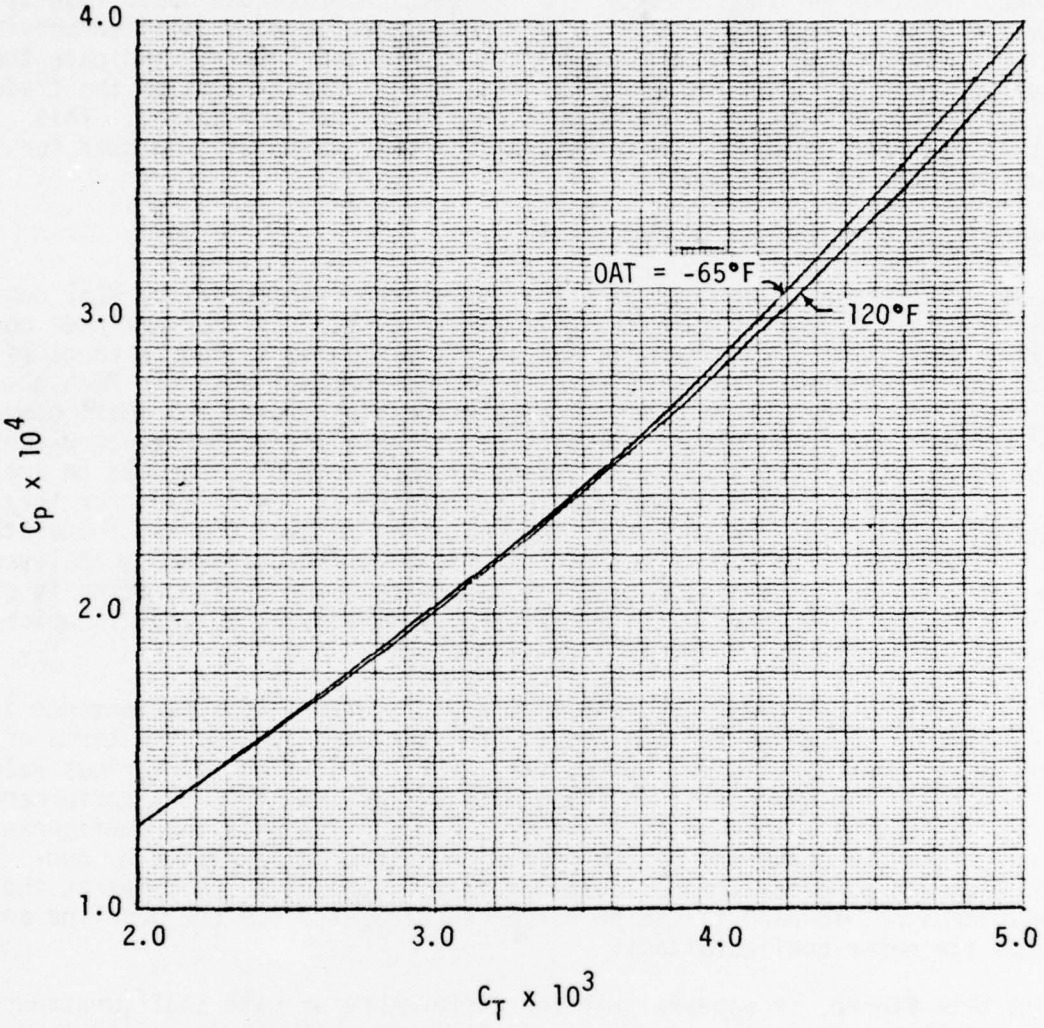

Figure 35. Effect of Mach number on power to hover.

TABLE 19. PERFORMANCE COMPARISON

Item	Units	Estimated	
		Standard rotor	Composite rotor
a. V_{NE}, sea level	kt-cas	120	120
b. Hover ceiling at IRP, OGE			
Std day	ft	8500	11000
95°F	ft	4250	6000
c. Hover ceiling at IRP, 4 ft skid height			
Std day	ft	12300	14800
95°F	ft	7300	9000
d. Vertical rate of climb at IRP			
Sea level	fpm	630	840
2000', 95°F	fpm	440	640
e. Maximum rate of climb at IRP			
2000', 95°F	fpm	1385	1385
f. Service ceiling at IRP	ft	16400	16400
g. Range (takeoff fuel allowance shall be 2 minutes at MCP at sea level and reserve fuel of 0.5 hr)			
2000', 95°F	nm	185	188
4000', 95°F	nm	---	199
h. Cruise speed for (g) above at MCP or less	kt-tas	100	100
i. Endurance (reserves and fuel allowance same as for (g) above)			
2000', 95°F	hr	2.8	2.8
j. Loiter speed, for (i) above	kt-tas	50	50

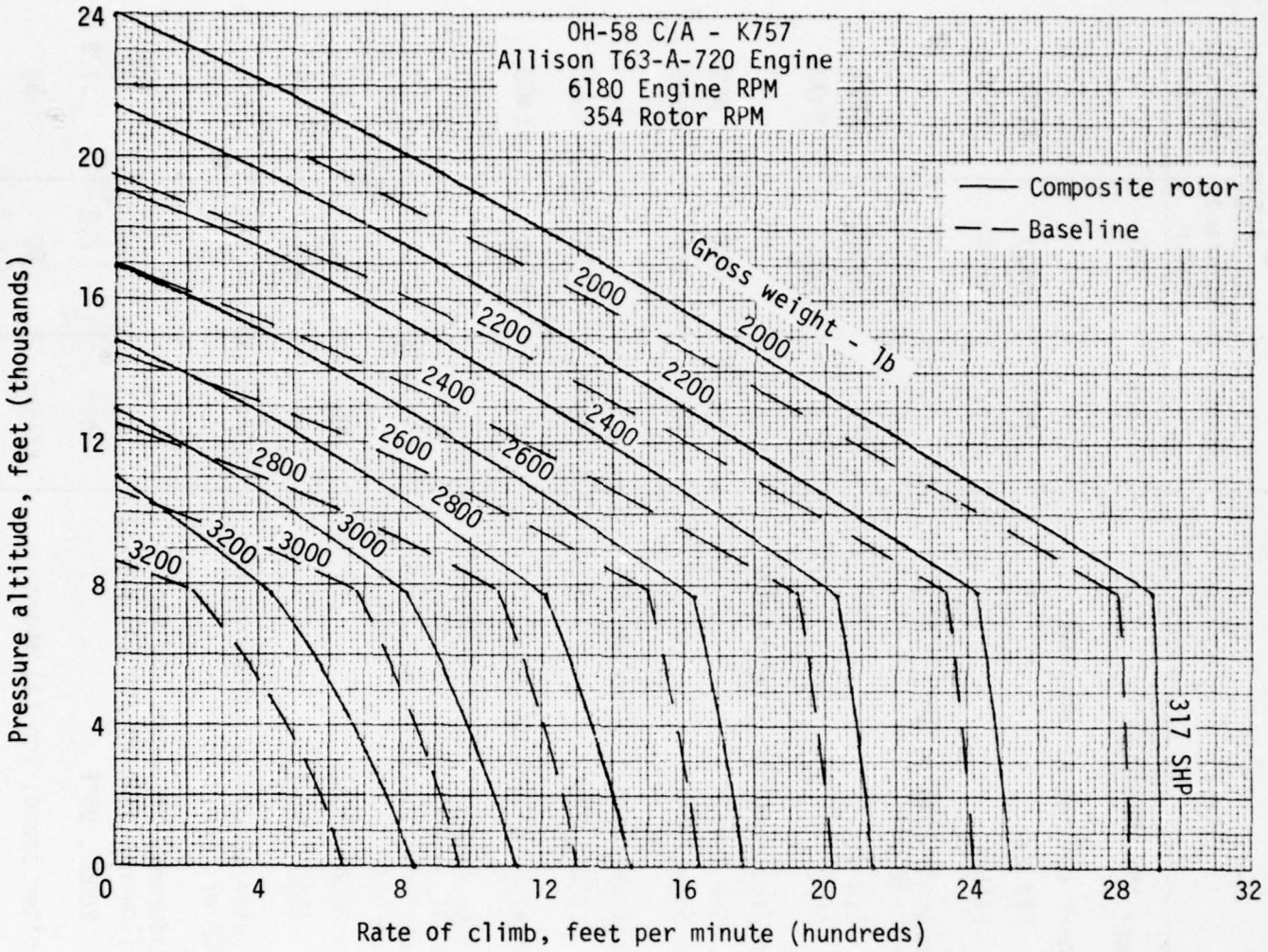

Figure 36. Vertical rate of climb, standard day.

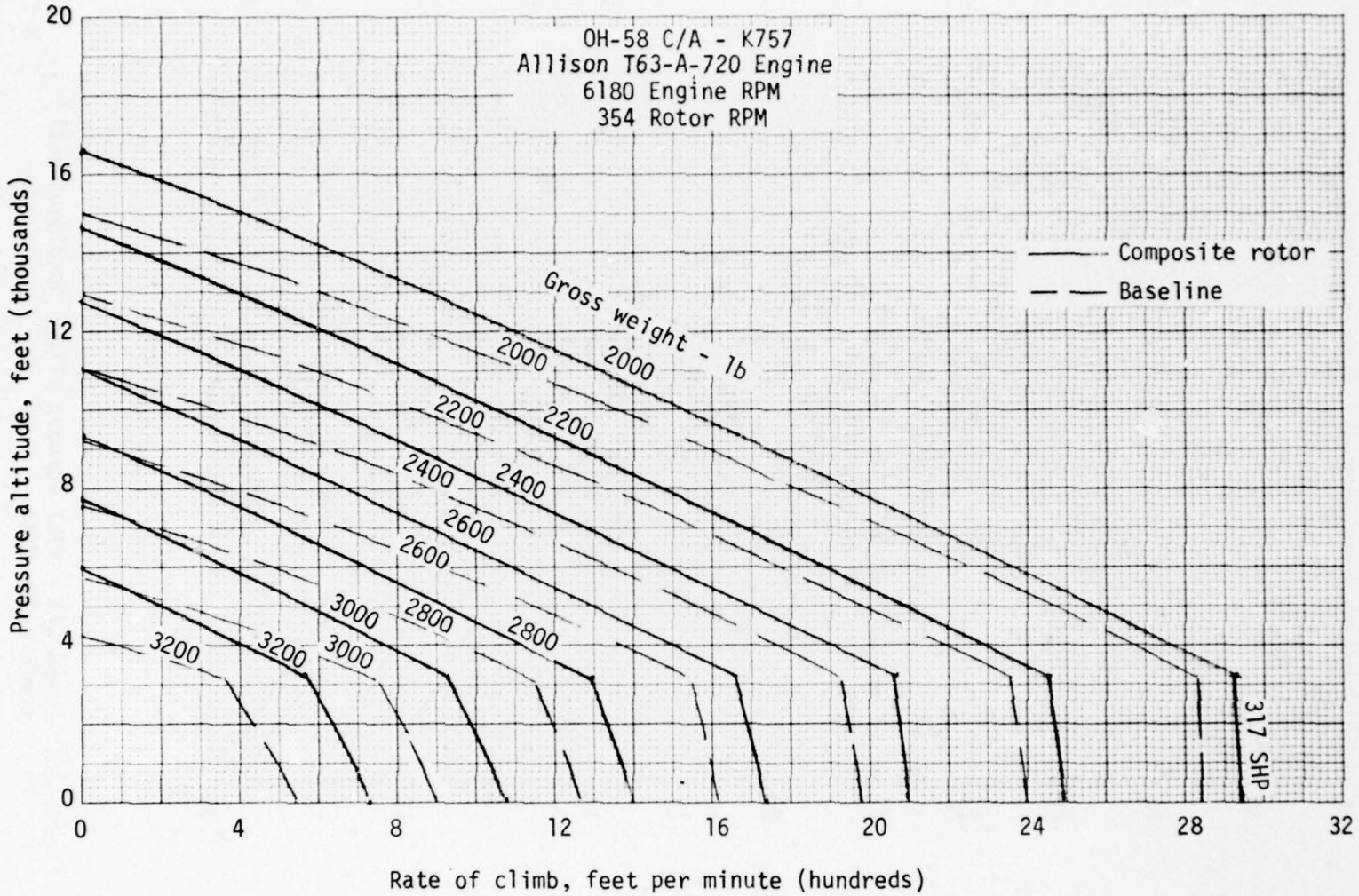

Figure 37. Vertical rate of climb, 95°F.

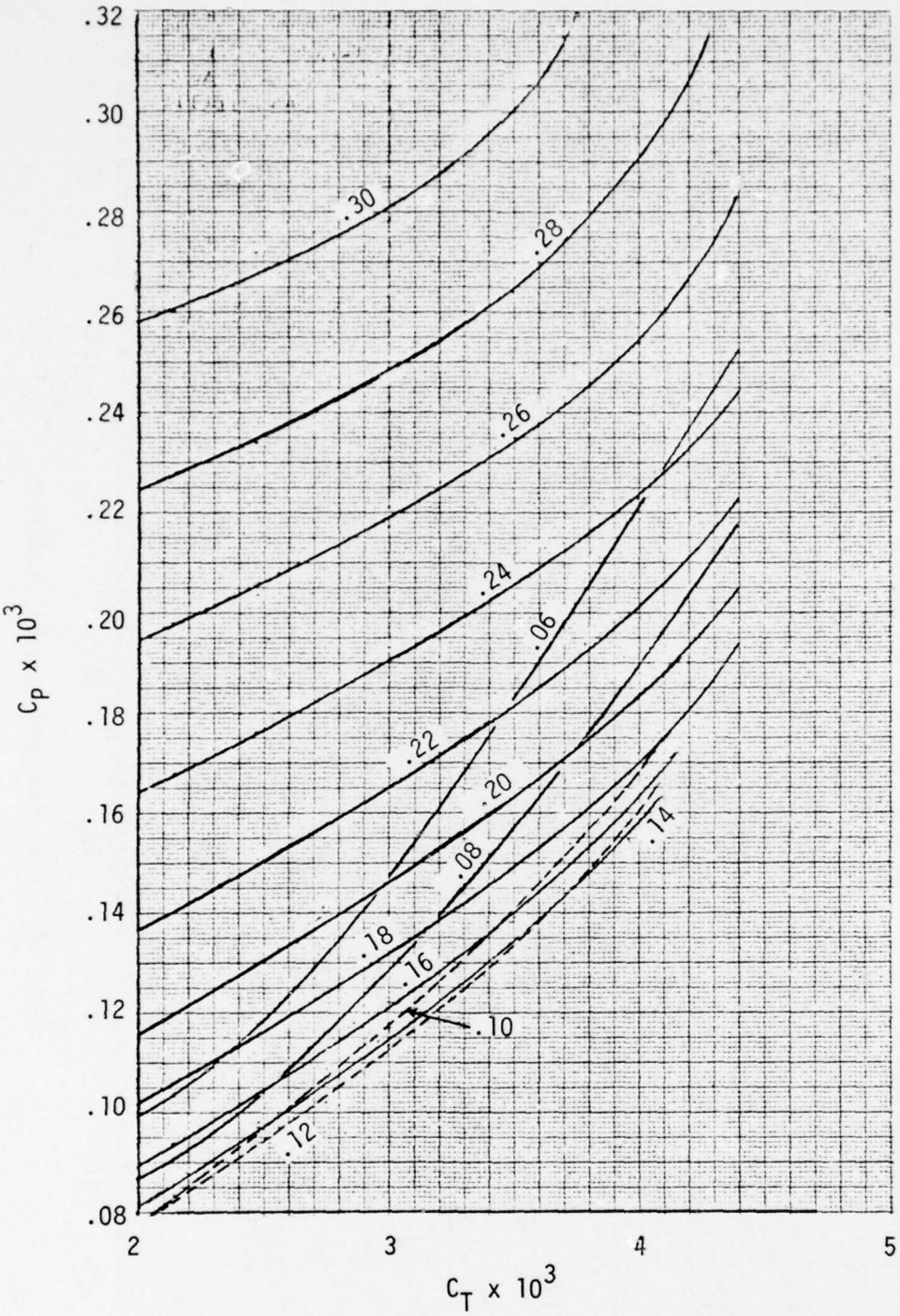

Figure 38. OH-58 C/A - K757 forward flight nondimensional performance data.

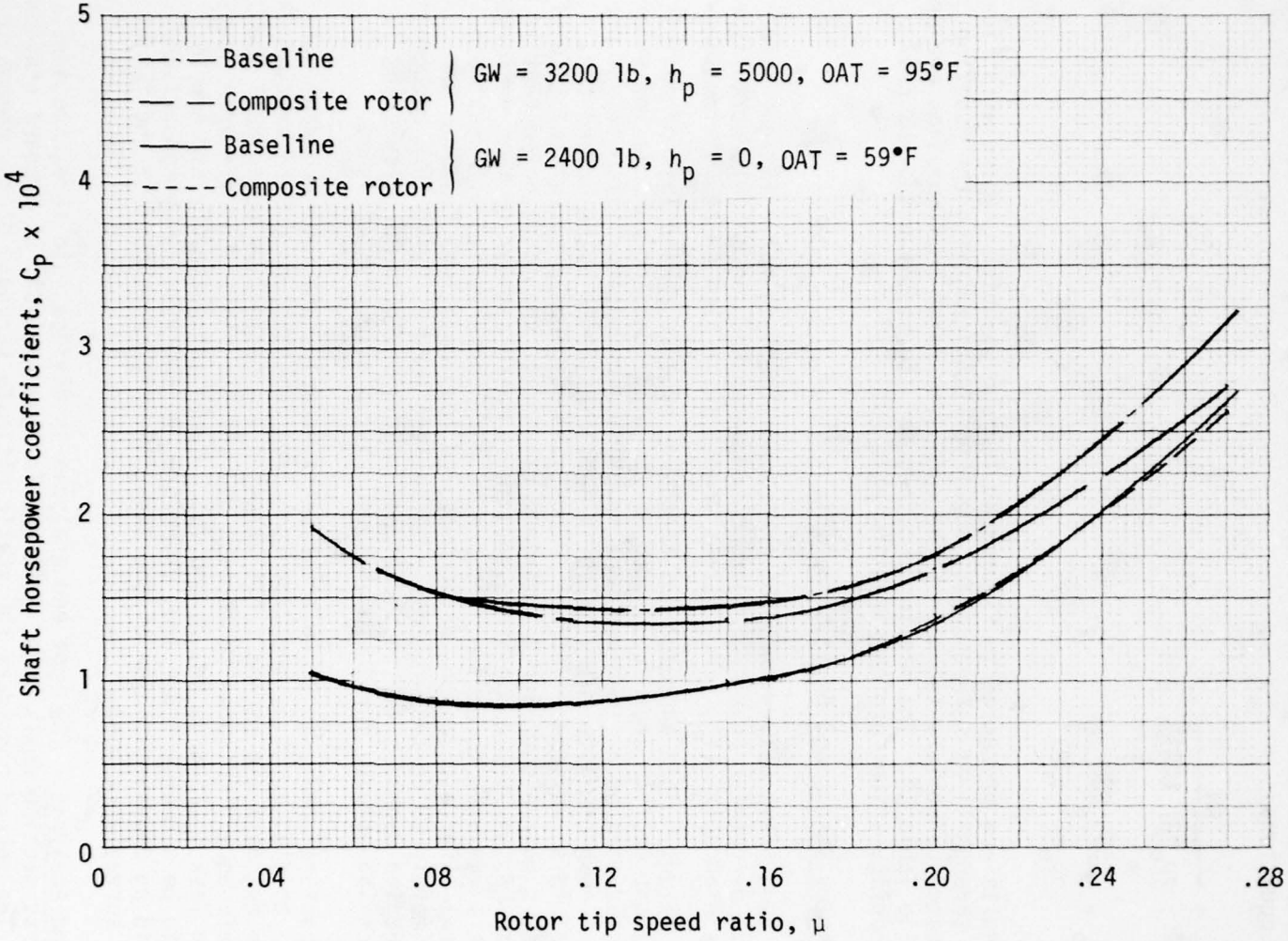

Figure 39. Forward flight performance, baseline and composite rotor configurations.

The dimensionalized forward flight performance which is affected by the K757 rotor blade configuration is calculated from Figure 38, using the following equations:

$$C_T = \frac{GW}{\sigma\rho_o \pi R^2 (\Omega R)^2}$$

$$C_P = \frac{550\ SHP}{\sigma\rho_o \pi R^2 (\Omega R)^3}$$

The results are presented in Figures 40 through 44 which compare with Figures 7 through 11 of Reference 3. Specific items comparing the baseline performance capability to that of the composite rotor configuration are presented in Table 19. The mission profiles for the baseline and the K757 rotor configurations are compared in Table 20.

Preliminary Stress and Fatigue Analysis

It has been previously shown that the composite blade has a fatigue life equal to or greater than 4703 hours based on an endurance limit established for the high speed (V_H) level flight condition at high GW and maximum density altitude. This approach was necessary because of the lack of definitive flight profile load data, such as the blade bending moments and shears associated with each time increment in the Government-furnished flight profile. A complete life calculation is also considered to be beyond the scope of this preliminary effort. Thus, the originally calculated life of 4703 hours may be considered a minimum value. It should be noted that in the case of the AH-1 composite blade, an approach similar to that performed in Task I was used to arrive at a preliminary conservative life estimate. The final life calculation, using measured load data, was found to be approximately twice the originally calculated number. With this background in mind, the emphasis in the structural analysis shifts to calculating stresses and strains for the high speed case previously mentioned.

The structural analysis is in three parts; namely, the root end from station 11 to station 36.5, the clean section from station 36.5 to station 180, and the outboard tip region. All stresses are calculated using Bell loads from Reference 9 (Figures 28 through 30) and the limit load criteria developed in Task I (Figures 24, 25 and 26). Loads calculated by Kaman were found to be somewhat lower and, therefore, unconservative by comparison. To avoid an underestimation of the task, the higher loads from the flight strain survey were used.

Root End Analysis. The root end analysis is divided into three sections. The first section deals with limit and fatigue analysis of inboard station 21.5. The second considers the static ultimate strength of the composite glass/graphite bearing retention plates, and the third section covers the stresses due to edgewise load reactions at the blade latch.

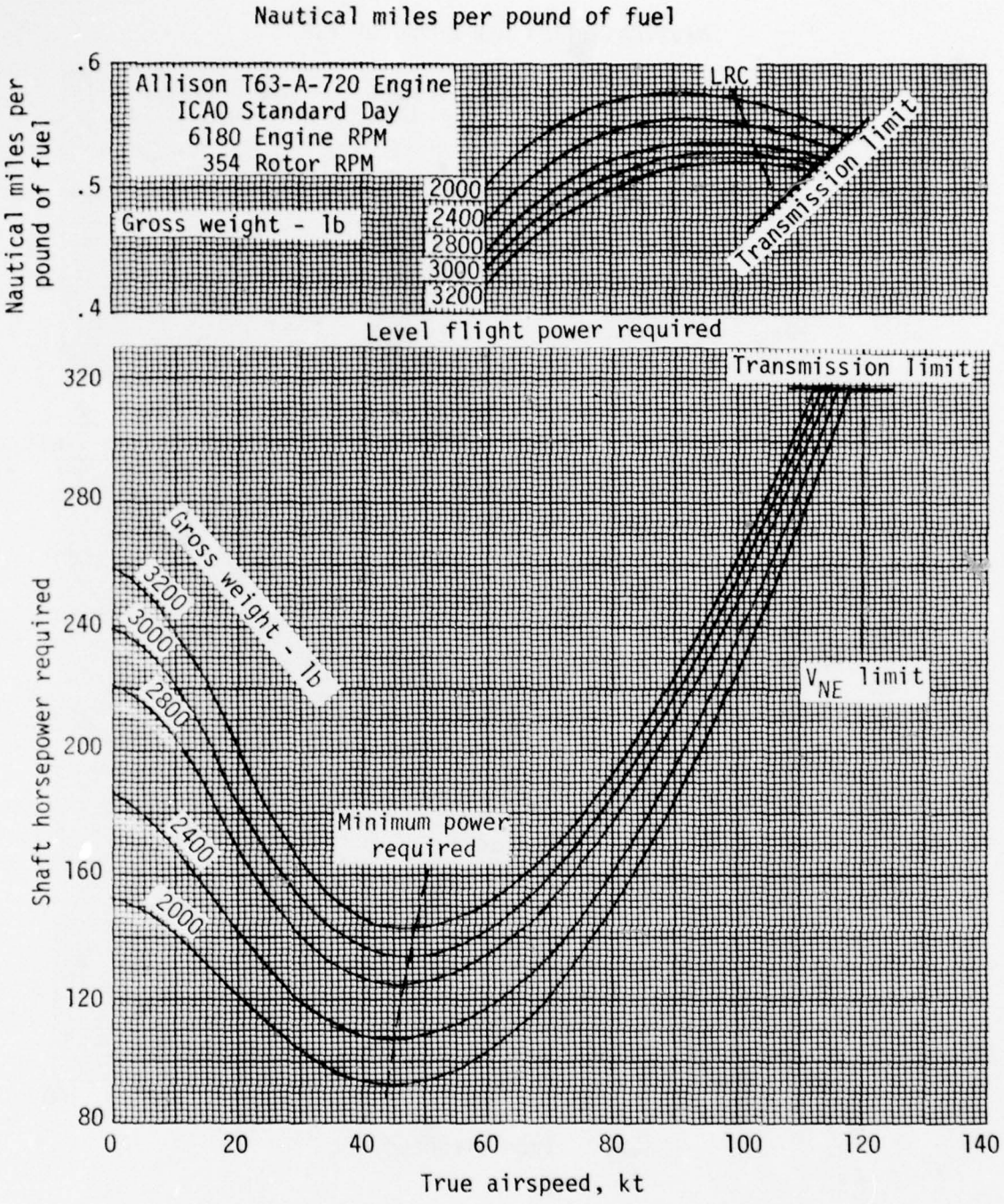

Figure 40. Level flight performance, sea level, standard day.

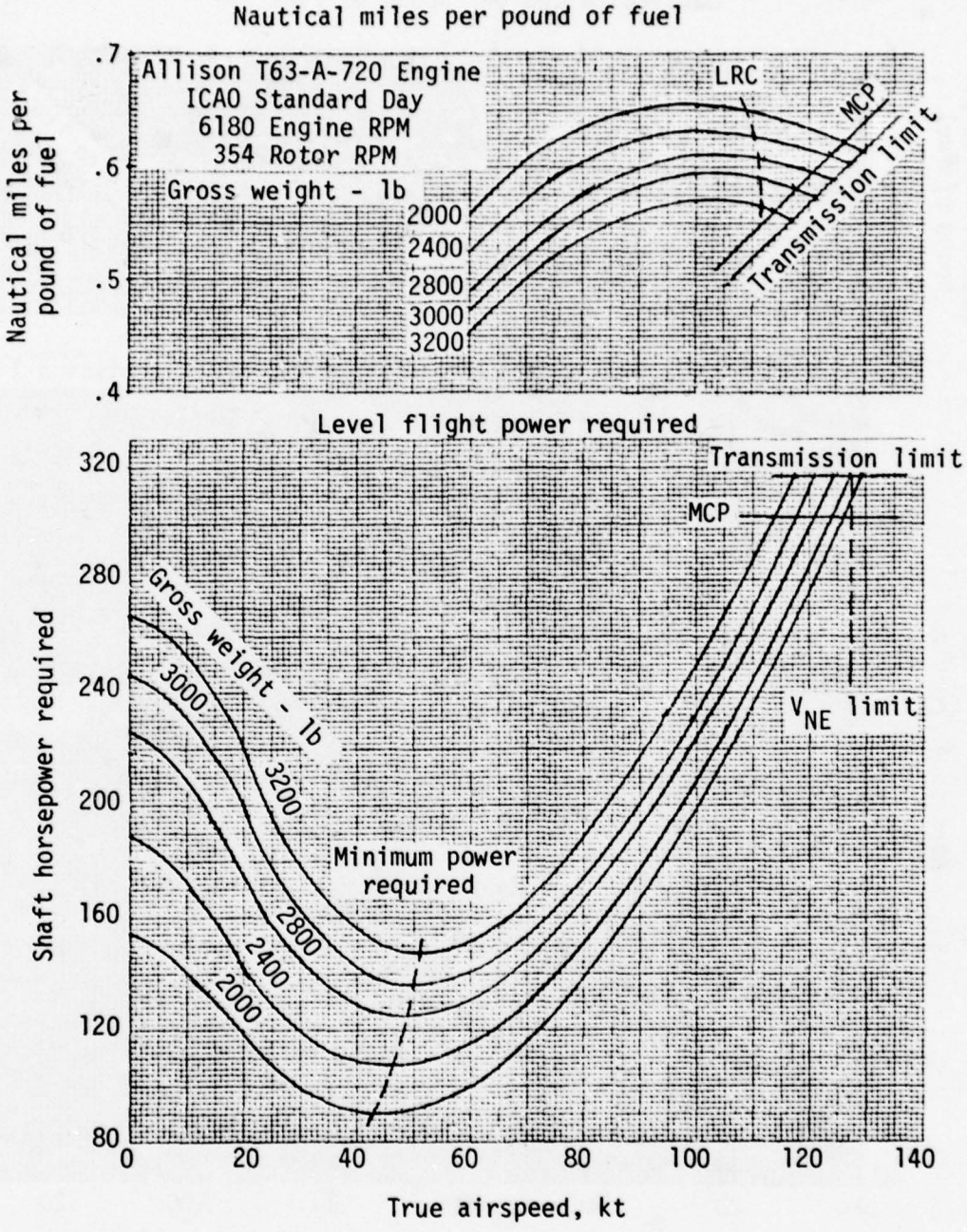

Figure 41. Level flight performance, 5000 feet, standard day.

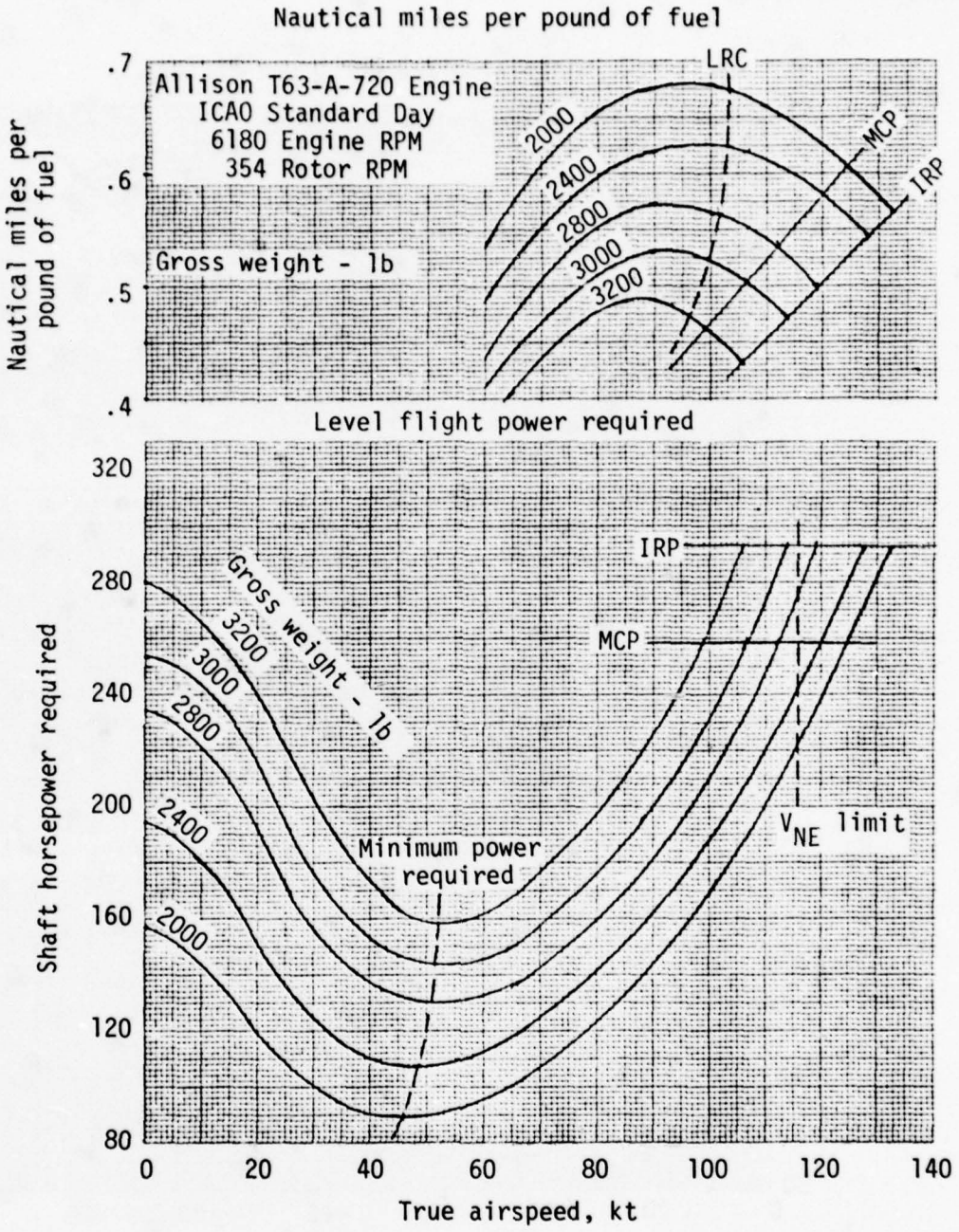

Figure 42. Level flight performance, 10000 feet, standard day.

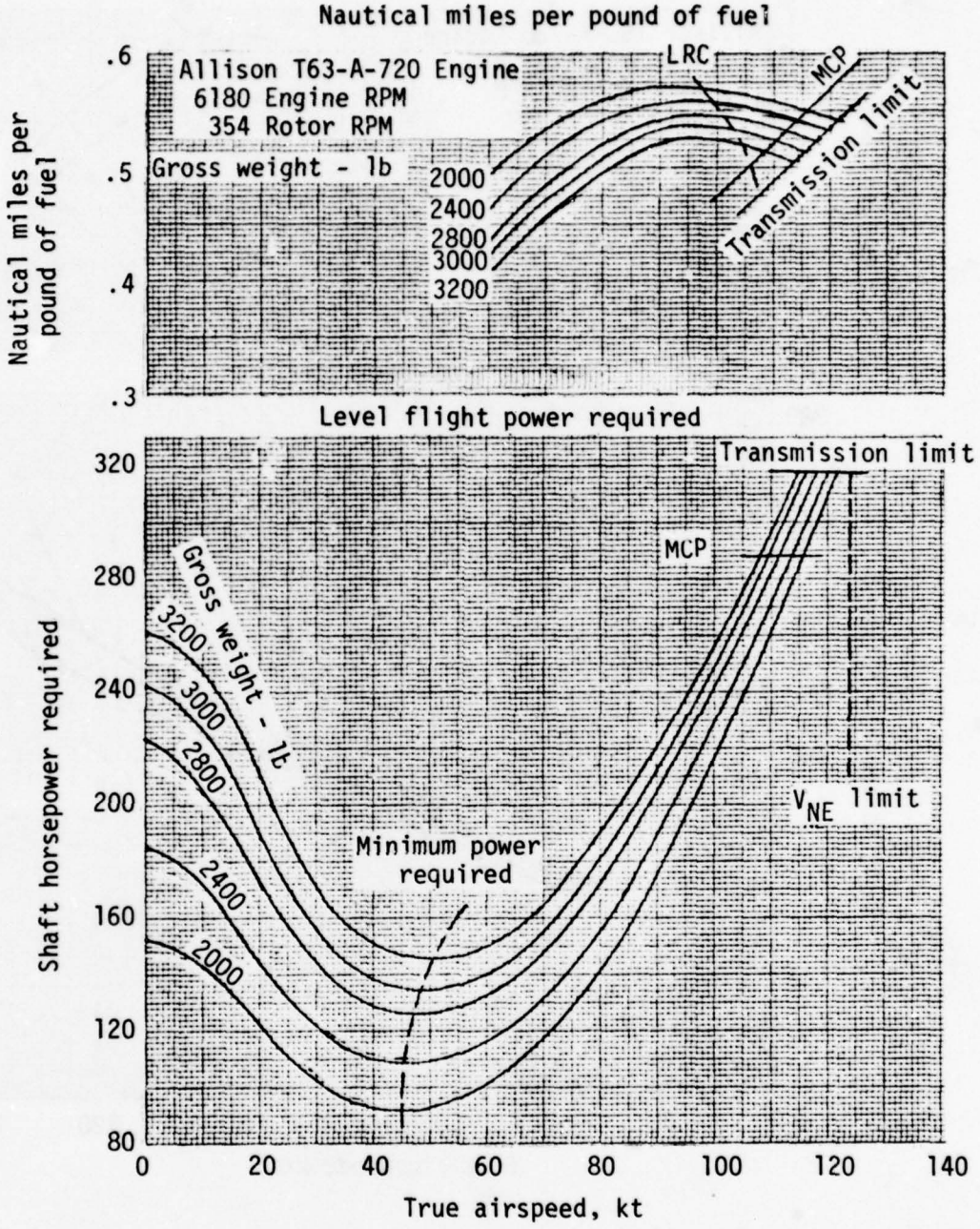

Figure 43. Level flight performance, sea level, 95°F.

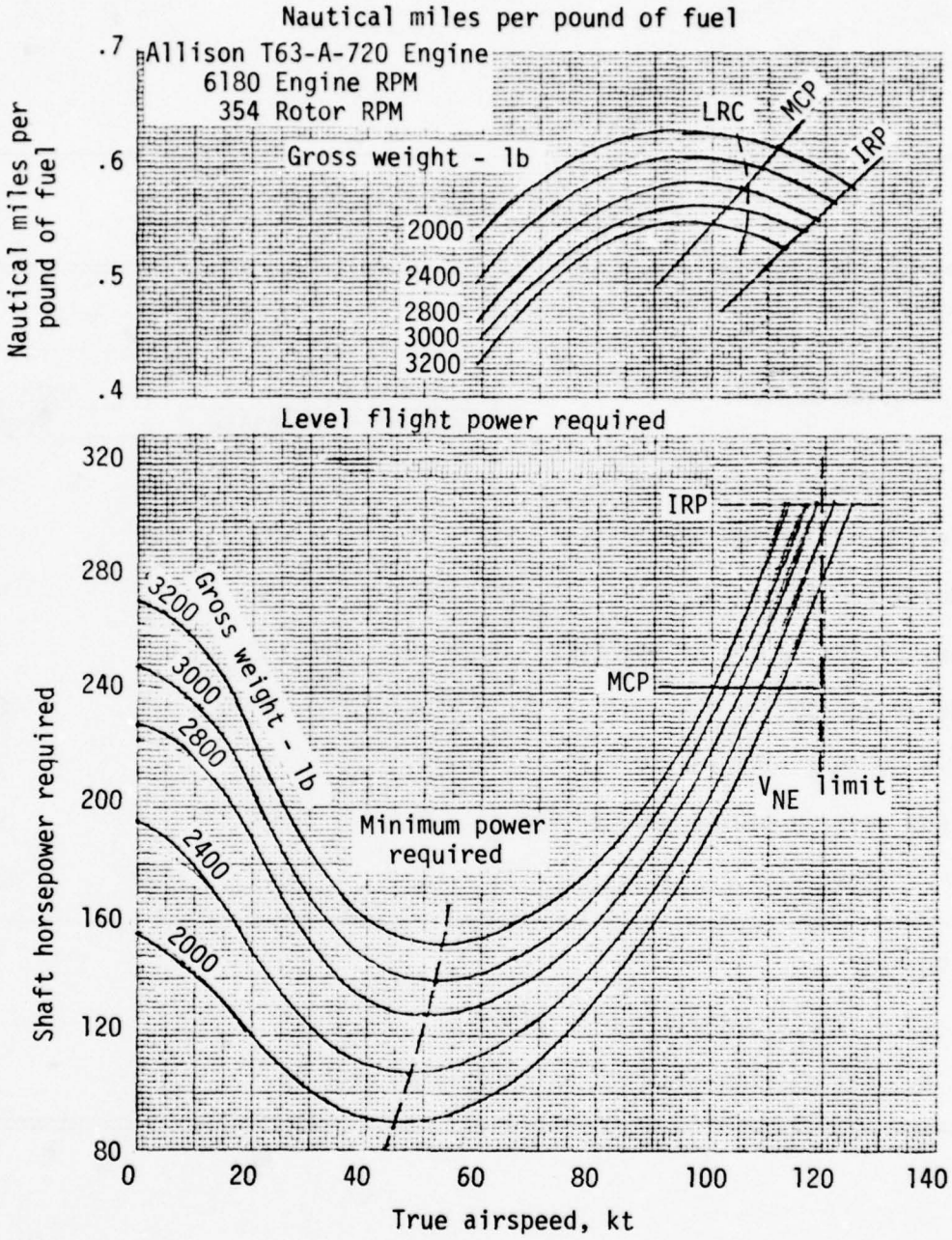

Figure 44. Level flight performance, 4000 feet, 95°F.

TABLE 20. MISSION PROFILE

Mission Segment	Fuel Used		
	2000', 95°F		4000', 95°F
	Baseline	Composite	Composite
8 minutes at ground idle	14	14	14
Cruise out at MCP for 10 min	33	33	30
Hover for 30 min OGE	104	98	98
Loiter for 30 min at V = 40KT	72	72	70
Hover for 30 min OGE	104	98	98
Cruise in at MCP for 10 min	33	33	30
Land with 30 min reserve at MCP	97	97	90
Total fuel for mission	457	445	430

Notes:

1) takeoff gross weight = 3200 lb
2) usable fuel = 457 lb
3) all mission segments calculated at 3200 lb

The stress analysis and section properties are determined using Kaman's CMAB program, which determines laminated plate properties and stress analyzes each lamina, and SHELLD, which calculates all section properties and determines bar stresses. CMAB is first used to determine the elastic properties of each specific bar. These are introduced into the SHELLD program for each bar location in the section model. For ultimate analysis, the section bar stress is reimposed in a recycle of the CMAB program to calculate the critical lamina stress. In the case of ultimate failure, the blade is not considered failed until the primary lamina is severed. Since a helicopter blade is a linear tension beam structure, its primary lamina is the uniaxial material. Therefore, the full bar load is imposed on the uniaxial material at failure; all other laminae undergo a quasi-yield, redistributing load to the uniaxial material prior to the actual failure.

In the case of fatigue analyses, stresses directly calculated in SHELLD are reduced to strains and compared with previously determined fatigue allowables (Figures 22 and 23). No CMAB reanalysis is necessary, since the allowables pertain to the bulk laminate performance of very similar composite structure tested in the AH-1 program.

Inherent in the CMAB static stress calculations is a general practice used at Kaman. Calculated stresses due to limit loads are compared to one-half of the allowable stress values. This incorporates an additional factor of safety of 1.333 beyond the usual 1.5. This is a reasonable allowance for general fabrication deviations and material quality variances.

The clean section analysis consists of cuts at stations 36.6, 60, 100, 140 and 179.916. Static and fatigue conditions are analyzed as previously discussed.

The outboard tip region analysis covers the critical conditions of rubber shear and tip GAG cyclic stresses.

Station 21.5 Static and Fatigue Analysis of Inboard Region. The SHELLD model of station 21.5 cross section appears in Figure 45. Page 185 of Appendix B lists tabulated data and page 186 indicates the resulting stress at bar number 9. Page 187 presents the CMAB analysis of the laminate at bar 9. This indicates a .30 margin of safety for lamina number 2 in the $\overline{22}$ (chordwise) direction. This is analogous to a yield condition, since the $\overline{22}$ modulus is highly nonlinear, being resin dominated. The actual failure margin is dependent on laminae 3, 6 and 9 which are uniaxial fibers. This margin is 4.85, as shown.

Pages 188 and 189 list the calculated vibratory and mean stresses for station 21.5. The highest stresses occur at bar 9 where mean and cyclic stresses are 6.9 ± 2.01 kips per square inch. Fatigue strains in the uniaxial S-glass material are determined as follows:

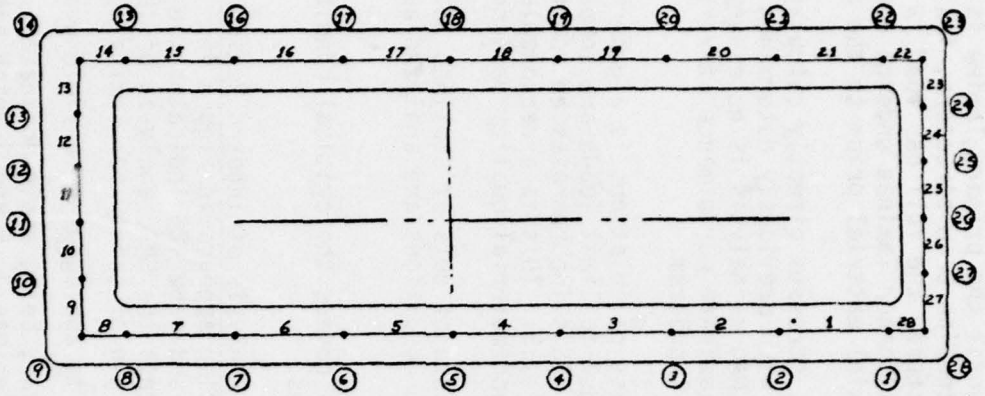

Figure 45. SHELLD structural model - station 21.5.

$$e = \frac{\text{Bar Stress}}{\text{Laminate Modulus}}$$

$$= \frac{(6.9 \pm 2.01)}{.57} \times \frac{10^3}{10^7}$$

$$= .00121 \pm .000353 \text{ in./in.}$$

From the Goodman diagram in Figure 22, we calculate a margin of safety in fatigue, as follows:

$$M.S. = \frac{.0016}{.000353} - 1 = 3.53$$

Station 18.5 Static Analysis of Inboard Attachment. Figure 46 indicates the blade root end attachment. Condition IX, a power off condition, is found to be critical for the bushing attachment. Limit loads are as follows:

$P_{\overline{CF}}$ = 50570.9 lb at 411 rpm (reference Figure 27)

M_B = 68000 lb-in. (reference Figure 24)

M_C = .75 x 50570.9 = 37928.2 lb-in.

M_{YZ} = 6400 lb-in. (reference Figure 26)

$$P_e = \frac{37928.2}{6} = 6321.4 \text{ lb}$$

Ultimate pin reactions for the bottom bushing are determined to be:

$$R_{CF_L} = \frac{1.168}{2.62} \times 50570.9 \times 1.5 = 33816.9 \text{ lb}$$

$$R_B = \frac{68000}{2.62} \times 1.5 = 38931.3 \text{ lb}$$

$$R_{e_L} = \frac{6321.4}{2} \times 1.5 = 4741.1 \text{ lb}$$

$$R_{YZ} = \frac{6400}{2.62} \times 1.5 = 3664.1 \text{ lb}$$

Therefore, the ultimate bearing load and stress is:

$$R_{BR_L} = \sqrt{72748.[illegible]^2 + 8405.2^2} = 73232.2 \text{ lb}$$

$$f_{BR_U} = \frac{73232.2}{2.25 \times .52} = 62591.6 \text{ psi}$$

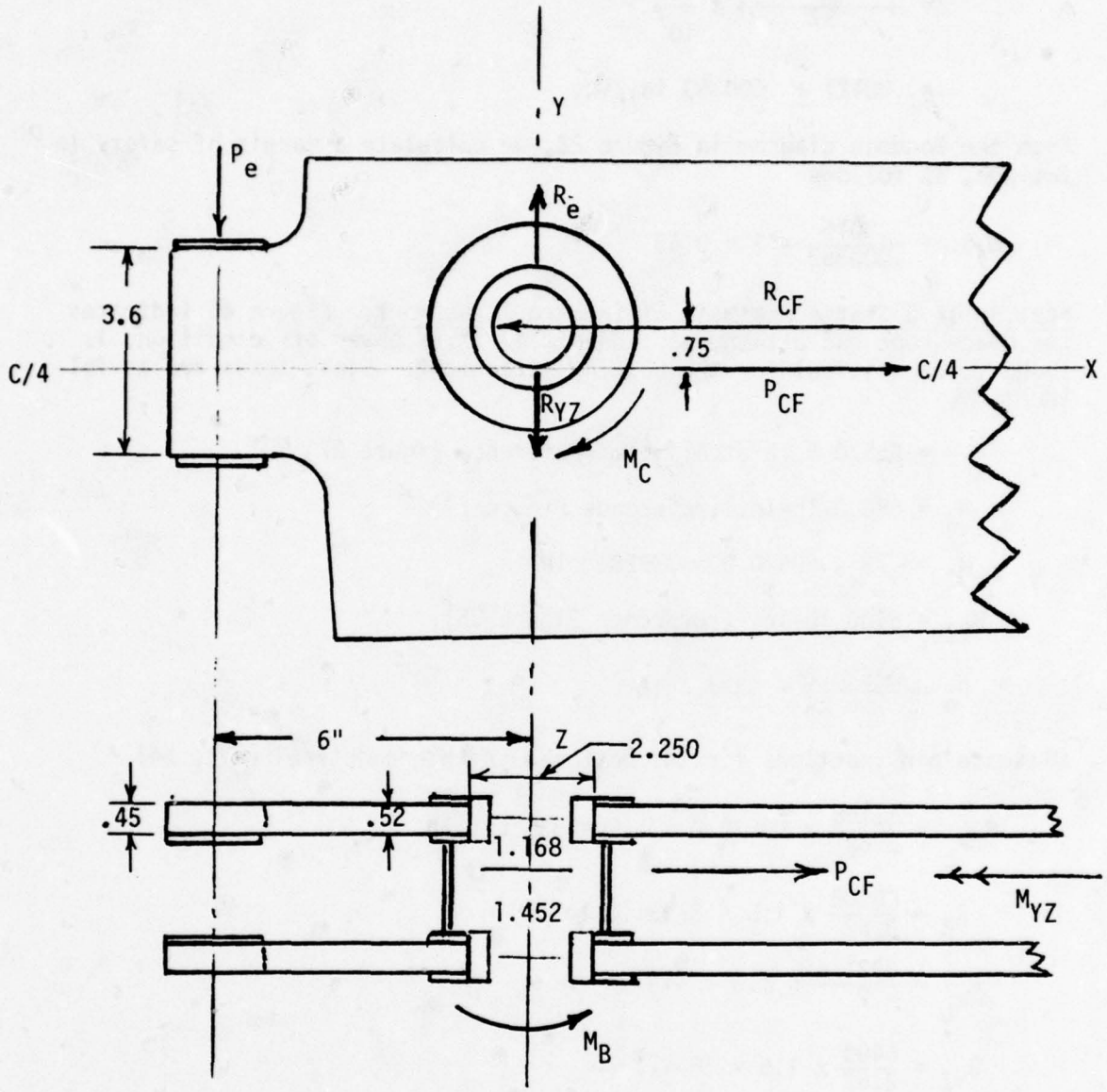

Figure 46. K757 root retention geometry.

Figure 47 indicates a mixed graphite/glass bearing allowable of 92,420 psi derived from Reference 11.

$$M.S. = \frac{92420}{62591.6} - 1 = .47 \text{ ultimate}$$

Ultimate shear stresses of the lower attachment are:

$$f_{S_U} = \frac{73232.2}{(6 - 1.125) \times 2 \times 5.2} = 14444 \text{ psi}$$

Figure 48 indicates a mixed graphite/glass shear allowable of 35915 psi also derived from Reference 11.

$$M.S. = \frac{35915}{14444} - 1 = 1.04 \text{ ultimate}$$

Station 11.5 static Analysis of Latch Engagement. The latch engagement stub (Figure 46) is critical in shear.

$$f_{S_U} = \frac{R_{e_L}}{(2)A_s} = \frac{4741.1}{.45 \times 3.6} = 2926.7$$

$$M.S. = \frac{35915}{2926.7} - 1 = \text{Large}$$

Static and Fatigue Analysis, Station 36.5 to 179.916. SHELLD models of stations 36.5 and 179.916 are shown in Figures 49 and 50. Station 36.5 is found to be critical for static and fatigue loading. Tabulated data appears on page 190 of Appendix B. Printout data on pages 191 and 192 indicates that critical combined stresses occur at bar 6 for uniaxial S-glass and bar 9 for uniaxial E-glass. Bar 24 has critical stresses for $\pm$ 45° S-glass. Fatigue strains are determined as follows:

$$e = \frac{\text{Bar Stress}}{\text{Laminate Modulus}}$$

Bar 6 Uni-S-Glass:

$$e = \frac{17.03 \pm 4.18}{.51} \times \frac{10^3}{10^7}$$

$$= .00334 \pm .00082 \text{ in./in.}$$

11. Hart-Smith, L. J., BOLTED JOINTS IN GRAPHITE-EPOXY COMPOSITES, NASA CR-144899, McDonnell Douglas Corporation, Long Beach, California, June 1976.

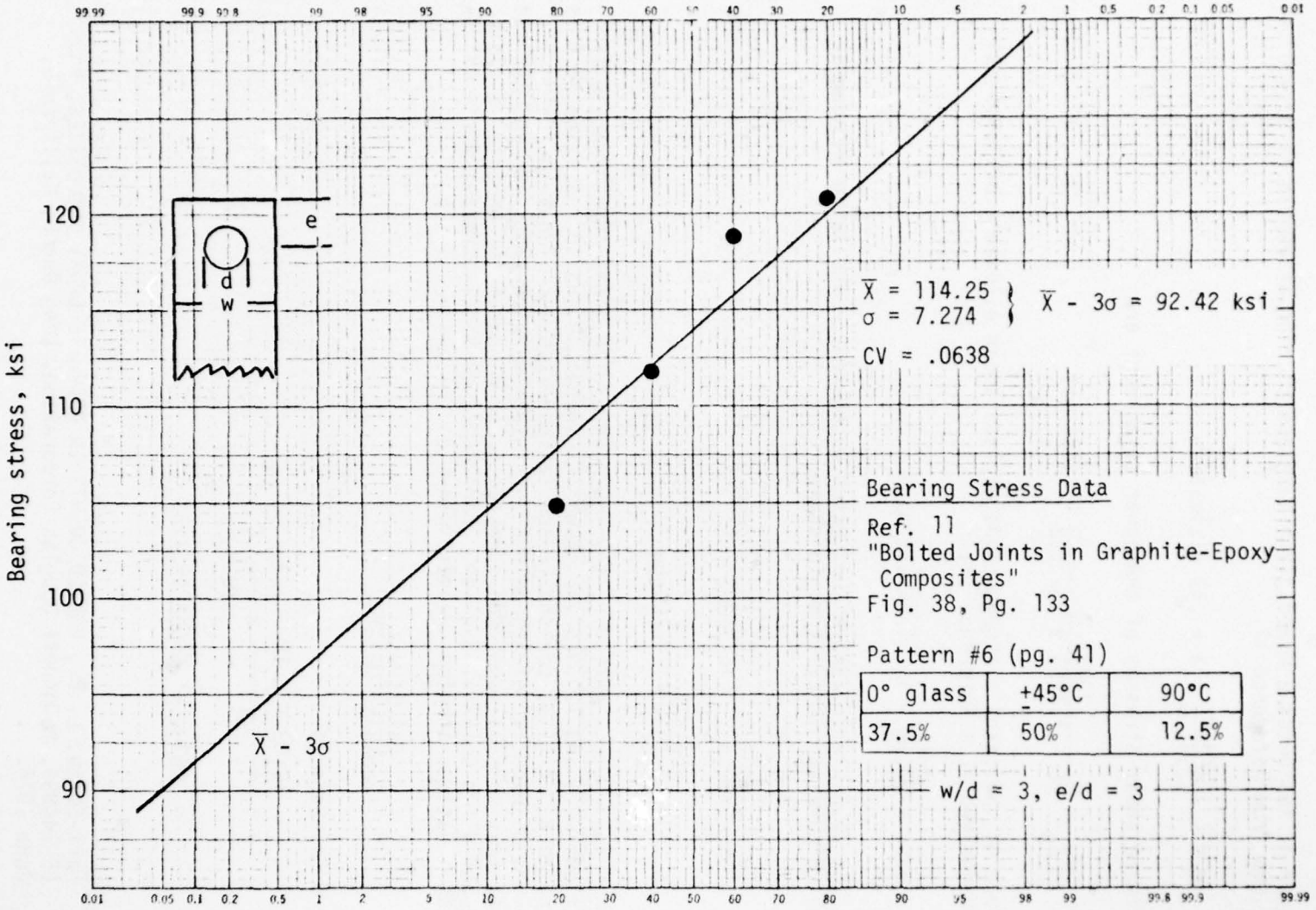

Figure 47. Bearing stress data.

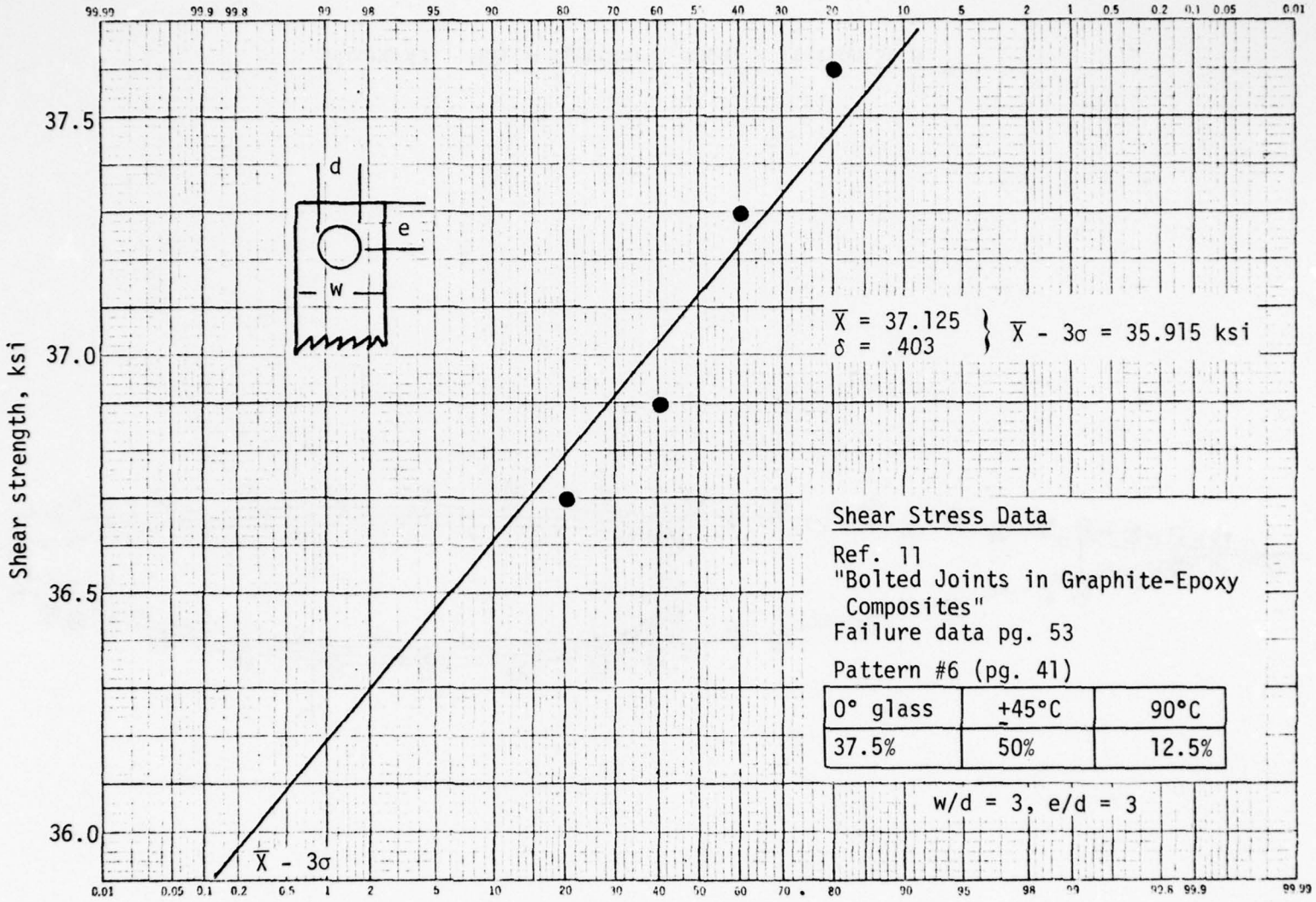

Figure 48. Shear stress data.

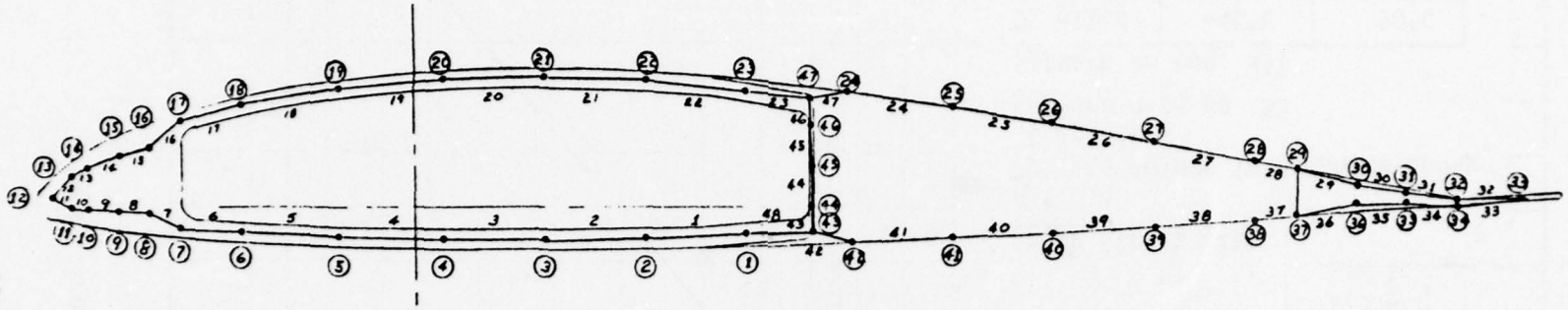

Figure 49. SHELLD structural model - station 36.5.

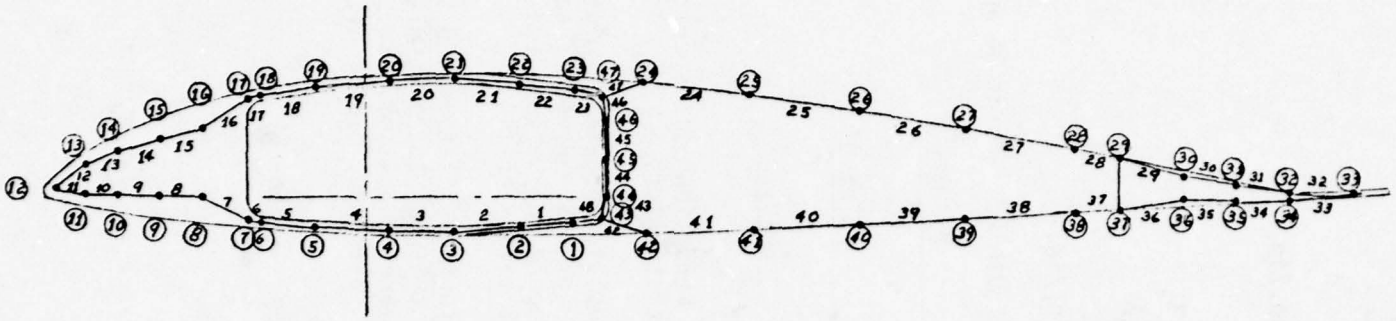

Figure 50. SHELLD structural model - station 179.916.

Bar 9 Uni-E-Glass:

$$e = \frac{15.85 \pm 3.49}{.50} \times \frac{10^3}{10^7}$$

$$= .00317 \pm .000698 \text{ in./in.}$$

Bar 24 $\pm$ 45° S-Glass:

$$e = \frac{-2.45 \pm 3.02}{.27} \times \frac{10^3}{10^7}$$

$$= -.00091 \pm .0011 \text{ in./in.}$$

Points 6 and 9 are plotted on Figure 22. Point 24 appears on Figure 23.

$$\text{M.S.} = \frac{.00115}{.00082} - 1 = .40 \quad \text{Point 6}$$

$$\text{M.S.} = \frac{.00075}{.000698} - 1 = .07 \quad \text{Point 9}$$

$$\text{M.S.} = \frac{.0017}{.00111} - 1 = .53 \quad \text{Point 24}$$

For static load considerations, Condition III is critical. Page 193 indicates that bar 4 has the highest stresses.

The CMAB stress analysis on page 194 indicates a minimum margin of safety in the transverse (22) direction of .03. However, actual blade failure will not occur until breakage occurs in the longitudinal (11) direction which has a calculated margin of safety of .44.

Tip Analysis - Rubber Bonded Interface, Station 130 to Station 211. Table 21 presents a calculation of centrifugal loads resulting from the cast steel weight and antinodal hardware at 354 rpm. Rubber shear stresses are critical for ultimate loadings. Ultimate load at 411 rpm is calculated as:

$$P_{CF} = 1.5 \times \left(\frac{411}{354}\right)^2 \times 22745 = 45989 \text{ lb}$$

Rubber shear area is 192.7 $in.^2$:

$$f_{S_{AVG}} = \frac{45989}{192.7} = 238.7 \text{ psi}$$

$$\text{M.S.} = \frac{600}{238.7} - 1 = 1.5.$$

TABLE 21. TIP WEIGHT CF DISTRIBUTION

Unit Weight lb/in.	Inboard Weight Sta. in. R_1	Outboard Weight Sta. in. R_2	Cumulative Weight lb	Cumulative CF lb
1.76	129	134.	8.8	22745
1.76	134	139	17.6	18613
.23	139	150	20.13	14324
.23	150	160	22.43	13018
.23	160	170	24.73	11745
.23	170	177	26.34	10390
.32	177	178	26.66	9392
.23	178	179.5	27.01	9189
.5	179.5	180	27.26	8969
.23	180	190	29.56	8809
.23	190	195	30.71	7289
.605	195	200	33.73	6599
.545	200	204	35.91	4365
.47	204	212	39.67	2793

The calculated average shear is approached in actual practice by proportioning the rubber thickness distribution to the active perimeter such that the load distribution is uniform. The analysis resulting in the actual thicknesses is a detailed procedure and beyond the scope of this study. The AH-1 composite blade has an identical tip mass support concept. Rubber thickness is .110 in. at the most inboard station. This decreases linearly to a nominal of .053 in., which extends to about 60% of the span length after which it decreases to .032 in. nominal in the tip region.

An additional significant feature of the tip mass concept is the built-in fail-safety. Should the rubber bond fail, the weight will be contained by the tapered spar configuration by a socketing action. This fail-safe principle has been demonstrated by test in the case of the AH-1 composite blade.

Tip Analysis - Low Cycle Fatigue of Weight, Station 204. At station 204, the tip is unsupported by the fiberglass shell. Therefore, the net section at 204 must react ground-air-ground cycle loads due to centrifugal force:

$$P_{CF} = 2793 \text{ lb @ } 354 \text{ rpm}$$

$$A_{204} = 1.11 \text{ in.}^2$$

$$f_T = \frac{2793}{1.11} = 2516.2 \text{ psi}$$

$$= 1258.1 \pm 1258.1 \text{ psi}$$

By inspection for cast stainless steel:

$$M.S. = \text{Large}$$

Section Properties. A determination of all section properties was made by SHELLD. These are presented in Figures 51 through 55.

Weight Calculation. A final weight calculation was performed. Figure 56 illustrates the weight distribution over the span. Total blade weight was found to be 89.33 lb. The span moment was calculated to be 10535.6. The net CG location was found to be .385 in. aft. The polar moment of inertia was calculated to be 341 slug ft^2, which is a 4.3% increase over the present value. These calculations were performed using 50% of the tip variable weight package and 2 lb of chordwise weights at the inboard end.

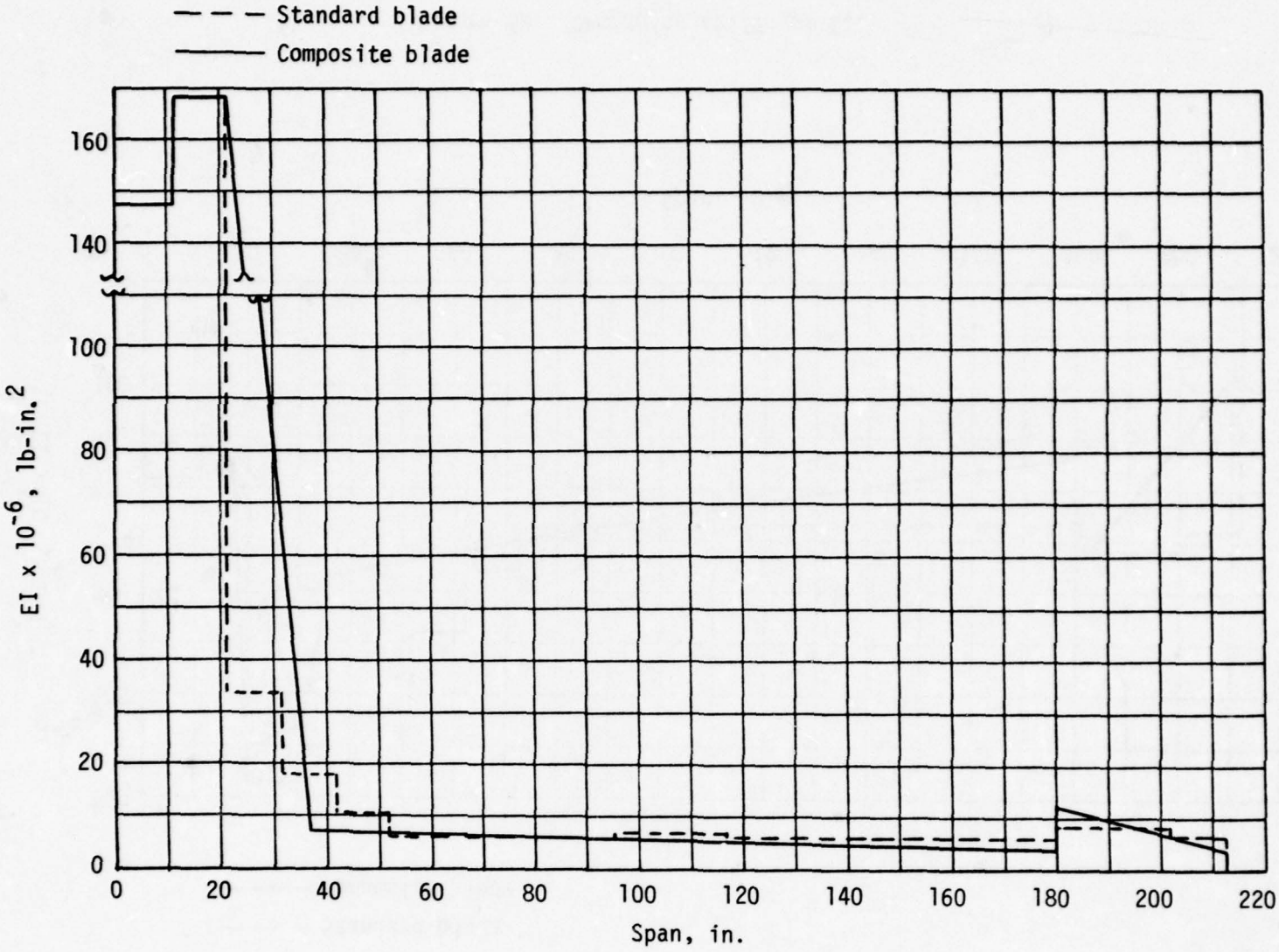

Figure 51. Beamwise stiffness EI.

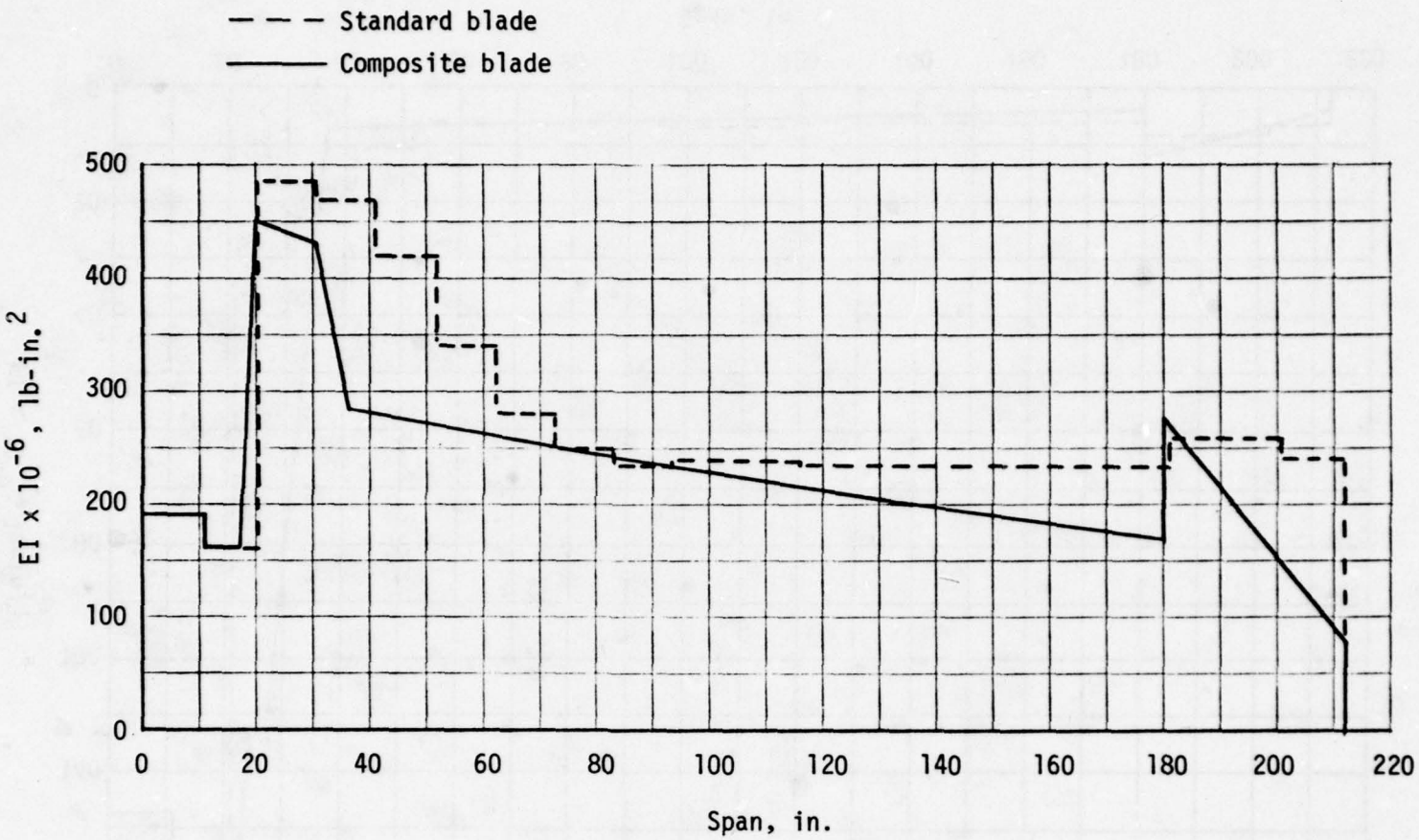

Figure 52. Chordwise stiffness EI.

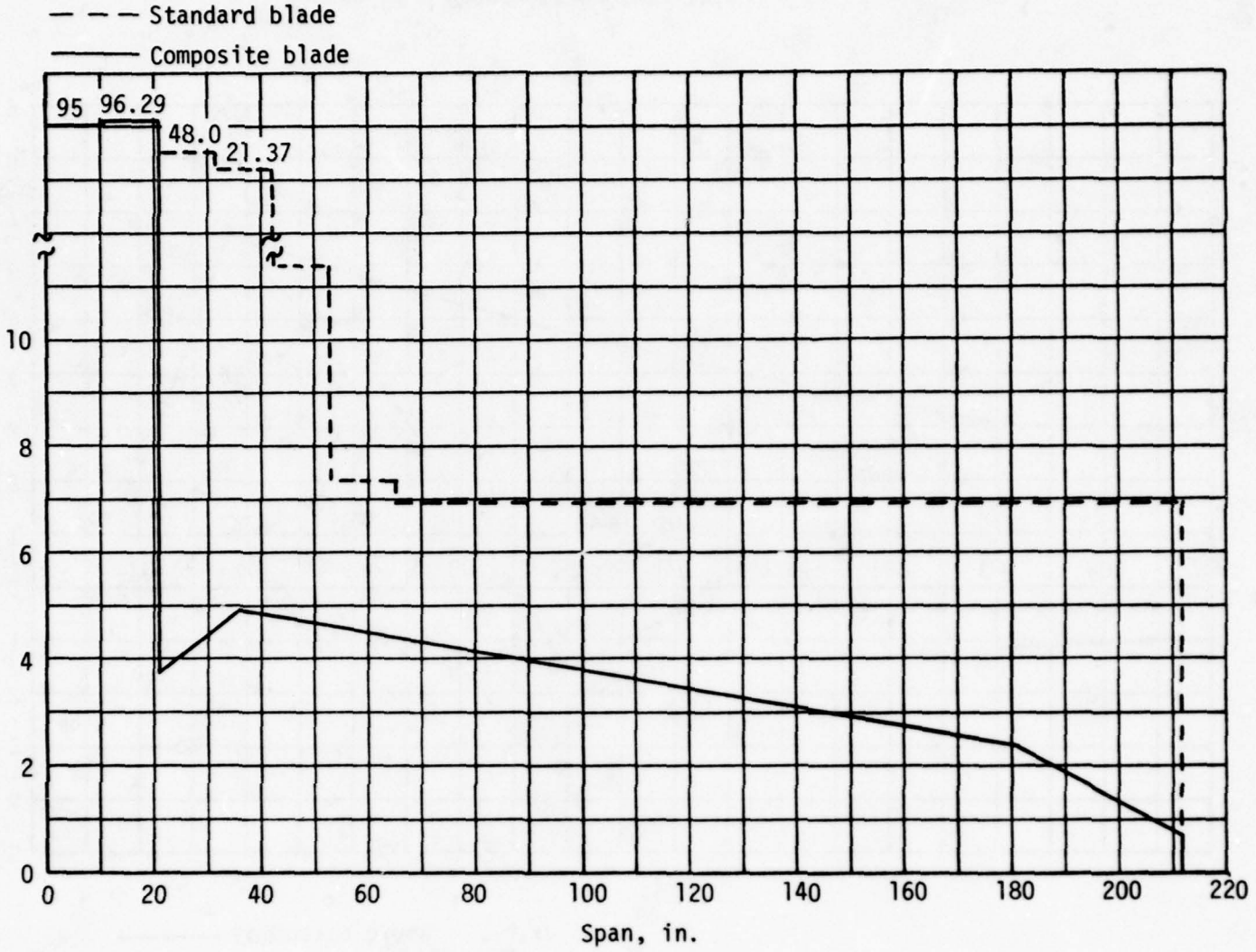

Figure 53. Torsional stiffness GJ.

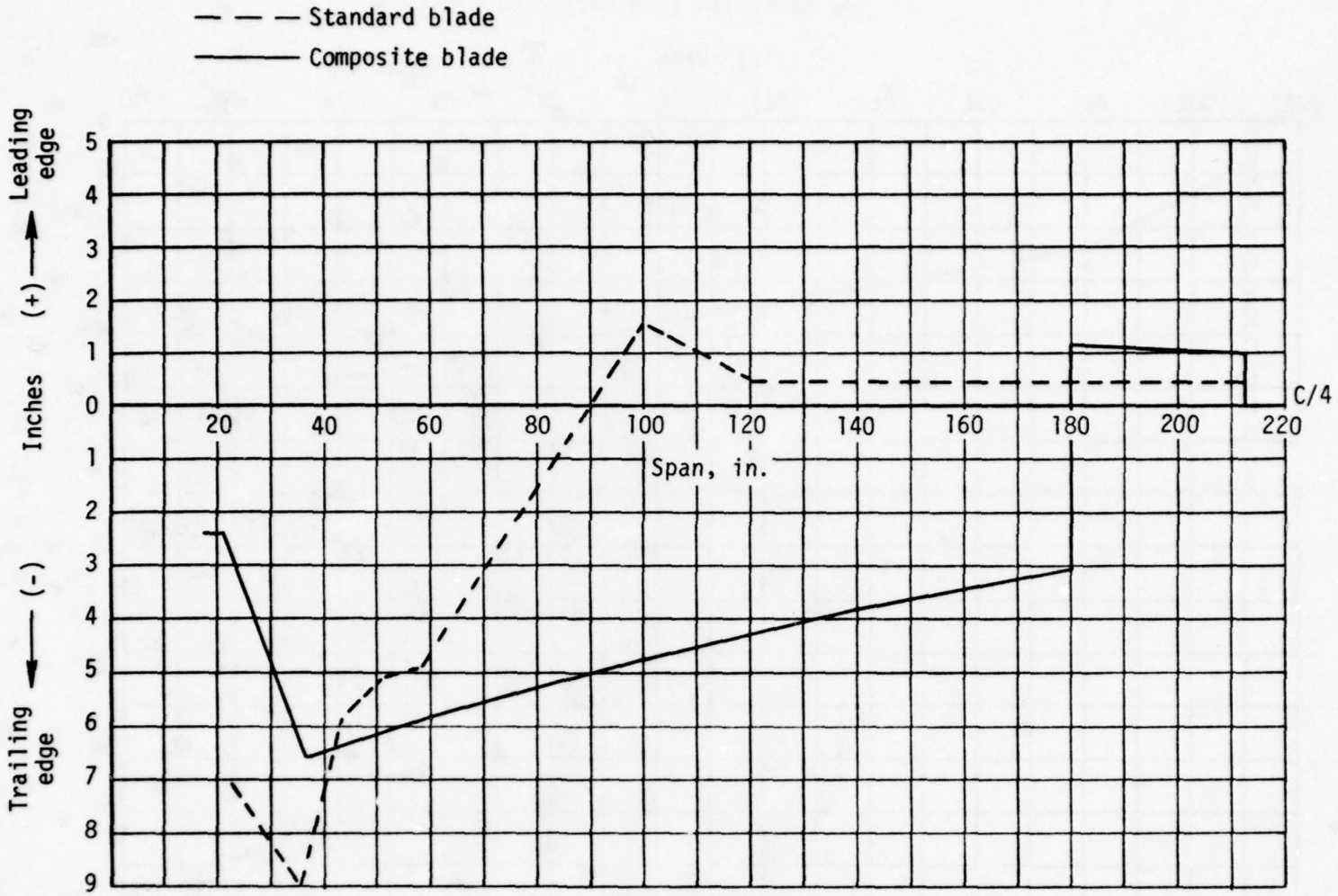

Figure 54. Chordwise neutral axis.

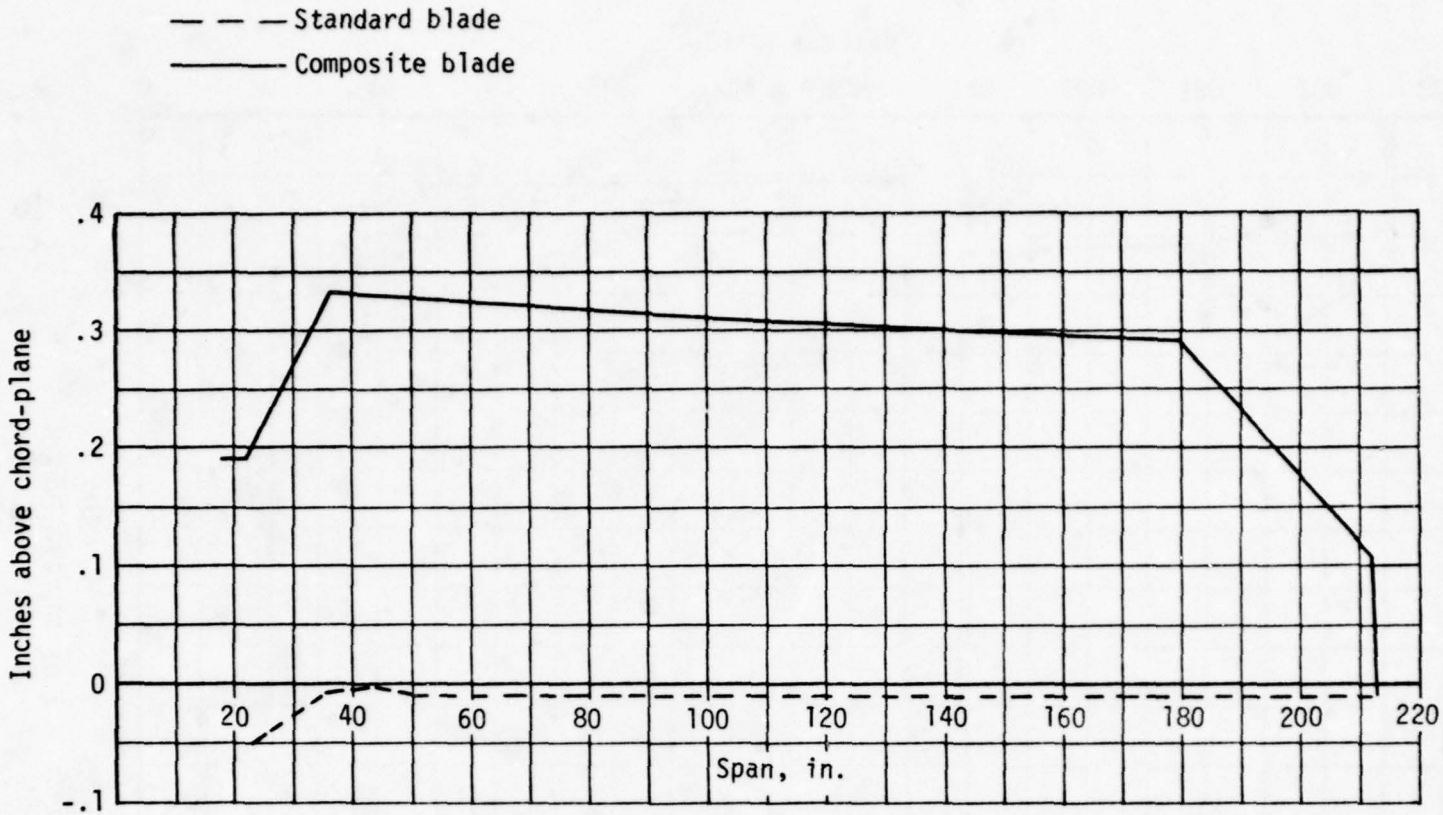

Figure 55. Vertical neutral axis.

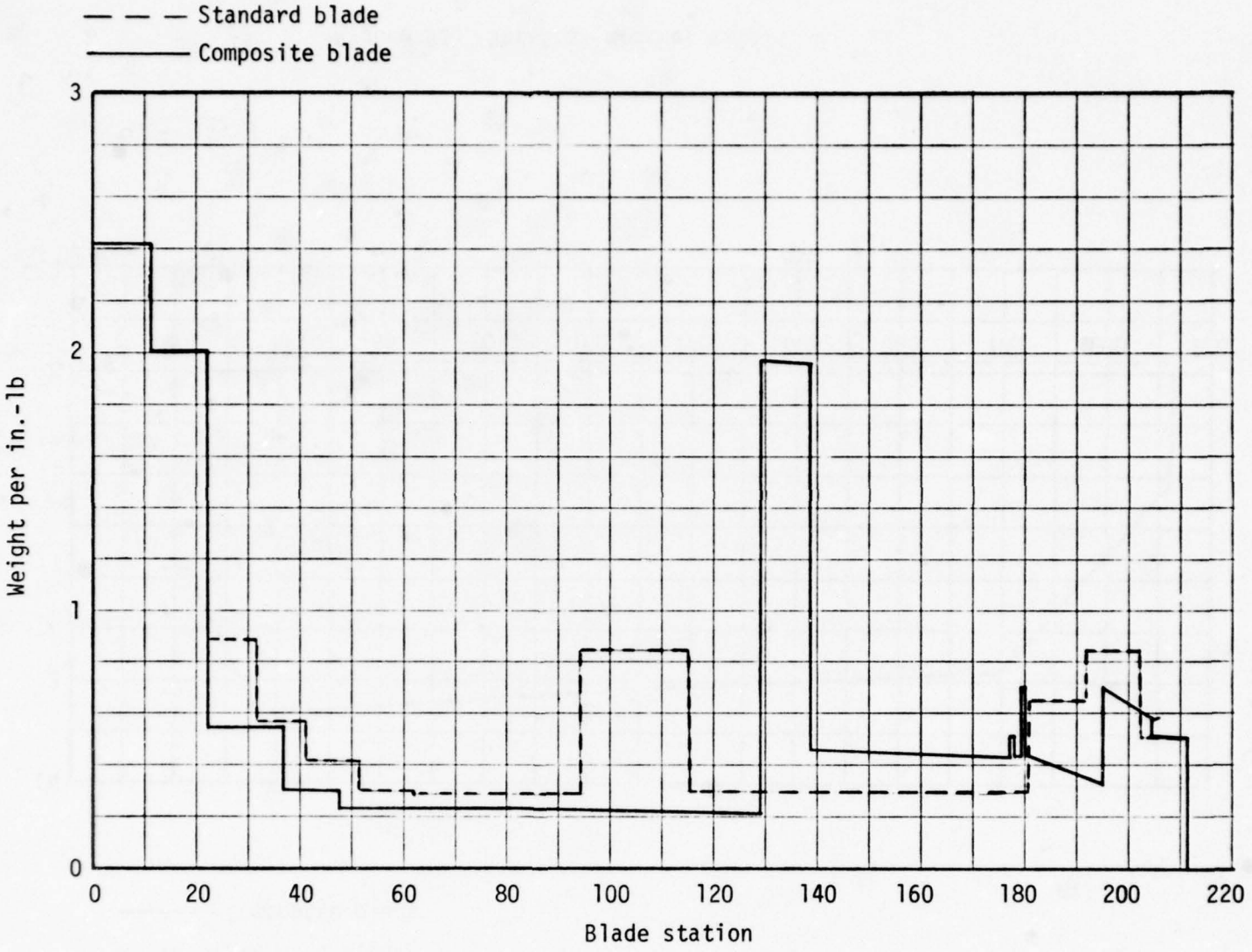

Figure 56. Blade weight distribution.

OH-58 Blade Dynamics and Load Determination

Blade Frequencies. In order to minimize development risk, development cost, and system integration cost, a new component for a successful vehicle with well known dynamic characteristics should be designed to have similar characteristics. This was the approach used in designing the K747 blade for the AH-1 helicopter.

Kaman designed a blade that closely approximates the dynamic characteristics of the B540 blade (standard blade) by matching the elastic and inertial properties of the structure to yield K747 blade natural frequencies that nearly match those of the B540.

The analysis used to calculate the blade natural frequencies for the B540 and K747 is the blade frequency computer program for nonuniform helicopter rotors developed by Rochester Applied Sciences Associates. This computer program determines the coupled natural frequencies and normal modes of a rotating, twisting beam with nonuniform mass and elastic properties. Fully coupled flatwise, edgewise and torsional motions are analyzed for the blades, and an automated frequency search method is used to determine the frequencies and modes for the blade natural frequencies.

Because the AH-1 uses a teetering hub, the coupled modes for both blades were analyzed for collective responses and cyclic responses. The collective responses correspond to a cantilever root end for flatwise motions and a pinned root end for edgewise motions. The cyclic responses correspond to a pinned root end for flatwise motions and a cantilever root end for edgewise motions. For all conditions, the torsion mode is assumed to be cantilevered. Table 22 compares the natural frequencies of both the standard B540 and the K747 blades of the normal operating rpm of the main rotor.

It is seen from Table 22 that the natural frequencies of the K747 blade are within the 10 percent of the B540 blade. Further shake tests of both blades confirmed this. In the development flight test of the K747 blade, no dynamic problems were encountered and a very successful program resulted.

This same philosophy is used in the preliminary design of the OH-58 K757 composite blade. In order to determine best EI distribution and mass distribution of the Kaman composite blade to match the standard OH-58 blade frequencies, Kaman's blade frequency program was used. This program is similar to the computer program for nonuniform helicopter rotors developed by Rochester Applied Sciences Associates, except that only uncoupled modes can be calculated. Table 23 gives the results of these calculations.

It is seen from Table 23, the uncoupled blade frequencies, that the Kaman K757 composite blades match the Bell standard blade frequencies very closely. The EI and mass distribution obtained from this phase of blade frequency matching was then used in the blade frequency computer program developed by Rochester Applied Sciences Associates to determine the coupled

TABLE 22. COUPLED BLADE NATURAL FREQUENCIES OF THE AH-1 HELICOPTER

Mode	Blade Frequency/Rev		Percent Deviation
	B540	K747	
Collective Mode			
First Flatwise	1.03	1.03	0
Second Flatwise	2.63	2.88	9.5
First Torsion	3.26	3.19	2.1
Third Flatwise	4.54	4.91	8.4
First Edgewise	6.73	6.88	2.2
Second Torsion	7.96	7.78	2.3
Cyclic Mode			
First Flatwise	.99	.95	4.0
First Edgewise	1.61	1.56	3.1
Second Flatwise	2.45	2.70	10.2
First Torsion	3.26	3.19	2.1
Third Flatwise	4.30	4.65	8.1
Second Torsion	7.60	7.59	0.1

TABLE 23. UNCOUPLED BLADE NATURAL FREQUENCIES OF THE OH-58 HELICOPTER

Mode	Blade Frequency/Rev		Percent Deviation
	Bell	Kaman	
Pin-Ended Modes			
First Flatwise	1.00	1.00	0
Second Flatwise	2.549	2.783	9.2
Third Flatwise	4.956	4.643	6.3
First Edgewise	0	0	0
Second Edgewise	4.676	5.040	7.8
Cantilever Modes			
First Flatwise	1.154	1.147	0.6
Second Flatwise	3.049	3.156	3.5
Third Flatwise	6.219	6.699	7.7
First Edgewise	1.011	.978	3.3
Second Edgewise	6.028	6,506	7.9

natural frequencies. It was realized, however, that the first cantilever edgewise mode was too close to 1/rev, which did not match Bell helicopter calculations of the first cantilever edgewise mode. Bell Helicopter Company fan plots which were Government-supplied data indicate a first edgewise cantilever mode of 1.314/rev as indicated in Table 24. Since the RASA blade frequency program could not reproduce this value using the supplied mass and stiffness properties increases in EI between station zero and 21 were made until the standard blade frequency was achieved. These EI values were then used to calculate the edgewise frequencies for the K757 blade. This is a reasonable approach since some undocumented parameter of the hub and retention hardware must account for the discrepancy.

Because the OH-58 uses a teetering hub, the coupled modes for both the standard and composite blades were analyzed for collective and cyclic responses. The collective responses correspond to a cantilever root end for flatwise motions and pinned root end for edgewise motions. This collective mode is excited by even harmonic excitations. The cyclic responses correspond to a pinned root end for flatwise conditions and a cantilever root end for edgewise motion. This cyclic mode is excited by odd harmonics of rotor excitation. For all conditions, the torsion mode is assumed cantilevered. Table 24 compares the natural frequencies of both the standard and improved rotor blades at the normal operating range of the main rotor. Figures 57 and 58 contain fan plots for the K757 and the standard blade.

TABLE 24. COUPLED BLADE NATURAL FREQUENCIES OF THE OH-58 HELICOPTER

Mode	Blade Frequency/Rev		Percent Deviation
	Bell	Kaman	
Collective Mode			
First Flatwise	1.148	1.147	0.1
Second Flatwise	3.031	2.917	3.7
First Edgewise	4.669	5.014	7.4
Third Flatwise	6.273	6.651	6.0
First Torsion	7.4038	7.614	2.9
Cyclic Mode			
First Flatwise	1.0	9.0	0
First Edgewise	1.314	1.284	2.3
Second Flatwise	2.542	2.685	5.6
Third Flatwise	4.976	4.816	3.2
Second Edgewise	6.809	6.898	1.3
First Torsion	7.098	7.256	2.2

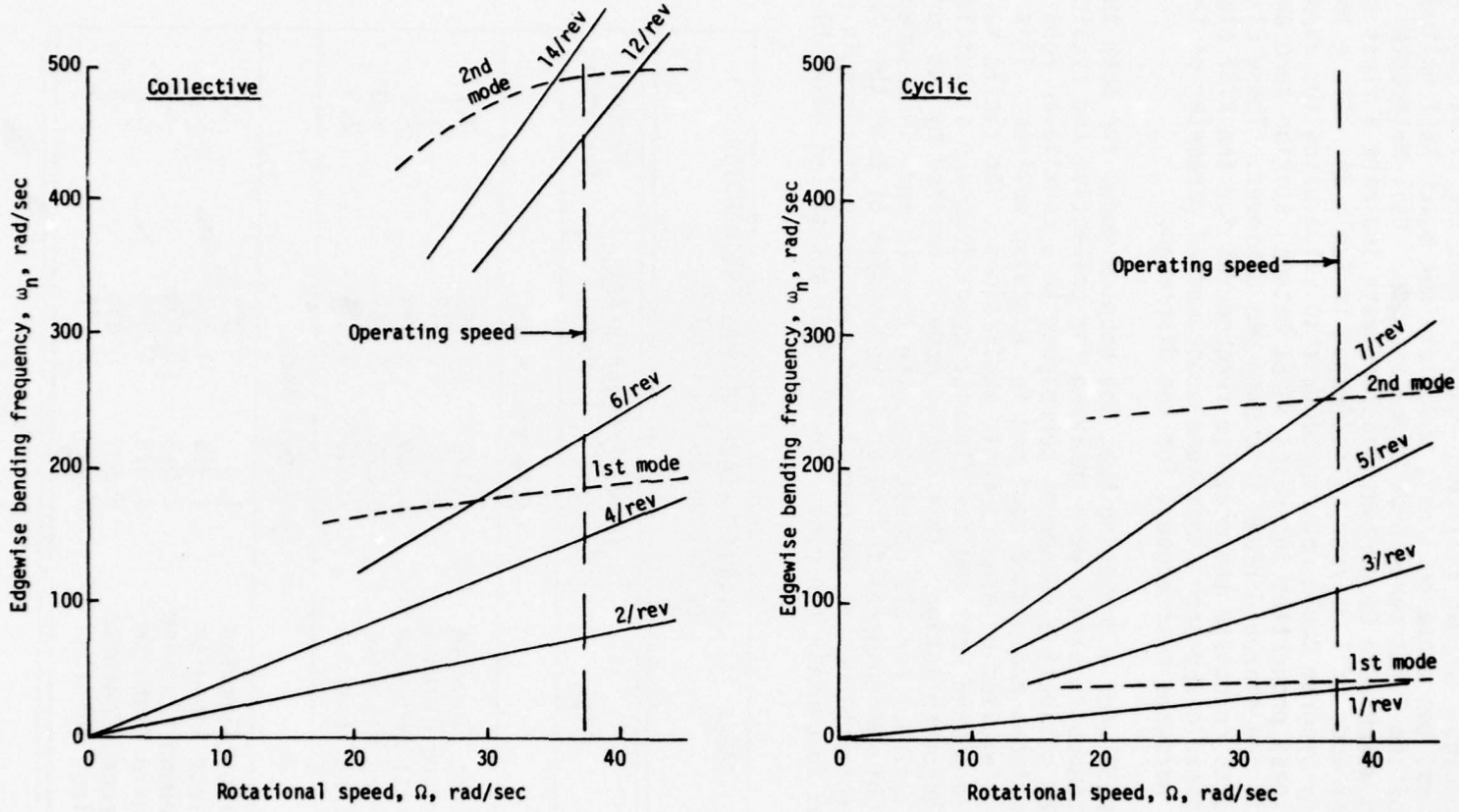

Figure 57. OH-58C/A, Kaman K757 blade, in-plane bending frequencies.

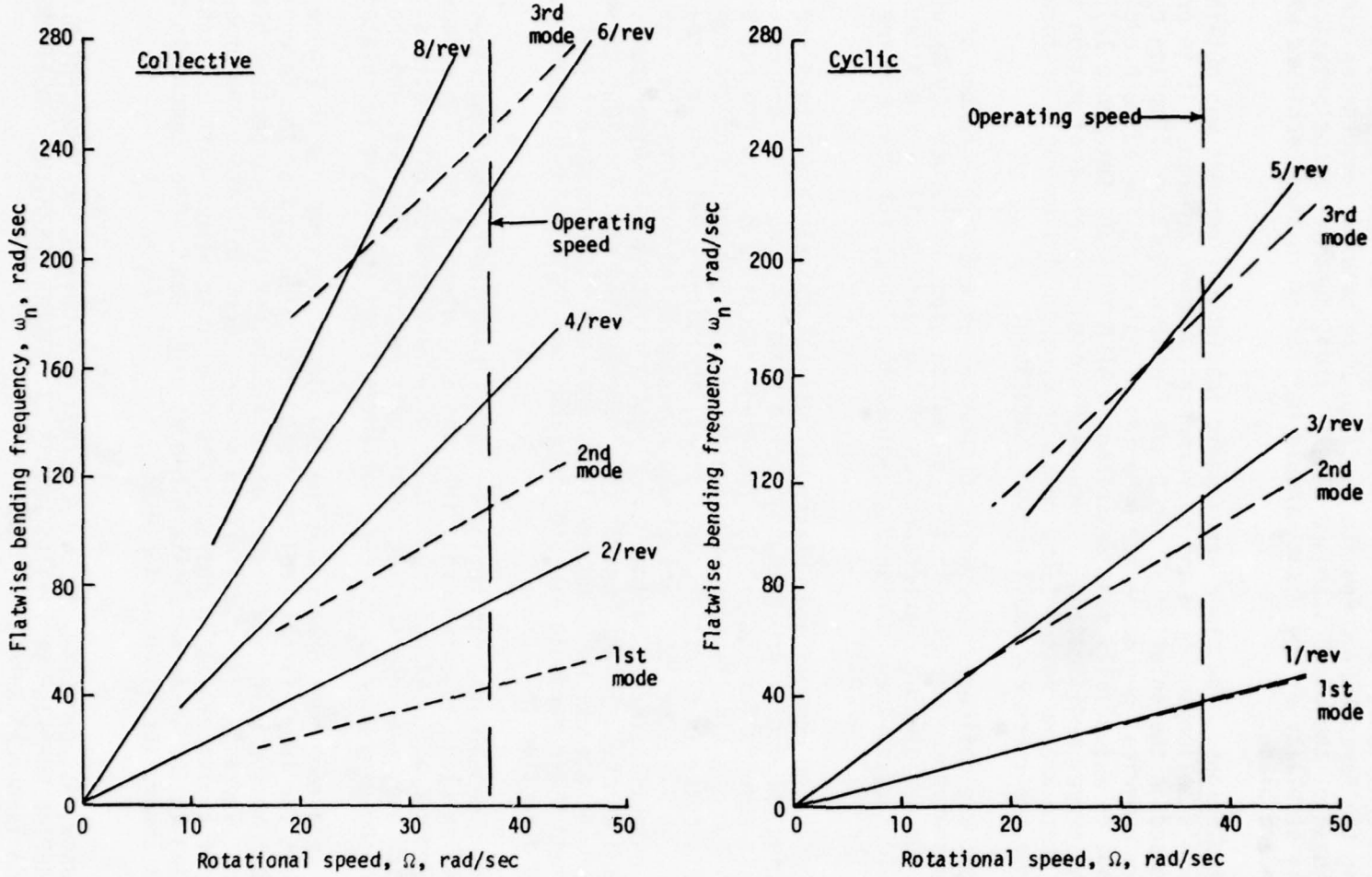

Figure 58. OH-58C/A, Kaman K757 blade, out-of-plane bending frequencies.

It is seen from Table 24 that excellent agreement has been achieved in designing the Kaman K757 composite blade to have natural frequencies similar to those of the OH-58 standard blade. Thus, dynamic characteristics, including stability of the blade, should be similar to those achieved with the standard blade.

Load Calculations. The blade aerodynamic loading environment was obtained from Kaman's helicopter trim and performance computer program. It is primarily based on the solution of the blade flapping equation of motion by an iterative numerical procedure for a series of points in the azimuth cycle. The method is essentially that described in NACA TN 3366 (Reference 12), but with several modifications. Because the actual equation of motion is solved, there are no restrictions on advance ratio, inflow ratio or forward speed, nor are there any small angle assumptions.

The blades are defined by geometric properties at a discrete number of spanwise stations. Any distribution of twist, taper or camber may be utilized. The aerodynamic characteristics of the blade sections are given in tabular form using Army-furnished two-dimensional data for the baseline and for the VR-7 airfoil.

Rotor forces and moments are obtained by utilizing a strip analysis and integrating the radial and azimuthal force distributions. The converged forces and moments for equilibrium flapping are utilized in a program which provides for the simultaneous solution of static equilibrium of the complete helicopter in all flight conditions, including level flight, steady turns and pull-ups, climb, partial power descents and autorotation. The program output includes, besides the flight attitutde, all integrated forces and moments, flight control requirements, the distributions of section angle of attack, Mach number, lift, drag and pitching moment coefficients, and blade harmonic airload distributions in both in-plane and out-of-plane directions.

The bending moment analysis begins by determining the response matrices on the rotating blade to unit loads, in-plane and out-of-plane. The steady and 4 harmonics of loadings from the trim and performance calculations, just described, are then applied to the unit response matrices, and the resulting bending moments, slopes, deflections and shears are calculated.

The net resultant root shears for the two blades are compared in Figure 59 throughout the level flight regime. Both were calculated by the foregoing analytical method using the proper airfoil data for their respective blade sections. There is little difference between them, indicating the probability of simlar vibration characteristics of both blades with a slight edge going to the Kaman composite blade at high speed. The components of the root shears are given in Table 25.

12. Gessow, A., and Crim, A. D., A METHOD OF STUDYING THE TRANSIENT BLADE FLAPPING BEHAVIOR OF LIFTING ROTORS AT EXTREME OPERATING CONDITIONS, NACA Technical Note 3366, 1955.

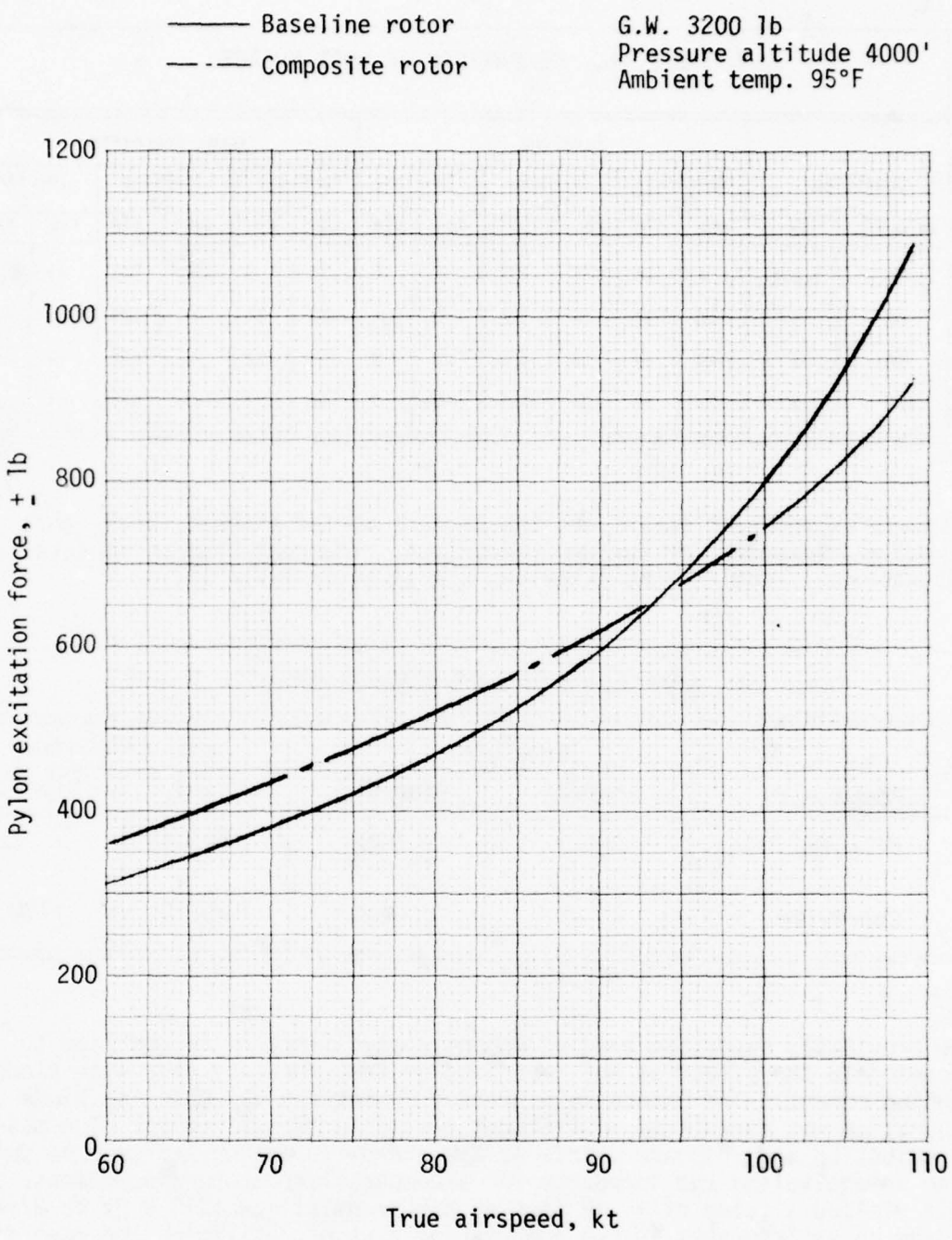

Figure 59. Comparison of resultant pylon excitation force.

TABLE 25. COMPARISON OF ROOT SHEARS

Condition		Baseline						Kaman Composite					
		Vertical 2Ω		In-Plane 1Ω		In-Plane 3Ω		Vertical 2Ω		In-Plane 1Ω		In-Plane 3Ω	
Velocity	n_z	cos	sin	cos	sin	cos	sin	cos	sin	cos	sin	cos	sin
60	1.414	4	-4	105	492	1	4	-34	3	153	543	-1	1
60	1	-6	32	46	300	-1	1	-22	12	81	346	<-.5	<.5
78	1	-9	48	26	435	-2	2	-32	22	70	491	-1	+1
109	1	25	78	-134	1075	-5	3	-56	83	-109	898	-1	-1

Inasmuch as the root shears are the highest at the highest speed, this condition was selected for further comparison. The root bending moments for the 109-knot, level-flight condition are given in Table 26.

TABLE 26. COMPARISON OF ROOT BENDING MOMENTS, IN.-LB

Component	Baseline		Kaman Composite	
	Steady	Vibratory	Steady	Vibratory
Flapwise	-3650	± 4522	-5199	± 2825
Chordwise	23183	±20000	20210	±18007

The previously described bending moment analysis had to be modified to accommodate the effect of hub impedance on the vibratory chordwise blade bending moment. The chordwise vibratory moment for the baseline blade configuration was correlated with flight test data (Reference 9). The mass distribution and response matrix of the chordwise motion was used to determine an equivalent hub impedance for a comparable root bending moment. This yielded a value of ± .78 inch of hub translation at 11.8 Hz or 2/rev of the rotor frequency in the nonrotating system. Utilizing the mass distribution and response matrix for the Kaman composite blade system yielded a hub translation of ± .64 inch at 11.8 Hz and a chordwise vibratory root bending moment of 18,007 in.-lb.

The foregoing table indicates that the root bending moments for the Kaman composite blade are very close to those for the baseline blade. The stress analyses for the Kaman composite blade utilizing the flight test bending moments of Reference 9 therefore will be slightly conservative.

The same flight condition was used to evaluate the blade torsional moment by means of the trim and performance program. The aerodynamic pitching moments and the rigid body centrifugal twisting moments for the Kaman composite blade were integrated, yielding the azimuthal variation shown in Figure 60. The indicated vibratory torsional moment of $\pm$ 550 in.-lb is significantly less than the design torsional vibratory moment given in Figure 30.

In general, the loading conditions on the Kaman composite blade are comparable to those obtained from the flight tests of the standard rotor, which was the basis of the stress analysis.

Manufacturing Methodology

The OH-58 K757 composite blade is designed with quality, simplicity and low cost in mind. This comes about largely because the fabrication technique, selected materials and configuration are mutually dependent parts of the design. Wet filmanet winding over a hard mandrel was selected because a tapered spar can efficiently be constructed with fibers laid in a predetermined, totally repeatable pattern. The technique is, however, dependent on the development of highly accurate hard tooling, e.g., internal mandrels and external molds, to produce consistently good spars. Experience with the AH-1 program has been that such tools can be developed within an anticipated development period.

The aft spar root reinforcement, nose block and trailing edge spline are linear filament windings of E-glass roving. This insures good fiber volume and fiber orientation control. The upper and lower spar caps are also linear windings but, in this instance, S-glass has been selected. These components are staged in closed molds to retain a tacky shape and are completely cured in the final assembly fixture. Sections are tapered by a well developed technique using a series of pins or blades to wind over and terminate a particular layer while allowing others to continue.

The upper and lower spar root reinforcements are lay-ups made from a scheduled series of preimpregnated uniglass and cross-ply carbon graphite pieces. These are fully cured in the final blade assembly.

Skins and doublers are filament wound on large diameter mandrels to produce a product with good weight control and, due to the resulting basket weave effect, excellent inherent damage resistance. This method results in the economical production of relatively large cross-ply pieces with little waste.

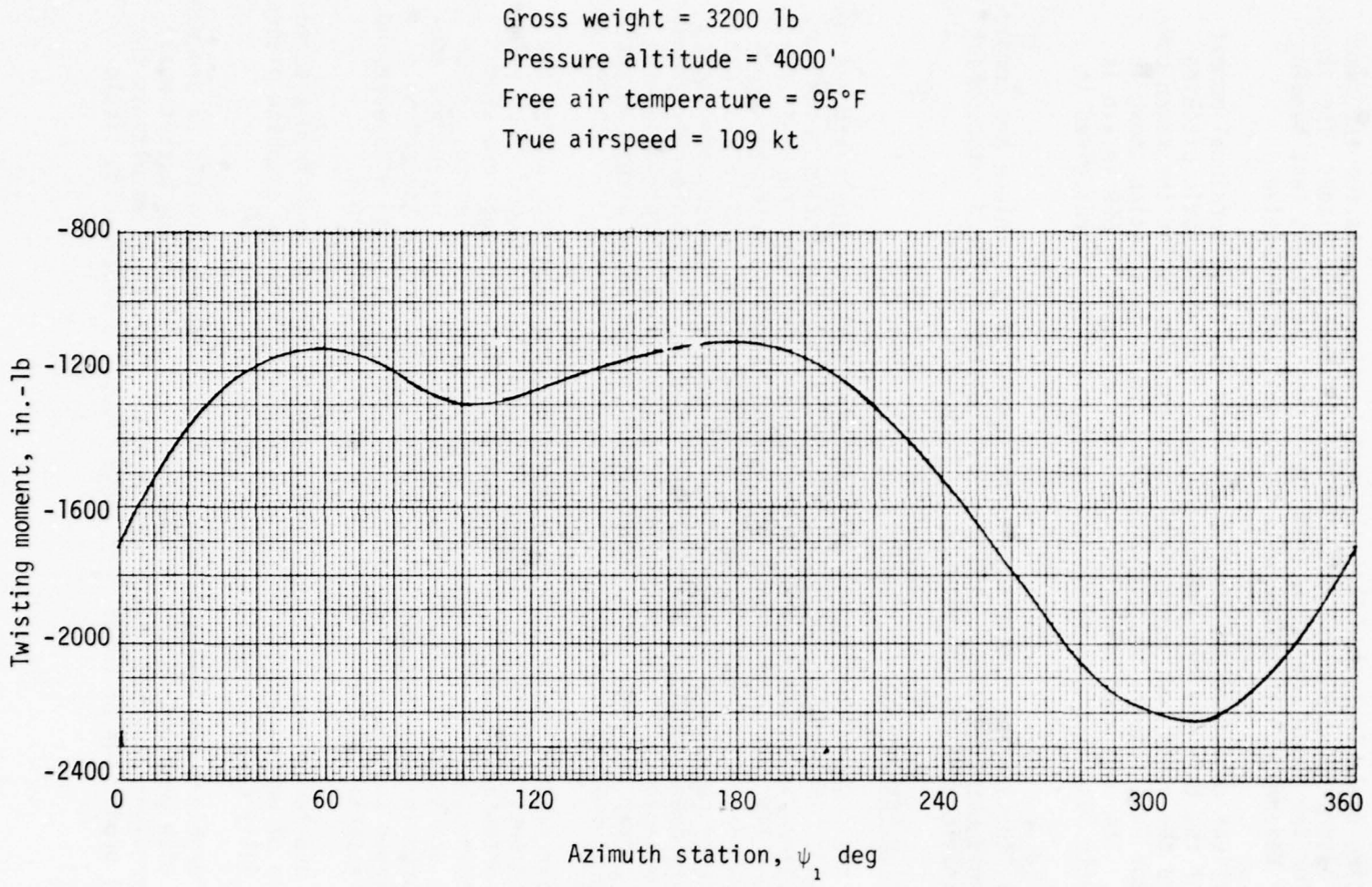

Figure 60. Net blade pitching moment at pitch control link - composite rotor blade.

The core material is shaped by forcing one side of the core block to conform and cutting the other surface to match. This results in a slight obliqueness of the cell orientation to one of the surfaces. Experience has shown this to have no significance to strength of efficiency.

The manufacturing sequence is shown in Figure 61. The mandrel is in three pieces. The tip weight serves as a permanent outboard mandrel. A mid-span mandrel mates with it; these two comprise the aerodynamic twist portion. Next, the inboard mandrel is mated. It has a reverse twist and allows an efficient structural section at the main retention. These mandrels are secured by means of a long "skewer bolt" which goes through holes in the removable mandrels and secures to a hole tapped in the tip ballast weight. With the mandrel assembled, it is mounted, using its trunnions, between the spindles of the filament winding machine.

Winding commences with 90° and cross-ply overwraps which secure the forward nose block longo and aft spar reinforcement. Thereafter, the upper and lower uniaxial cap and root reinforcements are added and a final securing cross-ply overwrap is applied. At this point, all the pre-cut and shaped components are assembled. These are builtup in the bonding fixture, laying one skin and its doublers on the bottom first. Next comes the spar, core and trailing edge spline; then the closing skin with its doublers. The fixture is closed and all components are co-cured. After curing, the blade is removed from the mold. The inboard mandrel is removed and the mid-span mandrel is pulled through the reverse-twist inboard section of the blade. This mandrel withdrawal history is illustrated in Figure 62. The completed blade has the mid-span ballast inserted and attached to the mandrel attach holes. Bushings, washers and end closures are added to complete the blade.

OH-58 Composite Blade Reliability, Maintainability and Life-Cycle Cost Analysis Report Sections

Reliability. The Contractor has participated in a number of programs specifically related to evaluating reliability and maintainability of Army helicopter rotor blades. Among these are the ongoing AH-1 Improved Main Rotor Blade program (IMRB), the Program for Phased Maintenance Check List Development, and the Field Repairable/Expendable Rotor Blade (FREB) program. In the two blade programs, extensive effort was spent in understanding the types of damage, both internal and external, that could occur on a helicopter main rotor blade in a combat environment. Based on the information supplied by the Army and measured in the field, a wide variety of repairs were both designed and tested under simulated field conditions. These repairs were subsequently whirl and flight tested during the structural demonstration parts of the programs. In the Phased Maintenance Check List program, data are presently being taken on Army helicopters to evaluate, among other things, the types of maintenance action required and the frequency of those actions. These programs are the most recent in a long series of programs in which the Contractor has participated and which have given him wide experience in both understanding the Army's blade maintenance problems and in developing and utilizing repair procedures designed to

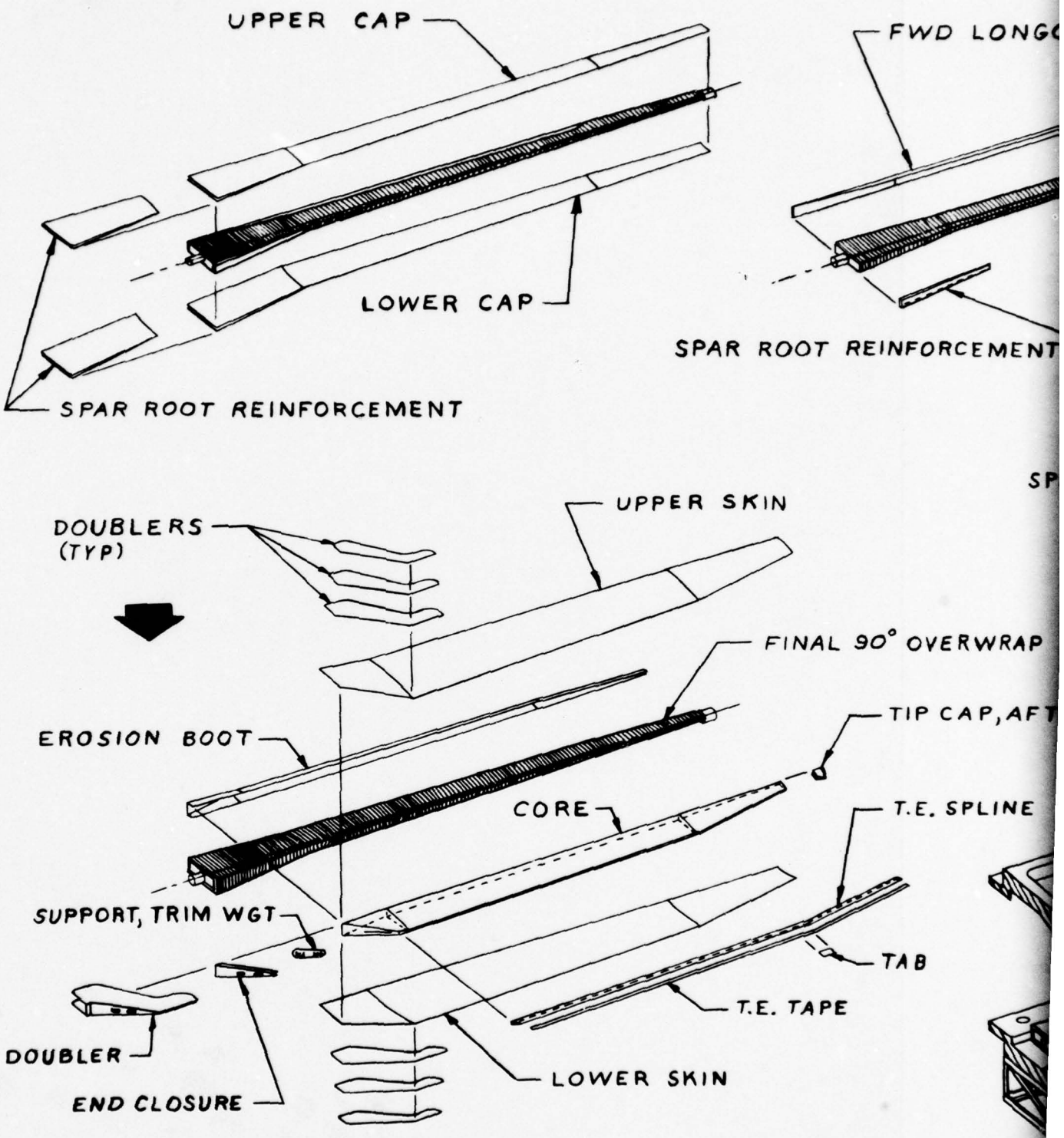

Figure 61. Manufacturing sequence.

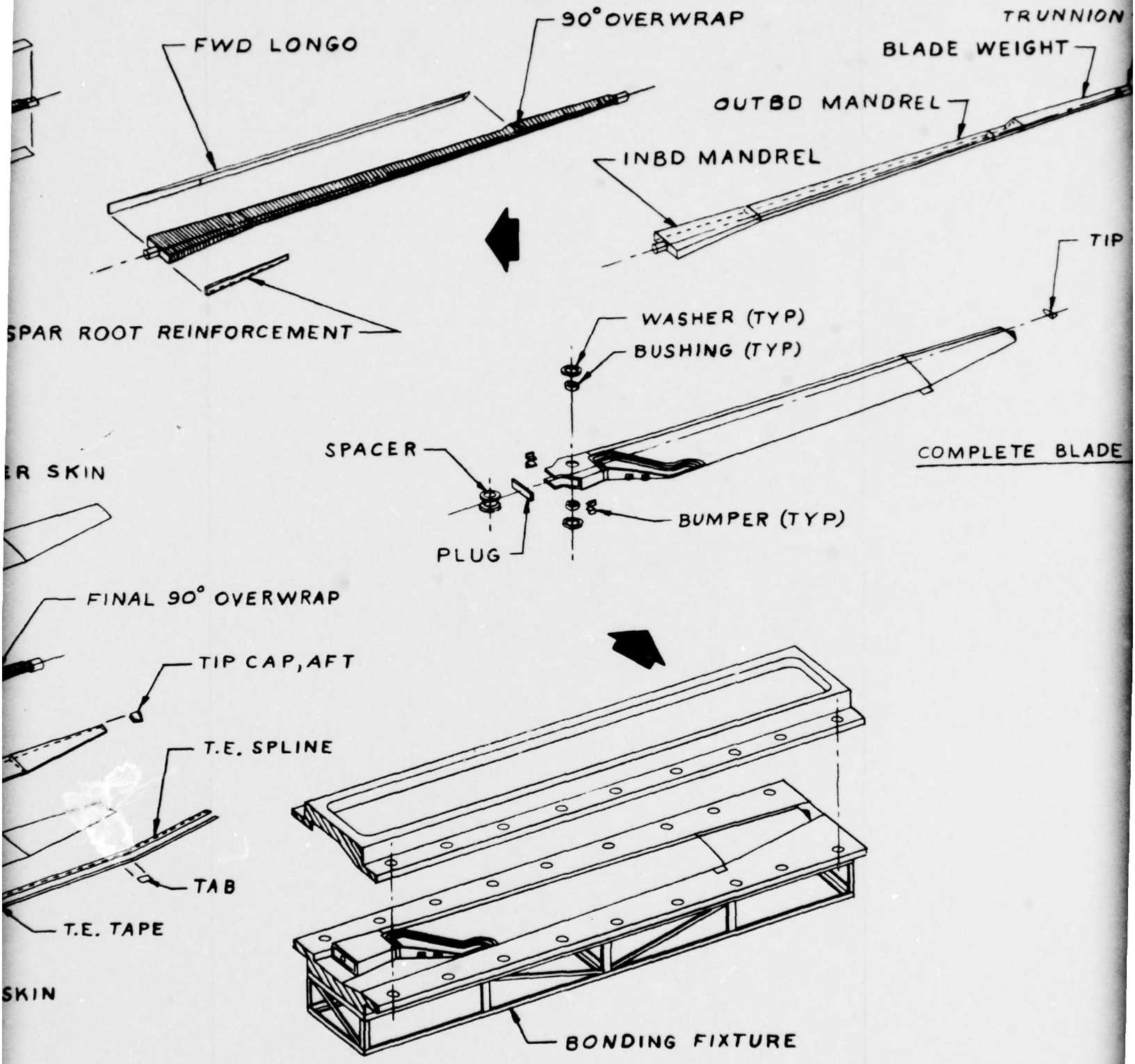
FWD LONGO
90° OVERWRAP
TRUNNION
BLADE WEIGHT
OUTBD MANDREL
INBD MANDREL
TIP
SPAR ROOT REINFORCEMENT
WASHER (TYP)
BUSHING (TYP)
SPACER
COMPLETE BLADE
BUMPER (TYP)
PLUG
FINAL 90° OVERWRAP
TIP CAP, AFT
T.E. SPLINE
TAB
T.E. TAPE
BONDING FIXTURE

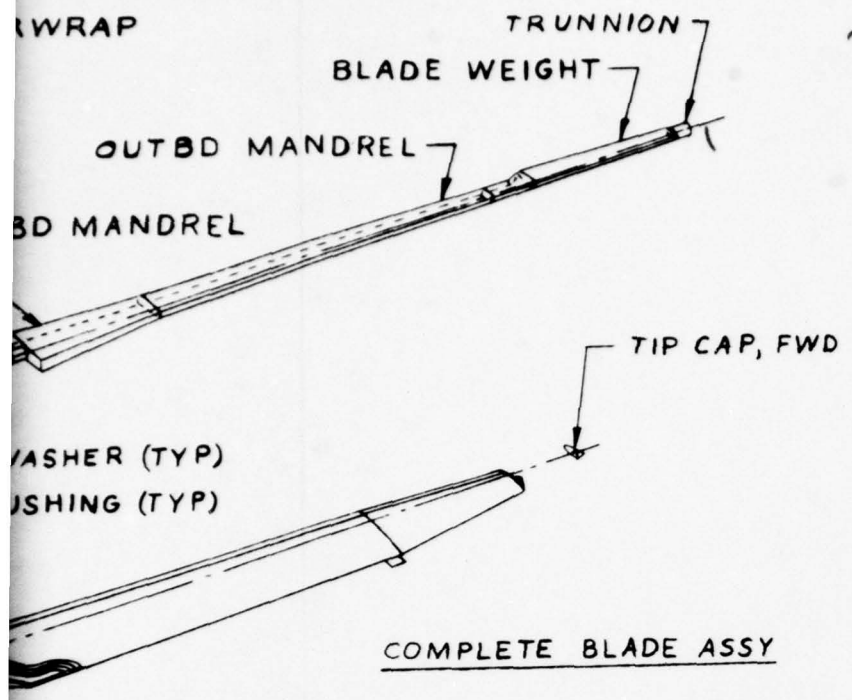

COMPLETE BLADE ASSY

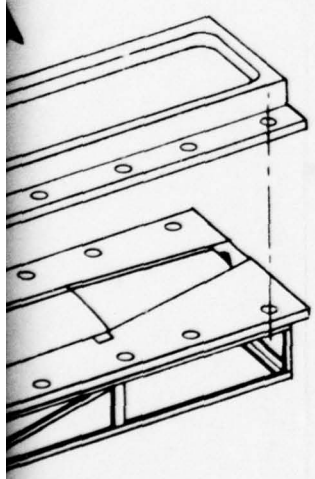

NG FIXTURE

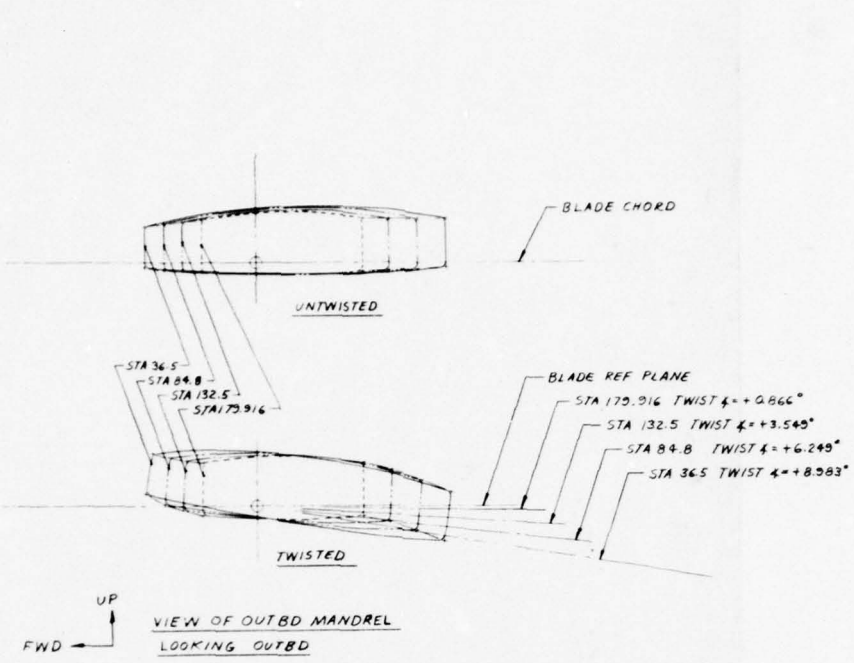

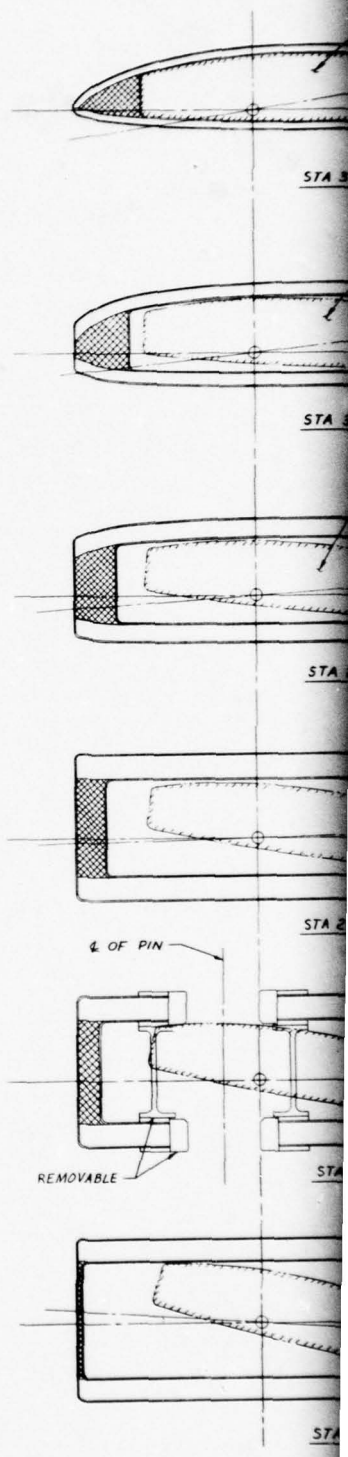

Figure 62. Mandrel withdrawal history.

1

2

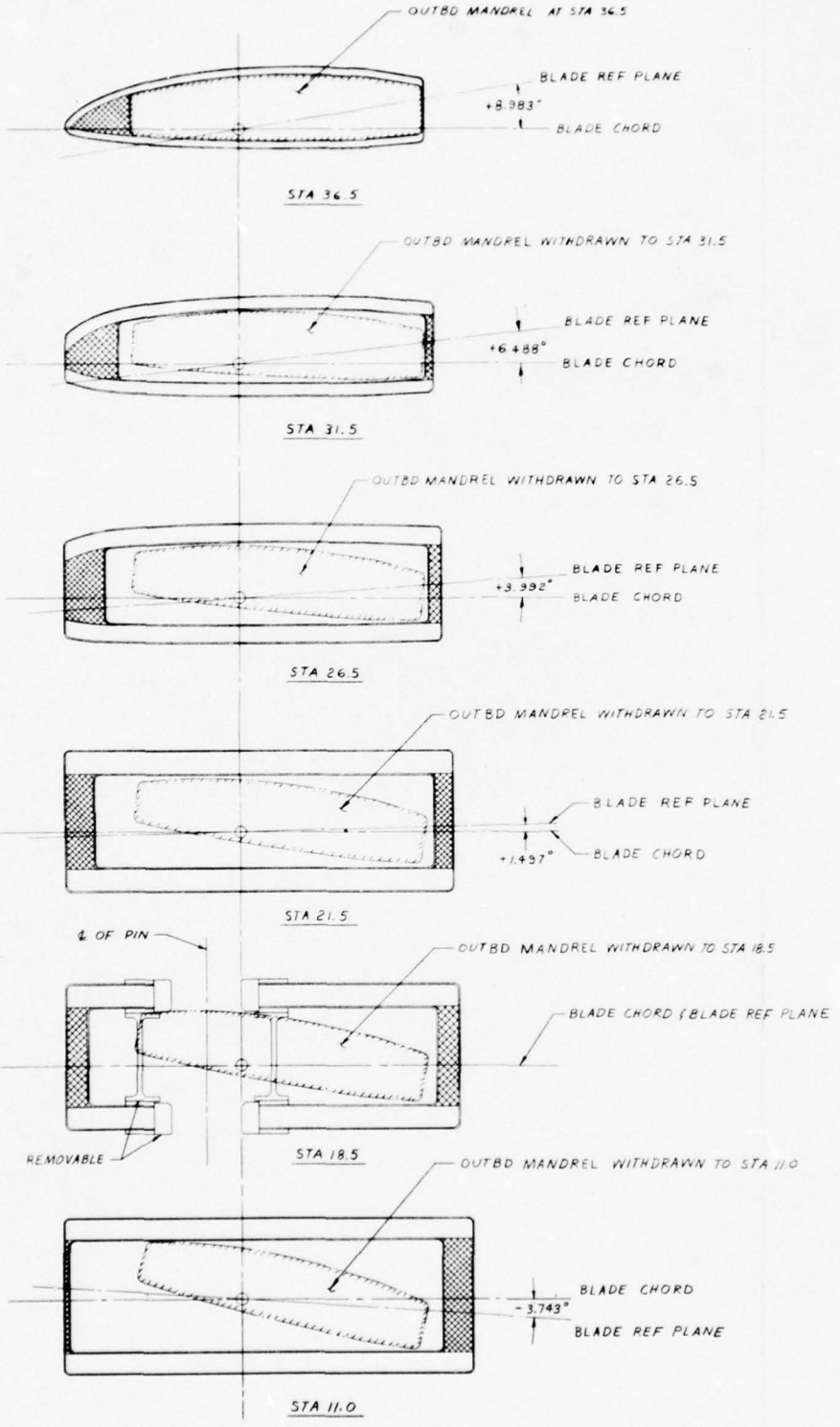

DE CHORD

REF PLANE
179.916 TWIST ℄ = +9.866°
STA 132.5 TWIST ℄ = +3.545°
STA 84.8 TWIST ℄ = +6.249°
STA 36.5 TWIST ℄ = +8.383°

efficiently and effectively reduce the Army's blade-related helicopter costs. This background of experience was drawn upon for this OH-58 composite main rotor program reliability and maintainability section of this report.

During the AH-1 program, methods were developed for both producing a highly damage resistant blade and for repairing the blade in the event damage did occur. Much of the effort in this program revolved around evaluating the required repairs to the AH-1 Improved Main Rotor Blade and developing suitable repairs that could be done in a minimum amount of time and at field level by MOS 67N20 personnel. Repairs were designed, damage was inflicted to the blade, testing was done to insure blade survivability during operation with damage, and then repairs were effected under simulated field conditions by MOS 67N20 personnel. During this full range of testing it was shown that a blade could survive damage and fly back to base of operation, and that repairs could be made successfully in the field. The knowledge gained in the development of these repairs for the actual AH-1 blade, and the first-hand repair experience developed by the Contractor were used as primary inputs in determining the reliability and maintainability parameters associated with the OH-58 composite blade.

The Army Phased Maintenance Check List program has given the Contractor further insight into the frequency and types of repairs that are encountered by typical blades in the Army helicopter fleet. This information, together with standard Army external damage prediction methods, was used to make the projection of mean time between failures (MTBF) for the K757 blades.

The Army *hundred-random-damage-scenario* method was used to evaluate the frequency of external damage on the OH-58 composite blade. By this method of analysis, an area of 30 x 300 inches is assumed to contain 100 different damages whose location and severity are randomly distributed. The OH-58 blade planform was placed in this area, and the centerline of rotation and quarter chords were superimposed on the area in the prescribed manner. Because the OH-58 composite blade is smaller in both chord and span than 30 x 300 inches, a large percentage of the hundred random damages will miss the blade completely. These misses were eliminated from the induced damages considered below. Table 27 shows the results of this distribution of damage. Twenty-seven actual events occur on the blade from random damages and, per the Statement of Work, this is interpreted as being representative of a mean time between failures due to induced damage of 1,000 blade hours.

In order to evaluate the frequency of inherent damages, the blade was compared to available data (Reference 13) for the IMRB. The primary differences between the two blades are as follows. First, the OH-58 blade is

13. Smyth, W. A., FINAL MAINTAINABILITY REPORT FOR THE IMPROVED MAIN ROTOR BLADE FOR THE AH-1 HELICOPTER, Kaman Report R-1355, Kaman Aerospace Corporation, Bloomfield, Connecticut, June 1977.

TABLE 27. INDUCED DAMAGE ESTIMATE AND DISPOSITION

#	Damage Type		Dimensional Description Span	Chord	Depth	Induced Damage Affected Blade Elements	Maint. Level Accept	Field	Depot	Scrap	Repair Type	Average Productive Time, hrs	Cure Time, hrs
1	Dent	E	.544	4.407	.235	Skin & core		X			5" skin	1.26	.5
13	Nick	E	1.164	1.832	.013	Boot/skin (over bearing plate/spar)	X						
19	Dent		2.277	3.540	<.001	Afterbody	X						
20	Battle damage	E	1.149	1.215	through	Skin & core		X			3" double plug	2.30	.75
21	Puncture	E	.341	.601	½ through	Skin & core		X			3" skin	1.15	.25
22	Dent	E	3.315	2.130	.028	Skin	X						
27	Puncture	E	.583	.862	½ through	Skin & core		X			3" plug	1.40	.75
28	Dent	E	.686	11.086	.001	Afterbody	X						
32	Dent	E	.793	8.681	.418	Afterbody		X			Double plug	1.55	1.0
34	Dent	E	.947	12.092	.262	Afterbody		X			Plug	1.31	.25
37	Nick	E	.958	1.877	.008	Skin	X						
38	Tear	E	.929	10.050	.971	Skin/core		X			Double skin	1.74	.5
39	Puncture	E	1.332	.625	½ through	Skin & core		X			Plug	1.083	.75
42	Puncture	E	.589	.877	½ through	Spar			X		Plug	16.0	
44	Puncture	E	.782	.585	½ through	Skin & core		X			Plug	1.403	.75
45	Dent	E	.024	4.61	.001	Skin & core	X						
56	Tear	E	.479	5.071	.558	Skin & core		X			Skin patch	1.0	.25
58	Battle damage	E	.148	1.021	through	Skin & core		X			Double plug	.89	1.0
63	Puncture	E	.717	2.047	½ through	Skin & core		X			Plug	1.408	.75
67	Puncture	E	.396	.709	½ through	Skin & core		X			Plug	1.408	.75
71	Battle damage	E	1.349	.863	through	Skin & core		X			Double plug	.89	1.0
73	Puncture	E	.98	1.15	½ through	Skin & core		X			Plug	1.40	.75
78	Nick	E	.964	.571	.035	Boot		X			Patch	.806	5.0
81	Battle damage	E	.945	.793	through	Skin & core		X			Double plug	1.56	1.0
92	Battle damage	E	1.463	.620	through	Boot, bearing plate, spar			X		Spar rep/boot rep	16.0	
97	Puncture	E	.701	2.192	½ through	Skin & core		X			Plug	1.41	.75
99	Battle damage	E	.954	.816	through	Skin & core		X			Double plug	1.56	1.0

smaller than the IMRB. Secondly, the single cell spar of the OH-58 blade extends further aft in percent chord than does the multiple cell spar of the AH-1 blade. Thirdly, the root attachment for the AH-1 blade composite cheek plate is built up and contains chordwise lugs at the root end. Metal fittings are used to connect between those chordwise lugs and the main and drag pins on the AH-1 hub. In the OH-58 blade, cross-ply graphite and unidirectional S-glass plates are introduced into the blade primary structure to provide the necessary bearing strength and accept the main and drag pins from the OH-58 hub. Because the spar is hollow, bushings and spacers are introduced into the composite spar to carry clamp-up loads, and they also improve the durability of the hole in the blade. Fourthly, the weight/tip blade configuration is significantly different for the K757 blade.

The IMRB reliability reports give inherent failure modes for that blade. Adjustments were made to account for the differences between the two blades, as well as the size and criticality of the relative parts. The result of these adjustments is given in damage events per million blade hours in Table 28. Based on the data in Tables 27 and 28, the overall mean time between failures for the OH-58 composite blade can be computed. The inherent failure modes are projected to occur at the rate of 236.7 per million blade hours, while the external failure modes are assumed to occur at 1000 per million blade hours. Combining these two numbers gives a combined mean time between failures of 808.6 hours. This is shown in the following calculation:

$$\frac{1}{MTBF} = \frac{1{,}000{,}000 \text{ Blade Hours}}{1000 \text{ External Failures}} + \frac{1{,}000{,}000 \text{ Blade Hours}}{236.7 \text{ Inherent Failures}}$$

$$MTBF = 808.6 \text{ hours}$$

Two other pertinent reliability parameters are flight-safety reliability and component durability. On the IMRB, mission configuration flight-safety reliability of .999998 for a mission of 1 hour was predicted. Because the primary loads are collected and concentrated at the root end of the helicopter main rotor blade, this number is related to complexity in the root area. The K757 blade has fewer parts and a more straightforward load path at its root end than does the AH-1 blade. Considering this fact, and assuming that the frequency and probability of tip weight loss are equal in both frequency and severity for the two blades, the mission configuration flight-safety reliability for the OH-58 blade can be conservatively assumed to be .999998 for a mission of 1 hour. As mentioned elsewhere in this report, the fatigue life of the OH-58 composite blade is calculated to be 4,703 hours by a conservative analysis. This figure is well above the 3600-hour requirement for a .9 probability of successful flight when weighed against inherent damage modes. Again, considering the relative complexity and simplicity of the IMRB and OH-58 blades, it can be conservatively assumed that the OH-58 composite blade will exhibit a flight-safety durability of .9 or better of surviving a minimum 3600-hour flight retirement life.

TABLE 28. INHERENT DAMAGE MODES AND DISPOSITIONS

Damage	Affected Blade Elements	Rate Per 10^6 Bld-hr	Maint. Level				Men @ Times MTTR		Repair Type
			Accept	Field	Depot	Scrap	Prod.	Cure	
Crack	Root closure	1.02	X	X			1.0	.5	Surface patch
Bond void or delamination	Root closure	1.17		X			1.0	.5	Surface patch
Delamination	Balance weight support	.45			X		7.0		Replace support
Crack	Balance weight support	.60			X		7.0		Replace support
Pin pilot wear	Balance weight support	2.31			X		7.0		Replace support
Corrosion	Balance weight assembly	1.79		X			1.0		Blend out
Cracks in lug	Balance weight assembly	.34			X		6.0		Replace fitting
Wear of pin in plate	Balance weight assembly	6.16			X		4.0		Replace pin
Loose/missing attach hardware	Balance weight assembly	12.10		X			.5		Replace hardware
Cracks	Spar, cell walls	26				X	6.4		Replace blade
Delamination	Spar, nose block	.29				X	6.4		Replace blade
Cracks	Spar, nose block	.26				X	6.4		Replace blade
Delamination	Bearing plates	1.31				X	6.4		Replace blade
Cracks	Bearing plates	1.19				X	6.4		Replace blade
Corrosion of metal inserts	Bearing plates	3.06		X			.25		Replace insert
Bushing wear	Bearing plates	6.16			X		4.0		Replace bushing
Delamination	Root end cell closure	.73		X			.5	.25	Surface patch
Cracks	Root end cell closure	.51		X			.5	.25	Surface patch
Delamination	Tip ballast weight	.15				X	6.4		Replace blade
Cracks	Tip ballast weight	.48				X	6.4		Replace blade
Loose/missing hardware	Tip ballast weight	6.6		X			.5		Replace hardware
Cracks	Tip cap	.13		X			1.5	.5	Replace tip cap

TABLE 28. INHERENT DAMAGE MODES AND DISPOSITIONS (CONTINUED)

Damage	Affected Blade Elements	Rate Per 10^6 Bld-hr	Maint. Level				Men @ Times MTTR		Repair Type
			Accept	Field	Depot	Scrap	Prod.	Cure	
Bond void/delamination from core	Skin	76.05		X			.92	.5	Skin patch
Bond void/delamination from spar	Skin	14.63		X			.25	.25	Inject filler
Bond void/delamination from spline	Skin	11.70		X			.25	.25	Inject filler
Cracks over core	Skin	31.36		X			.92	.5	Skin patch
Cracks over spar	Skin	5.93			X		.92	.5	Skin patch
Cracks over spline	Skin	5.09			X		.92	.5	Skin patch
Bond void/delamination	Skin doublers @ root	.625		X			.92	.5	Skin repair
Bond void/delamination	Skin doublers @ root	.625			X		6.0	3.0	Replace doublers
Cracks	Skin doublers @ root	.375			X		6.0	3.0	Replace doublers
Cracks	Skin doublers @ root	.375				X	6.4		Replace blade
Delamination from spar wall	Core	.73		X			.25	.25	Inject filler
Delamination from spar	Leading edge boot	10.96		X			.26	6.0	Repair boot
Delamination	Trailing edge spline	6.5		X			1.5	1.0	Spline repair
Cracks	Trailing edge spline	9.25		X			1.5	1.0	
Cracks	Trailing edge spline	3.08				X	6.4		Replace blade
Delamination	Trim tab	.29		X			.84	1.0	Replace trim tab
Cracks	Trim tab	2.81		X			.84	1.0	Replace trim tab
Corrosion	Trim tab	5.61		X			.84	1.0	Replace trim tab
Cracks	Aft tip cap	.32		X			1.5	.5	Surface patch
Delamination	Aft tip cap	3.3		X			1.5	.5	Surface patch

Maintainability. The Contractor's experience with the aforementioned IMRB program and the Field Repairable/Expendable Main Rotor Blade program allows the Contractor to closely estimate both the repair complexity and the repair time associated with maintenance action on the OH-58 blade program.

During both the IMRB and FREB programs, repairs were made under simulated field conditions by MOS 67N20 skill level personnel. These personnel were trained in the performance of the repair procedures. They subsequently demonstrated the repair procedures during both programs. Time studies were made of their efforts, and the results were recorded and published in numerous reports. The results of these programs allow very close estimates of the repair times that will be required by the OH-58 blade. The same repair goals used in these earlier programs were used for the K747 blade program. These goals include the minimization of additional tools required for the repairs, maximum simplicity of repair, minimum aircraft down time related to repair, and maximum percentage of repairs being made at the field level. Additionally, the K757 blade has been designed such that no scheduled maintenance will be required during the blade's fatigue life. The only expansion of IMRB repair techniques considered during the OH-58 program is depot level spar repair. Because the spar extends aft to a larger percentage of chord than did the IMRB spar and because the OH-58 spar is a single cell, a simple technique has been devised for the repair of the spar. This repair is shown schematically in Figure 63.

Damage from a through hit will be locally cleaned and tapered. Subsequently, the root closure of the spar and the main pin spacer will be removed, giving access to the spar internal cavity. A specially designed tool (the only one above AH-1 requirements for this program) will be inserted and will locate an internal patch against the internal surfaces of the spar. This tool is described in Figure 64. External filler pads will be bonded on the outside of the spar to bring the external surfaces back to contour. The spar internal tool will be pressurized and heated, and the resultant forces will be reacted by the existing or slightly modified afterbody repair tool. After a suitable cure cycle, the internal and external tools will be removed and some surface finishing and restoration will be completed. This process will restore the structural integrity of the spar. The damaged area on the spar's internal surface will be lapped with two unidirectional glass reinforcements. Because of the criticality of this repair for flight safety, and because of the additional skill level of the repairmen involved at this time, this repair has been designated for depot application. Tables 27 and 28 show both the reliability data mentioned above and the projected mean time to repair and repair type for the OH-58 blades.

During the OH-58 program, the possibility of installing anti-icing equipment on the blade was considered. Two methods are presently available for this purpose. The first method, used most frequently in the past, consists of electric heater elements installed as an integral part of the blade boot. The second method is a newly developed pneumatic system in which the boot's surfaces are made to flex from internal pneumatic pressure, thus shedding the ice.

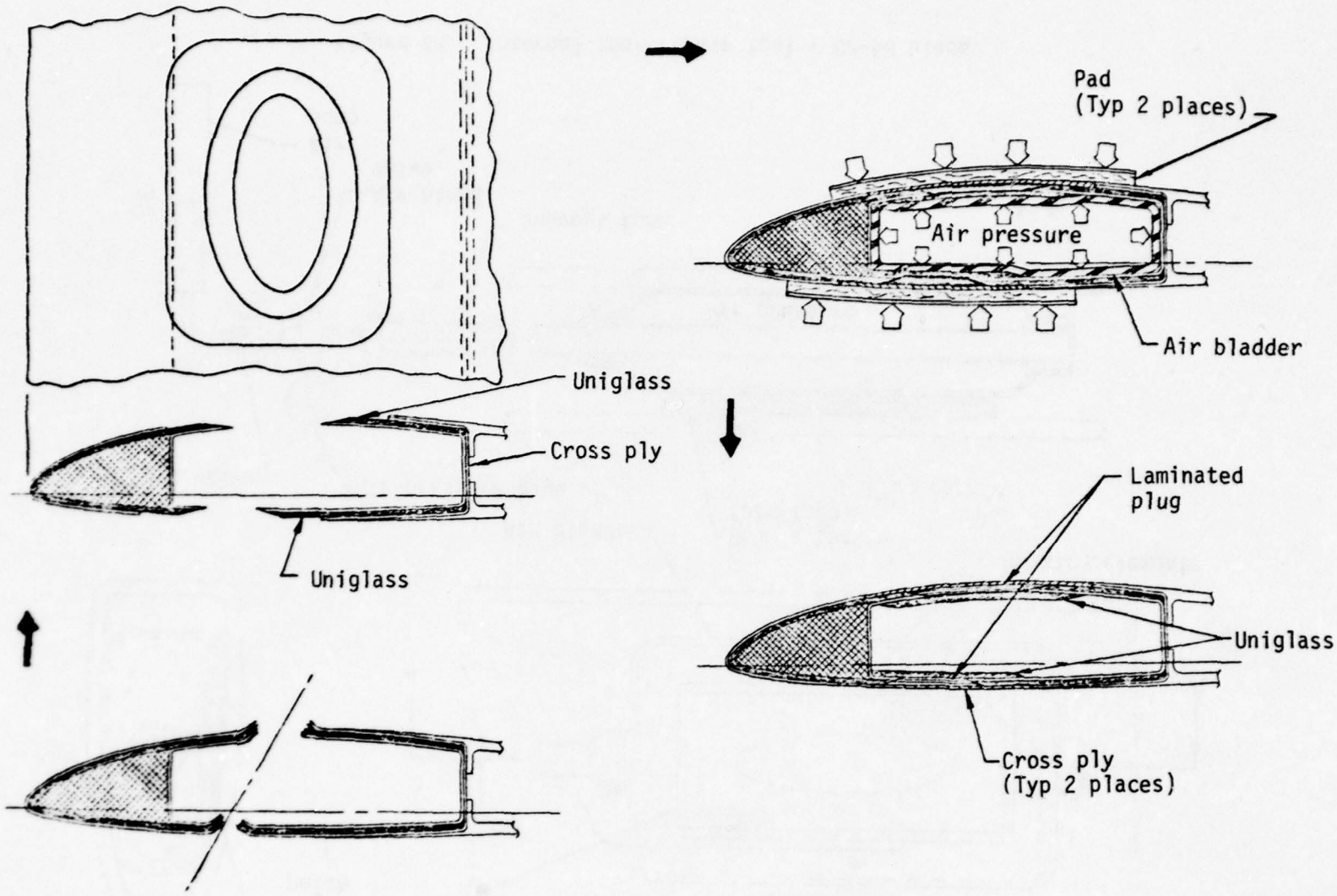

Figure 63. Spar repair technique - OH-58 blade.

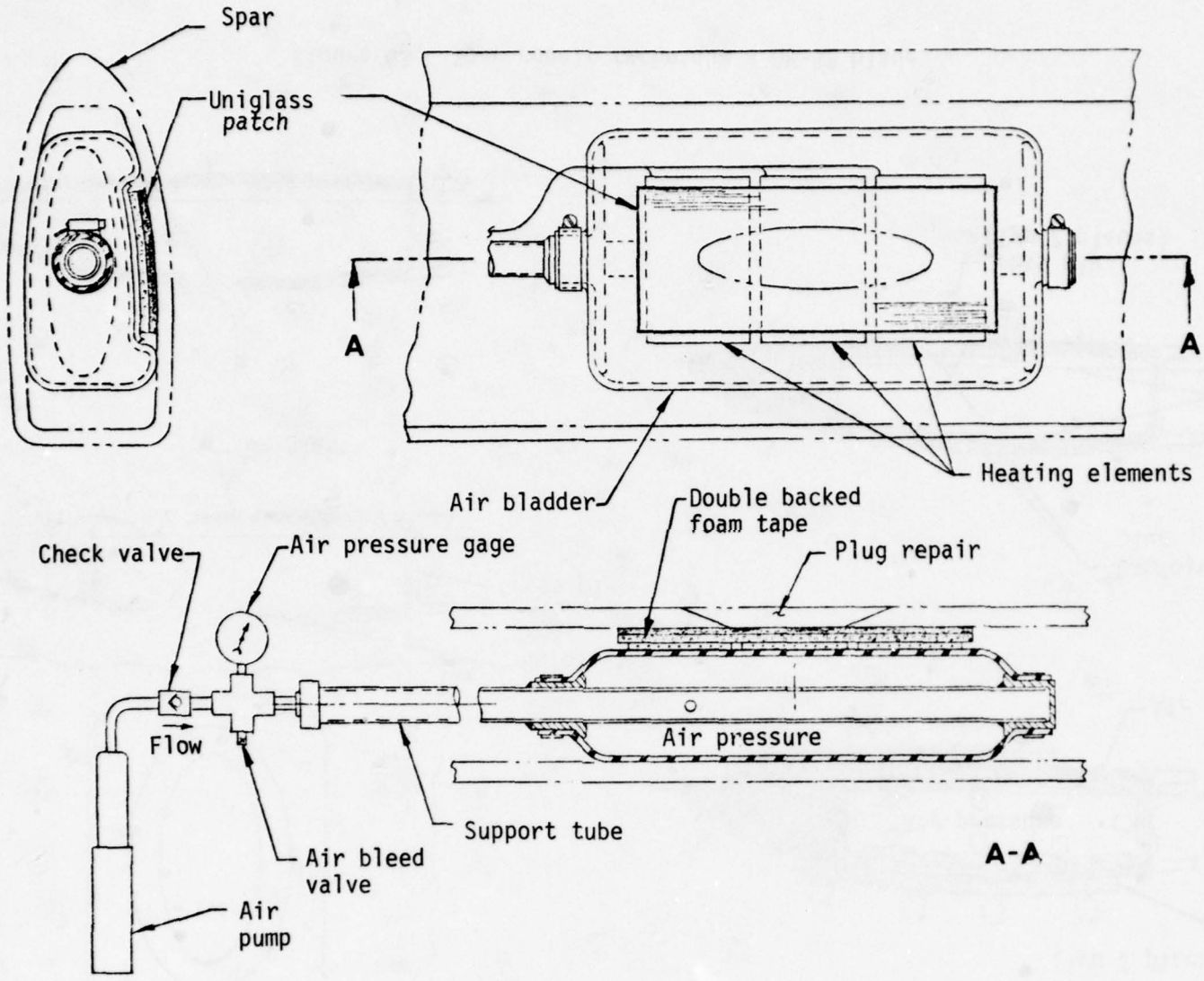

Figure 64. Internal spar repair tool - OH-58 blade.

Primary consideration was given to the electrothermal method of deicing because of its previous proven utility. The Contractor has had experience with this type of deicing system on the UH-2 helicopter and, based on this experience, concludes that with the exception of connection electric continuity checks, damage or functional problems will be delegated to a depot level repair for probable replacement.

The K757 rotor blade exhibits the same low repair times as the IMRB. The blade is projected to meet the 3-hour maximum repair time as described in the Statement of Work. This number is calculated as follows: the frequency of repair actions is divided into the total number of actions times their frequency of occurrence for mean times to repair. This average figure comes out to be 1.019 hours productive time. The same calculation is used with the cure times and results in .710 hour. A mathematical method (Reference 13) is used to convert the overall mean time to repair into the 95 percentile repair time, giving 2.28 hours. This is shown in the following calculation:

$$\text{Average productive repair time} = \frac{\text{Pro. repair time for inherent} + \text{Pro. repair time for external}}{\text{Inherent repair occurrences} + \text{External repair occurrences}}$$

$$= \frac{25{,}530 + 164.608}{25{,}000 + 201.245} = 1.019 \text{ hours}$$

Similarly,

$$\text{Average cure time} = \frac{17{,}750 + 154.288}{25{,}000 + 201.245} = .710 \text{ hour}$$

$$M_{95} = .710 + M_{95}, \text{ productive} = .710 + 2.28 = 2.99 \text{ hours}$$

Life-Cycle Cost Analysis. A method for predicting life-cycle cost analysis was developed for Army Contract DAAJ02-73-C-0006, Development Program for Field Repairable/Expendable Main Rotor Blades. This life-cycle cost analysis is described in Reference 14 and was used during both the FREB and the IMRB programs to determine sensitivity to various factors influencing blade-related life-cycle costs. The information available from this life-cycle cost analysis includes such maintainability parameters as mean time between maintenance actions and maintenance manhours per flight hour for a rotor system. In the Phased Maintenance Check List program, information is available on the mean time between failures for the present OH-58 main rotor

14. Miller, J. E., and Cook, T. N., DEVELOPMENT PROGRAM FOR FIELD-REPAIRABLE/EXPENDABLE MAIN ROTOR BLADES, USAAMRDL-TR-76-9, Eustis Directorate, U. S. Army Air Mobility R & D Laboratory, Fort Eustis, Virginia, September 1976, AD A030835.

blades. Based on this information, a mean time between failures of 245 hours can be calculated for the present OH-58 blade. This number includes failures requiring blade removal, as well as failures requiring retracking or adjustment of control linkages. This latter form probably occurs several times on a given blade before some deeper failure is diagnosed. Although this number, 245 hours, seems extremely low, it does permit a lower bound to be placed on the present blade's MTBF. For purposes of this analysis and comparison to the OH-58 composite blades, it will be considered that the mean time between failure for the present blade may be well above this number of 245.

As discussed in the reliability section of this report, the mean time between failure on a composite blade is projected to be 808.6 hours. Life cycle cost analyses for the OH-58 present blade and the OH-58 composite blades were run. The results of this study are presented in Figure 65. Cost estimations were made to provide a unit cost basis with and without deicing. Table 29 presents this cost breakdown for a production run of 3000 blades in terms of 1976 dollars. Pricing for the K757 blade is based on actual material costs and labor rates from the K747 blade program reduced to 1976 dollars. The overall blade prices cannot be compared, however, because the K747 has retention adapter hardware, a more complex spar, and because the cost impacts of subcontractor burdens will not occur for the K757 blade.

The composite blade, both with and without deicing, because of its high percentage of field repairability, is not only relatively low in life-cycle costs, but does not vary appreciably with mean time between failures. Because the present blade has such low field repairability, probably resulting in scrap for most damages, its life-cycle cost exhibits a much steeper gradient with mean time between failures. Thus, while MTBF may be considered from a number of positions and given different values for each of these positions, the composite blade is projected to have a life cycle cost at least 60% below that of the present blade. Table 30 shows the life cycle cost analysis program output for the OH-58 composite blade without deicing at a mean time between failures of 808.6 hours. This table gives a complete breakdown of the various frequencies of maintenance action, events for aircraft cycle and cost per aircraft life cycle. For the frequencies of repairs required, the maintenance man-hours per flight hour are shown to be .0116 for the two-bladed main rotor, or .0058 per blade flight hour. This number is below the specification of .01 maintenance man-hour per blade flight hour.

Natural Environmental Considerations

Since it is assumed that the composite rotor blade will be exposed to world-wide extremes of climate and weather, a large number of environmental considerations must be made. The impact of naturally occurring conditions is discussed in the following.

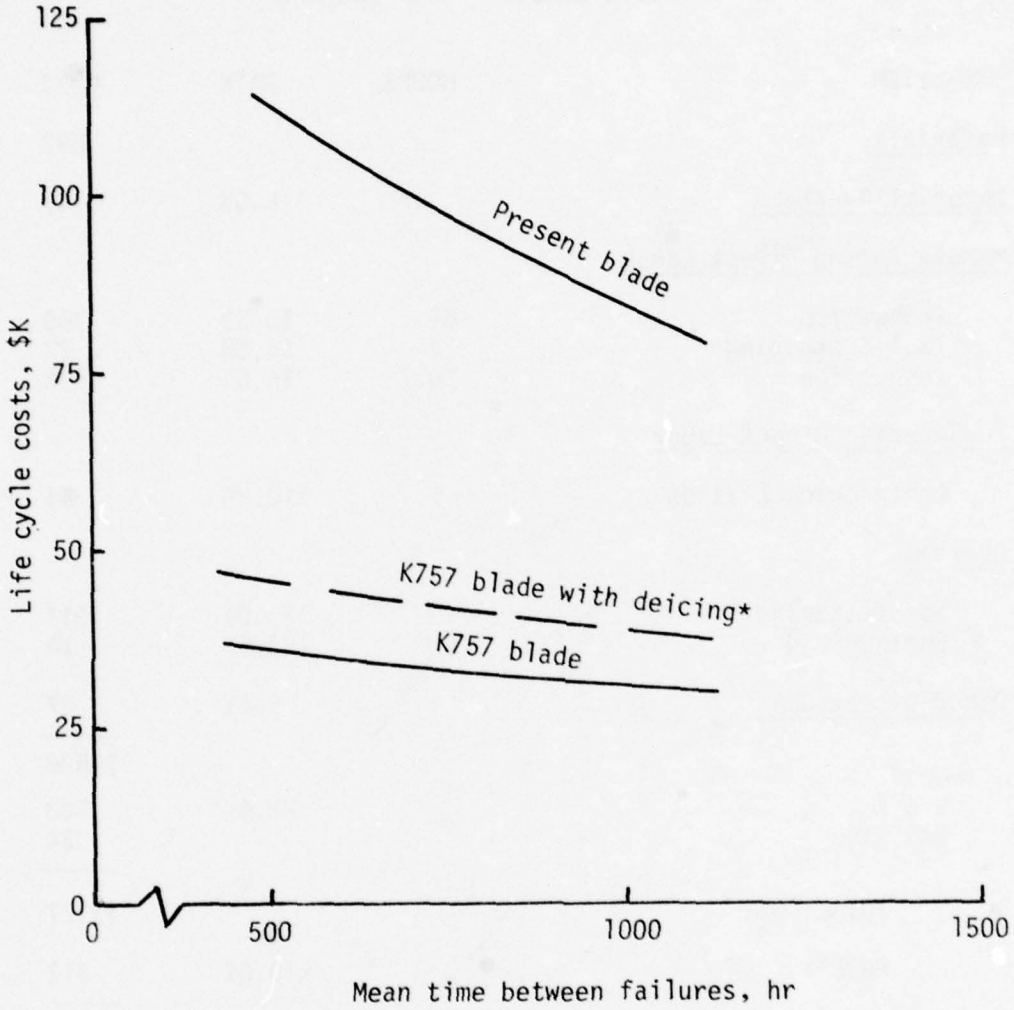

*Failure rate and costs are for deicing boot and blade only

Figure 65. Life-cycle cost study.

TABLE 29. K757 COMPOSITE MAIN ROTOR BLADE
3000 BLADES - 1976 DOLLARS

ITEM	HOURS	RATE	COST
Materials			892
Material Overhead		16.5%	147
Manufacturing Direct Labor			
Production	69	$5.33	368
Tool Sustaining	4	$6.85	27
Inspection	20.7	$6.65	138
Engineering Direct Labor			
Engineering Liaison	1	$10.88	11
Overhead			
Manufacturing		171.0%	911
Engineering		123.6%	14
Other Direct Cost		5.0%	27
			$2535
G & A		22.4%	568
CAS 414			24
TOTAL COST			$3127
PROFIT		10.0%	313
			$3440
Thermal-Electric Deicing			775
			$4215

TABLE 30. K757 BLADE LIFE-CYCLE COST BREAKDOWN

NEW BLADE PRICE	= $ 3040
MEAN TIME BETWEEN FAILURES	= 808.6 BLADE HOURS
FIELD REPAIRABILITY	= 76.2 PERCENT
MEAN TIME BETWEEN MAINTENANCE ACTIONS (BLADE HOURS):	
REPLACEMENTS	= 4299.6
REMOVALS FOR REPAIR OR REPLACEMENT	= 2022.9
REPAIRS	= 986.8
DAMAGE REPLACEMENTS	=30691.7
UNSCHEDULED MAINTENANCE	= 956.1
SCHEDULED MAINTENANCE (RETIREMENT)	= 5000.0
ALL MAINTENANCE ACTIONS	= 802.6
BLADE EVENTS PER AIRCRAFT LIFE CYCLE:	
NUMBER LOST TO ATTRITION	= 0.0000
NUMBER FATIGUE RETIRED UNDAMAGED	= 4.0000
NUMBER REPAIRED ON AIRCRAFT	= 15.0321
NUMBER REPAIRED OFF AIRCRAFT IN FIELD	= 0.0000
NUMBER SCRAPPED IN FIELD	= 0.0798
NUMBER DAMAGED AND RETIRED IN FIELD	= 0.0000
NUMBER REPAIRED AT DEPOT	= 5.2351
NUMBER SCRAPPED AT DEPOT	= 0.0000
NUMBER DAMAGED AND RETIRED AT DEPOT	= 0.5724
TOTAL NUMBER DAMAGED AND NOT REPAIRED	= 0.6516
TOTAL NUMBER ALL REPLACEMENTS	= 4.6516

TABLE 30. K757 BLADE LIFE-CYCLE COST BREAKDOWN (CONTINUED)

MAIN ROTOR BLADE COSTS PER AIRCRAFT LIFE CYCLE:

COST OF INITIAL PROCUREMENT:

NEW AIRCRAFT OUTFITTING COST	= $ 6880.00	
SPARES COST, WITH CONTAINERS	= $ 1141.20	
SPARE REPAIR MATERIALS	= $ 103.30	
REPAIR SUPPORT EQUIPMENT	= $ 848.00	
TOTAL INITIAL PROCUREMENT COST	=	$ 8972.60

COST OF REPLACEMENT BLADES FOR THOSE LOST AND UNSERVICEABLE (INCLUDING BLADE SHIPPING AND CONTAINER SHIPPING COSTS):

BLADES LOST TO ATTRITION	= $ 0.00	
DAMAGED BLADES NOT REPAIRED	= $ 3306.20	
TIME-EXPIRED UNDAMAGED BLADES	= $14760.00	
TOTAL REPLACEMENT COST	=	$18066.20

COST OF MAINTENANCE ACTIONS (LABOR AND MATERIAL TO INSPECT, REMOVE, REPAIR, REPLACE, ALIGN, AND TRACK):

FIELD REPAIR ON AIRCRAFT	= $ 2198.10	
FIELD REPAIR OFF AIRCRAFT	= $ 0.00	
FIELD SCRAP	= $ 2.80	
FIELD RETIREMENT	= $ 139.20	
DEPOT REPAIR	= $ 2879.50	
DEPOT SCRAP	= $ 0.00	
DEPOT RETIREMENT	= $ 120.10	
TOTAL MAINTENANCE COST	=	$ 5339.80
TOTAL LIFE-CYCLE BLADE COST PER AIRCRAFT		$32,378.50

MAINT'NCE MAN-HOURS/FLIGHT HOUR	=	0.0116
BLADE-RELATED AIRCRAFT DOWNTIME	=	43 HOURS

Ambient Temperature. Composite blades are slightly more temperature sensitive than metallic blades. Therefore, in the initial design phase, it has been necessary to use high temperature materials data in the determination of stresses and section properties. Elastomeric materials are cold-sensitive but, under dynamic flexing action, they rapidly reduce their stiffness until a stability point is reached. For these reasons, no significant effects due to ambient temperature variations will occur.

Humidity. Humidity produces reversible reductions in the strength and modulus of the epoxy matrix, and on matrix sensitive composite properties. For this reason, "wet" static properties are used for static stress analysis and fatigue properties are derived from fatigue tests of the AH-1 blade which included combined temperature/humidity effects.

Precipitation. Rain and sleet present classical erosion problems which are resisted by incorporation of a urethane elastomer leading edge boot.

Snow is harmless because of its low average density.

Hail is potentially damaging primarily in an erosion sense. Composite materials are much more damage resistant. Therefore, impact damage from hailstones will be negligible to all surfaces. As the impacted hailstones shatter, the resultant particles will cause relatively rapid erosion strip wear. However, the total time of exposure to hail conditions is estimated to be a small factor in the overall erosion life of the blade.

Erosion Protection. The erosion protection system consists of an elastomeric boot which extends from station 36.5 to the tip. It covers approximately 15% of the upper surface, wrapping around the leading edge to approximately 25% of the lower surface. The maximum thickness is .100 inch, which has been shown by Kaman test (Reference 15) to be satisfactory for the OH-58 tip speed condition.

Extensive materials testing was undertaken in the AH-1 composite program. Two major tests were performed to determine resistance to sand erosion and rain erosion. Rain erosion proved to be critical. The results indicated that a thermoplastic urethane elastomer produced by B. F. Goodrich as "Estane 165RN611" was the best. Extensive testing with this material indicated that .100 could protect the blade surface for 6 hours at a rainfall rate of 1 inch/hour for the AH-1 tip speed condition of 740 fps. Since less than .5% of aircraft time is anticipated in a rain environment, this was satisfactory to insure a 1200-hour life. Because the OH-58 tip speed is only 655 fps, a substantial increase in this performance is anticipated.

15. Hintermister, R. A., TEST REPORT FOR DEMONSTRATION OF THE AH-1 IMPROVED MAIN ROTOR BLADE EROSION PROTECTION SYSTEM, Kaman Report T-668, Kaman Aerospace Corporation, Bloomfield, Connecticut, February, 1977.

Salt Spray. Composite materials are not affected by salt spray. Metallic parts are damaged by salt, but these are held to a minimum in this design. The tip ballast weight is a stainless steel casting which has inherent corrosion resistance. Alloy steel surfaces which are not hermetically enclosed in an assembly will be cadmium plated and painted for protection. The highest susceptibility to salt spray corrosion is in fasteners securing secondary items such as chordwise and tip weights. Normal sanitation, such as fresh water flushing, in these areas will minimize or eliminate any corrosion problems.

Lightning Protection. Theoretical considerations, the published literature on lightning tests of composite structures, and specific experience with lightning tests of the AH-1 and HH-43 composite blades reveal two potentially serious modes of lightning damage in the proposed OH-58 blade.

In the first potentially destructive mode, the metal tip weight provides a partial internal current patch which can cause arc passage down the length of the hollow spar with attendant extreme internal pressures. Testing of the AH-1 blade demonstrated that this discharge mode can be prevented by providing an external conductive path over the weight.

In the case of the second potentially destructive mode, strokes flashing over the external surface will tend to enter and destroy the upper and lower blade root reinforcements, which contain graphite fiber. This can also be prevented by providing an external conductive path over the graphite containing area.

On both the AH-1 and HH-43 blades, the required external conductive paths have been successfully provided by applying a silver pigmented conductive coating under the normal paint finish system. This technique has been used because it does not affect blade performance and can be applied at relatively low cost. The effect on radar signature is slight compared to the overall signature of the compostie blade.

No other proven methods amenable to the selected fabrication technique were identified during this design study, and the use of the silver pigmented conductive coating is therefore the baseline approach for the OH-58 blade. During a blade development program, other methods (for example, provision of a thick dielectric plug inboard of the tip weight) would be explored in greater detail and tested if they appear to offer advantages.

Wind. Because of increased fatigue strength, composite blades are less susceptible to wind damage than metal blades. The greatest susceptibility is on the ground, where very high flapping moments can be generated unless the blades are restrained or tied down. Wind has no significant design impact.

Ice Protection. Under certain conditions of cold saturated air, ice may have a tendency to build up on rotor blades. Icing is resisted by the high centrifugal accelerations over the outer regions of the blade and the

natural flexing of the rotor blade as a beam. Nonetheless, extreme icing conditions do occur which demand treatment.

Blade deicing provisions have been considered for the composite OH-58 blade. The required meteorological conditions are defined in Figures 66 and 67 (Reference 16). Figure 66 defines the endurance deicing mission, while Figure 67 defines the maximum intermittent condition. These curves describe the typical cold saturated air conditions conducive to persistent ice formation. The physical requirements for deicing are that ice shall not be allowed to build up to the extent that it is detrimental to performance, stability, control, vibration level and structural integrity. The concept may also provide for clear-shedding where the expelled ice does not have the opportunity to damage the tail rotor or any other part of the helicopter. Several satisfactory systems are available which can fulfill these requirements.

Ice protection considerations fall into two categories: detail design considerations and system considerations. System considerations are not inconsiderable in that severe life-cycle cost penalties are generated from reduced overall reliability. This is because of the proliferation of onboard hardware requirements, such as wire bundles, distribution devices, slip rings and heavy-duty generating equipment. This report does not present overall system effects, but only effects on the blade alone. The detail design considerations are strongly dominated by the requirement that the deicing system must have a very minimum of impact on the blade design. This means that an ideal deicing system should be integrated into existing blade components with little or no detrimental effects. Kaman has investigated two deicing schemes which are applicable to the K757 blade design.

Thermal-Electric Design. This design consists of a urethane erosion boot with integral wires acting as electrical resistance heaters. The boot would extend along the leading edge all the way to the tip, covering 15% of the upper surface to 25% of the lower surface. The wires are waved so as not to be affected by blade strain. Heating is cyclic so that balanced shedding occurs at all times. Kaman has had extensive experience with an electrothermal system which was developed for the Navy UH-2 helicopter. This exposure to the overall system demands and constraints has provided a healthy appreciation of the overall aircraft impact. The UH-2 system consists of an electrically heated leading edge boot which also provides erosion protection to the inner portion of the blade. Beyond the 70% radius, only erosion protection is provided since the high G levels prevent the formation of ice.

16. Military Specification, MIL-E-38453A (USAF), ENVIRONMENTAL CONTROL, ENVIRONMENTAL PROTECTION, AND ENGINE BLEED AIR SYSTEMS, AIRCRAFT, GENERAL SPECIFICATION FOR, Department of Defense, Washington, D. C., 2 December 1971.

(1) Altitude: sea level to max. service ceiling

(2) Maximum vertical extent: 6500 ft

(3) Horizontal extent: max. end. mission

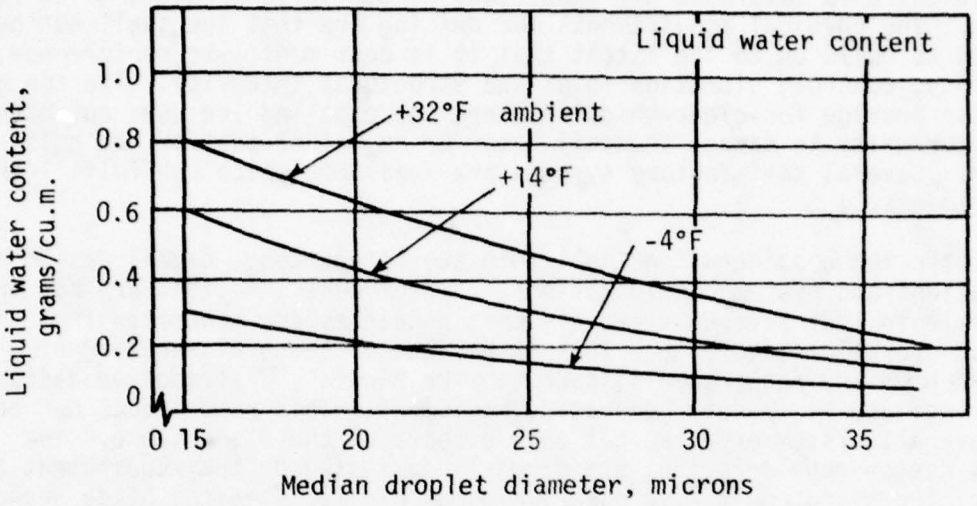

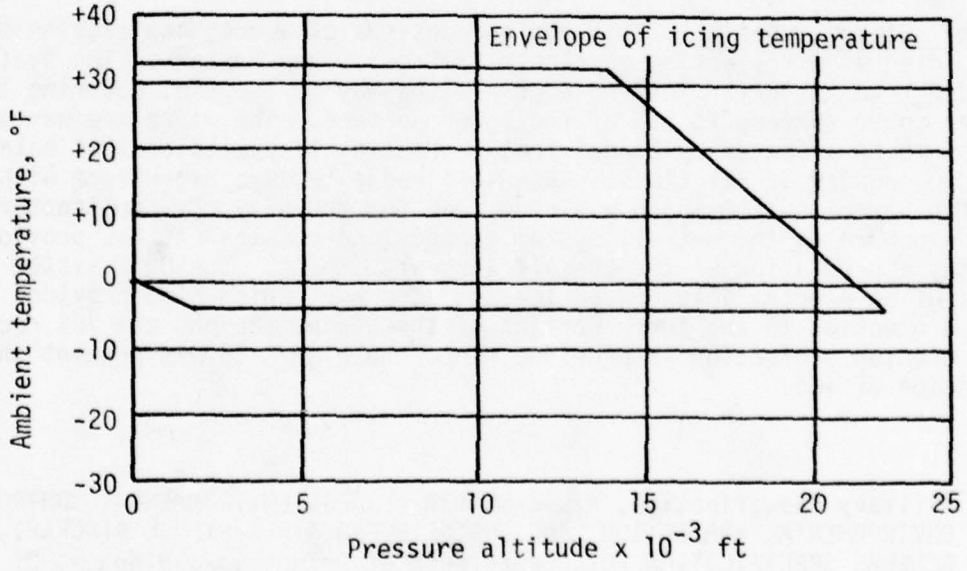

Figure 66. Continuous maximum icing conditions.

(1) Altitude: sea level to 22,000 ft

(2) Horizontal extent: 15 min.

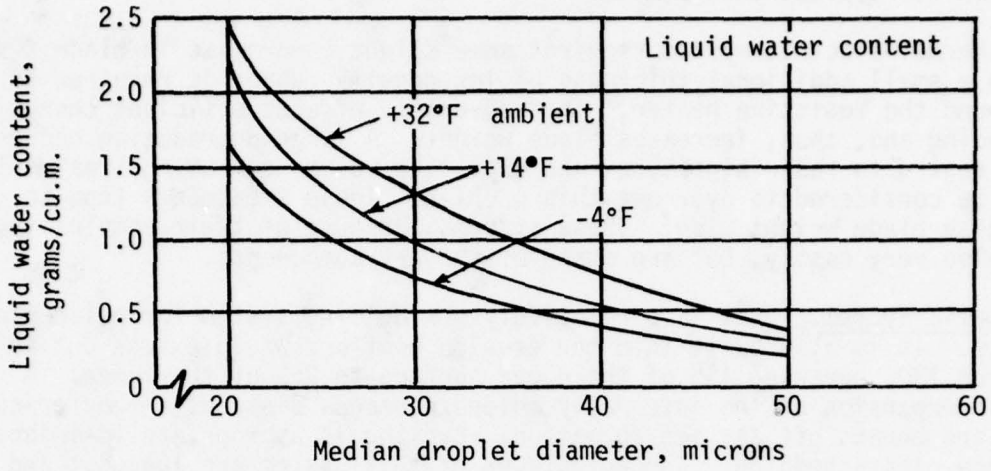

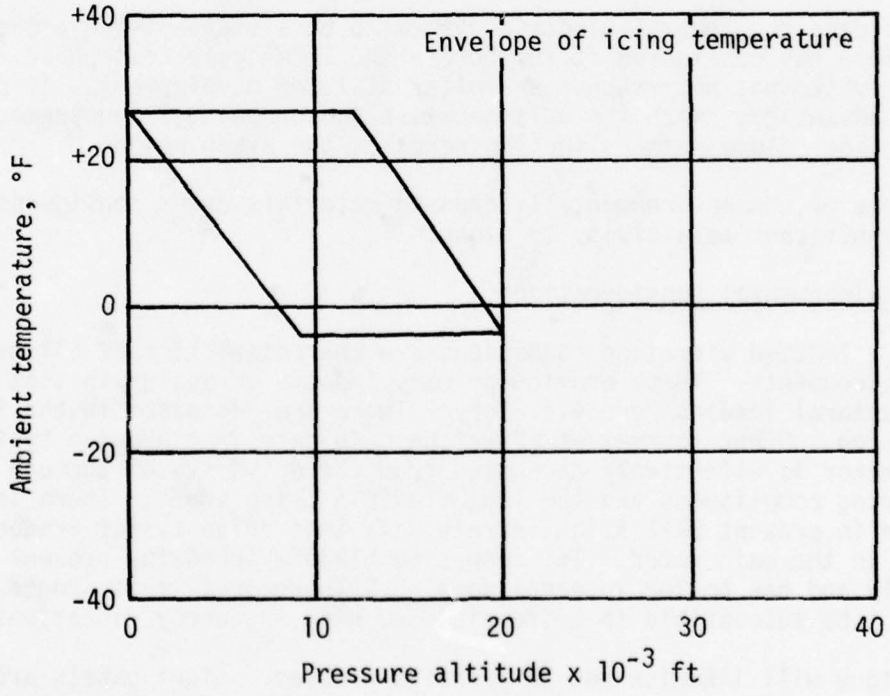

Figure 67. Intermittent maximum icing conditions.

The UH-2 system was thoroughly developed and completely successful, but did not see significant service use because blade bending deflections prevented icing from becoming a significant problem on this helicopter operating in its typical environment.

The thermal-electric system requires some slight compromise in blade design since a small additional thickness of low density rubber is required to surround the resistive heater. This adversely affects efficient chordwise balancing and, thus, increases blade weight. A large degradation occurs with regard to radar signature, and expensive volume consuming treatments must be considered to overcome this problem. These treatments tend to increase blade weight also. These systems, because of their complexity, are also very costly, but are state-of-the-art components.

Pneumatic System. This is a relatively new deicing system for helicopter blades. It is also built into the erosion boot and would extend out to station 180, covering 15% of the upper surface to 25% of the lower. A cyclic expansion of the integrally molded passages distends the outer surface and breaks off any ice formation. Cycling is appropriate to insure balance clear-shedding. The advantages of this system are low cost and good radar signature. The disadvantages are potential aerodynamic degradations and an increase in boot cross section which affects chordwise balance and increases blade weight and cost.

Kaman considers the thermal-electric system to be a state-of-the-art system and therefore has considered it further in the life cycle cost phase. The pneumatic system has not reached a similar state of development. It promises many advantages, with the only negative factor being a requirement for more blade volume which slightly increases the blade weight.

Ozone. None of the environmentally exposed materials under consideration has any significant sensitivity to ozone.

Induced Environmental Considerations

Vibration. Induced vibration conditions are characteristics of all helicopter environments. These provide primary impacts on design in that the major structural loadings are vibratory. These are addressed in the Structures section. Other sources of vibration originate in the drive system. The main rotor is effectively decoupled from the drive system through its pitch bearing compliances and the long flexible drive shaft. There is no indication in present Bell flight strain data that drive system frequencies are found in the main rotor. The composite blade matches the present blade dynamically and has better internal damping. Therefore, it is judged that it will not be susceptible to system-induced high frequency vibrations.

Sonic fatigue will likewise not be a design problem. Light panels are well damped such that large energy reactions can be supplied to the sonic excitation. No design impact is anticipated.

Transportation and Storage Constraints. No changes in transportation containers or storage techniques are anticipated. Internal support and restraint provisions will be needed in containers, but this does not impact blade design or operation in any way.

Ozone, Aircraft-Induced. The blade materials are not susceptible to ozone.

Aircraft Fluids Compatibility. All blade materials are unaffected by typical aircraft fluids such as rotor bearing greases, MIL-L-23699, and lubricating oils of MIL-L-7808 variety. Surface contamination from these fluids requires repair pretreatment cleaning prior to bonding. No design impact results from this consideration.

Thermal Shock. The selected blade materials, which are poor heat conductors, are not susceptible to thermal shock. A composite rotor blade may be considered to have a large thermal capacitance which resists rapid temperature changes and the attendant deleterious effects.

Cleaning Materials and Techniques. The K757 composite blade suffers no deleterious effects from existent cleaning materials and techniques presently in the Army system. No design or operational impact is accrued.

Aircraft Interior Noise. Interior aircraft noise levels will, most likely, be reduced in direct proportion to externally sensed noise. The low transmission efficiencies of the composite materials will insure that noise generated at the blade will not be transmitted to the cabin. Therefore, no design or operational impacts are anticipated.

Temperature (Induced). Conducted and radiated heat from the transmission and engine is dissipated by the natural forced convection of the moving rotor. The total amount of heat moved in this fashion is small due to long conducting paths and the relatively large offset distance of the rotor from the transmission and engine. No design impact was considered.

Moisture (Induced). Washing procedures do not provide any design or operational problems.

Salt Spray (Induced). The metallic components have a high susceptibility to salt spray corrosion. Therefore, cadmium plating and painting has been used as protection for all surfaces not hermetically sealed during assembly.

Damage Tolerance. The K757 blade is constructed of composite materials which have inherent internal redundancies limiting failure hazard. The "basket-weave cross-ply skin," which derives from the AH-1 composite blade program, proved to be highly damage resistant in ballistic tests. A spar pressurization system includes a Shrader valve to apply limited pressure to the sealed spar. Spar integrity is judged by the rate of pressure loss. This is a very simple, inexpensive system which is quite reliable once characteristic pressure-loss norms have been established.

Blade Obstacle Strike. The fiberglass nose block is a linear filament winding and, therefore, is a strong member with a large capacity to absorb impact energy. The shear strength of the nose block cross section is 12 times that of a 1-inch-diameter pine branch. The pine branch would be severed with only superficial abrasion damage to the erosion boot and blade surface.

Soft, unshielded copper wire exhibits brittle behavior under high strain rate conditions which prevail during impact. Over the outer 75% radius, a 1/4-inch-diameter wire would easily be severed with only superficial repairable damage to the blade.

Inboard of this point, the wire would suffer a large amount of tensile strain before failure, presenting some hazard to the control system. Damage to the blade would primarily be confined to the erosion boot.

External Aircraft Noise. Several of the design features of the composite OH-58 main rotor blade tend to promote reduced noise. These features, which include increased blade twist, blade planform and thickness taper, and the use of a trapezoidal tip shape and a high lift airfoil section, should result in a substantially reduced main rotor acoustic signature. Discussions of the qualitative effects of these design features are presented in the following paragraphs.

Noise radiation from a low to moderate tip speed helicopter rotor, such as the OH-58 main rotor, is largely due to the lift and drag forces which are developed on the rotor blades during flight. These forces, coupled with blade motion, generate local atmospheric pressure fluctuations, which propagate from the blades and are perceived as noise. Although the aerodynamic forces involved in this noise generation mechanism are continuously distributed along each rotor blade, it is possible to approximate this continuous distribution with a series of discrete forces. Each of these discrete forces can then be treated as a simple dipole noise source, with the total rotor noise signature equal to the sum of the contributions from all such sources. This approach provides a convenient means for evaluating the qualitative impact of the composite OH-58 rotor blade design features mentioned previously.

The noise radiated into the far field by a dipole noise source is given by:

$$P = \frac{-1}{4\pi C\,(1 - M_R)^2\,R} \left| \dot{F} + \frac{R_R \dot{M}_R}{(1 - M_R)} \right|$$

where

M_R = component of source Mach No. in the direction of the observer

$\dot{M}_R$ = time rate of change of source Mach No. in the direction of the observer

F_R = component of aerodynamic force in the direction of the observer

$\dot{F}_R$ = time rate of change of component of aerodynamic force in the direction of the observer

R_R = distance between source and observer

C = speed of sound

In the context of the present problem, the source motion terms M_R and $\dot{M}_R$ refer to the motion of an elemental length of blade span, and the aerodynamic force terms F_R and $\dot{F}_R$ refer to the summation of lift or drag over this length of blade span. It is clear from the equation that both relative blade motion and blade loading are important determinants of rotor noise, with noise decreasing with reductions in blade loading and/or relative motion.

It is also clear that low noise is promoted by distributing blade lift and drag forces in such a way that high forces occur over low velocity portions of the rotor blade. As shown in Figure 68, the spanwise lift distribution of the standard OH-58 rotor is such that high lift loads are generated at the blade tip, which has the highest velocity. For the composite OH-58 rotor, the use of increased twist, planform taper and the trapezoidal tip shape results in an inboard shift in the lift distribution. and this should substantially reduce the noise of this rotor.

Again, in accordance with the above equation, it can be seen that low noise is promoted by minimizing rapid fluctuations in blade loading. In practice, such fluctuations often occur as the result of interactions between the rotor and concentrated vortices shed at the rotor tip. Since the severity of these fluctuations and the magnitude of noise generated in this manner depends on the strength of the tip vortex, factors which influence tip vortex strength also affect noise. The trapezoidal tip used on the composite OH-58 rotor will result in reduced tip vortex strength and, to the extent that blade/vortex interaction occurs on this rotor, this will reduce the rotor noise signature.

As noted previously, both lift and drag forces generate noise. The airfoil section used on the present OH-58 rotor blade represents a compromise between good performance and manufacturing cost. This compromise resulted

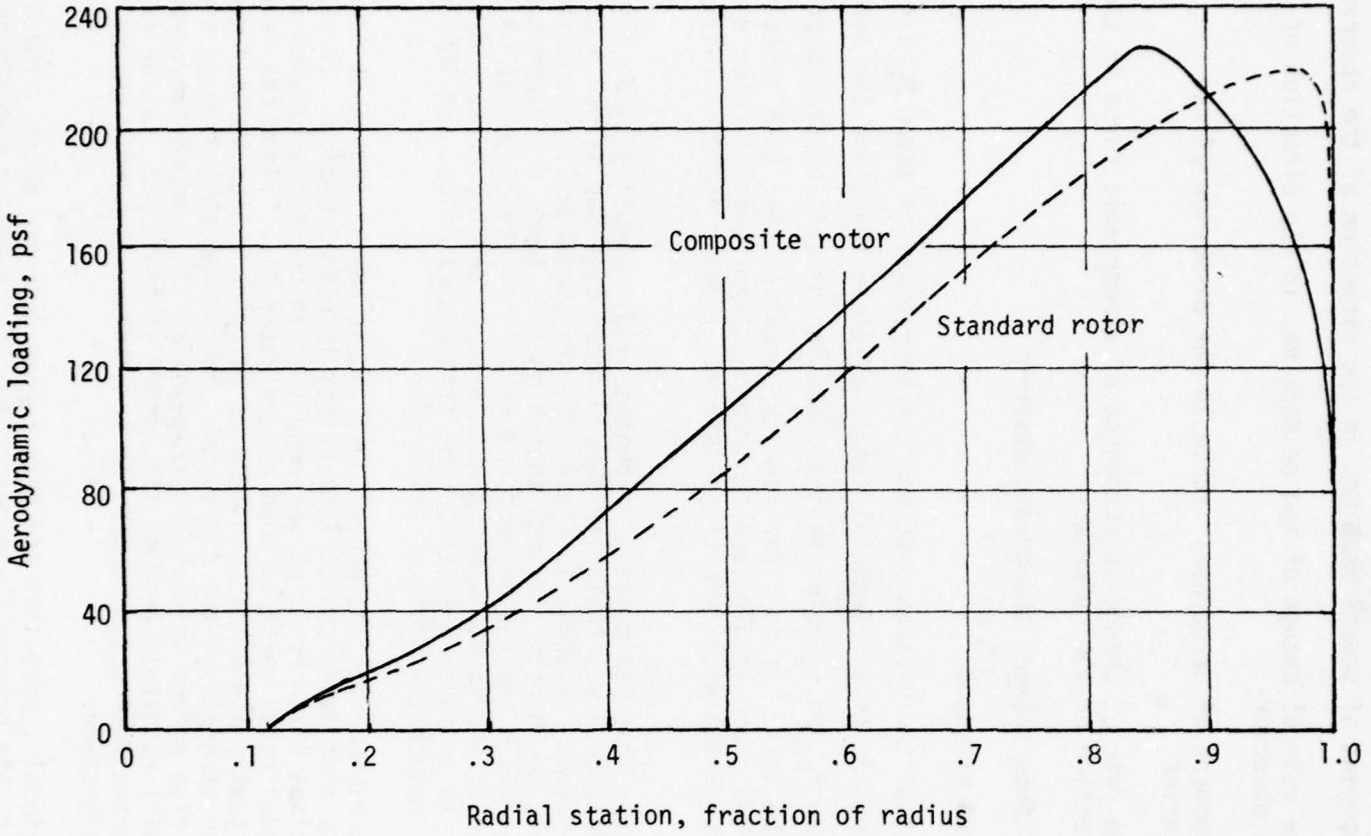

Figure 68. Comparison of composite and standard OH-58 rotor aerodynamic load distributions - hover.

in a relatively low lift-to-drag ratio for the present blade. The lift-to-drag ratio of the composite blade is considerably higher, and because of this, the component of rotor noise due to drag forces should be considerably reduced relative to the present blade, for comparable thrust requirements.

CONCLUSIONS

1. A simple, low-cost composite blade for the OH-58 helicopter can be fabricated using inexpensive hand tooling and wet filament winding technology obtained from experience on the Kaman AH-1 composite blade program. Blade cost is impacted primarily by fabrication techniques and number of joints. Blade configurations involving adapting metal parts proved to be about 20% more costly. Processes such as filament winding, braiding and pultruding proved to be low cost. Filament winding was selected because of its well developed background and ready adaptability to variable geometry blade configurations.

2. Analyses indicate that the composite blade life cycle cost is at least 60% below that of the present blade. A significant factor is the introduction of spar repairability at depot level.

3. The performance of the OH-58C in hover can be substantially improved by replacing the undesignated airfoil section currently used for the main rotor blade with one giving a higher lift-to-drag ratio.

4. The cambered VR-7 section is favored over the NACA 0012 for its superior lift-to-drag ratio at high lift coefficient and for its higher maximum lift coefficient.

5. Aerodynamic characteristics are generally secondary to structural and dynamic requirements in determination of blade planform.

6. A polar inertia increase of 4% is inherent in the K757 design. Blade weight is 6% lower. Blade CF and span moment are less than 4% higher which indicates little or no impact on the present OH-58 hub and controls.

7. Ballistic survivability is substantially enhanced in the case of the composite K757 blade.

8. Static strength equals or exceeds the present OH-58 metal blade.

9. The K757 blade has a conservatively calculated fatigue life of 4703 hours.

10. Considering first, second and third modes, the K757 natural frequencies match the present OH-58 blade within 8%. Torsional frequencies match within 3%.

11. Based on data from Appendix C, repairs are practical and achievable for planform-through damage of the K757 fiberglass spar; a spar repair for .50-caliber tumbled damage has no significant effect on the spar stiffness; and the test of a repaired K757 spar indicates no failure tendencies.

REFERENCES

1. Dadone, L. U., U. S. ARMY HELICOPTER DESIGN DATCOM, VOLUME I - AIRFOILS, USSAMRDL-TR-76-2, Eustis Directorate, U. S. Army Air Mobility R & D Laboratory, Fort Eustis, Virginia, September 1976.

2. Gregory, N., and Wilby, P. G., NPL 9615 AND NACA 0012 - A COMPARISON OF AERODYNAMIC DATA, CP No. 1261, Ministry of Defence (Procurement Executive), Aeronautical Research Council, London England, November 1968.

3. Hill, David A., DETAIL SPECIFICATION FOR THE OH-58C HELICOPTER INTERIM SCOUT, BHC 206-947-203, Bell Helicopter Corporation, Fort Worth, Texas, September 1975.

4. Yamakawa, George M., and Watts, Joseph C., AIRWORTHINESS AND FLIGHT CHARACTERISTICS TEST, PRODUCTION OH-58A HELICOPTER, UNARMED AND ARMED WITH XM27E1 WEAPON SYSTEM, USAASTA 68-30, U. S. Army Aviation Systems Test Activity, Edwards Air Force Base, California, September 1970, AD 875793L.

5. Noonan, Kevin W., and Bingham, Gene J., TWO-DIMENSIONAL AERODYNAMIC CHARACTERISTICS OF SEVERAL ROTORCRAFT AIRFOILS AT MACH NUMBERS FROM 0.35 TO 0.90, NASA TM X-73990, January 1977.

6. McKenzie, F. G., HLH/ATC ROTOR SYSTEM STRUCTURAL SUBSTANTIATION REPORT, Boeing-Vertol Report D301-10227-1, Boeing Company, Vertol Division, Morton, Pennsylvania, July 1973.

7. Jordan, G. L., STRUCTURAL DESIGN CRITERIA FOR 206A-1/OH-58A, BHC Report 206-099-200, Bell Helicopter Corporation, Fort Worth, Texas, August 1968.

8. Clinard, R. L., LOAD DETERMINATION AND STRUCTURAL ANALYSIS OF THE 206-011-001-3 MAIN ROTOR HUB AND BLADE ASSEMBLY FOR THE 206A-1 HELICOPTER, BHC Report 206-099-107, Bell Helicopter Corporation, Fort Worth, Texas, January 1969.

9. Martin, Bill, MODEL 206A-1 CERTIFICATION FLIGHT LOAD SURVEY, VOLUME II OF VI, BHC Report 206-194-062, Bell Helicopter Corporation, Fort Worth, Texas, April 1969.

10. Hardersen, C. P., FINAL STRESS ANALYSIS OF K747 MAIN ROTOR BLADE FOR AH-1Q/S HELICOPTER, Kaman Report S230-1, Kaman Aerospace Corporation, Bloomfield, Connecticut, June 1977.

11. Hart-Smith, L. J., BOLTED JOINTS IN GRAPHITE-EPOXY COMPOSITES, NASA CR-144899, McDonnell Douglas Corporation, Long Beach, California, June 1976.

12. Gessow, A., and Crim, A. D., A METHOD OF STUDYING THE TRANSIENT BLADE FLAPPING BEHAVIOR OF LIFTING ROTORS AT EXTREME OPERATING CONDITIONS, NACA Technical Note 3366, 1955.

13. Smyth, W. A., FINAL MAINTAINABILITY REPORT FOR THE IMPROVED MAIN ROTOR BLADE FOR THE AH-1 HELICOPTER, Kaman Report R-1355, Kaman Aerospace Corporation, Bloomfield, Connecticut, June 1977.

14. Miller, J. E., and Cook, T. N., DEVELOPMENT PROGRAM FOR FIELD-REPAIRABLE/EXPENDABLE MAIN ROTOR BLADES, USAAMRDL-TR-76-9, Eustis Directorate, U. S. Army Air Mobility R & D Laboratory, Fort Eustis, Virginia, September 1976, AD A030835.

15. Hintermister, R. A., TEST REPORT FOR DEMONSTRATION OF THE AH-1 IMPROVED MAIN ROTOR BLADE EROSION PROTECTION SYSTEM, Kaman Report T-668, Kaman Aerospace Corporation, Bloomfield, Connecticut, February, 1977.

16. Military Specification, MIL-E-38453A (USAF), ENVIRONMENTAL CONTROL, ENVIRONMENTAL PROTECTION, AND ENGINE BLEED AIR SYSTEMS, AIRCRAFT, GENERAL SPECIFICATION FOR, Department of Defense, Washington, D. C., 2 December 1971.

```
// JOB CH58HOVR P433                                    22.09.29
// ASSGN SYS010,X'235'
// OPTION NODUMP
// DLBL IJSYS10,'AIRFOIL DATA BANK-DO NOT DELETE-FKDUNN',99/365
// EXTENT SYS010,ENG003,1,,3300,200
// EXEC HOVERSP5
```

VERTOL VR-7 FROM BINGHAM

Trailing edge tab from x/c = .76 to x/c = 1.01
Tab angle = -4.7°

CL TABLE 1

ALPHA	MACH 0.350	MACH 0.400	MACH 0.500	MACH 0.610	MACH 0.680	MACH 0.750	MACH 0.850	MACH 0.900	MACH
0.0	0.1100	0.1300	0.1300	0.1500	0.1900	0.2500	0.1800	0.2000	
1.00	0.2400	0.2600	0.2750	0.3000	0.3500	0.4000	0.2600	0.3500	
2.00	0.3700	0.3900	0.4200	0.4400	0.5000	0.5100	0.3400	0.4700	
3.00	0.5000	0.5100	0.5500	0.5900	0.6400	0.6000	0.4100	0.5600	
4.00	0.6200	0.6400	0.6900	0.7300	0.7400	0.6600	0.4800	0.6400	
6.00	0.8600	0.8900	0.9500	0.9900	0.8500	0.7800	0.6100	0.7800	
8.00	1.1100	1.1200	1.2700	1.1800	0.9800	0.9100	0.8300	0.9100	
10.00	1.3600	1.3400	1.2950	1.2200	1.0900	1.0300	1.0300	1.0300	
11.00	1.4500	1.4100	1.3370	1.2200	1.1400	1.0900	1.0900	1.0900	
12.00	1.5300	1.4000	1.3600	1.2600	1.1900	1.1400	1.1400	1.1400	
12.50	1.5400	1.3680	1.3680	1.2600	1.2115	1.1700	1.1700	1.1700	
13.00	1.5100	1.3400	1.3700	1.2620	1.2286	1.2000	1.2000	1.2000	
13.00	1.4800	1.3100	1.3750	1.2750	1.2508	1.2300	1.2300	1.2300	
14.00	1.4500	1.2800	1.3780	1.2800	1.2692	1.2600	1.2600	1.2600	
14.50	1.4300	1.2600	1.3530	1.2800	1.2854	1.2900	1.2900	1.2900	
15.00	1.3800	1.3550	1.3550	1.2700	1.2969	1.3200	1.3200	1.3200	
16.00	1.3900	1.1900	1.3250	1.2500	1.2742	1.2950	1.2950	1.2950	
16.50	1.3570	1.1600	1.3100	1.2500	1.2769	1.3000	1.3000	1.3000	
17.00	1.3263	1.1500	1.3000	1.2550	1.2879	1.3162	1.3162	1.3162	
20.00	1.1722	1.1722	1.1722	1.1722	1.2939	1.3983	1.3983	1.3983	
25.00	0.8922	0.8922	0.8922	0.8922	1.0364	1.1600	1.1600	1.1600	
30.00	0.9950	0.9950	0.9950	0.9950	0.9950	0.9950	0.9950	0.9950	
45.00	1.1800	1.1800	1.1800	1.1800	1.1800	1.1800	1.1800	1.1800	
60.00	0.8802	0.8802	0.8802	0.8802	0.8802	0.8802	0.8802	0.8802	
90.00	0.0627	0.0627	0.0627	0.0627	0.0627	0.0627	0.0627	0.0627	
135.00	-1.0000	-1.0000	-1.0000	-1.0000	-1.0000	-1.0000	-1.0000	-1.0000	
170.00	-0.7452	-0.7452	-0.7452	-0.7452	-0.7452	-0.7452	-0.7452	-0.7452	
175.00	-0.5200	-0.5200	-0.5200	-0.5200	-0.5200	-0.5200	-0.5200	-0.5200	
180.00	0.0	0.0	0.0	0.0	0.0	0.0	0.0	0.0	
185.00	0.4875	0.4875	0.4875	0.4875	0.4875	0.4875	0.4875	0.4875	
190.00	0.7509	0.7509	0.7509	0.7509	0.7509	0.7509	0.7508	0.7509	
225.00	1.0000	1.0000	1.0000	1.0000	1.0000	1.0000	1.0000	1.0000	
270.00	-0.0627	-0.0627	-0.0627	-0.0627	-0.0627	-0.0627	-0.0627	-0.0627	
300.00	-0.8802	-0.8802	-0.8802	-0.8802	-0.8802	-0.8802	-0.8802	-0.8802	
315.00	-1.1800	-1.1800	-1.1800	-1.1800	-1.1800	-1.1800	-1.1800	-1.1800	
330.00	-0.9950	-0.9950	-0.9950	-0.9950	-0.9950	-0.9950	-0.9950	-0.9950	
335.00	-0.8922	-0.8922	-0.8922	-0.8922	-0.8922	-0.8922	-0.8922	-0.8922	
340.00	-0.8260	-0.8260	-0.8260	-0.8260	-0.8260	-0.8260	-0.8260	-0.8260	
346.00	-0.8100	-0.8100	-0.8100	-0.8100	-0.7831	-0.7600	-0.7600	-0.7600	
348.00	-0.8160	-0.8160	-0.8160	-0.8160	-0.7864	-0.7610	-0.7610	-0.7610	
349.00	-0.8160	-0.8160	-0.8160	-0.8160	-0.7864	-0.7610	-0.7610	-0.7610	
350.00	-0.7665	-0.7660	-0.7665	-0.7665	-0.7584	-0.7514	-0.7514	-0.7514	
352.00	-0.6556	-0.6700	-0.6556	-0.6700	-0.6785	-0.6858	-0.6858	-0.6858	
354.00	-0.5043	-0.5400	-0.5300	-0.5600	-0.6250	-0.6808	-0.6808	-0.6805	
356.00	-0.3400	-0.3500	-0.3400	-0.3700	-0.4400	-0.5000	-0.5000	-0.5000	
357.00	-0.2400	-0.2500	-0.2400	-0.2700	-0.3131	-0.3530	-0.3530	-0.3500	
358.00	-0.1400	-0.1500	-0.1300	-0.1500	-0.1608	-0.1700	-0.1700	-0.1700	
359.00	-0.0300	-0.0300	0.0	-0.0100	0.0061	0.0200	0.0200	0.0200	
360.00	0.0900	0.0950	0.1200	0.1200	0.1631	0.2000	0.2000	0.2000	

VERTOL VR-7 FROM BINGHAM

CD TABLE 1

ALPHA	MACH 0.350	MACH 0.400	MACH 0.500	MACH 0.610	MACH 0.680	MACH 0.750	MACH 0.850	MACH 0.900	MACH
0.0	0.0075	0.0083	0.0083	0.0088	0.0082	0.0105	0.0445	0.0120	
1.00	0.0075	0.0086	0.0084	0.0089	0.0091	0.0138	0.0495	0.0130	
2.00	0.0075	0.0086	0.0083	0.0089	0.0105	0.0180	0.0540	0.0200	
3.00	0.0076	0.0087	0.0084	0.0089	0.0145	0.0295	0.0640	0.0320	
4.00	0.0078	0.0087	0.0088	0.0090	0.0250	0.0635	0.0720	0.0460	
6.00	0.0080	0.0097	0.0090	0.0110	0.0425	0.0860	0.0900	0.0860	
8.00	0.0095	0.0110	0.0220	0.0260	0.0815	0.1320	0.1325	0.1320	
10.00	0.0130	0.0200	0.0250	0.0820	0.1340	0.1760	0.1760	0.1760	
11.00	0.0230	0.0290	0.0395	0.1190	0.1590	0.1970	0.1970	0.1970	
12.00	0.0625	0.0435	0.0500	0.1450	0.1832	0.2160	0.2160	0.2160	
12.50	0.0650	0.0500	0.0675	0.1670	0.2020	0.2320	0.2320	0.2320	
13.00	0.0710	0.0575	0.0675	0.1950	0.2208	0.2430	0.2430	0.2430	
13.00	0.0775	0.0664	0.0750	0.2080	0.2344	0.2570	0.2570	0.2570	
14.00	0.0820	0.0700	0.0750	0.2200	0.2464	0.2690	0.2690	0.2690	
14.50	0.0850	0.0765	0.1590	0.2350	0.2603	0.2820	0.2820	0.2820	
15.00	0.0860	0.1590	0.1590	0.2500	0.2740	0.2945	0.2945	0.2945	
16.00	0.0900	0.1300	0.2065	0.2810	0.3017	0.3195	0.3195	0.3195	
16.50	0.1055	0.1475	0.2250	0.2960	0.3148	0.3310	0.3310	0.3310	
17.00	0.1350	0.1630	0.2440	0.3100	0.3282	0.3440	0.3440	0.3440	
20.00	0.2382	0.2673	0.3377	0.3709	0.3942	0.4141	0.4141	0.4141	
25.00	0.4500	0.4500	0.4500	0.4500	0.4877	0.5200	0.5200	0.5200	
30.00	0.6000	0.6000	0.6000	0.6000	0.6000	0.6000	0.6000	0.6000	
45.00	1.1940	1.1940	1.1940	1.1940	1.1940	1.1940	1.1940	1.1940	
60.00	1.6620	1.6620	1.6620	1.6620	1.6620	1.6620	1.6620	1.6620	
90.00	2.0220	2.0220	2.0220	2.0220	2.0220	2.0220	2.0220	2.0220	
135.00	1.1945	1.1945	1.1945	1.1945	1.1945	1.1945	1.1945	1.1945	
170.00	0.1320	0.1320	0.1320	0.1320	0.1320	0.1320	0.1320	0.1320	
175.00	0.0620	0.0620	0.0620	0.0	0.0620	0.0620	0.0620	0.0620	
180.00	0.0220	0.0220	0.0220	0.0220	0.0220	0.0220	0.0220	0.0220	
185.00	0.0620	0.0620	0.0620	0.0620	0.0620	0.0620	0.0620	0.0620	
190.00	0.1320	0.1320	0.1320	0.1320	0.1320	0.1320	0.1320	0.1320	
225.00	1.1945	1.1945	1.1945	1.1945	1.1945	1.1945	1.1945	1.1945	
270.00	2.0220	2.0220	2.0220	2.0220	2.0220	2.0220	2.0220	2.0220	
300.00	1.6620	1.6620	1.6620	1.6620	1.6620	1.6620	1.6620	1.6620	
315.00	1.1940	1.1940	1.1940	1.1940	1.1940	1.1940	1.1940	1.1940	
330.00	0.6000	0.6000	0.6000	0.6000	0.6000	0.6000	0.6000	0.6000	
335.00	0.4500	0.4500	0.4500	0.4500	0.4500	0.4500	0.4500	0.4500	
340.00	0.2990	0.2990	0.2990	0.2990	0.2990	0.2990	0.2990	0.2990	
346.00	0.1930	0.1970	0.1970	0.1970	0.2008	0.2040	0.2040	0.2040	
348.00	0.1815	0.1835	0.1835	0.1835	0.1902	0.1960	0.1960	0.1960	
349.00	0.1720	0.1730	0.1730	0.1730	0.1830	0.1915	0.1915	0.1915	
350.00	0.1500	0.1520	0.1600	0.1610	0.1742	0.1856	0.1856	0.1856	
352.00	0.0830	0.1040	0.1160	0.1295	0.1478	0.1635	0.1635	0.1635	
354.00	0.0460	0.0650	0.0775	0.0920	0.1122	0.1295	0.1295	0.1295	
356.00	0.0230	0.0350	0.0440	0.0550	0.0674	0.0780	0.0780	0.0780	
357.00	0.0150	0.0220	0.0300	0.0390	0.0465	0.0530	0.0530	0.0530	
358.00	0.0100	0.0110	0.0160	0.0200	0.0270	0.0330	0.0330	0.0330	
359.00	0.0078	0.0078	0.0100	0.0122	0.0159	0.0190	0.0190	0.0190	
360.00	0.0079	0.0079	0.0080	0.0081	0.0102	0.0120	0.0120	0.0120	

BELL CH-58C/A MAIN ROTOR CONF. OT-2R WITH 12 DEG TWIST, VR-7, DATA BANK 228
13 STATIONS
NO STA=13
0.172 0.300 0.450 0.600 0.700 0.750 0.800 0.850 0.875 0.900 0.924 0.952 0.977
15 GOLDSTEIN NO OF BLADES COLUMN 10
NUMBER OF BLADES FOR GOLDSTEIN USE= 2

16 SPEED OF SOUND 4000 FT., 95 DEGS.

MACH NO.=VT * X /(1155.0)
17 TWIST TABLE,12. DEGREES FULL SPAN
6.94 5.40 3.60 1.80 0.60 0.0 -0.60 -1.20 -1.50 -1.80 -2.09 -2.42 -2.72
18 AIRFOIL USED FIRST CARD IFOIL
START SECTION END SECTION

0.1160 1.0000
19 PROP FACTOR 8. FREE PROP 4. SHROUDED

SIGMA*CL= 8.00*X*KG*SIN(PHI)*TAN(PHI)
20 INTEGRATION LIMITS

CT XO= 0.116 CT XEND= 1.000 INDUCED CP XO= 0.0 CP XEND= 1.000 PROFILE CP XO= 0.0 CP XEND= 1.000
22 ITERATION LIMITS
ITERATION LIMIT ON PHI = 60 ITERATION LIMIT ON CT/SIGMA = 0
23 TOLERANCES

TOLERANCE ON PHI =0.2500 RELATIVE TOLERANCE ON CT/SIGMA =0.00020
30 BLADE CHORDS FEET CONFIGURATION CT-2R3

STATION	0.172	0.300	0.450	0.600	0.700	0.750	0.800	0.850	0.875	0.900	0.924	0.952	0.977
CHORD	1.234	1.198	1.155	1.112	1.084	1.070	1.055	1.042	0.946	0.859	0.775	0.673	0.586

25 **********
********** NEW CASE **********
THET75 REQD= 5.000 EQUIVALENT CHORD= 0.964 SIGMA EQUIVALENT=0.03474

RHO=0.001920 OMEGAR= 655.0 RADIUS= 17.67 ADELTA= 0.0 DELTA= 0.0

THETA 75 = 5.00 CT/SIGMA = 0.06628 CP/SIGMA INDUCED = 0.002497 CP/SIGMA PROFILE = 0.000980 CP/SIGMA = 0.003477

P/T = 0.0625 FIGURE OF MERIT = 0.6468 HP= 116.18 BLADE AREA= 16.897

STATION	MACH NO.	ALPHA	CL	CD	L/D	PHI	CT	CP IND.	CP PRO.
0.172	0.350	4.04	0.6244	0.0078	80.02	7.899	0.0003978	0.0000095	0.0000009
0.300	0.350	4.16	0.6390	0.0078	81.76	6.241	0.0012184	0.0000400	0.0000045
0.450	0.350	3.74	0.5890	0.0077	76.01	4.859	0.0024540	0.0000940	0.0000145
0.600	0.350	3.00	0.4994	0.0076	65.72	3.804	0.0035764	0.0001428	0.0000327
0.700	0.397	2.25	0.4195	0.0086	49.01	3.345	0.0039923	0.0001635	0.0000571
0.750	0.425	1.96	0.3924	0.0085	46.02	3.039	0.0042340	0.0001688	0.0000691
0.800	0.454	1.63	0.3549	0.0085	41.96	2.771	0.0043012	0.0001667	0.0000821
0.850	0.482	1.29	0.3134	0.0084	37.25	2.512	0.0042346	0.0001581	0.0000967
0.875	0.496	1.19	0.3022	0.0084	36.02	2.308	0.0039305	0.0001387	0.0000956
0.900	0.510	1.08	0.2885	0.0084	34.19	2.123	0.0036079	0.0001205	0.0000951
0.924	0.524	0.93	0.2704	0.0085	31.81	1.980	0.0032136	0.0001027	0.0000934
0.952	0.540	0.75	0.2468	0.0086	28.84	1.830	0.0027072	0.0000825	0.0000895
0.977	0.554	0.59	0.2264	0.0086	26.31	1.689	0.0022763	0.0000657	0.0000846

GOLDSTEIN FACTORS

0.99978 0.99948 0.99861 0.99902 0.99716 0.99543 0.99589 0.99835 0.99523 0.99588 0.92658 0.84187 0.77160
25 **********

THET75 REQD= 7.000 EQUIVALENT CHORD= 0.964 SIGMA EQUIVALENT=0.03474

RHO=0.001920 OMEGAR= 655.0 RADIUS= 17.67 ADELTA= 0.0 DELTA= 0.0

THETA 75 = 7.00 CT/SIGMA = 0.09504 CP/SIGMA INDUCED = 0.004277 CP/SIGMA PROFILE = 0.000986 CP/SIGMA = 0.005263

P/T = 0.0659 FIGURE OF MERIT = 0.7337 HP= 175.85 BLADE AREA= 16.897

STATION	MACH NO.	ALPHA	CL	CD	L/D	PHI	CT	CP IND.	CP PRO.
0.172	0.350	5.09	0.7503	0.0079	94.87	8.850	0.0004751	0.0000127	0.0000009
0.300	0.350	5.42	0.7898	0.0079	99.45	6.985	0.0014999	0.0000552	0.0000045
0.450	0.350	5.08	0.7501	0.0079	94.85	5.516	0.0031170	0.0001355	0.0000148
0.600	0.350	4.38	0.6651	0.0078	84.86	4.424	0.0047534	0.0002208	0.0000336
0.700	0.397	3.77	0.6095	0.0086	70.52	3.827	0.0057901	0.0002713	0.0000575
0.750	0.425	3.38	0.5711	0.0087	65.92	3.616	0.0061530	0.0002918	0.0000701
0.800	0.454	3.01	0.5324	0.0085	62.34	3.393	0.0064434	0.0003058	0.0000828
0.850	0.482	2.62	0.4945	0.0084	58.75	3.177	0.0066732	0.0003151	0.0000966
0.875	0.496	2.52	0.4864	0.0084	58.15	2.979	0.0063180	0.0002879	0.0000951
0.900	0.510	2.41	0.4761	0.0084	56.72	2.789	0.0059469	0.0002609	0.0000944
0.924	0.524	2.27	0.4602	0.0085	54.45	2.645	0.0054624	0.0002333	0.0000927
0.952	0.540	2.08	0.4377	0.0085	51.35	2.500	0.0047975	0.0001997	0.0000891
0.977	0.554	1.91	0.4176	0.0086	48.56	2.362	0.0041953	0.0001692	0.0000845

GOLDSTEIN FACTORS

0.99893 0.99870 0.99816 0.99837 0.99532 0.99021 0.98353 0.97329 0.96187 0.95476 0.88366 0.79636 0.72392

25

********** NEW CASE **********

THET75 REQD= 8.000 EQUIVALENT CHORD= 0.964 SIGMA EQUIVALENT=0.03474

RHO=0.001920 OMEGAR= 655.0 RADIUS= 17.67 ADELTA= 0.0 DELTA= 0.0

THETA 75 = 8.00 CT/SIGMA = 0.10977 CP/SIGMA INDUCED = 0.005330 CP/SIGMA PROFILE = 0.000998 CP/SIGMA = 0.006328

P/T = 0.0687 FIGURE OF MERIT = 0.7573 HP= 211.47 BLADE AREA= 16.897

STATION	MACH NO.	ALPHA	CL	CD	L/D	PHI	CT	CP IND.	CP PRO.
0.172	0.350	5.69	0.8226	0.0080	103.23	9.248	0.0005191	0.0000146	0.0000009
0.300	0.350	6.06	0.8680	0.0080	107.85	7.336	0.0016450	0.0000636	0.0000046
0.450	0.350	5.78	0.8331	0.0080	104.43	5.824	0.0034572	0.0001588	0.0000149
0.600	0.350	5.09	0.7511	0.0079	94.97	4.707	0.0053624	0.0002651	0.0000339
0.700	0.397	4.49	0.7002	0.0089	78.85	4.108	0.0066456	0.0003344	0.0000591
0.750	0.425	4.10	0.6651	0.0088	75.88	3.902	0.0071596	0.0003665	0.0000708
0.800	0.454	3.72	0.6285	0.0087	72.31	3.683	0.0076000	0.0003916	0.0000842
0.850	0.482	3.33	0.5883	0.0086	68.72	3.471	0.0079335	0.0004093	0.0000982
0.875	0.496	3.23	0.5806	0.0085	68.31	3.270	0.0075366	0.0003770	0.0000966
0.900	0.510	3.12	0.5711	0.0085	67.24	3.076	0.0071281	0.0003450	0.0000955
0.924	0.524	2.98	0.5559	0.0085	65.35	2.933	0.0065946	0.0003123	0.0000933
0.952	0.540	2.78	0.5351	0.0086	62.44	2.791	0.0058609	0.0002724	0.0000895
0.977	0.554	2.62	0.5164	0.0086	59.86	2.657	0.0051847	0.0002352	0.0000847

GOLDSTEIN FACTORS

0.99858 0.99834 0.99790 0.99808 0.99424 0.98762 0.97777 0.96224 0.94743 0.93701 0.86511 0.77658 0.70300

25 **********

********** NEW CASE **********

THET75 REQD= 8.500 EQUIVALENT CHORD= 0.964 SIGMA EQUIVALENT=0.03474

RHO=0.001920 OMEGAR= 655.0 RADIUS= 17.67 ADELTA= 0.0 DELTA= 0.0

STATION	MACH NO.	ALPHA	CL	CD	L/D	PHI	CT	CP IND.	CP PRO.
0.172	0.350	6.93	0.9765	0.0087	112.25	10.004	0.0006116	0.0000186	0.0000009
0.300	0.350	7.38	1.0329	0.0090	114.29	8.017	0.0019487	0.0000824	0.0000051
0.450	0.350	7.18	1.0080	0.0089	113.41	6.416	0.0041700	0.0002111	0.0000166
0.600	0.350	6.56	0.9295	0.0084	110.43	5.244	0.0066215	0.0003648	0.0000360
0.700	0.397	5.97	0.8850	0.0096	92.33	4.626	0.0083838	0.0004752	0.0000636
0.750	0.425	5.58	0.8522	0.0094	91.09	4.420	0.0091574	0.0005312	0.0000755
0.800	0.454	5.19	0.8186	0.0091	90.02	4.212	0.0098801	0.0005824	0.0000879
0.850	0.482	4.78	0.7815	0.0089	87.66	4.021	0.0105204	0.0006291	0.0001021
0.875	0.496	4.67	0.7757	0.0089	87.41	3.825	0.0100529	0.0005885	0.0001007
0.900	0.510	4.57	0.7682	0.0089	86.07	3.628	0.0095744	0.0005466	0.0001002
0.924	0.524	4.43	0.7546	0.0090	84.13	3.481	0.0089397	0.0005027	0.0000982
0.952	0.540	4.23	0.7350	0.0090	81.91	3.342	0.0080398	0.0004475	0.0000936
0.977	0.554	4.06	0.7181	0.0089	80.38	3.211	0.0072004	0.0003949	0.0000876

GOLDSTEIN FACTORS

0.99791 0.99763 0.99718 0.99752 0.99226 0.98293 0.96727 0.94152 0.91986 0.90302 0.82973 0.73916 0.66375

25 **********

********** NEW CASE **********

THET75 REQD=10.500 EQUIVALENT CHORD= 0.964 SIGMA EQUIVALENT=0.03474

RHO=0.001920 OMEGAR= 655.0 RADIUS= 17.67 ADELTA= 0.0 DELTA= 0.0

THETA 75 = 10.50 CT/SIGMA = 0.14738 CP/SIGMA INDUCED = 0.008393 CP/SIGMA PROFILE = 0.001075 CP/SIGMA = 0.009468

P/T = 0.0765 FIGURE OF MERIT = 0.7875 HP= 516.38 BLADE AREA= 16.897

STATION	MACH NO.	ALPHA	CL	CD	L/D	PHI	CT	CP IND.	CP PRO.
0.172	0.350	7.25	1.0165	0.0089	113.71	10.164	0.0006354	0.0000197	0.0000010
0.300	0.350	7.72	1.0748	0.0093	115.71	8.181	0.0020254	0.0000874	0.0000053
0.450	0.350	7.54	1.0526	0.0092	114.97	6.559	0.0043510	0.0002253	0.0000170
0.600	0.350	6.93	0.9758	0.0087	112.23	5.374	0.0069467	0.0003923	0.0000372
0.700	0.397	6.35	0.9291	0.0098	94.52	4.746	0.0087971	0.0005117	0.0000652
0.750	0.425	5.96	0.9000	0.0095	94.67	4.541	0.0096660	0.0005762	0.0000766
0.800	0.454	5.56	0.8666	0.0092	94.20	4.335	0.0104557	0.0006345	0.0000889
0.850	0.482	5.15	0.8297	0.0090	92.39	4.148	0.0111635	0.0006887	0.0001028
0.875	0.496	5.05	0.8240	0.0089	92.41	3.953	0.0106747	0.0006458	0.0001012
0.900	0.510	4.95	0.8167	0.0090	90.81	3.754	0.0101750	0.0006012	0.0001009
0.924	0.524	4.80	0.8032	0.0091	88.46	3.608	0.0095118	0.0005542	0.0000994
0.952	0.540	4.61	0.7836	0.0091	85.79	3.469	0.0085679	0.0004949	0.0000952
0.977	0.554	4.44	0.7665	0.0091	83.90	3.339	0.0076834	0.0004382	0.0000895

GOLDSTEIN FACTORS

0.99775 0.99746 0.99700 0.99738 0.99180 0.98183 0.96482 0.93674 0.91352 0.89520 0.82160 0.73058 0.65472

25 **********

********** NEW CASE **********

THET75 REQD=11.000 EQUIVALENT CHORD= 0.964 SIGMA EQUIVALENT=0.03474

RHO=0.001920 OMEGAR= 655.0 RADIUS= 17.67 ADELTA= 0.0 DELTA= 0.0

THETA 75 = 11.00 CT/SIGMA = 0.15493 CP/SIGMA INDUCED = 0.009067 CP/SIGMA PROFILE = 0.001101 CP/SIGMA = 0.010168

P/T = 0.0782 FIGURE OF MERIT = 0.7904 HP= 339.76 BLADE AREA= 16.897

STATION	MACH NO.	ALPHA	CL	CD	L/D	PHI	CT	CP IND.	CP PRO.
0.172	0.350	7.58	1.0578	0.0092	115.14	10.354	0.0006599	0.0000208	0.0000010
0.300	0.350	8.06	1.1170	0.0096	116.38	8.344	0.0021025	0.0000926	0.0000054
0.450	0.350	7.90	1.0974	0.0094	116.44	6.701	0.0045325	0.0002398	0.0000175
0.600	0.350	7.30	1.0222	0.0090	113.92	5.502	0.0072729	0.0004206	0.0000383
0.700	0.397	6.74	0.9734	0.0101	96.56	4.863	0.0092128	0.0005490	0.0000668
0.750	0.425	6.34	0.9482	0.0102	92.53	4.660	0.0101784	0.0006227	0.0000826
0.800	0.454	5.94	0.9150	0.0093	98.30	4.456	0.0110346	0.0006884	0.0000899
0.850	0.482	5.53	0.8781	0.0090	97.09	4.273	0.0118098	0.0007505	0.0001035
0.875	0.496	5.42	0.8726	0.0090	97.39	4.079	0.0112999	0.0007054	0.0001016
0.900	0.510	5.32	0.8655	0.0091	95.50	3.879	0.0107791	0.0006581	0.0001017
0.924	0.524	5.18	0.8521	0.0092	92.71	3.732	0.0100868	0.0006080	0.0001006
0.952	0.540	4.98	0.8324	0.0093	89.56	3.593	0.0090985	0.0005445	0.0000968
0.977	0.554	4.81	0.8153	0.0093	87.30	3.464	0.0081692	0.0004833	0.0000915

GOLDSTEIN FACTORS

0.99760 0.99729 0.99683 0.99725 0.99135 0.98075 0.96242 0.93205 0.90730 0.88753 0.81360 0.72214 0.64588

28

OH-58, BINGHAM'S VR-7, CONFIG. DT-2R3, SPEED SWEEP, 1/24/78

5.000000	5.000000	0.005000	0.005000	0.013000	0.010000	0.050000	0.001000
10	12	10	0	1	1	15	0

1 0.0 0.10

2 0.12 1.00

RADIAL STA	TWIST	BLADE CHORD	MASS/LBS/IN
0.172	6.94	1.234	0.0
0.300	5.40	1.198	0.0
0.450	3.60	1.155	0.0
0.600	1.80	1.112	0.0
0.700	0.60	1.084	0.0
0.750	0.0	1.070	0.0
0.850	-1.20	1.042	0.0
0.900	-1.80	0.859	0.0
0.950	-2.42	0.673	0.0
0.977	-2.72	0.586	0.0

RADIUS	GAMMA	NO BLADES	SIGMA	DELTA 3	OFFSET RATIO
1.76700E 01	5.41000E 00	2.00000E 00	3.47000E-02	0.0	0.0

BLADE START	BLADE END
1.00000E-01	1.00000E 00

SB	I1	IR
1.80000E 01	2.00000E 02	0.0

RHO	SPEED SOUND
1.92000E-03	1.15500E 03

ROLL RATE	PITCH RATE	MANEUVER FCT
0.0	0.0	0.0

PROP INCID(LG)	PROP INCID(LAT)	BETA 1(RAD)	BETA2(RAD)	DNWASH WING	DNWASH TAIL	DNWASH AT PROP	X DIST CABLE
0.0	0.0	0.0	0.0	0.0	3.50000E-02	0.0	0.0

X DIST HUB	Z DIST HUB	Y DIST HUB	X DIST WING	Z DIST WING	Y DIST WING	(DEP/DALFA)WG	(DEP/DALFA)TAIL
0.0	4.99000E 00	0.0	0.0	0.0	0.0	0.0	0.0

X DIST H.TAIL	Z DIST H.TAIL	Y DIST H.TAIL	X DIST PROP	Z DIST PROP	Y DIST PROP	X VERT TAIL	Z VERT TAIL
1.21200E 01	7.13000E-01	0.0	0.0	0.0	0.0	1.96100E 01	1.43000E 00

CLO(FUSE)	CNO(FUSE)	CL DELTA AIL	CL DELTA RUDR	CN DELTA AIL	CN DELTA RUDR	Z DIST CABLE	Y DIST CABLE
0.0	0.0	0.0	0.0	0.0	0.0	0.0	0.0

CL ALFA WING	CLWING/AIL	CLO WING	CDC WING	CL ALFA H.TAIL	CL DELTA ELEV	CLO H.TAIL	CDO H.TAIL
1.00000E 00	0.0	0.0	0.0	3.72500E 00	3.72500E 00	-2.38000E-01	1.00000E-02

CL ALFA FUSE	CLO FUSE	CDO FUSE	CLVTAIL/RUDR	CLO VERT TAIL	CDO VERT TAIL	CMO WING	CM WING/AIL
1.37000E-02	1.21000E-03	1.42800E-02	0.0	0.0	1.00000E-02	0.0	0.0

AR WING	AR H.TAIL	AR VERT TAIL	AR FUSE	AREA WING	AREA H.TAIL	AREA VERT TAIL	MAC WING	RAD
1.00000E 01	4.30000E 00	4.53000E 00	3.00000E-01	1.00000E-01	9.66000E 00	9.11000E 00	1.67E 01	1.67E 01

SPAN-FCT WING	SPAN-FCT H.T.	SPAN-FCT FUSE	SPAN-FCT VT	QT/Q	DALFA/DAIL	FUSE REF AREA	CABLE TENSION
1.00000E 00	7.50000E-01	1.00000E 00	7.50000E-01	7.00000E-01	0.0	9.80500E 02	1.00000E 00

PROP TORQ FCTR	PROP PITCH FCT	PROP YAW FCT	NO PROP FCTR	RADIUS PROP	EFF PROP	OMEGAR PROP	PROP FORCE FCTR
0.0	0.0	0.0	1.00000E 00	0.0	0.0	0.0	0.0

DELTA AIL(RAD)	DELTA ELEV(RAD)	DELTA RUDR	CMO FUSE	CM ALFA FUSE	FLAP HNGE SPR	FITZ FCTR	PHI CABLE(RAD)
0.0	0.0	0.0	-2.13000E-03	1.88000E-02	2.15528E 05	0.0	0.0

GROSS WEIGHT	LOAD FCTR Z	LOAD FCTR X	ALFA FUSE(RAD)	NO ITER NZ	NO ITER ALFAF	NO ITER Q	TR DIRECTION
3.20000E 03	1.00000E 00	0.0	8.10000E-03	40	40	0	1.00000E 00

PRINT CONTROL	HARM CONTROL	NO HARMONICS	ITER WING,PROP	WING LIFT REQD	PROP THRST RQD	TOL WING LIFT	TOL PROP THRST
1	0	0	40	0.0	0.0	2.00000E 01	5.00000E 01

MU	THETA 75	LAMBDA	TORQ FCTR	HFORCE FCTR	WING INCID	H TAIL INCID	OMEGAR
2.00000E-01	6.70000E 00	-2.90000E-02	1.01800E 00	1.56300E 00	0.0	0.0	6.55000E 02

DELTA LAMB	H TAIL INCR	PROP/WING CTL	ACON	ALFAF FCTR	BUILT IN CONE	AUTOR CONTR	ACON MULT
2.00000E-03	0.0	0.0	1.50000E-01	1.78600E-02	5.23000E-02	0.0	1.00000E 00

```
 OH-58, BINGHAM'S VR-7, CONFIG. DT-2R3,  SPEED SWEEP, 1/24/78
CASE NO=                          NUMBER OF ITERATIONS ON PROP THRUST AND WING LIFT=

NZ ITER LIMIT=40     FUSELAGE ANG ITER LIMIT=40     NZ(REQ)=      1.00

  RADIUS=   17.67          GAMMA=    4.37          OMEGAR=  655.00       NO BLADES=    2.
SOLIDITY=  0.0347        DELTA 3=    0.0        CFF.RATIO=     0.0        BLADE ROOT CUT OUT=  0.100

NO RADIAL STA=10       NO AZIMUTH STA=12       BETA ITER LIMIT=10
TOL ON BETA  = 5.00    TOL ON BETADOT= 5.00

BL FLAPPING STATIC MOM= 18.0 BL FLAPPING INERTIA=    200. PROD OF INERTIA=  0.0  BL FLPNG HNGE SPR.RATE= 215528.

FLIGHT CONDITION
  MU= 0.200       GR WT=   3200.     NZ= 1.00     NX= 0.0     RADIAL FLOW CORR(CP)= 1.0180  RADIAL FLOW CORR(CH)= 1.5630
TH75= 6.787      ALAMO= -0.0370     CT= 0.00408     CH= 0.00025     CY= 0.00013     CQ=0.0001448

ROTOR PARAMETERS
    THRUST=  3295.      HP=   139.      HFORCE=  201.      YFORCE= -105.      MX=     0.      MY=     0.
FORCE NORMAL TO FLIGHT PATH= 3292.      FORCE PARALLEL TO FLIGHT PATH=  241.      ROTOR ANGLE OF ATTACK= -0.1339RAD =  -7.6708
TAIL ROTOR THRUST(LBS)=  105.           TAIL ROTOR TORQUE(FT.LB)= -62.0

PROPELLER LONGITUDINAL INCIDENCE=  0.0          WING INCIDENCE=  0.0       HORIZONTAL TAIL INCIDENCE=  0.0
  AILERON   DEFLECTION=  0.0  RUDDER DEFLECTION=  0.0  CABLE TENSION=    1.00  CABLE ANGLE=  0.0

    ALAMO SHAFT= -0.0266          ROTOR ANGLE OF ATTACK= -4.6987DEG          MU SHAFT= 0.201

TRIM DATA
    FEATHERING ANGLES(RAD)          FLAPPING ANGLES(DEG)
        A1S=  0.0239                    B1S= -0.2837
        B1S=  0.0519                    A1S= -0.6142

  SMALL A1(RAD)=  0.0412        SMALL B1(RAD)= -0.0288        CONING ANGLE(RAD)=  0.0395

   CL TAIL(IN)=-0.6738  ALPHA TAIL-IN(RAD)=-0.1170    CL TAIL(OUT)=-0.6647  ALPHA TAIL-OUT(RAD)=-0.1145
    HORIZONTAL TAIL LOAD=    -75.4          TAIL INCIDENCE ZERO(RAD)=  0.0
    PROPELLER   THRUST  =      0.1          VELOCITY(FT/SEC)= 132.184  (KNOTS)=  78.253
   FUSELAGE ANGLE (DEG)= -4.6310           U=  131.752
        ROLL ANGLE(RAD)=-.0249=  -1.43DEG   W=  -10.671
     PITCH RATE(RAD/SEC)= 0.0               RATE OF CLIMB(FT/MIN)=     0.0
         WING LIFT(LBS)=      -0.1          FUSELAGE LIFT(LBS)=      1.4      FUSELAGE PITCHING MOMENT(FT LBS)=  -1008.4
```

BLADE ANGLE OF ATTACK DISTRIBUTION (DEG)

AZIMUTH STA	NON DIMENSIONAL BLADE RADIUS									
	0.172	0.300	0.450	0.600	0.700	0.750	0.850	0.900	0.950	0.977
0.0	-0.30	3.11	3.58	2.92	2.22	1.81	0.94	0.47	-0.03	-0.27
30.0	3.32	4.10	3.66	2.64	1.80	1.34	0.39	-0.10	-0.63	-0.88
60.0	5.49	5.43	4.60	3.39	2.48	1.99	1.00	0.48	-0.06	-0.32
90.0	7.25	6.92	5.92	4.63	3.68	3.18	2.15	1.63	1.08	0.81
120.0	8.55	8.18	7.14	5.80	4.83	4.32	3.23	2.75	2.19	1.92
150.0	9.11	9.06	8.13	6.83	5.86	5.35	4.31	3.78	3.22	2.94
180.0	7.86	9.29	8.83	7.70	6.78	6.30	5.29	4.76	4.22	3.95
210.0	-1.19	8.15	9.04	8.32	7.54	7.10	6.16	5.67	5.14	4.88
240.0	-79.47	4.43	8.45	8.39	7.80	7.42	6.58	6.11	5.62	5.37
270.0	-120.91	-0.21	7.07	7.59	7.16	6.84	6.07	5.64	5.17	4.94
300.0	-78.51	-0.06	5.59	6.04	5.63	5.33	4.58	4.17	3.70	3.48
330.0	-12.45	1.94	4.34	4.25	3.71	3.37	2.57	2.14	1.67	1.44

AZIMUTH	BETA	BETAD
0.	-0.003	1.431
30.	0.021	1.431
60.	0.049	1.431
90.	0.069	1.431
120.	0.082	1.431
150.	0.085	1.431
180.	0.080	1.431
210.	0.064	1.431
240.	0.039	1.431
270.	0.012	1.431
300.	-0.009	1.431
330.	-0.015	1.431

BLADE MACH NUMBER DISTRIBUTION

AZIMUTH STA	NON-DIMENSIONAL BLADE RADIUS									
	0.172	0.300	0.450	0.600	0.700	0.750	0.850	0.900	0.950	0.977
0.0	0.10	0.17	0.26	0.34	0.40	0.43	0.48	0.51	0.54	0.55
30.0	0.16	0.23	0.31	0.40	0.46	0.48	0.54	0.57	0.60	0.61
60.0	0.20	0.27	0.35	0.44	0.50	0.52	0.58	0.61	0.64	0.65
90.0	0.21	0.28	0.37	0.45	0.51	0.54	0.60	0.62	0.65	0.67
120.0	0.20	0.27	0.35	0.44	0.49	0.52	0.58	0.61	0.64	0.65
150.0	0.15	0.23	0.31	0.40	0.45	0.48	0.54	0.57	0.59	0.61
180.0	0.10	0.17	0.25	0.34	0.40	0.42	0.48	0.51	0.54	0.55
210.0	0.04	0.11	0.20	0.28	0.34	0.40	0.45	0.48	0.51	0.53
240.0	0.05	0.07	0.16	0.24	0.30	0.38	0.43	0.46	0.51	0.53
270.0	0.07	0.06	0.14	0.23	0.28	0.31	0.43	0.45	0.48	0.50
300.0	0.07	0.07	0.16	0.24	0.30	0.33	0.39	0.41	0.44	0.46
330.0	0.06	0.12	0.20	0.28	0.34	0.37	0.43	0.45	0.48	0.50

CL DISTRIBUTION

AZIMUTH STA	NON DIMENSIONAL BLADE RADIUS									
	0.172	0.300	0.450	0.600	0.700	0.750	0.850	0.900	0.950	0.977
0.0	0.05376	0.51368	0.56984	0.49016	0.44661	0.39278	0.26576	0.20079	0.11659	0.08608
30.0	0.53844	0.63239	0.57919	0.50207	0.39048	0.32488	0.19504	0.10711	0.03527	0.00607
60.0	0.79845	0.79191	0.69944	0.60503	0.48189	0.42375	0.29306	0.22260	0.12940	0.09975
90.0	1.01655	0.97459	0.88510	0.77204	0.64833	0.58932	0.46004	0.39923	0.34157	0.31094
120.0	1.17836	1.13231	1.01051	0.92464	0.79750	0.73983	0.61777	0.55123	0.48566	0.46288
150.0	1.24846	1.24309	1.12660	1.07297	0.93143	0.86564	0.74368	0.68246	0.61443	0.58114
180.0	1.09257	1.27156	1.21348	1.07211	1.06521	0.99762	0.85720	0.79263	0.73146	0.70150
210.0	-0.05124	1.12889	1.24043	1.15022	1.05274	1.04356	0.97583	0.90659	0.83802	0.80442
240.0	-0.34960	0.67133	1.16588	1.15846	1.08479	1.03799	1.00566	0.96831	0.90005	0.86823
270.0	0.66729	0.06504	0.99416	1.05849	1.00508	0.96527	0.90374	0.89850	0.84229	0.81207
300.0	-0.37590	0.08316	0.81063	0.86522	0.81408	0.77936	0.74126	0.71140	0.66664	0.63665
330.0	-0.81464	0.36213	0.66113	0.64941	0.58514	0.56586	0.49471	0.43834	0.37186	0.33826

CD DISTRIBUTION

AZIMUTH STA	NON DIMENSIONAL BLADE RADIUS									
	0.172	0.300	0.450	0.600	0.700	0.750	0.850	0.900	0.950	0.977
0.0	0.00787	0.00762	0.00772	0.00759	0.00830	0.00832	0.00838	0.00840	0.00811	0.00889
30.0	0.00766	0.00781	0.00773	0.00835	0.00832	0.00837	0.00852	0.00841	0.01054	0.01191
60.0	0.00795	0.00794	0.00796	0.00856	0.00835	0.00844	0.00877	0.00885	0.00522	0.01104
90.0	0.00894	0.00869	0.00837	0.00896	0.00870	0.00863	0.00882	0.00911	0.00509	0.00892
120.0	0.01046	0.00981	0.00933	0.00898	0.00888	0.00893	0.00881	0.00889	0.00576	0.00977
150.0	0.01144	0.01136	0.00973	0.01392	0.00899	0.00894	0.00899	0.00887	0.00886	0.00889
180.0	0.00940	0.01176	0.01095	0.00927	0.01362	0.01093	0.00893	0.00895	0.00895	0.00888
210.0	0.00822	0.00976	0.01133	0.01006	0.00916	0.01143	0.01005	0.00897	0.00691	0.00889
240.0	1.89566	0.00784	0.01028	0.01018	0.00935	0.00907	0.01132	0.00974	0.00896	0.00894
270.0	1.45357	0.00788	0.00880	0.00919	0.00887	0.00863	0.00859	0.00890	0.00892	0.00889
300.0	1.88408	0.00789	0.00796	0.00803	0.00796	0.00793	0.00854	0.00882	0.00668	0.00859
330.0	0.18410	0.00750	0.00783	0.00782	0.00774	0.00801	0.00836	0.00831	0.00833	0.00836
END OF CASE										

CH-58 COMPOSITE BLADE STA 21.5 ANALYSIS — SHELL-D USES
CH-58 BLADE LIMIT LOADS STA 21.5 CONDIX — INCH-KIP SYSTEM

CASE 11.12
INPUT DATA

BASIC MODULI
STRINGER E = 10000.
SKIN G = 1000.

	STATION 21.50 COORDINATES		STATION 0.0 COORDINATES		COMP.	TENS.	CRITICAL STRESS		REL.	SKIN	SKIN			
ELEM.	Y	Z	Y	Z	AREA	AREA	COMP.	TENS.	MOD.	THICK.	MOD.	AST	CF	TF
1	-4.00	-1.130	0.0	0.0	0.2278	0.3387	-100.00	100.00	0.57	0.5243	1056.	0.0000	0.5	0.500
2	-3.00	-1.130	0.0	0.0	0.2749	0.5243	-100.00	100.00	0.57	0.5243	1056.	0.0000	0.5	0.500
3	-2.00	-1.130	0.0	0.0	0.2749	0.5243	-100.00	100.00	0.57	0.5243	1056.	0.0000	0.5	0.500
4	-1.00	-1.130	0.0	0.0	0.2749	0.5243	-100.00	100.00	0.57	0.5243	1056.	0.0000	0.5	0.500
5	0.0	-1.130	0.0	0.0	0.2749	0.5243	-100.00	100.00	0.57	0.5243	1056.	0.0000	0.5	0.500
6	1.00	-1.130	0.0	0.0	0.2749	0.5243	-100.00	100.00	0.57	0.5243	1056.	0.0000	0.5	0.500
7	2.00	-1.130	0.0	0.0	0.2749	0.5243	-100.00	100.00	0.57	0.5243	1056.	0.0000	0.5	0.500
8	3.00	-1.130	0.0	0.0	0.2749	0.3696	-100.00	100.00	0.57	0.5243	1056.	0.0000	0.5	0.500
9	3.41	-1.130	0.0	0.0	0.3487	0.3122	-100.00	100.00	0.57	0.6500	1056.	0.0000	0.5	0.500
10	3.41	-0.500	0.0	0.0	0.4225	0.3673	-100.00	100.00	0.51	0.6500	604.	0.0000	0.5	0.500
11	3.41	0.0	0.0	0.0	0.4225	0.3250	-100.00	100.00	0.51	0.6500	604.	0.0000	0.5	0.500
12	3.41	0.500	0.0	0.0	0.4225	0.3250	-100.00	100.00	0.51	0.6500	604.	0.0000	0.5	0.500
13	3.41	1.000	0.0	0.0	0.4225	0.3276	-100.00	100.00	0.51	0.6500	604.	0.0000	0.5	0.500
14	3.41	1.508	0.0	0.0	0.3487	0.2726	-100.00	100.00	0.57	0.5243	1056.	0.0000	0.5	0.500
15	3.00	1.508	0.0	0.0	0.2749	0.3696	-100.00	100.00	0.57	0.5243	1056.	0.0000	0.5	0.500
16	2.00	1.508	0.0	0.0	0.2749	0.5243	-100.00	100.00	0.57	0.5243	1056.	0.0000	0.5	0.500
17	1.00	1.508	0.0	0.0	0.2749	0.5243	-100.00	100.00	0.57	0.5243	1056.	0.0000	0.5	0.500
18	0.0	1.508	0.0	0.0	0.2749	0.5243	-100.00	100.00	0.57	0.5243	1056.	0.0000	0.5	0.500
19	-1.00	1.508	0.0	0.0	0.2749	0.5243	-100.00	100.00	0.57	0.5243	1056.	0.0000	0.5	0.500
20	-2.00	1.508	0.0	0.0	0.2749	0.5243	-100.00	100.00	0.57	0.5243	1056.	0.0000	0.5	0.500
21	-3.00	1.508	0.0	0.0	0.2749	0.5243	-100.00	100.00	0.57	0.5243	1056.	0.0000	0.5	0.500
22	-4.00	1.508	0.0	0.0	0.2749	0.3565	-100.00	100.00	0.57	0.5243	1056.	0.0000	0.5	0.500
23	-4.36	1.508	0.0	0.0	0.2278	0.2023	-100.00	100.00	0.49	0.4250	620.	0.0000	0.5	0.500
24	-4.36	1.000	0.0	0.0	0.1806	0.2142	-100.00	100.00	0.49	0.4250	620.	0.0000	0.5	0.500
25	-4.36	0.500	0.0	0.0	0.1806	0.2125	-100.00	100.00	0.49	0.4250	620.	0.0000	0.5	0.500
26	-4.36	0.0	0.0	0.0	0.1806	0.2125	-100.00	100.00	0.49	0.4250	620.	0.0000	0.5	0.500
27	-4.36	-0.500	0.0	0.0	0.1806	0.2401	-100.00	100.00	0.49	0.4250	620.	0.0000	0.5	0.500
28	-4.36	-1.130	0.0	0.0	0.1806	0.2104	-100.00	100.00	0.49	0.4250	620.	0.0000	0.5	0.500

CH-58 COMPOSITE BLADE STA 21.5 ANALYSIS — SHELL-D USES INCH-KIP SYSTEM

CH-58 BLADE LIMIT LOADS STATION 21.5 COND III

CASE 11.13 LOAD Y = 0.0 MXX = 6.150 FXX = 35.000

STA. 21.50 POINT Z = 0.0 MXY = -68.000 FXY = 0.0

MXZ = -58.000 FXZ = 0.0

NO.	AXIAL STRESS	M.S.	COMPONENTS OF FORCE X	Y	Z	SHEAR FLOW	SHEAR STRESS	SKIN FORCE COMP. Y	Z
1	6.46	14.47	2.189	0.0	0.0	0.150	0.29	0.102	0.0
2	7.29	12.72	3.821	0.0	0.0	0.150	0.29	0.150	0.0
3	8.11	11.33	4.252	0.0	0.0	0.150	0.29	0.150	0.0
4	8.93	10.20	4.683	0.0	0.0	0.150	0.29	0.150	0.0
5	9.75	9.25	5.114	0.0	0.0	0.150	0.29	0.150	0.0
6	10.58	8.46	5.545	0.0	0.0	0.150	0.29	0.150	0.0
7	11.40	7.77	5.976	0.0	0.0	0.150	0.29	0.150	0.0
8	12.22	7.18	4.517	0.0	0.0	0.150	0.29	0.106	0.0
9	12.56	6.96	3.921	0.0	0.0	0.150	0.23	0.031	0.047
10	8.62	10.60	3.165	0.0	0.0	0.150	0.23	0.0	0.085
11	6.48	14.42	2.137	0.0	0.0	0.150	0.23	0.0	0.075
12	4.35	22.01	1.412	0.0	0.0	0.150	0.23	0.0	0.075
13	2.21	44.26	0.724	0.0	0.0	0.150	0.23	0.0	0.076
14	0.04	99.00	0.012	0.0	0.0	0.150	0.29	-0.031	0.038
15	-0.29	99.00	-0.108	0.0	0.0	0.150	0.29	-0.106	0.0
16	-1.12	88.64	-0.585	0.0	0.0	0.150	0.29	-0.150	0.0
17	-1.94	50.61	-1.016	0.0	0.0	0.150	0.29	-0.150	0.0
18	-2.76	35.24	-1.447	0.0	0.0	0.150	0.29	-0.150	0.0
19	-3.58	26.92	-1.878	0.0	0.0	0.150	0.29	-0.150	0.0
20	-4.40	21.71	-2.309	0.0	0.0	0.150	0.29	-0.150	0.0
21	-5.23	18.14	-2.740	0.0	0.0	0.150	0.29	-0.150	0.0
22	-6.05	15.53	-2.156	0.0	0.0	0.150	0.29	-0.102	0.0
23	-5.55	17.03	-1.122	0.0	0.0	0.150	0.35	-0.027	-0.038
24	-3.44	28.07	-0.737	0.0	0.0	0.150	0.35	0.0	-0.076
25	-1.37	72.20	-0.290	0.0	0.0	0.150	0.35	0.0	-0.075
26	0.71	99.00	0.150	0.0	0.0	0.150	0.35	0.0	-0.075
27	2.78	34.96	0.668	0.0	0.0	0.150	0.35	0.0	-0.085
28	5.39	17.54	1.135	0.0	0.0	0.150	0.35	0.027	-0.047

X-TWIST = 0.000164047 RAD./IN. CHECKS, MXX = 6.150 FXX = 35.000 IYZ = -0.1091 AREA = 6.031

Y-CURV. = -0.000837751 RAD./IN. MXY = -68.000 FXY = -0.000 IYY = 8.9030 YCENT = -0.236

Z-CURV. = -0.000145190 RAD./IN. MXZ = -58.000 FXZ = -0.000 IZZ = 44.9955 ZCENT = 0.193

AD-A064 159 KAMAN AEROSPACE CORP BLOOMFIELD CONN F/G 1/3
PRELIMINARY DESIGN STUDY OF A COMPOSITE MAIN ROTOR BLADE FOR TH--ETC(U)
SEP 78 C HARDERSEN, W BLACKBURN DAAJ02-77-C-0075
UNCLASSIFIED R-1532-VOL-1 USARTL-TR-78-29A NL

3 OF 3
AD
A064 159

END
DATE
FILMED
3-79
DDC

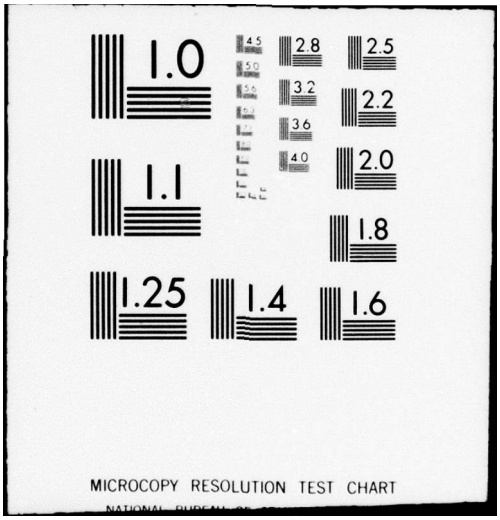
1.0
1.1
1.25
1.4
1.6
1.8
2.0
2.2
2.5
2.8
3.2
3.6
4.0
4.5
5.0
MICROCOPY RESOLUTION TEST CHART

PROG...CMAB

OH-58 INBOARD RETENTION BEARING PLATE

MAT.	ALLOWABLE STRESS, UNIAXIAL 11	11	22	22	12	12	MODULI E11	E22	G	NU12
6	-42.5	62.5	-10.0	2.70	-4.50	4.50	5200.	1300.	550.	0.260
30	-37.8	103.0	-7.1	2.30	-2.73	2.73	7820.	2504.	865.	0.300
31	-75.3	95.0	-19.2	3.20	-3.87	3.87	19500.	1570.	580.	0.330

LAMINA	1	2	3	4	5	6	7	8	9	10	11
MATERIAL	6	6	30	31	31	30	31	31	30	6	6
THICKNESS	0.0170	0.0170	0.0530	0.0366	0.0366	0.2040	0.0366	0.0366	0.0530	0.0085	0.0085
ANGLE	63.	-63.	0.	-45.	45.	0.	45.	-45.	0.	-62.	62.

LAMINATE PROPERTIES	EX	EY	G
K*S UNRESTRAINED	5755.	3146.	2102.
K*S = 0	5768.	3146.	2104.

BUCKLING PARAMETERS, VALID FOR L*L/R BETWEEN 0.14161E 02 AND 0.14161E 04
BUCKLING LOAD FX,CR= 0.22993E 05 NX,CR= 0.36595E 04 /R

BEHAVIOR FOR NX= 6.565 NY= 0.0 NXY= 0.150 KX= 0.0 KY= 0.0 KXY= 0.0

LAM. NO.	STRESSES X	Y	XY	STRAINS 11	22	12	11	22	12	M.S. 11	22	12	MIN.
11	2.4	-2.2	-0.5	-1.6	1.8	-1.6	-0.000350	0.001429	-0.002947	19.96	0.45	1.78	0.45
10	2.3	-2.5	0.8	-2.1	1.9	1.5	-0.000506	0.001546	0.002790	15.14	0.34	1.93	0.34
9	17.2	-1.4	0.1	17.2	-1.4	0.1	0.002250	-0.001211	0.000141	4.85	1.34	21.46	1.34
8	7.2	3.2	-4.0	9.1	1.2	2.0	0.000449	0.000590	0.003461	9.85	2.45	0.93	0.93
7	8.4	4.4	5.4	11.8	1.0	-2.0	0.000590	0.000449	-0.003461	7.26	3.53	0.93	0.93
6	17.2	-1.4	0.1	17.2	-1.4	0.1	0.002250	-0.001211	0.000141	4.85	1.34	21.46	1.34
5	8.4	4.4	5.4	11.8	1.0	-2.0	0.000590	0.000449	-0.003461	7.26	3.53	0.93	0.93
4	7.2	3.2	-4.0	9.1	1.2	2.0	0.000449	0.000590	0.003461	9.85	2.45	0.93	0.93
3	17.2	-1.4	0.1	17.2	-1.4	0.1	0.002250	-0.001211	0.000141	4.85	1.34	21.46	1.34
2	2.2	-2.7	0.9	-2.4	1.9	1.5	-0.000554	0.001594	0.002717	13.74	0.30	2.01	0.30
1	2.3	-2.4	-0.5	-1.8	1.8	-1.6	-0.000441	0.001480	-0.002882	17.54	0.40	1.84	0.40
ALL	13.0	0.0	0.3				0.002250	-0.001211	0.000141				0.30

CH-58 COMPOSITE BLADE STA 21.5 ANALYSIS — SHELL-D USES
CH-58 BLADE FATIGUE LOADS AT STATION 21.5 — INCH-KIP SYSTEM

CASE 11.14 — LOAD Y = 0.0 — MXX = 1.550 — FXX = 0.0
STA. 21.50 — POINT Z = 0.0 — MXY = -12.000 — FXY = 0.0
MXZ = -22.000 — FXZ = 0.0

NO.	AXIAL STRESS	M.S.	COMPONENTS OF FORCE X	Y	Z	SHEAR FLOW	SHEAR STRESS	SKIN FORCE COMP. Y	Z
1	-0.03	59.00	-0.010	0.0	0.0	0.038	0.07	0.026	0.0
2	0.24	59.00	0.128	0.0	0.0	0.038	0.07	0.038	0.0
3	0.52	55.00	0.272	0.0	0.0	0.038	0.07	0.038	0.0
4	0.79	59.00	0.417	0.0	0.0	0.038	0.07	0.038	0.0
5	1.07	52.48	0.561	0.0	0.0	0.038	0.07	0.038	0.0
6	1.34	72.37	0.705	0.0	0.0	0.038	0.07	0.038	0.0
7	1.62	60.14	0.849	0.0	0.0	0.038	0.07	0.038	0.0
8	1.89	51.78	0.700	0.0	0.0	0.038	0.07	0.027	0.0
9	2.01	48.81	0.627	0.0	0.0	0.038	0.06	0.008	0.012
10	1.38	71.62	0.506	0.0	0.0	0.038	0.06	0.0	0.021
11	1.03	55.63	0.336	0.0	0.0	0.038	0.06	0.0	0.019
12	0.69	59.00	0.225	0.0	0.0	0.038	0.06	0.0	0.019
13	0.35	59.00	0.115	0.0	0.0	0.038	0.06	0.0	0.019
14	0.00	59.00	0.001	0.0	0.0	0.038	0.07	-0.008	0.010
15	-0.11	59.00	-0.041	0.0	0.0	0.038	0.07	-0.027	0.0
16	-0.38	59.00	-0.202	0.0	0.0	0.038	0.07	-0.038	0.0
17	-0.66	59.00	-0.346	0.0	0.0	0.038	0.07	-0.038	0.0
18	-0.93	59.00	-0.490	0.0	0.0	0.038	0.07	-0.038	0.0
19	-1.21	81.67	-0.634	0.0	0.0	0.038	0.07	-0.038	0.0
20	-1.48	66.36	-0.778	0.0	0.0	0.038	0.07	-0.038	0.0
21	-1.76	55.63	-0.923	0.0	0.0	0.038	0.07	-0.038	0.0
22	-2.03	48.15	-0.725	0.0	0.0	0.038	0.07	-0.026	0.0
23	-1.87	52.61	-0.377	0.0	0.0	0.038	0.09	-0.007	-0.010
24	-1.53	64.45	-0.327	0.0	0.0	0.038	0.09	0.0	-0.019
25	-1.20	82.63	-0.254	0.0	0.0	0.038	0.09	0.0	-0.019
26	-0.86	59.00	-0.184	0.0	0.0	0.038	0.09	0.0	-0.019
27	-0.53	59.00	-0.128	0.0	0.0	0.038	0.09	0.0	-0.021
28	-0.11	59.00	-0.024	0.0	0.0	0.038	0.09	0.007	-0.012

X-TWIST = 0.0000041345 RAD./IN. — CHECKS, MXX = 1.550 — FXX = 0.000 — IYZ = -0.1091 — AREA = 6.031
Y-CURV. = -0.0001241911 RAD./IN. — MXY = -12.000 — FXY = -0.000 — IYY = 8.9030 — YCENT = -0.236
Z-CURV. = -0.0000485EE RAD./IN. — MXZ = -22.000 — FXZ = -0.000 — IZZ = 44.9955 — ZCENT = 0.193

CH-58 COMPOSITE BLADE STA 21.5 ANALYSIS — SHELL-D USES
CH-58 MEAN LOADS AT STATION 21.5 — INCH-KIP SYSTEM

CASE 11.15 — LOAD Y = 0.0 — MXX = -0.300 — FXX = 35.000
STA. 21.50 — POINT Z = 0.0 — MXY = -8.000 — FXY = 0.0
MXZ = -44.000 — FXZ = 0.0

NO.	AXIAL STRESS	M.S.	COMPONENTS OF FORCE X	Y	Z	SHEAR FLOW	SHEAR STRESS	SKIN FORCE COMP. Y	Z
1	2.05	47.80	0.694	0.0	0.0	-0.007	-0.01	-0.005	0.0
2	2.70	35.98	1.418	0.0	0.0	-0.007	-0.01	-0.007	0.0
3	3.36	28.77	1.761	0.0	0.0	-0.007	-0.01	-0.007	0.0
4	4.01	23.91	2.105	0.0	0.0	-0.007	-0.01	-0.007	0.0
5	4.67	20.42	2.448	0.0	0.0	-0.007	-0.01	-0.007	0.0
6	5.32	17.78	2.792	0.0	0.0	-0.007	-0.01	-0.007	0.0
7	5.98	15.72	3.135	0.0	0.0	-0.007	-0.01	-0.007	0.0
8	6.64	14.07	2.453	0.0	0.0	-0.007	-0.01	-0.005	0.0
9	6.90	13.45	2.156	0.0	0.0	-0.007	-0.01	-0.002	-0.002
10	5.69	16.57	2.090	0.0	0.0	-0.007	-0.01	0.0	-0.004
11	5.27	17.97	1.714	0.0	0.0	-0.007	-0.01	0.0	-0.004
12	4.85	19.60	1.577	0.0	0.0	-0.007	-0.01	0.0	-0.004
13	4.43	21.55	1.453	0.0	0.0	-0.007	-0.01	0.0	-0.004
14	4.45	21.46	1.213	0.0	0.0	-0.007	-0.01	0.002	-0.002
15	4.18	22.91	1.546	0.0	0.0	-0.007	-0.01	0.005	0.0
16	3.53	27.35	1.850	0.0	0.0	-0.007	-0.01	0.007	0.0
17	2.87	33.81	1.506	0.0	0.0	-0.007	-0.01	0.007	0.0
18	2.22	44.10	1.163	0.0	0.0	-0.007	-0.01	0.007	0.0
19	1.56	63.01	0.819	0.0	0.0	-0.007	-0.01	0.007	0.0
20	0.91	99.00	0.476	0.0	0.0	-0.007	-0.01	0.007	0.0
21	0.25	99.00	0.132	0.0	0.0	-0.007	-0.01	0.007	0.0
22	-0.43	99.00	-0.144	0.0	0.0	-0.007	-0.01	0.005	0.0
23	-0.56	99.00	-0.113	0.0	0.0	-0.007	-0.02	0.001	0.002
24	-0.15	99.00	-0.031	0.0	0.0	-0.007	-0.02	0.0	0.004
25	0.26	99.00	0.055	0.0	0.0	-0.007	-0.02	0.0	0.004
26	0.67	99.00	0.142	0.0	0.0	-0.007	-0.02	0.0	0.004
27	1.07	92.18	0.258	0.0	0.0	-0.007	-0.02	0.0	0.004
28	1.59	62.05	0.333	0.0	0.0	-0.007	-0.02	-0.001	0.002

X-TWIST = -0.000008002 RAD./IN. — CHECKS, MXX = -0.300 — FXX = 35.000 — IYZ = -0.1091 — AREA = 6.031
Y-CURV. = -0.000164180 RAD./IN. — MXY = -8.000 — FXY = 0.000 — IYY = 8.9030 — YCENT = -0.236
Z-CURV. = -0.000115709 RAD./IN. — MXZ = -44.000 — FXZ = 0.000 — IZZ = 44.9955 — ZCENT = 0.193

OH-58 COMPOSITE BLADE--PROPERTIES BETWEEN 36.5 AND 179.916 RUN = 3 SHELL-D USES
OH-58 LIMIT LOADS AT STATION 179.916 INCH-KIP SYSTEM

CASE 15.12
INPUT DATA

BASIC MODULI
STRINGER E = 10000.
SKIN G = 1000.

	STATION 179.92 COORDINATES		STATION 36.50 COORDINATES		COMP.	TENS.	CRITICAL STRESS		REL.	SKIN	SKIN			
ELEM.	Y	Z	Y	Z	AREA	AREA	COMP.	TENS.	MOD.	THICK.	MOD.	AST	CF	TF
1	-1.50	-0.240	-3.29	-0.280	0.0361	0.0688	-100.00	100.00	0.51	0.1900	1056.	0.0000	0.5	0.500
2	-1.50	-0.280	-2.30	-0.310	0.0361	0.1048	-100.00	100.00	0.51	0.1900	1056.	0.0000	0.5	0.500
3	-0.80	-0.320	-1.30	-0.320	0.0361	0.1236	-100.00	100.00	0.51	0.1900	1056.	0.0000	0.5	0.500
4	-0.20	-0.300	-0.30	-0.320	0.0361	0.1236	-100.00	100.00	0.51	0.1900	1056.	0.0000	0.5	0.500
5	0.50	-0.270	0.70	-0.300	0.0361	0.1142	-100.00	100.00	0.51	0.1900	1056.	0.0000	0.5	0.500
6	1.00	-0.240	1.70	-0.270	0.0361	0.0584	-100.00	100.00	0.51	0.1900	1056.	0.0000	0.5	0.500
7	1.11	-0.210	2.30	-0.210	0.1863	0.1444	-100.00	100.00	0.51	0.5800	604.	0.0000	0.5	0.500
8	1.52	0.0	2.60	-0.070	0.2932	0.2386	-100.00	100.00	0.50	0.5000	612.	0.0000	0.5	0.500
9	1.94	0.0	2.90	-0.060	0.2050	0.1870	-100.00	100.00	0.50	0.4000	628.	0.0000	0.5	0.500
10	2.35	0.0	3.20	-0.025	0.1312	0.1285	-100.00	100.00	0.49	0.3200	646.	0.0000	0.5	0.500
11	2.64	0.020	3.39	-0.015	0.0850	0.0828	-100.00	100.00	0.49	0.2600	677.	0.0000	0.5	0.500
12	2.51	0.090	3.58	0.090	0.0620	0.0780	-100.00	100.00	0.47	0.1800	677.	0.0120	0.5	0.500
13	2.64	0.280	3.39	0.300	0.0775	0.0846	-100.00	100.00	0.49	0.3500	646.	0.0000	0.5	0.500
14	2.35	0.400	3.20	0.350	0.1537	0.1468	-100.00	100.00	0.49	0.4300	628.	0.0000	0.5	0.500
15	1.94	0.520	2.90	0.480	0.2225	0.2020	-100.00	100.00	0.50	0.5100	612.	0.0000	0.5	0.500
16	1.52	0.620	2.60	0.560	0.3101	0.2591	-100.00	100.00	0.50	0.6000	604.	0.0000	0.5	0.500
17	1.11	0.900	2.30	0.815	0.1981	0.1596	-100.00	100.00	0.51	0.1900	1056.	0.0000	0.5	0.500
18	1.00	0.920	1.70	0.970	0.0361	0.0587	-100.00	100.00	0.51	0.1900	1056.	0.0000	0.5	0.500
19	0.50	1.030	0.70	1.140	0.0361	0.1150	-100.00	100.00	0.51	0.1900	1056.	0.0000	0.5	0.500
20	-0.20	1.080	-0.30	1.225	0.0361	0.1240	-100.00	100.00	0.51	0.1900	1056.	0.0000	0.5	0.500
21	-0.80	1.090	-1.30	1.250	0.0361	0.1237	-100.00	100.00	0.51	0.1900	1056.	0.0000	0.5	0.500
22	-1.50	1.040	-2.30	1.210	0.0361	0.1050	-100.00	100.00	0.51	0.1900	1056.	0.0000	0.5	0.500
23	-1.90	0.990	-3.29	1.100	0.0361	0.0652	-100.00	100.00	0.51	0.1900	1056.	0.0000	0.5	0.500
24	-2.58	1.070	-4.30	1.110	0.0003	0.0120	-100.00	100.00	0.27	0.0170	2331.	0.0000	0.5	0.500
25	-3.60	0.930	-5.30	0.970	0.0003	0.0173	-100.00	100.00	0.27	0.0170	2331.	0.0000	0.5	0.500
26	-4.60	0.800	-6.30	0.800	0.0003	0.0171	-100.00	100.00	0.27	0.0170	2331.	0.0000	0.5	0.500
27	-5.59	0.620	-7.30	0.620	0.0003	0.0173	-100.00	100.00	0.27	0.0170	2331.	0.0000	0.5	0.500
28	-6.60	0.450	-8.30	0.430	0.0003	0.0122	-100.00	100.00	0.27	0.0170	2331.	0.0000	0.5	0.500
29	-7.00	0.380	-8.70	0.370	0.0182	0.0630	-100.00	100.00	0.46	0.1900	703.	0.0000	0.5	0.500
30	-7.60	0.280	-9.30	0.180	0.0241	0.0873	-100.00	100.00	0.43	0.1100	799.	0.0000	0.5	0.500
31	-8.10	0.130	-9.78	0.100	0.0079	0.0428	-100.00	100.00	0.38	0.0600	927.	0.0000	0.5	0.500
32	-8.60	0.090	-10.30	0.070	0.0023	0.0237	-100.00	100.00	0.27	0.0300	2331.	0.0000	0.5	0.500
33	-9.17	0.030	-10.89	0.030	0.0369	0.0532	-100.00	100.00	0.27	0.0300	2331.	0.0360	0.5	0.500
34	-8.60	0.0	-10.30	0.0	0.0023	0.0236	-100.00	100.00	0.27	0.0600	927.	0.0000	0.5	0.500
35	-8.10	0.0	-9.78	0.005	0.0103	0.0475	-100.00	100.00	0.38	0.1300	799.	0.0000	0.5	0.500
36	-7.60	0.0	-9.30	0.0	0.0285	0.0933	-100.00	100.00	0.43	0.2000	703.	0.0000	0.5	0.500
37	-7.00	-0.100	-8.70	-0.100	0.0202	0.0642	-100.00	100.00	0.46	0.0170	2331.	0.0000	0.5	0.500
38	-6.60	-0.120	-8.30	-0.125	0.0003	0.0120	-100.00	100.00	0.27	0.0170	2331.	0.0000	0.5	0.500
39	-5.59	-0.200	-7.30	-0.200	0.0003	0.0170	-100.00	100.00	0.27	0.0170	2331.	0.0000	0.5	0.500
40	-4.60	-0.240	-6.30	-0.240	0.0003	0.0169	-100.00	100.00	0.27	0.0170	2331.	0.0000	0.5	0.500
41	-3.60	-0.295	-5.30	-0.300	0.0003	0.0172	-100.00	100.00	0.27	0.0170	2331.	0.0000	0.5	0.500
42	-2.58	-0.330	-4.30	-0.340	0.0003	0.0119	-100.00	100.00	0.27	0.0170	2331.	0.0000	0.5	0.500
43	-2.22	-0.200	-3.95	-0.250	0.0182	0.0339	-100.00	100.00	0.51	0.0500	2331.	0.0000	0.5	0.500
44	-2.22	0.0	-3.95	0.0	0.0000	0.0000	-100.00	100.00	0.27	0.0500	2331.	0.0000	0.5	0.500
45	-2.22	0.360	-3.95	0.380	0.0000	0.0000	-100.00	100.00	0.27	0.0500	2331.	0.0000	0.5	0.500
46	-2.22	0.760	-3.95	0.790	0.0000	0.0000	-100.00	100.00	0.27	0.0500	2331.	0.0000	0.5	0.500
47	-2.22	0.930	-3.95	1.040	0.0182	0.0342	-100.00	100.00	0.51	0.0170	2331.	0.0000	0.5	0.500
48										0.1900	1056.			

CH-58 COMPOSITE BLADE--PROPERTIES BETWEEN 36.5 AND 179.916 RUN = 3 SHELL-D USES

OH-58 FATIGUE LOADS AT STATION 36.60 INCH-KIP SYSTEM

CASE 11.13 LOAD Y = 0.0 MXX = -1.500 FXX = 0.0

STA. 36.60 POINT Z = 0.0 MXY = -7.500 FXY = 0.0

MXZ = -22.000 FXZ = 0.0

NO.	AXIAL STRESS	M.S.	COMPONENTS OF FORCE X	Y	Z	SHEAR FLOW	SHEAR STRESS	SKIN FORCE COMP. Y	Z
1	2.11	46.46	0.330	0.003	0.000	0.074	0.39	0.061	-0.002
2	2.69	36.19	0.510	0.003	0.000	0.074	0.39	0.074	-0.001
3	3.17	30.57	0.602	0.002	0.0	0.074	0.39	0.074	-0.000
4	3.59	26.83	0.683	0.000	0.000	0.073	0.39	0.073	0.001
5	3.91	24.55	0.744	-0.001	0.000	0.072	0.38	0.073	0.002
6	4.18	22.91	0.637	-0.003	0.000	0.072	0.38	0.058	0.003
7	4.12	23.27	0.632	-0.005	0.0	0.071	0.12	0.032	0.007
8	3.43	28.13	0.587	-0.004	0.000	0.070	0.14	0.021	0.005
9	3.49	27.67	0.473	-0.003	0.000	0.070	0.17	0.021	0.002
10	3.39	28.49	0.308	-0.002	0.000	0.069	0.22	0.017	0.002
11	3.37	28.65	0.198	-0.001	0.000	0.069	0.27	0.013	0.004
12	2.86	34.00	0.188	-0.001	0.0	0.069	0.38	0.000	0.011
13	1.80	54.62	0.109	-0.001	-0.000	0.069	0.20	-0.013	0.009
14	1.49	66.10	0.156	-0.001	0.000	0.068	0.16	-0.017	0.006
15	0.72	59.00	0.107	-0.001	0.000	0.068	0.13	-0.020	0.007
16	0.18	99.00	0.036	-0.000	0.000	0.068	0.11	-0.020	0.011
17	-1.29	76.80	-0.227	0.002	-0.000	0.068	0.36	-0.030	0.014
18	-2.36	41.41	-0.366	0.002	0.000	0.068	0.36	-0.054	0.011
19	-3.68	26.18	-0.705	0.001	0.001	0.068	0.36	-0.068	0.009
20	-4.55	20.56	-0.867	-0.001	0.001	0.069	0.36	-0.068	0.004
21	-5.11	18.56	-0.972	-0.003	0.001	0.070	0.37	-0.069	-0.001
22	-5.33	17.77	-1.013	-0.006	0.001	0.071	0.37	-0.070	-0.005
23	-5.17	18.34	-0.814	-0.008	0.001	0.072	0.38	-0.059	-0.006
24	-3.02	32.10	-0.035	-0.000	0.000	0.012	0.68	-0.008	-0.000
25	-2.85	34.04	-0.049	-0.001	0.000	0.012	0.69	-0.012	-0.002
26	-2.60	37.43	-0.045	-0.001	0.0	0.012	0.69	-0.012	-0.002
27	-2.32	42.05	-0.040	-0.000	0.0	0.012	0.69	-0.012	-0.002
28	-2.01	48.63	-0.024	-0.000	-0.000	0.012	0.70	-0.008	-0.001
29	-3.29	29.39	-0.208	-0.002	-0.000	0.012	0.66	-0.006	-0.002
30	-2.41	40.46	-0.209	-0.002	-0.000	0.013	0.12	-0.007	-0.002
31	-1.98	49.45	-0.084	-0.001	-0.000	0.013	0.21	-0.006	-0.001
32	-1.46	67.71	-0.036	-0.000	-0.000	0.013	0.43	-0.007	-0.000
33	-1.48	66.70	-0.079	-0.001	0.0	0.013	0.44	0.000	-0.000
34	-1.26	78.45	-0.031	-0.000	0.0	0.013	0.22	0.007	-0.000
35	-1.61	61.17	-0.075	-0.001	0.000	0.013	0.10	0.007	-0.000
36	-1.62	60.87	-0.149	-0.002	0.0	0.014	0.07	0.007	-0.001
37	-1.04	95.21	-0.067	-0.001	0.0	0.014	0.83	0.007	-0.001
38	-0.45	99.00	-0.005	-0.000	-0.000	0.014	0.83	0.010	-0.001
39	-0.01	99.00	-0.000	-0.000	0.0	0.014	0.84	0.014	-0.001
40	0.33	99.00	0.006	0.000	0.0	0.014	0.84	0.014	-0.001
41	0.73	99.00	0.012	0.000	0.000	0.014	0.84	0.014	-0.001
42	1.07	92.75	0.012	0.000	0.000	0.014	0.84	0.010	0.000
43	1.67	58.68	0.109	0.001	0.000	-0.060	-1.21	0.027	-0.008
44	0.19	99.00	0.000	0.000	0.0	-0.060	-1.21	0.0	-0.019
45	-0.88	99.00	-0.000	-0.000	.000	-0.060	-1.21	0.0	-0.024
46	-2.04	48.05	-0.000	-0.000	.00	-0.060	-1.21	0.0	-0.020
47	-5.13	18.48	-0.336	-0.004	0.000	0.012	0.68	-0.025	-0.009
48						0.075	0.39	0.0	0.0

X-TWIST = 0.000309849 RAD./IN. CHECKS, MXX = 1.500 FXX = 0.000 IYZ = 0.1607 AREA = 2.083

Y-CURV. = -0.001333714 RAD./IN. MXY = -7.500 FXY = 0.000 IYY = 0.7407 YCENT = -0.659

Z-CURV. = -0.000003244 RAD./IN. MXZ = -22.000 FXZ = -0.000 IZZ = 28.4150 ZCENT = 0.332

CH-58 COMPOSITE BLADE--PROPERTIES BETWEEN 36.5 AND 179.916 RUN = 3 SHELL-D USES
CH-58 MEAN LOADS AT STATION 36.60 INCH-KIP SYSTEM

CASE 11.14 LOAD Y = 0.0 MXX = -0.215 FXX = 32.200
STA. 36.60 POINT Z = 0.0 MXY = -4.000 FXY = 0.0
MXZ = -42.500 FXZ = 0.0

NO.	AXIAL STRESS	M.S.	COMPONENTS OF FORCE X	Y	Z	SHEAR FLOW	SHEAR STRESS	SKIN FORCE COMP. Y	Z
1	11.11	8.00	1.743	0.017	0.000	-0.004	-0.02	-0.003	0.000
2	12.63	6.92	2.393	0.013	0.001	-0.004	-0.02	-0.004	0.000
3	13.94	6.18	2.647	0.005	0.0	-0.005	-0.03	-0.005	0.000
4	15.14	5.60	2.877	0.002	0.000	-0.006	-0.03	-0.005	-0.000
5	16.14	5.20	3.067	-0.004	0.001	-0.007	-0.04	-0.006	-0.000
6	17.03	4.87	2.593	-0.013	0.001	-0.008	-0.04	-0.006	-0.000
7	17.13	4.84	2.626	-0.022	0.0	-0.010	-0.02	-0.004	-0.001
8	15.68	5.38	2.693	-0.020	0.001	-0.011	-0.02	-0.003	-0.001
9	15.85	5.31	2.148	-0.014	0.001	-0.013	-0.03	-0.004	-0.000
10	15.65	5.39	1.423	-0.008	0.000	-0.013	-0.04	-0.003	-0.000
11	15.57	5.42	0.914	-0.005	0.000	-0.014	-0.05	-0.003	-0.001
12	14.40	5.94	0.946	-0.004	0.0	-0.015	-0.08	0.000	-0.002
13	12.45	7.03	0.746	-0.004	-0.000	-0.015	-0.04	0.003	-0.002
14	11.90	7.40	1.246	-0.007	0.000	-0.016	-0.04	0.004	-0.001
15	10.38	8.64	1.551	-0.010	0.000	-0.016	-0.03	0.005	-0.002
16	9.26	9.80	1.928	-0.014	0.001	-0.017	-0.03	0.005	-0.003
17	6.45	14.51	1.141	-0.005	0.001	-0.018	-0.09	0.008	-0.004
18	4.11	23.32	0.638	-0.003	-0.000	-0.018	-0.09	0.014	-0.003
19	1.13	67.13	0.217	-0.000	-0.000	-0.017	-0.09	0.017	-0.002
20	-0.56	59.00	-0.182	-0.000	0.000	-0.016	-0.09	0.017	-0.001
21	-2.42	40.27	-0.461	-0.002	0.001	-0.015	-0.08	0.015	0.000
22	-3.21	30.13	-0.611	-0.003	0.001	-0.013	-0.07	0.014	0.001
23	-3.27	29.62	-0.515	-0.005	0.000	-0.011	-0.06	0.010	0.001
24	-2.45	35.82	-0.028	-0.000	0.000	-0.005	-0.30	0.003	0.000
25	-2.31	42.21	-0.040	-0.000	0.000	-0.005	-0.29	0.005	0.001
26	-2.01	48.69	-0.035	-0.000	0.0	-0.005	-0.28	0.005	0.001
27	-1.65	59.43	-0.025	-0.000	0.0	-0.005	-0.28	0.005	0.001
28	-1.24	79.56	-0.015	-0.000	-0.000	-0.005	-0.27	0.003	0.001
29	-1.98	49.54	-0.125	-0.001	-0.000	-0.004	-0.02	0.002	0.000
30	-0.77	59.00	-0.067	-0.001	-0.000	-0.003	-0.02	0.002	0.000
31	-0.50	59.00	-0.021	-0.000	-0.000	-0.002	-0.04	0.001	0.000
32	-0.53	59.00	-0.013	-0.000	-0.000	-0.002	-0.06	0.001	0.000
33	-0.68	59.00	-0.037	-0.000	0.0	-0.001	-0.05	0.000	0.000
34	-1.14	59.00	-0.003	-0.000	0.0	-0.001	-0.02	-0.001	0.000
35	0.24	59.00	0.011	0.000	-0.000	-0.001	-0.01	-0.000	-0.000
36	0.80	59.00	0.074	0.001	0.0	0.000	0.00	-0.000	-0.000
37	2.47	39.92	0.159	0.002	0.0	0.001	0.06	0.000	-0.000
38	1.85	53.05	0.022	0.000	0.000	0.001	0.07	0.001	-0.000
39	2.91	33.33	0.050	0.001	0.0	0.001	0.07	0.001	-0.000
40	3.78	25.45	0.064	0.001	0.0	0.001	0.08	0.001	-0.000
41	4.76	20.01	0.081	0.001	0.000	0.001	0.08	0.001	-0.000
42	5.63	16.77	0.065	0.001	0.000	0.001	0.08	0.001	0.000
43	10.01	8.99	0.654	0.009	0.000	0.006	0.11	-0.001	0.001
44	3.96	24.26	0.000	0.000	0.0	0.006	0.11	0.0	0.002
45	1.84	53.29	0.000	0.000	-0.000	0.006	0.11	0.0	0.002
46	-0.44	59.00	-0.000	-0.000	0.000	0.006	0.11	0.0	0.002
47	-3.43	28.15	-0.225	-0.003	0.000	-0.005	-0.30	0.005	0.001
48						-0.004	-0.02	0.0	0.0

X-TWIST = -0.000046129 RAD./IN. CHECKS, MXX = -0.215 FXX = 32.200 IYZ = 0.1607 AREA = 2.083
Y-CURV. = -0.000236515 RAD./IN. MXY = -4.000 FXY = 0.000 IYY = 0.7407 YCENT = -0.659
Z-CURV. = -0.000239671 RAD./IN. MXZ = -42.500 FXZ = -0.000 IZZ = 28.4150 ZCENT = 0.332

CH-58 COMPOSITE BLADE--PROPERTIES BETWEEN 36.5 AND 179.516 RUN = 3 SHELL-D USES
CH-58 LIMIT LOADS AT STATION 36.60 INCH-KIP SYSTEM

CASE 11.12 LOAD Y = 0.0 MXX = 5.900 FXX = 45.500
STA. 36.60 POINT Z = 0.0 MXY = -48.000 FXY = 0.0
MXZ = 0.0 FXZ = 0.0

NO.	AXIAL STRESS	M.S.	COMPONENTS OF FORCE X	Y	Z	SHEAR FLOW	SHEAR STRESS	SKIN FORCE COMP. Y	Z
1	35.92	1.78	5.632	0.055	0.002	0.286	1.51	0.237	-0.009
2	38.01	1.63	7.204	0.040	0.002	0.283	1.49	0.284	-0.006
3	39.24	1.55	7.454	0.026	0.0	0.280	1.47	0.282	-0.001
4	40.02	1.50	7.604	0.005	0.001	0.276	1.45	0.278	0.003
5	39.93	1.50	7.568	-0.011	0.002	0.273	1.44	0.274	0.007
6	39.41	1.54	6.001	-0.025	0.001	0.270	1.42	0.217	0.012
7	37.26	1.68	5.711	-0.047	0.0	0.267	0.46	0.131	0.027
8	30.67	2.26	5.248	-0.040	0.003	0.264	0.53	0.080	0.020
9	30.32	2.30	4.108	-0.028	0.002	0.262	0.66	0.079	0.006
10	28.73	2.48	2.608	-0.015	0.000	0.261	0.81	0.064	0.006
11	28.35	2.57	1.646	-0.005	0.000	0.260	1.00	0.049	0.015
12	23.28	3.30	1.530	-0.007	0.0	0.259	1.44	0.000	0.041
13	14.97	5.68	0.897	-0.005	-0.000	0.259	0.74	-0.049	0.034
14	12.92	6.74	1.253	-0.008	0.000	0.258	0.60	-0.063	0.023
15	7.31	12.67	1.093	-0.007	0.000	0.258	0.51	-0.078	0.027
16	3.69	26.07	0.729	-0.005	0.000	0.255	0.43	-0.078	0.043
17	-7.62	12.12	-1.349	0.011	-0.001	0.261	1.37	-0.117	0.053
18	-14.38	5.72	-2.339	0.011	0.001	0.263	1.38	-0.210	0.043
19	-23.10	3.33	-4.428	0.006	0.004	0.267	1.41	-0.265	0.034
20	-27.61	2.62	-5.256	-0.004	0.005	0.272	1.43	-0.269	0.015
21	-29.49	2.39	-5.606	-0.020	0.006	0.277	1.46	-0.274	-0.002
22	-28.53	2.51	-5.424	-0.030	0.006	0.282	1.48	-0.279	-0.021
23	-24.50	3.08	-2.859	-0.038	0.003	0.286	1.51	-0.234	-0.024
24	-13.75	6.27	-0.160	-0.002	0.000	0.045	2.89	-0.033	-0.002
25	-10.90	8.18	-0.198	-0.002	0.000	0.049	2.90	-0.049	-0.008
26	-7.34	12.62	-0.127	-0.002	0.0	0.050	2.91	-0.049	-0.009
27	-3.55	27.17	-0.061	-0.001	0.0	0.050	2.92	-0.050	-0.009
28	0.48	59.00	0.006	-0.000	0.000	0.050	2.93	-0.035	-0.006
29	2.91	33.39	0.184	0.002	0.000	0.050	0.27	-0.025	-0.006
30	9.26	9.80	0.802	0.010	0.000	0.051	0.46	-0.027	-0.007
31	10.56	8.47	0.448	0.005	0.000	0.051	0.85	-0.025	-0.003
32	8.06	11.41	0.197	0.002	0.000	0.051	1.70	-0.028	-0.002
33	8.75	10.43	0.470	0.006	0.0	0.051	1.71	0.000	-0.002
34	9.70	9.31	0.237	0.003	0.0	0.051	0.85	0.028	-0.001
35	13.66	6.32	0.640	0.007	-0.000	0.051	0.39	0.026	-0.000
36	15.87	5.30	1.461	0.017	0.0	0.051	0.26	0.028	-0.003
37	21.59	3.63	1.397	0.016	0.0	0.051	3.02	0.026	-0.003
38	13.46	6.43	0.161	0.002	0.000	0.051	3.01	0.036	-0.003
39	15.64	5.39	0.267	0.003	0.0	0.051	3.01	0.051	-0.003
40	17.00	4.88	0.289	0.003	0.0	0.051	3.01	0.051	-0.003
41	18.82	4.21	0.321	0.004	0.000	0.051	3.00	0.051	-0.003
42	20.18	3.96	0.234	0.003	0.000	0.051	2.99	0.034	0.001
43	34.09	1.93	2.227	0.027	0.001	-0.239	-4.77	0.103	-0.032
44	12.37	7.08	0.000	0.000	0.0	-0.239	-4.77	0.0	-0.075
45	3.48	27.16	0.000	0.000	-0.000	-0.239	-4.77	0.0	-0.094
46	-6.12	15.25	-0.000	-0.000	-0.000	-0.239	-4.77	0.0	-0.079
47	-22.39	3.47	-1.467	-0.018	0.001	0.049	2.88	-0.102	-0.037
48						0.289	1.52	0.0	0.0

X-TWIST = 0.001198289 RAD./IN. CHECKS, MXX = 5.900 FXX = 45.501 IYZ = 0.1607 AREA = 2.083
Y-CURV. = -0.000855549 RAD./IN. MXY = -48.000 FXY = -0.000 IYY = 0.7407 YCENT = -0.659
Z-CURV. = -0.000153692 RAD./IN. MXZ = -0.000 FXZ = -0.000 IZZ = 28.4150 ZCENT = 0.332

PROG...CMAB

BASIC BLADE SECTION CH-58 STA 36.5 S-GLASS UNI ONLY FOR CRITICAL ELEMENT

MAT.	ALLOWABLE STRESS, UNIAXIAL 11	11	22	22	12	12	MODULI E11	E22	G	NU12
30	-37.8	103.0	-7.1	2.30	-2.73	2.73	7820.	2504.	865.	0.300

LAMINA 1

MATERIAL 30

THICKNESS 0.1060

ANGLE 0.

LAMINATE PROPERTIES	EX	EY	G
K*S UNRESTRAINED	7820.	2504.	865.
K*S = 0	7820.	2504.	865.

BUCKLING PARAMETERS, VALID FOR L*L/R BETWEEN 0.17865E 01 AND 0.17865E 03

BUCKLING LOAD FX,CR= 0.13007E 04 NX,CR= 0.20701E 03 /R

BEHAVIOR FOR NX= 7.604 NY= 0.0 NXY= 0.280 KX= 0.0 KY= 0.0 KXY= 0.0

LAM. NO.	STRESSES X	Y	XY	STRAINS 11	22	12	11	22	12	M.S. 11	22	12	MIN.
1	71.7	-0.0	2.6	71.7	-0.0	2.6	0.009173	-0.002752	0.003054	0.44	0.03	0.03	0.03
ALL	71.7	0.0	2.6				0.009173	-0.002752	0.003054				0.03

APPENDIX C

OH-58 BLADE SPAR REPAIRABILITY

INTRODUCTION

Kaman has recently completed the repairability program for the composite AH-1 blade. This program included afterbody repair and, for the first time, a high order of trailing edge spline repair. Because of the multicelled cross section of the AH-1 blade, it was not considered practical to repair spar damage since there exists a high probability of severe internal wall damage and the relatively small cells render the repair tooling schemes impractical. Also, the emphasis in the AH-1 program was repairability of damage due to the 23mm HEI threat. Spar damage due to this threat was so extensive as to preclude any consideration of repair. The Kaman K757 OH-58 composite blade will have the same afterbody repairability but, in addition, it will provide a practical opportunity for spar repairs. This is because the chordwise dimension of the single cell spar approaches 50% of the total chord which provides adequate opportunity for wound dressing and repair on the top and bottom surfaces. Kaman proposed to include, as part of Contract No. DAAJ02-77-C-0075, the OH-58 composite blade program, a Kaman-funded spar repairability study. The repairability scheme envisioned the repair of ballistic damage to the top and/or bottom surfaces of the airfoil. It did not include repairs of the solid fiberglass leading edge nose piece or the afterbody core-spar wall juncture. Tests were proposed to prove the practicality of repair.

DISCUSSION

The repairability evaluation program consisted of the following primary steps:

1. Construct prototype spar section (Figure C-1).
2. Test the spar in a free-free beam rig for 10^6 cycles (Figure C-2). Use loads corresponding to high speed straight and level flight for the present blade.
3. Submit the successfully tested spar to ballistic damage.
4. Repair specimen.
5. Retest for 10^6 cycles using high speed straight and level flight loads.

Step 1 was performed by tape winding, using 2-inch prepreg tapes, over a mandrel made up of spanwise tapered segments. Spanwise uniaxial filaments were also 2-inch tapes which were butted. The material used was 3M XP250 Uni-E-Glass. E-glass is considered to be a conservative choice for the purposes of this program. Cure was accomplished on the mandrel under 35 psi

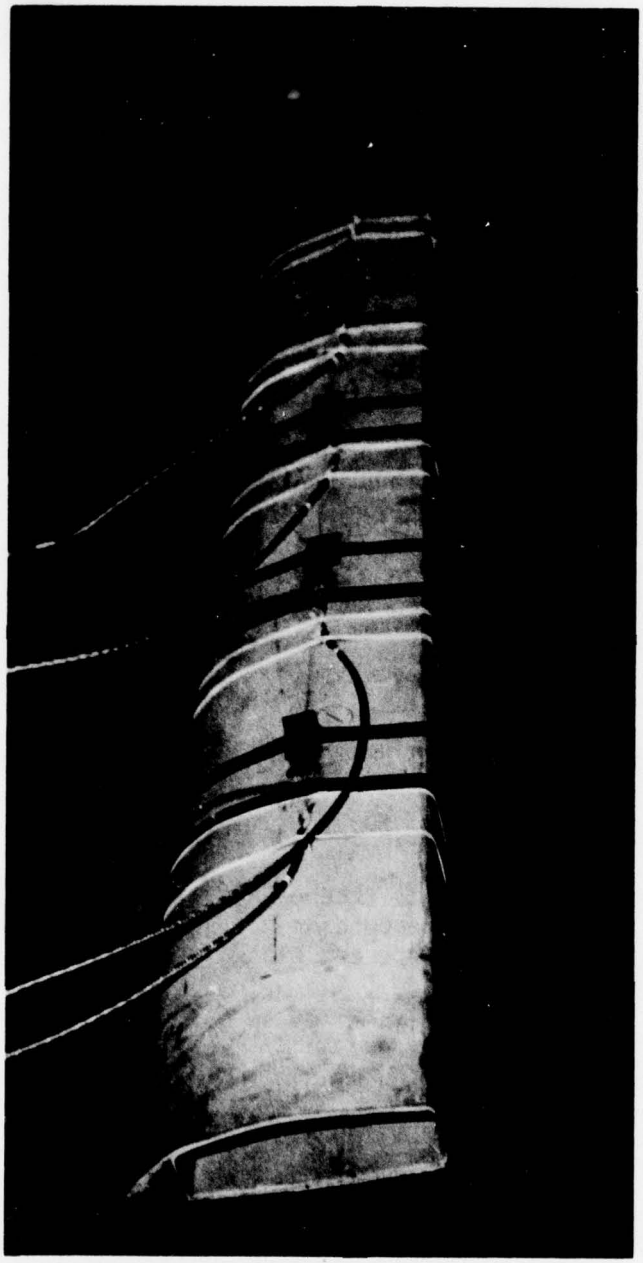

Figure C-1. Filament-wound OH-58 spar.

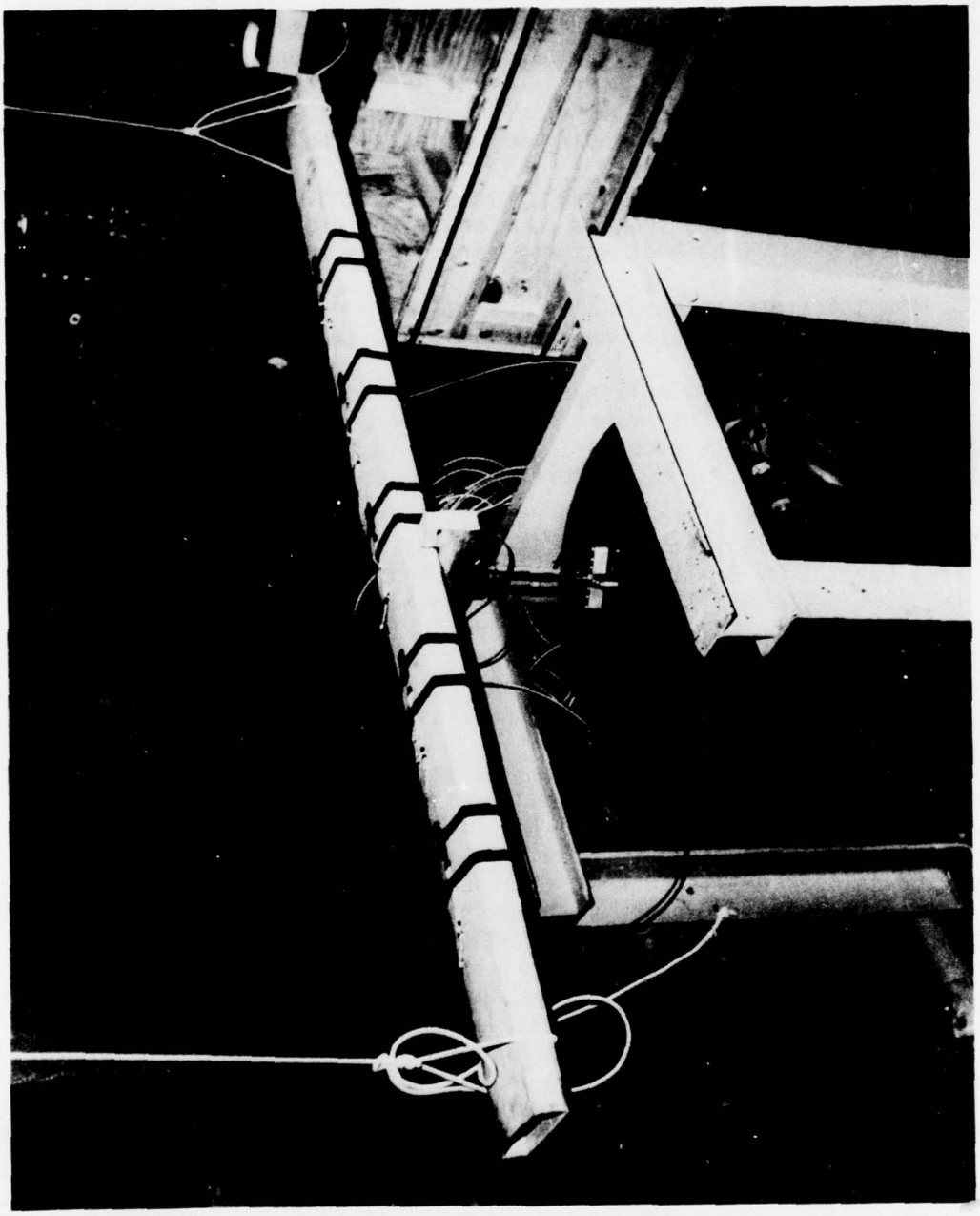

Figure C-2. Free-free beam test rig.

autoclave pressure for 90 minutes, minimum, at 250°F to 270°F. The schedule of material and the distribution are illustrated in Figure C-3.

The spar was completed before the final blade definition and, therefore, was not totally representative of the final configuration. Basically, there are three significant differences which would tend to minimize ballistic damage:

1. An additional ± 45° winding was added to the cross section.

2. The afterbody "basketweave" skin was extended over the top and bottom of the spar to tuck under the erosion boot in the design. The boot was not part of the prototype spar.

3. The thickness of uniaxial plies was reduced from .140 inch to .106 inch. (Total thickness is .170 inch.)

Step 2 was performed using only beamwise cyclic bending of ± 3000 in.-lb peak since the free-free rig vibrates in the beamwise or out-of-plane direction only. This slightly exceeds loadings at station 60, and exceeds all values outboard of station 60 (Reference 9, Figure 225, for the V_H condition). Therefore, 75% of the blade span is tested or approximately 91% of the rotor disc vulnerability area. Step 3 was performed at the Applied Technology Laboratory Ballistic Facility. Figures C-4 through C-7 illustrate the test setup and the blade condition before and after the test. Test apparatus at the ballistic laboratory included a Hewlett-Packard measuring system, electronic ballistic velocity screens, firing control system, video monitoring system, speedgraphic camera, .50-caliber Mann barrel and .50-caliber ammunition (APM2 w/225 grains of IMR5010 powder).

The blade was mounted in a wood frame and secured to the mounting ring to present the spanwise axis at a 90° angle with respect to the impact point. No loads were imposed during test. The impact was located 36 inches from the right end and 5 inches down from the leading edge (Figure C-5). The tumbled .50-caliber APM2 struck at a velocity of 2568 fps. The most notable results are the extensive spanwise brooming of the internal uniaxial material and the chordwise brooming of the 90° plies on the exit side. The cross plies were "holed" by the strike with a limited amount of delamination. By contrast, the uniaxial plies suffered extensive surface delamination and internal brooming. The basketweave extension would have reduced the surface delamination and the additional cross ply winding would have further restrained internal brooming. It is judged that the damage generated by the test exceeds that expected of the final cross section and that the test is conservative from a repair point of view.

Step 4 was performed in the Kaman Materials Laboratory. All delaminated material was removed, resulting in clean holes as shown in Figure C-8. Next, a patch conforming to the spanwise cross section shown in Figure C-9 was applied to both inlet and exit holes. Both the isotropic (0, 60, 120) and uniaxial patches were made from Uni-E-Glass (3M XP250). Outer and

Basic spar cross section

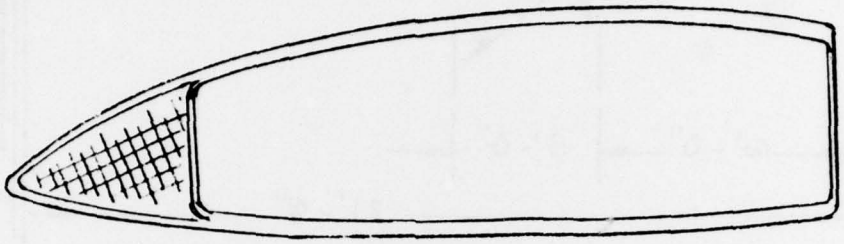

Winding schedule

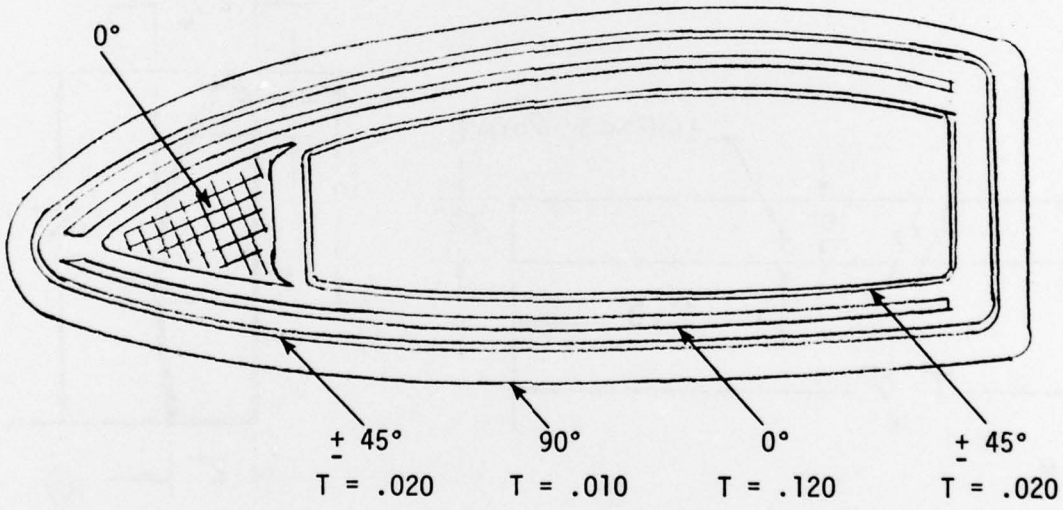

Figure C-3. Material distribution.

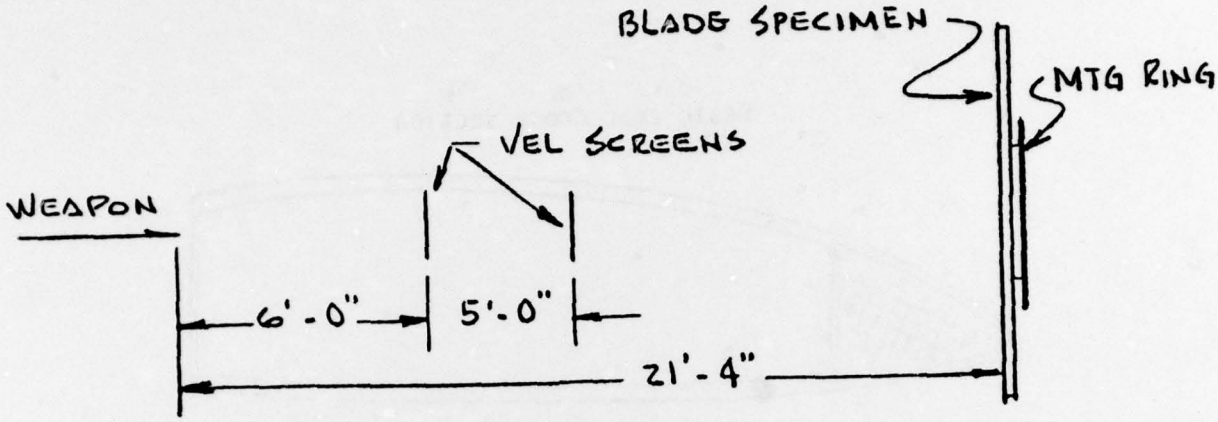

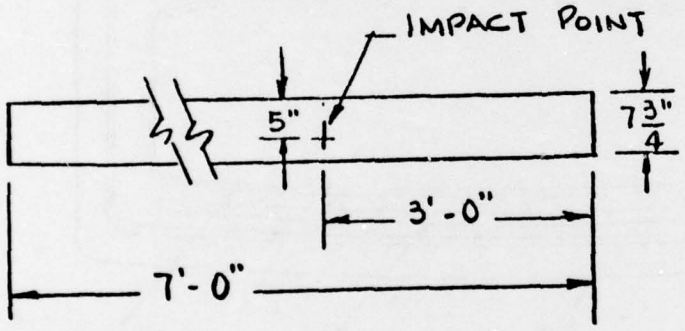

BLADE SPECIMEN
NTS

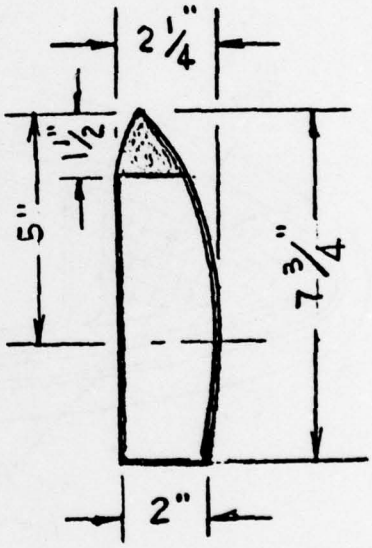

END VIEW
NTS

Figure C-4. Test set-up.

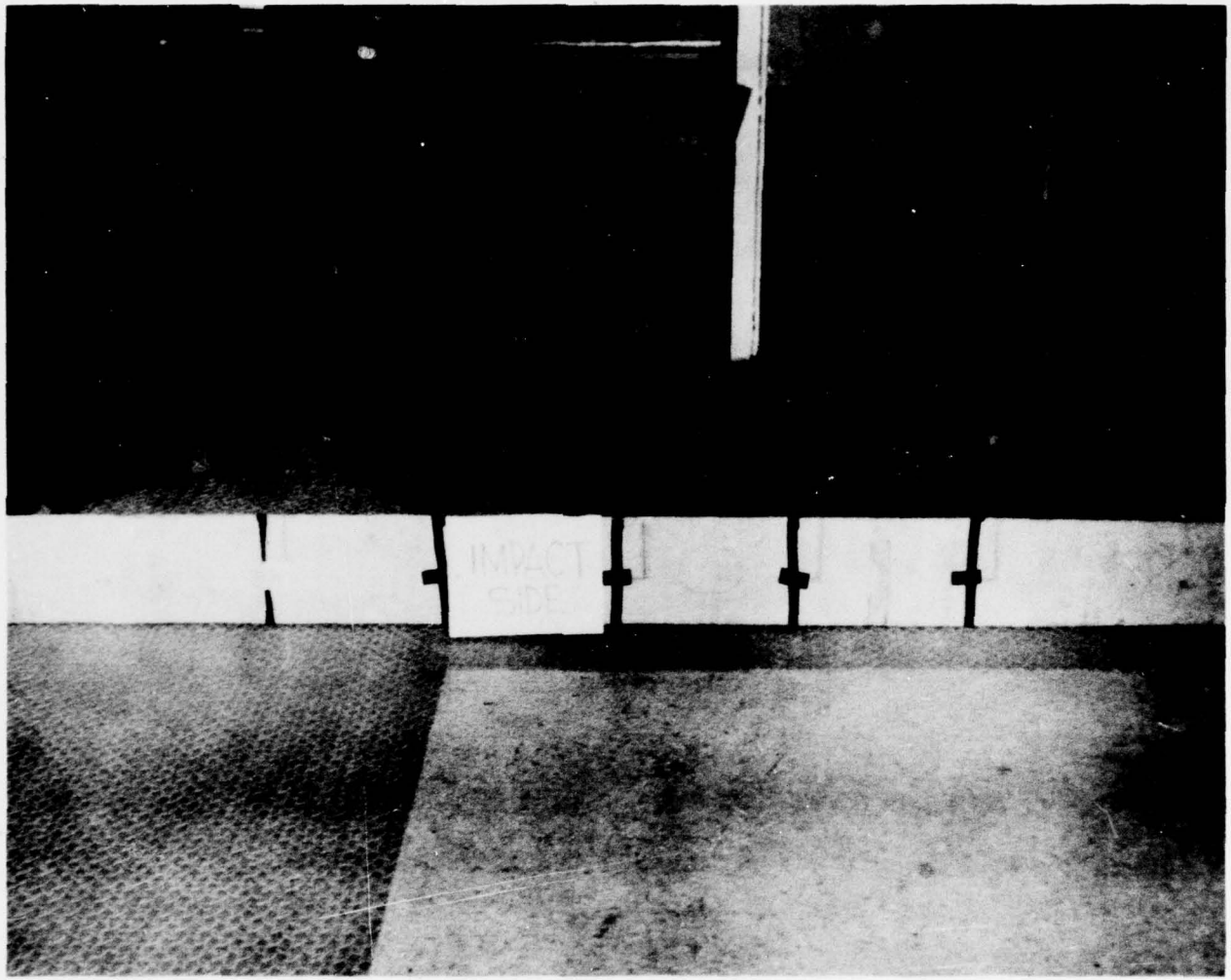

Figure C-5. View of blade before impact.

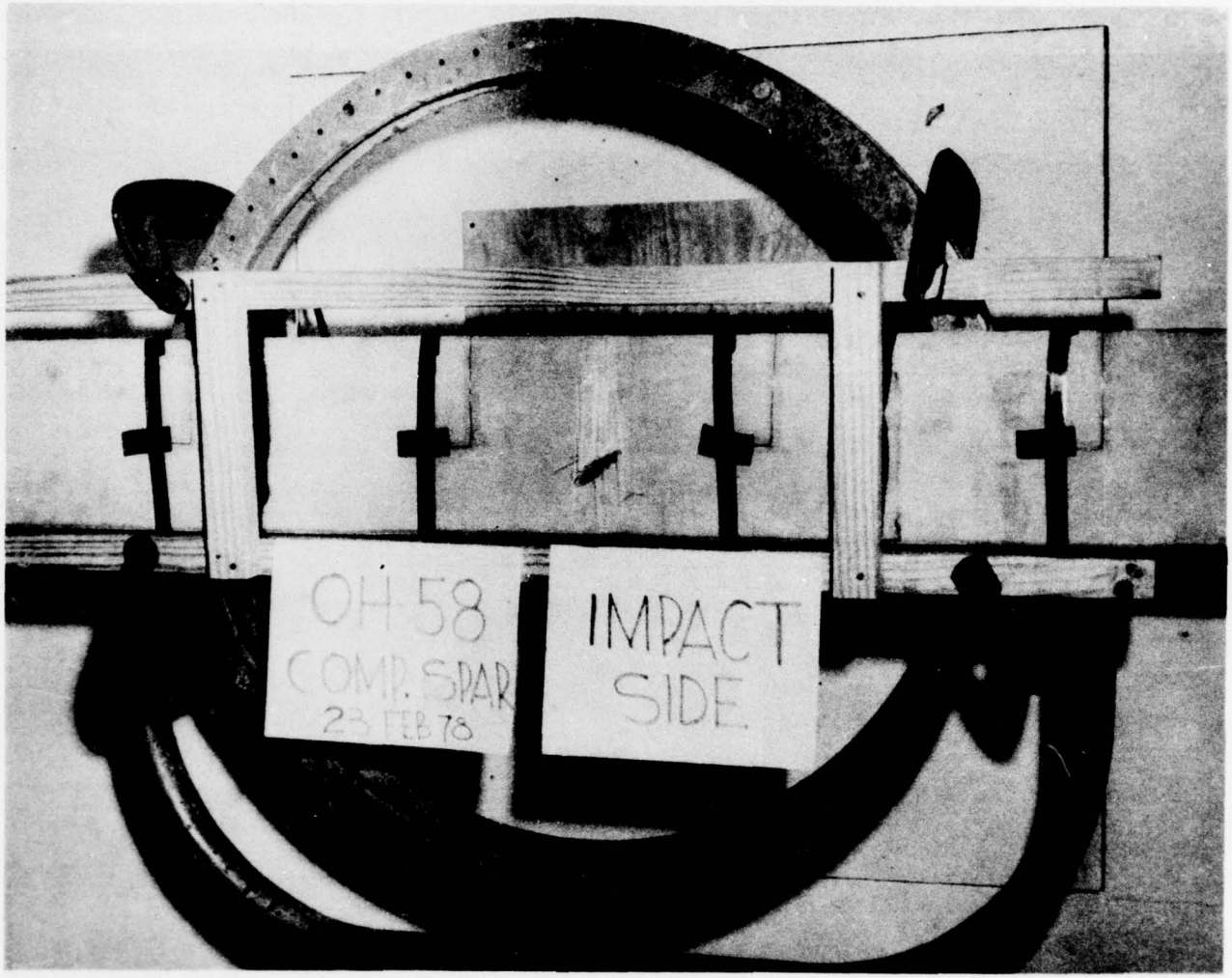

Figure C-6. Impact side of .50-caliber tumbled strike.

Figure C-7. Exit side - .50-caliber strike.

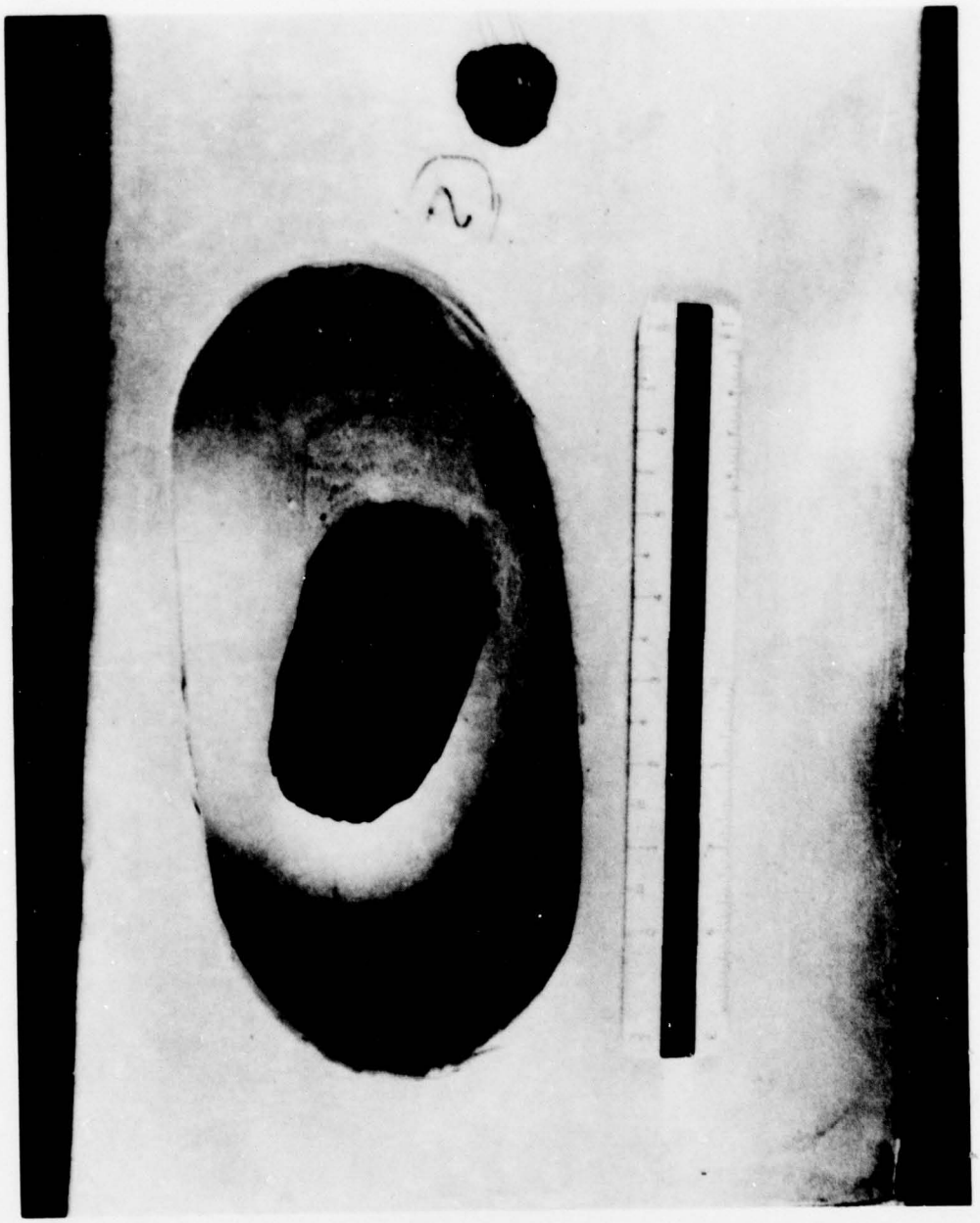

Figure C-8. Cleanup of entrance and exit holes.

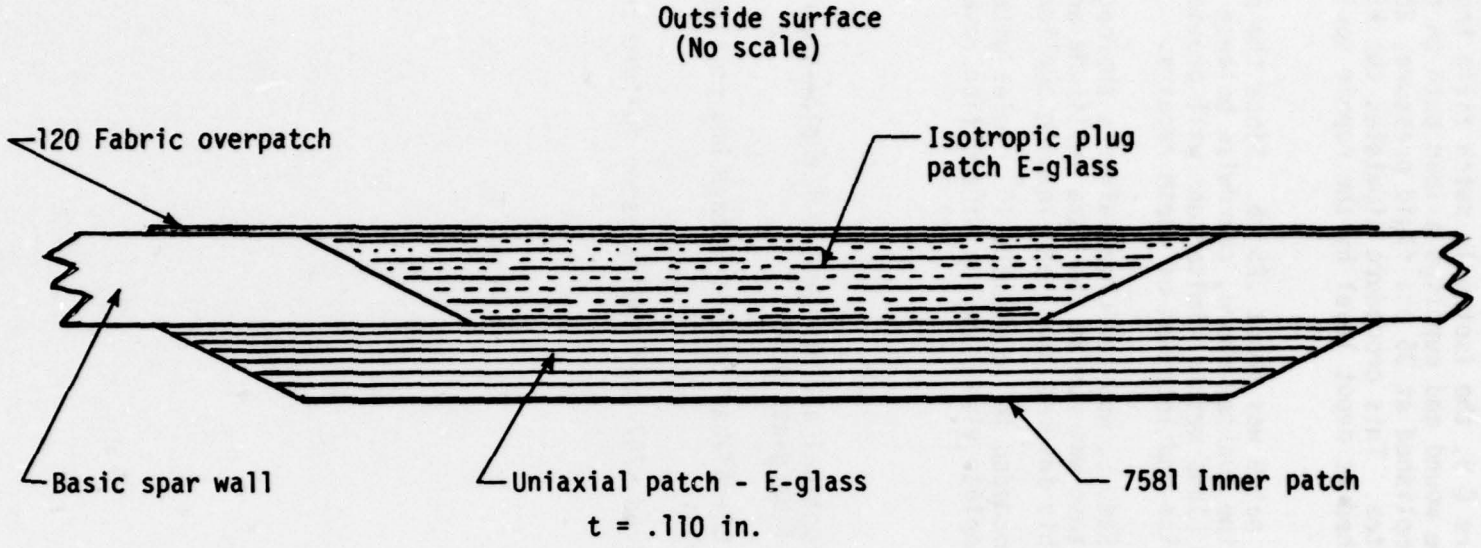

Figure C-9. Spanwise cross section of patch.

inner prepreg cover patches were 7581 and 120 Fabric, American Cyanamid BP919. As shown in Figure C-9, the isotropic patch fills the hole while the uni-patch bridges the wound and supplies a load path on the inside of the spar. Cure was accomplished at 35 psi fluid pressure, 250°F to 270°F for a minimum of 90 minutes. This procedure simulates the kind of repair which would be accomplished at depot level by the repair tools illustrated in Figures 63 and 64.

The total weight of this patch was about .25 lb. Since the patch will center approximately at the quarter-chord, chordwise balance will be unaffected. Span moment and blade weight limitations will provide working limits for the number, size and location of these repairs.

The final fatigue test, Step 5, was performed after a thorough inspection of the spar patch. The test was run at the same amplitude and frequency as in the original test. This insures that test loading duplicated the original levels. The test proceeded to accumulate 10^6 cycles without any indication of failure. A complete visual and tap-inspection revealed no deficiencies.

CONCLUSIONS

1. Spar repairs are practical and achievable for plan-form through damage of the K757 fiberglass spar.

2. A spar repair for .50-caliber tumbled damage has no significant effect on the spar stiffness.

3. The test of a repaired K757 spar indicates no failure tendencies.